ECMWF COPERNICUS REPORT

Copernicus Atmosphere Monitoring Service

Validation report of the CAMS near-real time global atmospheric composition service

Period September – November 2020

Issued by: KNMI

Date: 12 March 2021

Ref: CAMS84_2018SC3_D1.1.1_SON2020

IMPLEMENTED BY ECMWF

Validation report of the CAMS near-real-time global atmospheric composition service: Period September - November 2020

EDITORS:
N. Sudarchikova (MPG), M. Schulz (MetNo),
Q. Errera (BIRA-IASB), M. Ramonet (LSCE), H.J. Eskes (KNMI)

AUTHORS:
S. Basart (BSC), A. Benedictow (MetNo), Y. Bennouna (CNRS-LA),
A.-M. Blechschmidt (IUP-UB), S. Chabrillat (BIRA-IASB),
Y. Christophe (BIRA-IASB), E. Cuevas (AEMET), A. El-Yazidi (LSCE),
H. Flentje (DWD), P. Fritzsche (DWD), K. M. Hansen (AU), U. Im (AU),
J. Kapsomenakis (AA), B. Langerock (BIRA-IASB),
A. Richter (IUP-UB), V. Thouret (CNRS-LA), A. Wagner (MPG),
T. Warneke (UBC), C. Zerefos (AA)

REPORT OF THE COPERNICUS ATMOSPHERE MONITORING SERVICE, VALIDATION SUBPROJECT.

AVAILABLE AT:
http://atmosphere.copernicus.eu/quarterly_validation_reports

CITATION:
Sudarchikova, N., M. Schulz, Q. Errera, M. Ramonet, H. J. Eskes, S. Basart, A. Benedictow, Y. Bennouna, A.-M. Blechschmidt, S. Chabrillat, Christophe, Y., E. Cuevas, A. El-Yazidi, H. Flentje, P. Fritzsche, K.M. Hansen, U. Im, J. Kapsomenakis, B. Langerock, A. Richter, V. Thouret, A. Wagner, T. Warneke, C. Zerefos, Validation report of the CAMS near-real-time global atmospheric composition service: Period September - November 2020, Copernicus Atmosphere Monitoring Service (CAMS) report, CAMS84_2018SC3_D1.1.1_SON2020.pdf, March 2021, doi: 10.24380/rysv-7371.

STATUS:
Version 1, final

DATE:
12 March 2021

Executive Summary

The Copernicus Atmosphere Monitoring Service (http://atmosphere.copernicus.eu, CAMS) is a component of the European Earth Observation programme Copernicus. The CAMS global near-real time (NRT) service provides daily analyses and forecasts of reactive trace gases, greenhouse gases and aerosol concentrations. This document presents the validation statistics and system evolution of the CAMS NRT service for the period up to 1 December 2020, with a focus on September-November 2020 (SON-2020). Updates of this document appear every 3 months, e.g. Ramonet et al. (2021). A detailed description of the measurement datasets used is provided in Eskes et al. (2021). Automated verification plots are made available through the CAMS global evaluation server, https://global-evaluation.atmosphere.copernicus.eu.

This summary is split according to service themes as introduced on the CAMS website: air quality & atmospheric composition, climate forcing, ozone layer and UV. Specific attention is given to the ability of the CAMS system to capture recent events. We focus on the 'o-suite' composition fields, which are the daily analyses and forecasts produced by the IFS (Integrated Forecast System) modelling system at ECMWF, using the available meteorological and atmospheric composition observations which are ingested in the ECMWF 4D-Var assimilation system. The model and assimilation configurations are summarised in section 2. We furthermore assess the impact of the composition observations by comparing the validation results from the 'o-suite' to a 'control' configuration without atmospheric composition data assimilation. Also, the pre-operational delayed-mode analyses and high-resolution forecasts of CO_2 and CH_4 are assessed in this report.

Air quality and atmospheric composition

Tropospheric ozone (O_3)

The CAMS o-suite ozone is validated with surface and free tropospheric ozone observations from the GAW and ESRL networks, ozone sondes, IAGOS aircraft profiles and IASI tropospheric ozone retrievals. For free tropospheric ozone against ozone sondes, the o-suite modified normalized mean biases (MNMBs) are on average small, ±10% over the Northern Hemisphere (NH), between ±30% for stations in the Tropics, and ±20% for the Arctic in the recent years (Fig. S.1). Over Antarctica o-suite biases are observed between 0% and ±20% for the recent years, whereas the control run shows larger negative biases. For SON 2020, good agreement is found over the NH mid latitudes (MNMBs of o-suite within 10%), Arctic (MNMBs of o-suite within 20%) and Antarctica (MNMBs of o-suite within ± 15%) in the free troposphere.

The time series show no indication of substantial changes in tropospheric ozone biases after the upgrade to Cy47R1 on October 6, 2020. Note that the Cy47R1 data record covered by this report is still too short (7 weeks) to draw quantitative conclusions.

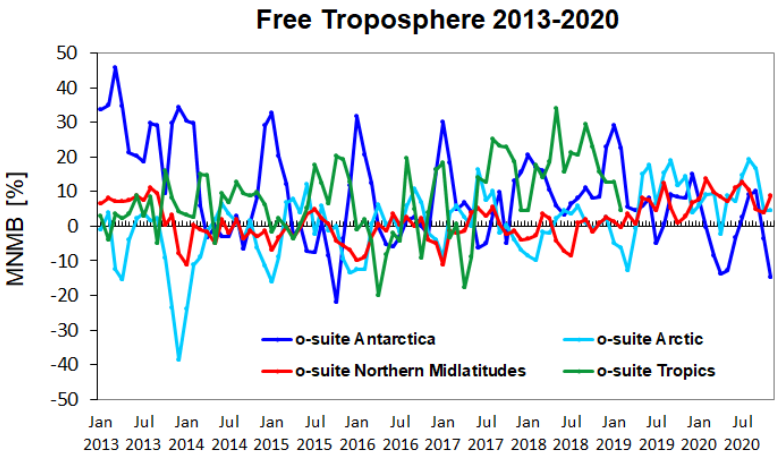

Figure S.1: Time series of MNMB of ozone in the o-suite, compared against ozone sondes, averaged over different latitude bands. The free troposphere is defined here as the layer between 750 and 300 hPa.

Ozone is well represented in the low troposphere by both runs with on average a positive MNMB of less than 15% up to 2000 m and a correlation of about 80%. In the UTLS region the bias is larger and the results from the two runs differ. Ozone is mostly overestimated by the o-suite with an average MNMB of more than 40%, whereas the control run does not present a systematic behaviour. Due to the COVID-19 pandemic, air travel was largely reduced during June-November 2020 and the number of available IAGOS aircraft profiles that could be included in this report was very limited.

The comparison with GAW surface stations shows that O_3 surface mixing ratios in SON are overestimated with MNMBs within 28% for Europe (exception: CGR station with higher bias) and within 26% for Asian stations. Correlation coefficients for European stations are between 0.48 and 0.77 and between 0.58 and 0.92 for Asian stations. The timeseries of modelled surface ozone show in general a good correspondence with the observations. The validation with ESRL stations likewise shows overestimations of ozone mixing ratios mostly within 30% (exception: THD station in USA). The comparison with surface observations in megacities in China show significant correlations with $0.6 < r < 0.9$. The o-suite mostly underestimates surface ozone values in Chinese cities north of 30°N and overestimates south of 30°N.

The validation with IASI satellite data shows that o-suite run is in good agreement with observations with a difference within ±10%. The model run captured well record-low ozone values over the Arctic in March and over Antarctic during September-November 2020 (higher bias up to 20% can be seen in October). The new control run shows relatively good results with bias within 10%, linked to the update of the modelling of stratospheric ozone in 47R1. The overestimation of about 20% can be seen over the southern high latitudes in October and November (Figure S.2) which may be related to the very stable vortex, strong ozone depletion and long duration of the ozone hole season in 2020, which deviates from the climatology in the hybrid linear stratospheric ozone scheme.

The validation with IASOA surface observations shows that the CAMS simulations do not capture ozone depletion events in March – June in 2015 – 2020 at any of the sites. These events are related to halogen chemistry reactions that are not represented in the CAMS simulations. The simulations are on average in good agreement with the observations apart from the spring depletion events.

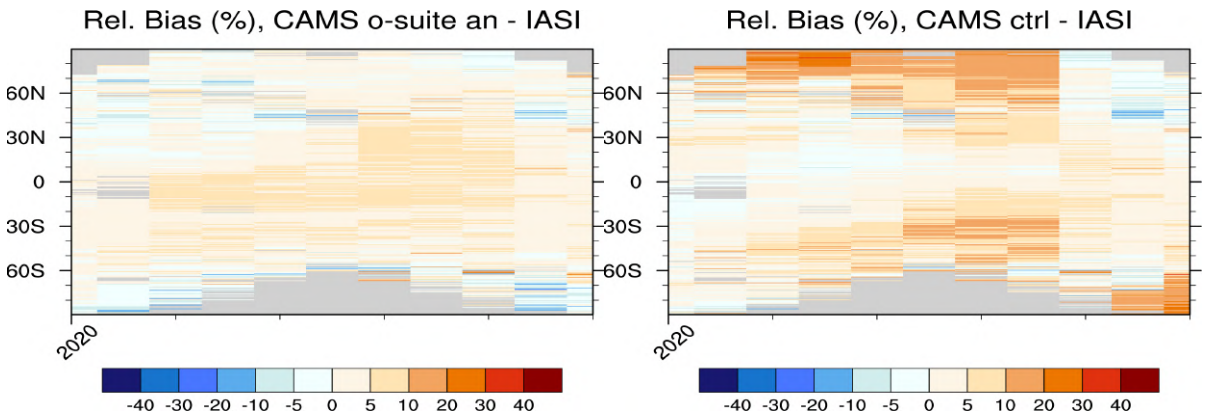

Figure S.2: Relative difference between the model runs and IASI Metop-A O_3 total column as function of latitude and time from January to November 2020: o-suite analysis (left) and control run (right). Grey colour indicates missing values. The upgrade of 6 October results in a clear improvement of stratospheric ozone in the model, as demonstrated by the control run.

Tropospheric Nitrogen dioxide (NO_2)

Model validation with respect to GOME-2/MetOp-A and Sentinel-5P TROPOMI NO_2 data shows that tropospheric NO_2 columns are well reproduced by the NRT model runs, indicating that emission patterns and NO_x photochemistry are generally well represented, although modelled shipping signals are more pronounced than in the satellite retrievals. Tropospheric NO_2 columns over some local emission hotspots (e.g. Moscow, and Red Basin in China) are overestimated, while wintertime and springtime values over Europe around Benelux are underestimated. The long-term development over East-Asia (and Europe) for previous years (Figure S.3), associated with the development of emissions, is not in agreement with the observations. Between spring and autumn, the models regularly show an overestimation over several regions with boreal forest fire activity (Canada, Alaska, Siberia). With respect to months affected by COVID-19 lockdown time periods, the o-suite generally fails to reproduce observed reductions in tropospheric NO_2 for large areas over China and South Asia, but performs better for Europe. We do not see clear evidence of a change in concentrations in the time series during the upgrade to Cy47R1 of 6 October 2020, but the Cy47R1 data record covered by this report is only short (October-November).

With respect to months affected by COVID-19 lockdown time periods, the o-suite generally fails to reproduce observed reductions in tropospheric NO_2 for large areas over China and South Asia, but performs better for Europe.

The comparison with surface observations in megacities in China show significant correlations with $0.3 < r < 0.9$. For stations in the latitudinal belt 30°N-40°N the o-suite strongly overestimates surface NO_2 values with MNMBs varying between 20% and 100%. For the stations south of the 30° N parallel, the o-suite MNMB varies between -50% and +40%. The time series do not show an obvious change in bias during the upgrade to 47R1 on 6 October 2020.

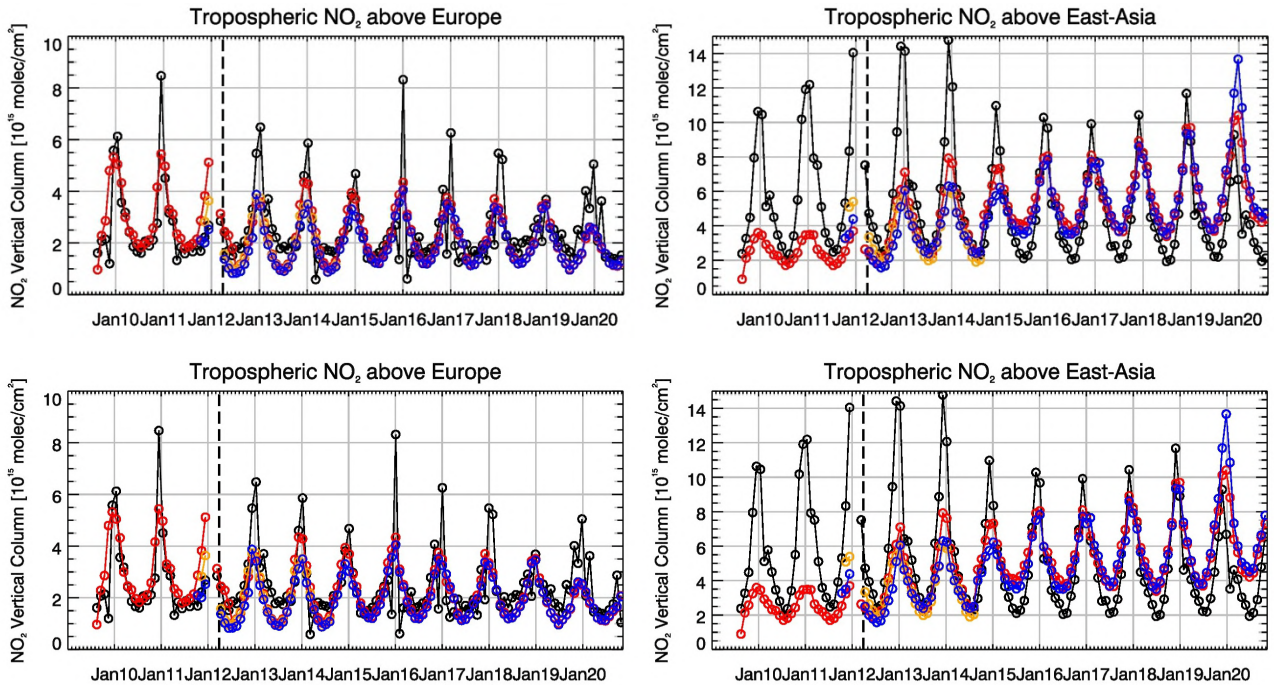

Figure S.3: Time series of tropospheric NO_2 columns from SCIAMACHY (up to March 2012) and GOME-2 (from April 2012 onwards) compared to model results for Europe and East-Asia. Black lines show the observations, red shows the o-suite, blue lines show CAMS control results including older configurations from the MACC projects before September 2014, orange shows the forecast from the MACC project, based on the Mozart-IFS model.

Tropospheric Carbon Monoxide (CO)

Model validation with respect to GAW network surface observations, FTIR observations (NDACC and TCCON) and MOPITT / IASI satellite retrievals reveals that the absolute values, latitude dependence and seasonality, as well as day-to-day variability of CO can be reproduced well by the CAMS-global analyses and forecasts. Compared to GAW stations, the o-suite run is underestimated within 13% for European stations, within 28% for Asian stations and within 14% for stations located in the Southern Hemisphere. The control run shows larger negative biases (up to -28%) for European stations and similar range of biases for Asian stations. The comparisons with EEA AirBase surface observations in Europe shows high temporal correlations, small biases over Spain, Belgium, Germany, Switzerland and the Czech Republic and larger negative biases over Cyprus, Poland and the Estonia (down to -75%).

The model upgrade (60 to 137 levels) implemented in July 2019 changes the overall biases in both the troposphere and stratosphere. The negative bias for the tropospheric columns increased in the most recent quarterly reports to -6% in JJA, -7.5% in MAM, -8.5% in DJF (compared to -2% before July 2019) and is larger than the reported measurement uncertainty. The stratospheric column bias also changed to -8.5% in JJA 2020 and -13% in MAM 2020 compared to values well above +10% before July 2019.

For TCCON data, the o-suite shows a slight underestimation of CO for all available sites except Pasadena. For the control model the underestimation is significantly higher. The comparison with

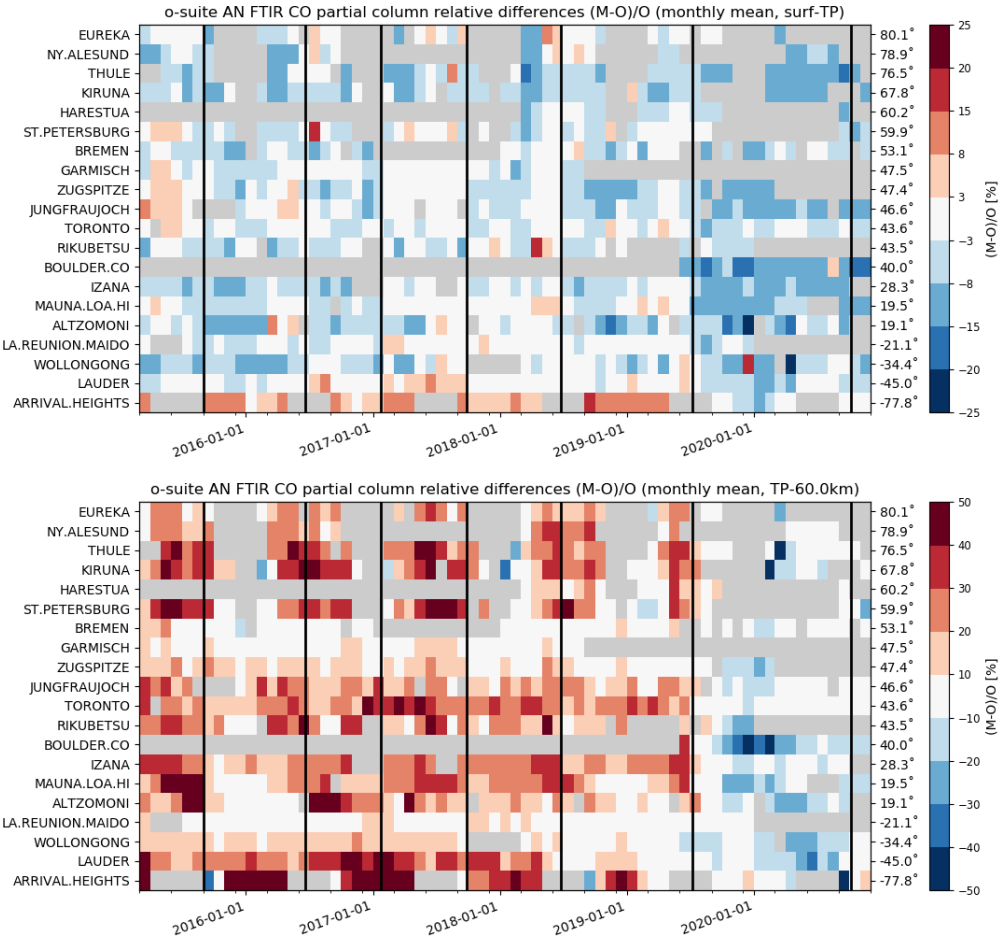

Figure S.4: Monthly-mean bias from 2015 up to the period SON 2020 for tropospheric CO columns (top, mean relative difference in %) and stratospheric CO columns (bottom). The o-suite upgrades are indicated in black vertical lines, stations are sorted by latitude. The overall uncertainty for the CO measurements is approximately 3% on the tropospheric columns and 10% for the stratospheric columns. The o-suite analysis averaged bias in tropospheric columns increased to -6% for SON compared to -2% bias before the model update in July 2019. The bias in the stratosphere reduced to -8.5% compare to +18% before July 2019 and is comparable to the measurement's uncertainty.

the NDACC data is presented on the Figure S.4. The 6 October 2020 upgrade (47R1) shows similar biases to the period before, while the 46R1 configuration shows significantly lower CO in both the troposphere and stratosphere.

Due to the covid-19 crisis the number of flights including the IAGOS instrument package has been very limited, and only a few IAGOS profiles are included in this SON-2020 report.

For the evaluation with MOPITT satellite data in SON, the o-suite run shows relatively good agreement with a negative bias within 10%. The better agreement can be seen over Europe and East and South Asian regions with bias within 5%. For the control run, the strong increase of negative bias in September-October can be seen over Europe, US, Siberian and Alaskan fire regions and over South African region. The evaluation with IASI satellite date, shows underestimation by the o-suite within 20% and by up to 50% by the control run.

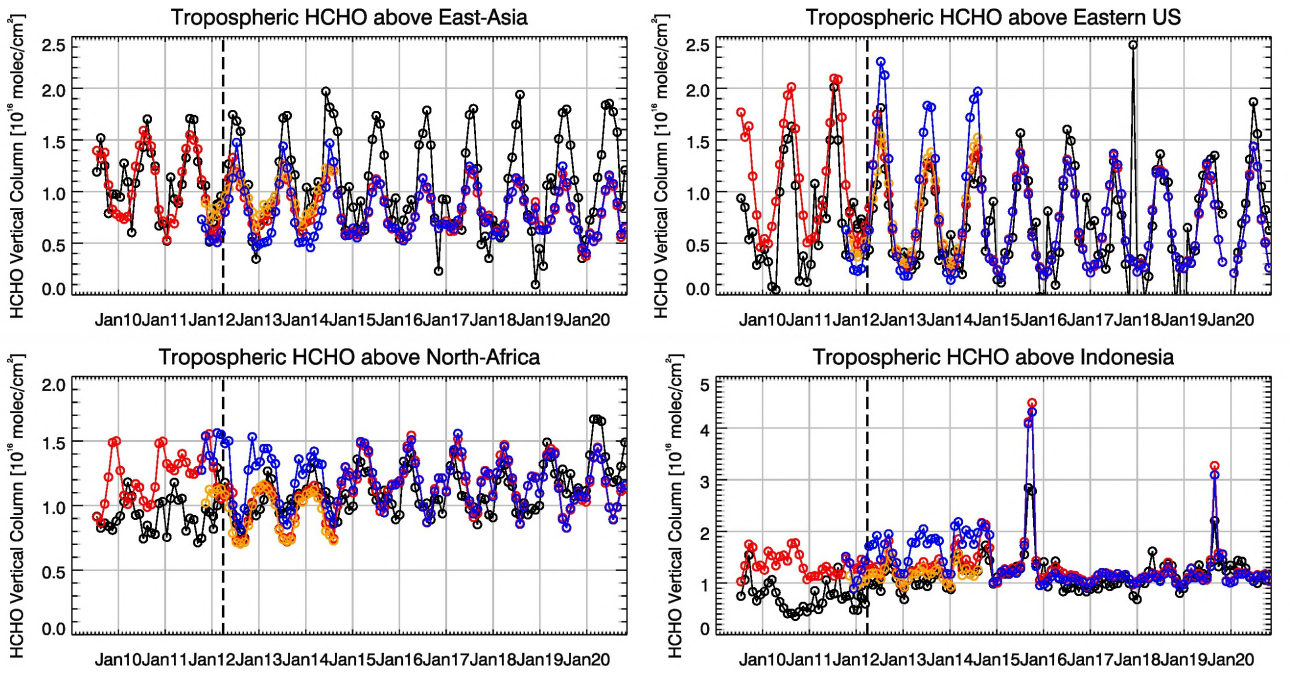

Figure S.5: Time series of average tropospheric HCHO columns [10^{16} molec cm^{-2}] from SCIAMACHY (up to March 2012, black) and GOME-2 (from April 2012 onwards, black) compared to model results (red – o-suite, blue - MACC_fncrt_TM5/MACC_CIFS_TM5/control, orange - MACC_fcnrt_MOZ) for different regions. The blue line shows MACC_fcnrt_TM5 from November 2011 to November 2012, MACC_CIFS_TM5 results from December 2012 to August 2014 and control results from September 2014 onwards (the model run without data assimilation is termed control since Sep 2014). The regions differ from those used for NO_2 to better focus on HCHO hotspots: East-Asia (25-40°N, 110-125°E), Eastern US (30-40°N, 75-90°W), Northern Africa (0-15°N, 15°W-25°E) and Indonesia (5°S-5°N, 100-120°E). Negative satellite retrieved values over Eastern US are due to a lack of data (caused by instrument degradation) during Northern Hemisphere winter months for this region. Vertical dashed black lines mark the change from SCIAMACHY to GOME-2A based comparisons in April 2012.

Formaldehyde

Model validation, with respect to SCIAMACHY/Envisat HCHO data (before April 2012), GOME-2/MetOp-A and Sentinel-5P TROPOMI HCHO data, shows that modelled monthly HCHO columns represent well the magnitude of oceanic and continental background values and the overall spatial distribution in comparison with mean satellite HCHO columns (Fig. S.5). Compared to GOME-2 satellite retrievals, an overestimation of values regularly occurs over Australia and Central Africa, which could be both related to biogenic emissions and fire emissions. For time series over East-Asia and the Eastern US, both regions where HCHO columns are probably dominated by biogenic emissions, models and retrievals agree rather well, but the yearly cycle over East-Asia is underestimated by the models.

The time series do not show evidence of a jump in regional HCHO concentration levels after the Cy47R1 upgrade.

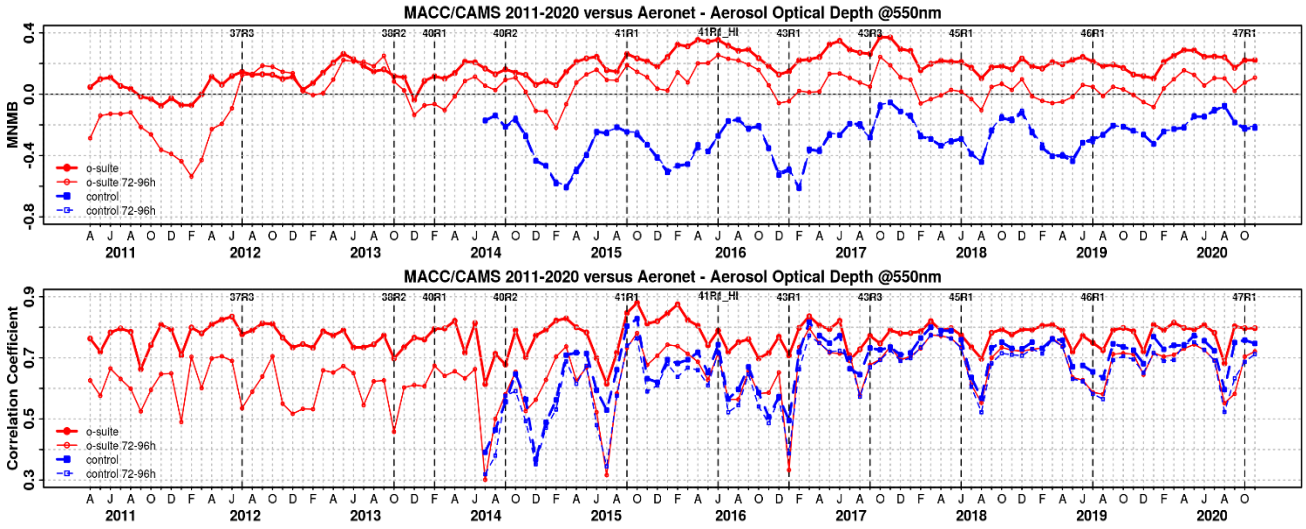

Figure S.6. Aerosol optical depth at 550nm in IFS 00Z model simulations for April 2011 – November 2020 against daily matching Aeronet Version3 level 1.5 data. a) Modified normalized mean bias (MNMB); o-suite (thick red curve); o-suite at last forecast day (light red curve); Control (blue dashed); Control at last forecast day (light blue dashed); b) Corresponding correlation coefficient. Model version changes are marked as vertical bars.

Aerosol

We estimate that the o-suite aerosol optical depth showed an average positive bias in the latest three months of +20%, measured as modified normalized mean bias against daily Aeronet (V3 level 1.5) sun photometer data. The 3-day forecasted aerosol distribution shows 13% less aerosol optical depth (AOD) than that from the initial forecast day, as shown in Fig. S.6-a. Spatiotemporal correlation, shown in Fig. S.6-b, shows month-to-month variation in SON 2020 similar to autumn 2019, indicating the simulation reproduces approximately 46% of the day to day AOD variability across all Aeronet stations. The o-suite forecast at +3 days shows slightly lower correlation, as a consequence of imperfect forecasted meteorology and fading impact of the initial assimilation of MODIS AOD and MODIS fire info on model performance. The o-suite forecast running each day at 12UTC shows almost identical performance as the forecast starting at 00UTC.

The AOD performance of the o-suite with respect to the AERONET data exhibits no pronounced seasonal cycle but somewhat less correlation in late summer. Since the latest upgrade in October 2020, the largest contributions to global AOD come from organics, sulphate and sea salt, dust decreased globally. All species AOD decreased due to the model upgrade in July 2019 with nitrate now contributing to AOD.

The aerosol Ångström exponent (AE) contains information about the size distribution of the aerosol, and implicitly about composition. The o-suite AE became more positive indicating a change to slightly more fine particles since the model upgrade to version 47R1 in October 2020, along with a decrease in correlation. MNMB Bias in AE increased from unbiased before to +25% in October/November. The change is probably linked to a change in the seasalt parameterisation with smaller particles coming from the marine source.

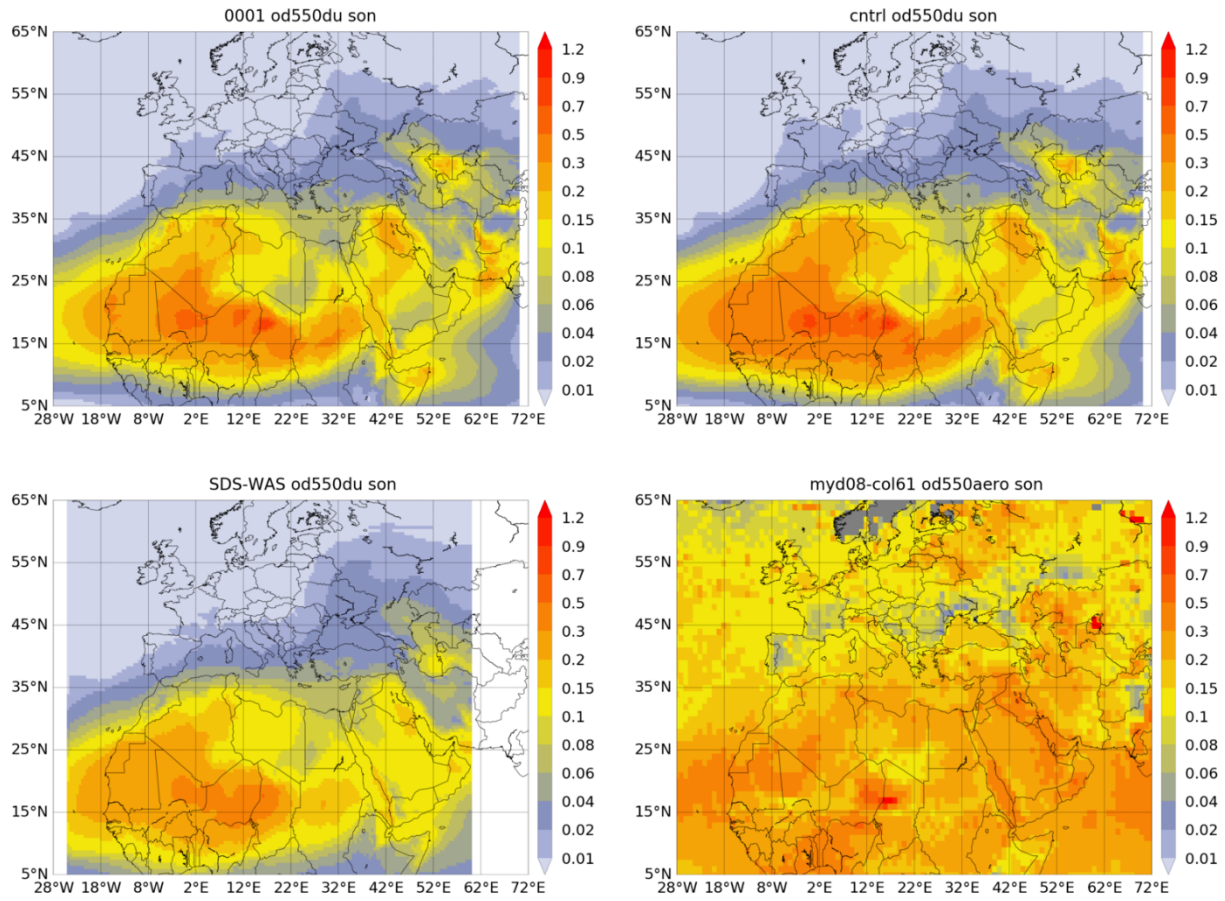

Figure S.7: Averaged DOD 24h forecast from o-suite (top left) and control (top right), DOD of the multi-model SDS-WAS Median product (bottom left) as well as AOD from MODIS/Aqua Collection 6.1 Level 3 combined Dark Target and Deep Blue product (bottom right) for the study period.

PM10 and PM2.5, as defined by the IFS aerosol model, are evaluated against NRT data globally and a climatology. NRT data for 2020 suggest on average for North America, Europe and China a PM10 MNMB bias of -5%, +13%, -2% respectively and for PM2.5 a MNMB bias of +14%, -3% and +13% respectively. Local variations of the bias are large.

The IFS climatology represents an average from rural and background site data in the period 2000-2009 at 160 sites in North America and Europe. Note that observed PM levels from that period where higher than today. Apart from that the findings are consistent with the NRT bias mentioned above. Against a climatology IFS PM10 concentrations exhibit on average in the latest period an underestimation with MNMB bias of -33% in Europe and a slight overestimation of 2% in North America. PM25 concentrations are underestimated with -40% in Europe and overestimated with 21% in North America. The fraction of PM simulated data within a factor 2 of observed values stayed similar since September 2017 for both PM10 and PM2.5. PM2.5 seems to have deteriorated compared to periods before mid-2017, while PM10 shows an improvement. However with the model version upgrade in July 2019 the PM2.5 has improved significantly, and both PM2.5 and PM10 have a more clear seasonal variation. The time series for the October 2020 upgrade (Cy47R1) is too short to draw conclusions.

Anthropogenic black carbon and organic aerosol (OA) emissions were found to be shifted by 180 degrees in longitude since January 2020, corrected with the upgrade in October 2020. This resulted in erroneous, shifted black carbon fields. OA results are less affected, since secondary aerosol formation and biomass burning sources are more important for OA fields. PM and total optical depth were not impacted to a large extent.

During this season, satellites (see MODIS in Figure S.7) show that significant dust activity in Northern Africa (seasonal AOD above 0.5) is concentrated in latitudes between 15 and 25ºN with maximum seasonal AOD values over 0.7 in Mali and Chad. Meanwhile, in the Middle East, high AOD values up to 0.5 are observed in Iraq. Overall, the o-suite shows lower season AOD values than the control run, as observed in previous season which are in general higher than the SDS-WAS multi-median product particularly in Iraq and Eastern Sahara as well as in regions around the Caspian Sea and the Afghanistan/Pakistan border. Both CAMS runs reproduce high DOD dust activity in the region of Mali, Mauritania, and Algeria, but overestimate them in Iraq, Eastern Sahara, the Caspian Sea and the Afghanistan /Pakistan border in comparison with MODIS. Seasonal DOD over Central Saudi Arabia, Iran and Afghanistan /Pakistan border appears overestimated in comparison with MODIS and the SDS-WAS multi-model ensemble (see Figure S.7). However, both CAMS runs can reproduce the dust transport over the North Atlantic region. On 6th October 2020, there was an upgrade of the CAMS model (to Cy47R1) that affected the desert dust module. This upgrade revised the desert dust source mapping and dust emissions. From this date, dust emissions are lower in comparison with the previous model version as seen in the AERONET comparison at sites in desert dust regions. From September to November, the o-suite (control) reproduces the daily variability of AERONET dust-filtered observations, with a correlation coefficient of 0.70 (0.70) averaged over all AERONET sites, which is lower than the SDS-WAS multi-model product which has a correlation coefficient of 0.82. Regarding mean bias (MB), the o-suite tends to slightly underestimate the AERONET observations with an MB of -0.01 while the control slightly overestimates them (MB of 0.01). and the SDS-WAS multi-model underestimates the AERONET observations (MB of -0.01).

The vertical profiles of backscatter are evaluated for 21 ceilometer stations evenly distributed over Germany. After changes in the model upgrade of July 2019 (Cy46R1) a notable lower positive bias of the model backscatter combined with higher correlations then before are observed. The step at the top of the PBL is captured notably better with 137 levels than with 60 levels (51L instead of 27L <8 km altitude), same for o-suite and control. The amplitude of the model vertical profile is now very close the observation (reference), with a larger bias of the model backscatter during summer in comparison to fall 2020. A bias remains, but depends on the weather situation. The amplitude of the model vertical profile is close to the observation. Concluding, the 3-hourly averages of Pearson's correlation coefficients show a better clustering of the data, also hinting to more consistent results with outliers lowering the overall standard deviation (r= 0.1-0.7). The Cy47R1 time series is too short for a quantitative evaluation of the upgrade, but in October and November 2020 the median profiles show a very good match with the ceilometers.

System performance in the Arctic

The CAMS runs are validated using surface ozone measurements from the ESRL-GMD and the IASOA networks (5 sites) and ozone concentrations in the free troposphere, UTLS and the stratosphere are evaluated using balloon sonde measurement data.

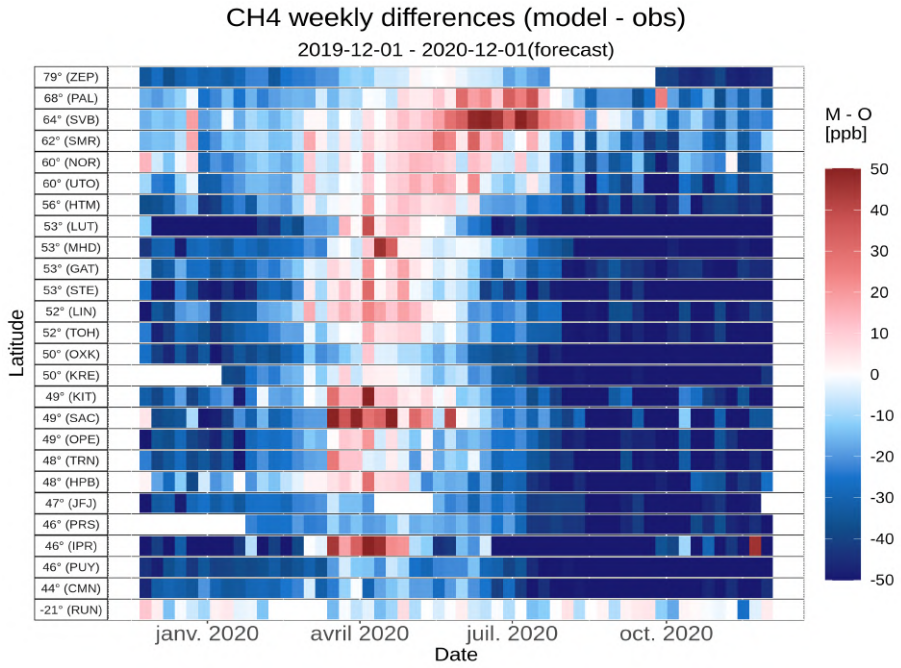

Figure S.8: Mosaic plot of CH_4 biases (in ppb) of the CAMS analysis, compared to surface station observations. Each vertical coloured line represents a weekly mean.

For the period from September to November 2020, the simulations of the surface ozone concentrations are on average in fair agreement with the observations (MNMB = -5% – 16%). There is no indication of a change in performance during the upgrade to Cy47R1.

During September– November 2020 there is an overestimation of the ozone concentrations in the Arctic free troposphere and UTLS (MNMB up to 20%), while it is well described in the stratosphere with low bias.

Comparison with FTIR observations from the NDACC network shows that the CO tropospheric columns are underestimated at Thule with bias of -14% for the o-suite with larger bias for the control run (-20), while the bias for the stratospheric column is lower with bias of -6% (o-suite) and 6% (control).

System performance in the Mediterranean

During autumn, both CAMS runs do reproduce the daily variability of AERONET AOD observations, although present general overestimation in the whole Mediterranean Basin. The correlation coefficient decreases from (0.20, 0.53 and 0.41) for control to (0.14, 0.43 and 0.32) and MB slightly increases from (0.08, 0.10 and 0.12) for control to (0.12, 0.14 and 0.15) for o-suite respectively for Western, Central and Eastern Mediterranean. Overestimations are linked to an enhanced background aerosols that are not directly linked to natural contributions.

At surface levels, both CAMS runs show a higher correlation coefficient in Northwestern Europe (above 0.7) in comparison with the 3-hourly EEA PM10 and PM2.5 observations. For PM10, both CAMS runs show underestimations (MB under -4 $\mu g/m^3$) except in Central Europe and Eastern

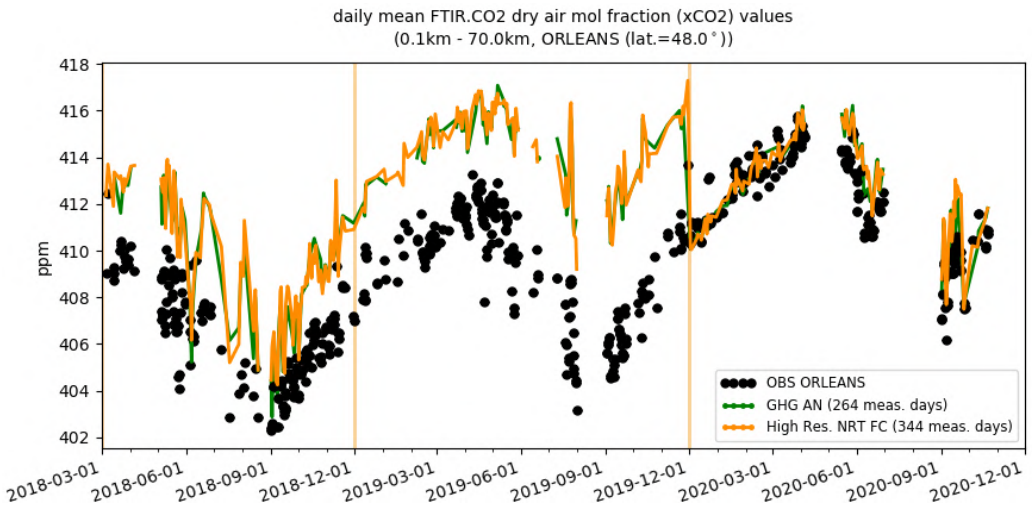

Figure S.9: Comparison of the CO_2 CAMS configurations with TCCON CO_2 at Orleans.

Iberian Peninsula which appear overestimated (MB above 4 µg/m^3). Despite the PM2.5 comparison shows lower difference, the overestimations observed in PM10 o-suite in Central Europe are also detected in the PM2.5 o-suite comparison (MB above 4 µg/m^3).

During September, both CAMS runs predict peaks above 50 µg/m^3 for PM10 (see Figure 8.4.5) that in most of the cases overestimated the EEA observations. This tendency changes with the model upgrade to CY47R1 on 6 October. This change has a clear signal in the surface concentrations, reducing the PM10 and PM2.5 levels. PM10 levels are reduced more than 60% at some sites. This reduces the number of predicted PM10 daily exceedances. Coarse aerosol contributions (coming from desert dust and sea-salt contributions) were predicted in Southern Europe during this season as it is indicated the low observed PM2.5/PM10 ratio (which indicated the dominance of coarse particles).

The model is compared to surface O_3 observations from the AirBase network. Our analysis shows that model MNMBs vary between -15% and 35% depending on the station. Temporal correlation coefficients between simulated and observed surface ozone for both the o-suite and control runs are highly significant over the entire Mediterranean from Gibraltar to Cyprus.

Climate forcing

Greenhouse gases

CO_2 and CH_4 surface concentrations from ICOS network, and total or partial columns from TCCON and NDACC stations have been used to validate the analysis and high-resolution forecast experiments.

Since the new experiments started in December 2019 both ICOS (surface) and TCCON (total columns) observations showed CH_4 negative biases ranging from -10 to -50 ppb (Fig. S.8). The bias turns positive at most ICOS sites in North hemisphere between April and July depending on the latitude, and is also decreased in June for North hemisphere TCCON sites. NDACC partial columns indicate also negative biases in the troposphere, but slight positive biases in the stratosphere.

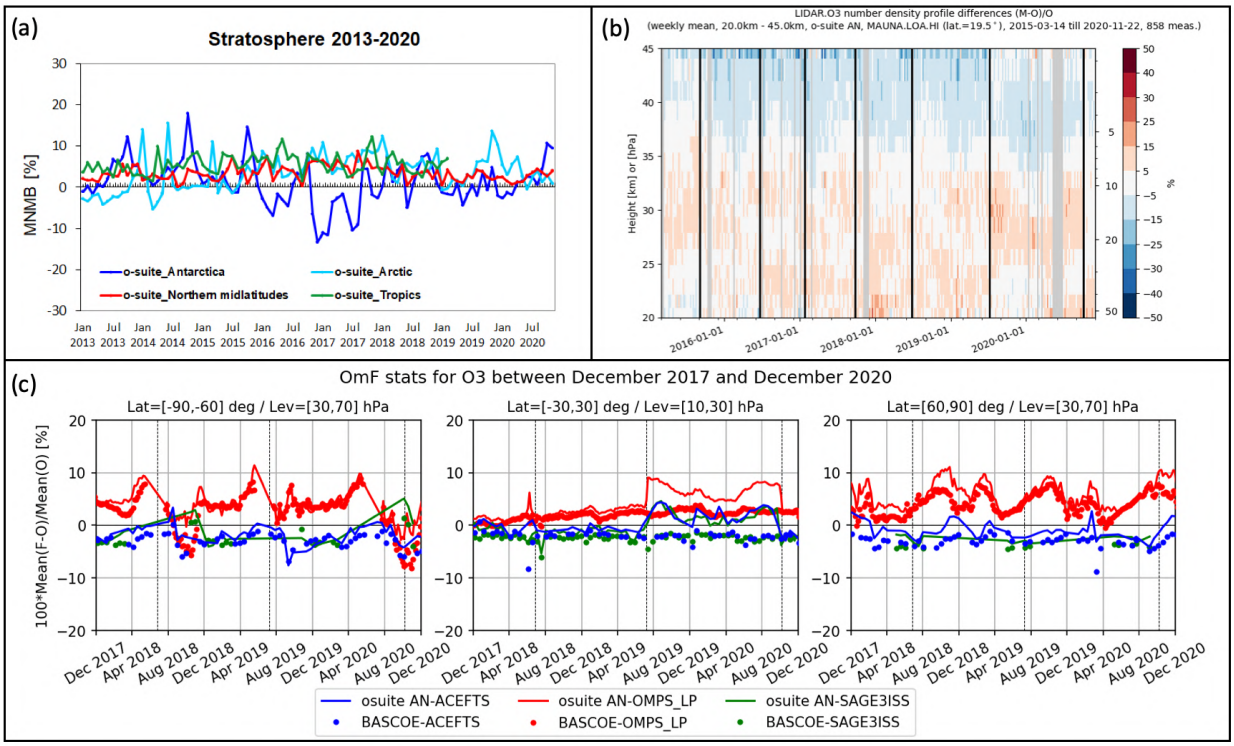

Figure S.10. (a): MNMBs (%) of ozone in the stratosphere from the o-suite against aggregated ozonesonde data in the Arctic (light blue), Antarctic (dark blue) northern midlatitudes (red) and tropics (green) from 2013 to November 2020.The stratosphere is defined as the altitude region between 60 and 10 hPa in the tropics and between 90 and 10 hPa elsewhere. (b): Comparison of the weekly mean profile bias between the O_3 mixing ratios of the 1-d forecast and the NDACC LIDAR at Mauna Loa. (c): Time series comparing model runs to observations for the period 2017-12-01 to 2020-11-30 in three latitude bands and three pressure layers (left: 90°S-60°S between 30 and 70 hPa, centre: 30°S-30°N S between 10 and 30 hPa and right: 60°N-90°N between 30 and 70 hPa) for the o-suite analyses (solid lines) and BASCOE (dotted lines) against observations from OMPS-LP v2.5 (red), ACE-FTS v3.6 (blue) and SAGE-III v5.1 (green). Shown is the normalized mean bias (model-obs)/obs (%).

For CO_2 both surface measurements and total column shows biases generally within ±1%, with a maximum in late spring or summer at the surface, and later (September) for the TCCON sites (Fig. S.9). Higher biases are observed in autumn 2020, when the CAMS experiments fail to reproduce the high CO_2 enhancements observed for several days especially in Northern Europe.

Ozone layer and UV

Ozone partial columns and vertical profiles

The SON 2020 period was marked by two noticeable facts. The first one was the exceptionally deep ozone hole that happened above Antarctica. The second one was the implementation of the new CY47r1 o-suite on October 6, 2020. Stratospheric ozone from the CAMS o-suite seems not to have been affected by the first fact where the agreement with independent observations was similar to previous years (see the time series against ACE-FTS in Fig. S.10.c for the South Pole region). The second fact, on the other hand, allowed an improvement in the agreement with independent

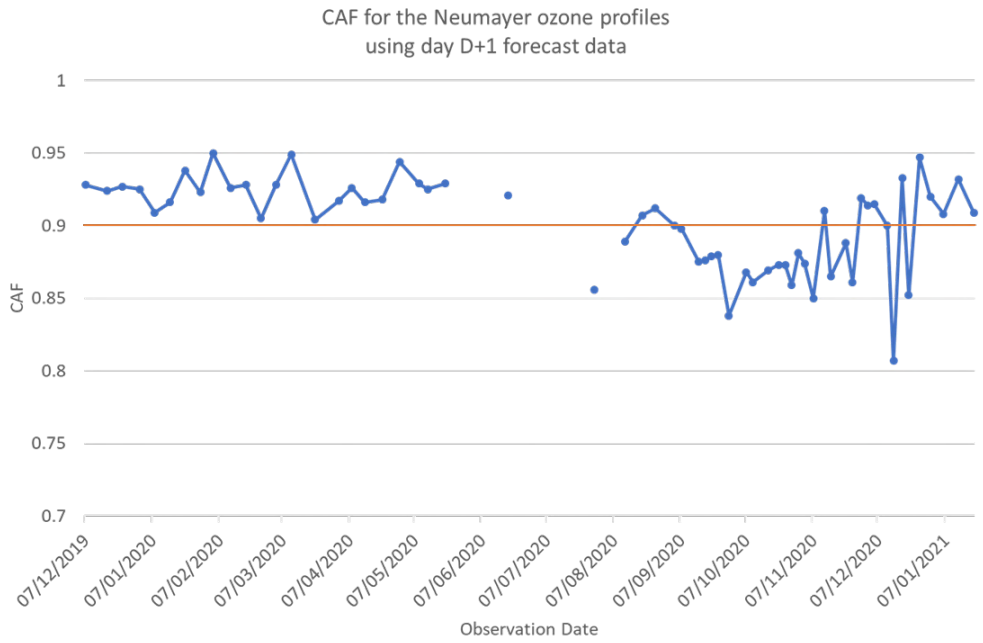

Figure S.11. Time series of the CAF values calculated between CAMS model 1-day forecast data and balloon O_3 sonde measurements at Neumayer station in Antarctica. The orange line corresponds to the KPI target minimum value of 0.9.

observations in the tropical region (see the discontinuity in the time series against lidar observations above Mauna Loa site in Fig. S.10.b and independent satellite profiles in the tropics in Fig. S.10.c).

Detailed comparisons between CAMS stratospheric ozone and independent observations include observations from ozonesonde profiles, ground-based instruments from NDACC (Network for the Detection of Atmospheric Composition Change, http://www.ndacc.org) and vertical profiles from 3 satellite instruments (OMPS-LP, ACE-FTS and SAGE-III). Furthermore, o-suite analyses are also compared with the analyses delivered by the independent BASCOE assimilated analyses.

In summary, the o-suite O_3 partial pressures are slightly overestimated in all latitude bands (MNMBs between -0.5 to 4.3% for SON 2020). Comparisons with the NDACC observations show a generally good agreement, with small performance differences between the analysis and the 1-day forecasts. The comparison with independent satellite profiles is generally in good agreement for the considered period, usually within 10%.

Other stratospheric trace gases

Due to the lack of stratospheric chemistry in the C-IFS-CB05 scheme, the only useful product in the stratosphere is ozone. Stratospheric NO_2 has been evaluated, confirming that this product is not yet mature.

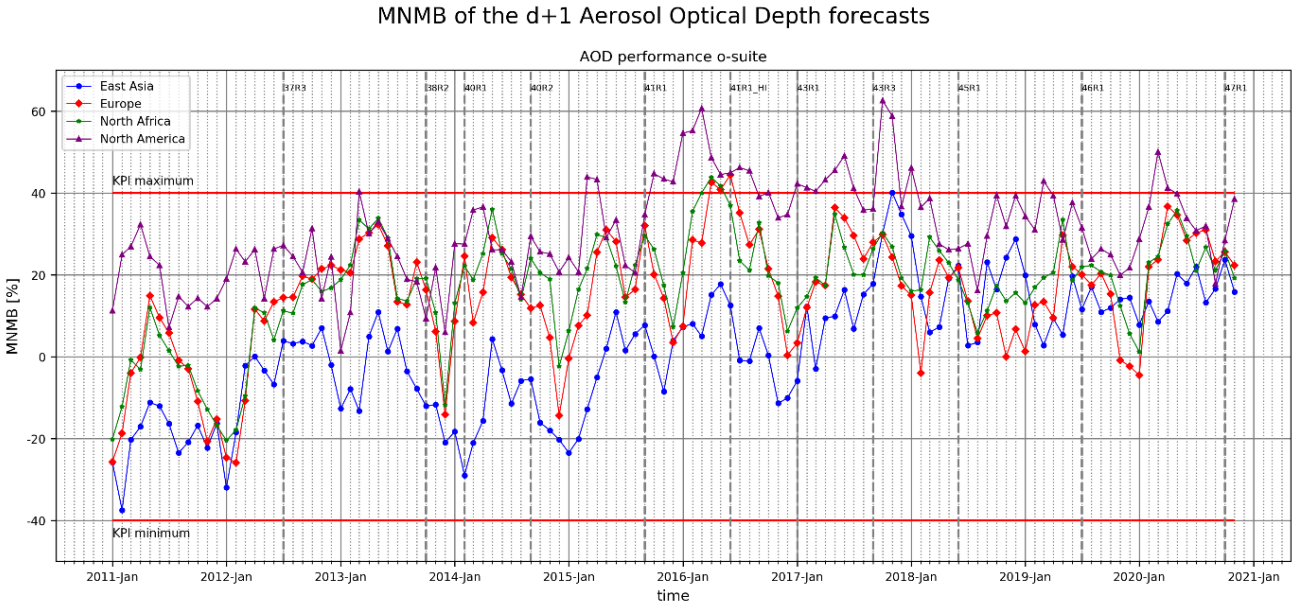

Figure S.12. Modified Normalized Mean Bias (MNMB) for the d+1 Aerosol Optical Depth (AOD) at four main regions, based on observations from AERONET stations. The horizontal red lines show allowed minimum and maximum values for this KPI. The vertical dashed lines correspond to the dates when new CAMS o-suite upgrades became operational.

Events

Dust event in November 2020 in Europe: In early-November 2020, MODIS satellite detected an intense dust outbreak that reached the Iberian Peninsula and northern Europe. The comparison with MODIS shows that the o-suite reproduces the spatial and temporal distribution of the observed AOD plume with the origin of the plume over Algeria and following an arc that was crossing Spain, France, United Kingdom, and Germany. PM10 values are slightly overestimated compared to surface observations.

Key performance indicators for the CAMS o-suite

Two statistical measures with chosen threshold values, plus a production requirement were introduced as Key Performance Indicators (KPIs) for the CAMS global o-suite.

The CAMS production KPI is defined as the percentage of cycles in which all the general data dissemination tasks are completed before the deadlines: 10 UTC for the 00:00 and 22 UTC for the 12:00 UTC run. The o-suite data delivery for the reporting period September, October and November 2020 was excellent, with an on-time percentage of 100%.

The ozone profile Common Area Fraction (CAF) is a measure of the level of agreement between the CAMS ozone profile and corresponding measurements from balloon sondes. For the KPI these are evaluated for the observations at the Neumayer station in Antarctica. Here a CAF value of 1 indicates a perfect match between the measured and forecasted profiles. For the KPI a challenging target minimum value of 0.9 is chosen. Values of CAF for collocated measured and modelled ozone profiles for the period from end of 2019 to beginning of 2021 are shown in Fig. S.11. The gaps in the

middle of the time series correspond to cases where the balloon did not reach the 30 hPa level, which is the minimum height required for a meaningful comparison.

The CAMS o-suite fulfills the ozone CAF predefined requirement mainly at the first half and at the end of the examined period. In the period September-December 2020, CAF values generally lie somewhat below the 0.9 value threshold. This corresponds to local ozone hole conditions, which are accompanied by strong gradients in the ozone profile, posing an additional challenge for the analysis.

The Modified Normalized Mean Bias of the Aerosol Optical Depth (MNMB AOD) is an indicator of the agreement (in terms of statistical bias) between the o-suite 1-day forecast AOD of CAMS and corresponding estimations from AERONET stations. Values are reported separately for East Asia, Europe, North Africa and North America. The KPI target is for MNMB AOD values to lie within the range ±40%. Results, reported on a monthly basis, are shown in Fig. S.12. The time series begins in 2011, allowing for all model versions since then to be evaluated (vertical dashed lines in the figure correspond to commencement of successive model versions). Overall, the results lie within the KPI limits, with the exception of some cases in North America in the middle of the time series. In the second half of the time series, results from the four regions converge to positive values, but below the KPI limit.

Table of Contents

1. Introduction

The Copernicus Atmosphere Monitoring Service (CAMS, http://atmosphere.copernicus.eu/) is a component of the European Earth Observation programme Copernicus. The CAMS global near-real time (NRT) service provides daily analyses and forecasts of trace gas and aerosol concentrations. The CAMS near-real time services consist of daily analysis and forecasts with the ECMWF IFS system with data assimilation of trace gas concentrations and aerosol properties. This document presents the system evolution and the validation statistics of the CAMS NRT global atmospheric composition analyses and forecasts. The validation methodology and measurement datasets are discussed in Eskes et al. (2015).

In this report the performance of the system is assessed in two ways: both the longer-term mean performance (seasonality) as well as its ability to capture recent events are documented. Table 1.1 provides an overview of the trace gas species and aerosol aspects discussed in this CAMS near-real time validation report. This document is updated every 3 months to report the recent status of the near-real time service. The report covers results for a period of at least one year to document the seasonality of the biases. Sometimes reference is made to other model versions or the reanalysis to highlight aspects of the near-real time products.

This validation report is accompanied by the "Observations characterization and validation methods" report, Eskes et al. (2019), which describes the observations used in the comparisons, and the validation methodology. This report can also be found on the global validation page, http://atmosphere.copernicus.eu/user-support/validation/verification-global-services.

Key CAMS NRT products and their users are: Boundary conditions for regional air quality models (e.g. AQMEII, air quality models not participating in CAMS); Long range transport of air pollution (e.g. LRTAP); Stratospheric ozone column and UV (e.g. WMO, DWD); 3D ozone fields (e.g. SPARC). As outlined in the MACC-II Atmospheric Service Validation Protocol (2013) and MACC O-INT document (2011), relevant user requirements are quick looks of validation scores, and quality flags and uncertainty information along with the actual data. This is further stimulated by QA4EO (Quality Assurance Framework for Earth Observation, http://www.qa4eo.org) who write that “all earth observation data and derived products is associated with it a documented and fully traceable quality indicator (QI)”. It is our long-term aim to provide such background information. The user is seen as the driver for any specific quality requirements and should assess if any supplied information, as characterised by its associated QI, are "fit for purpose" (QA4EO task team, 2010).

CAMS data are made available to users as data products (grib or netcdf files) and graphical products, accessible through the Atmosphere Data Store on http://atmosphere.copernicus.eu/data.

A summary of the system and its recent changes is given in section 2. Subsequent sections give an overview of the performance of the system for various species, and during recent events. Routine validation results can be found online via regularly updated verification pages, http://atmosphere.copernicus.eu/user-support/validation/verification-global-services.
Table 1.2 lists all specific validation websites that can also be found through this link.

Table 1.1: Overview of the trace gas species and aerosol aspects discussed in this CAMS near-real time validation report. Shown are the datasets assimilated in the Cy47R1 CAMS analysis (second column) and the datasets used for validation, as shown in this report (third column). Green colours indicate that substantial data is available to either constrain the species in the analysis, or substantial data is available to assess the quality of the analysis. Yellow boxes indicate that measurements are available, but that the impact on the analysis is not very strong or indirect (second column), or that only certain aspects are validated (third column).

Species, vertical range	Assimilation	Validation
Aerosol, optical properties	MODIS Aqua/Terra AOD PMAp AOD	AOD, Ångström: AERONET, GAW, Skynet, MISR, OMI, lidar, ceilometer
Aerosol mass (PM10, PM2.5)	MODIS Aqua/Terra	European AirBase stations
O_3, stratosphere	MLS, GOME-2, OMI, OMPS, TROPOMI	Sonde, lidar, MWR, FTIR, OMPS, ACE-FTS, SAGE3-ISS and BASCOE analyses
O_3, UT/LS	MLS	IAGOS, ozone sonde
O_3, free troposphere	Indirectly constrained by limb and nadir sounders	IAGOS, ozone sonde, IASI
O_3, PBL / surface		Surface ozone: WMO/GAW, NOAA/ESRL-GMD, AIRBASE
CO, UT/LS	IASI, MOPITT	IAGOS
CO, free troposphere	IASI, MOPITT	IAGOS, MOPITT, IASI, TCCON
CO, PBL / surface	IASI, MOPITT	Surface CO: WMO/GAW, NOAA/ESRL
NO_2, troposphere	OMI, GOME-2, partially constrained due to short lifetime	TROPOMI, SCIAMACHY, GOME-2, MAX-DOAS
HCHO		TROPOMI, GOME-2, MAX-DOAS
SO_2	GOME-2, TROPOMI (Volcanic eruptions)	
Stratosphere, other than O_3		NO_2 column only: SCIAMACHY, GOME-2
CO_2, surface, PBL		ICOS
CO_2, column	GOSAT	TCCON
CH_4, surface, PBL		ICOS
CH_4, column	GOSAT, IASI	TCCON

Table 1.2: Overview of quick-look validation websites of the CAMS system.

The CAMS global evaluation server
https://global-evaluation.atmosphere.copernicus.eu
Reactive gases – Troposphere
IAGOS tropospheric ozone and carbon monoxide: http://www.iagos.fr/cams/ Surface ozone from EMEP (Europe) and NOAA-ESRL (USA): http://www.academyofathens.gr/cams Tropospheric nitrogen dioxide and formaldehyde columns against satellite retrievals: http://www.doas-bremen.de/macc/macc_veri_iup_home.html Tropospheric CO columns against satellite retrievals: http://www.mpimet-cams.de GAW surface ozone and carbon monoxide: https://atmosphere.copernicus.eu/charts/cams_gaw_ver/v0d_gaw_oper_operfc_nrt_sites?facets=undefined&time=2018060100,0,2018060100&fieldpair=CO&site=cmn644n00
Reactive gases - Stratosphere
Stratospheric composition: http://www.copernicus-stratosphere.eu NDACC evaluation in stratosphere and troposphere (the NORS server) http://nors-server.aeronomie.be
Aerosol
Evaluation against Aeronet stations: http://aerocom.met.no/cams-aerocom-evaluation/ More in-depth evaluations are available from the Aerocom website. WMO Sand and Dust Storm Warning Advisory and Assessment System (SDS-WAS) model intercomparison and evaluation: http://sds-was.aemet.es/forecast-products/models Aeronet verification of CAMS NRT forecasts: https://atmosphere.copernicus.eu/charts/cams_aeronet_ver/?facets=undefined&time=2019020100,0,2019020100&site=ARM_Graciosa
Satellite data monitoring
Monitoring of satellite data usage in the Near-Real-Time production: https://atmosphere.copernicus.eu/charts/cams/cams_satmon?facets=undefined&time=2016071800&Parameter=AURA_MLS_profile_Ozone_1_GLOBE

The CAMS global evaluation server, https://global-evaluation.atmosphere.copernicus.eu, became available in Summer 2019. This server combines many of the individual verification results shown on the other CAMS web pages listed in Table 1.2, and presents the comparisons through a uniform interface.

Naming and color-coding conventions in this report follow the scheme as given in Table 1.3.

Table 1.3. Naming and colour conventions as adopted in this report.

Name in figs	experiment	Colour
{obs name}	{obs}	black
o-suite D+0 FC	0001	red
control	gsyg	blue
GHG high-resolution run	gqpe / ghqy	orange
GHG global analysis	gqiq	green

2. System summary and model background information

The specifics of the different CAMS model versions are given below (section 2.1) including an overview of model changes. Other systems used in CAMS are listed in section 2.2. An overview of products derived from this system is given in section 2.3. Timeliness and availability of the CAMS products is given in section 2.4.

2.1 System based on the ECMWF IFS model (the o-suite and control run)

Key model information is given on the CAMS data-assimilation and forecast run o-suite and its control experiment, used to assess the performance of the assimilation. The forecast products are listed in Table 2.1. Table 2.2 provides information on the satellite data used in the o-suite. Further details on the different model runs and their data usage can be found at http://atmosphere.copernicus.eu/documentation-global-systems.

Table 2.1: Overview of model runs assessed in this validation report.

Forecast system	Exp. ID	Brief description	Upgrades (e-suite ID)	Cycle
O-suite	0001	Operational CAMS DA/FC run	20201006-present 20190709-20201006 20180626-20190708 20170926-20180625 20170124-20170926 20160621-20170124 20150903-20160620 20140918-20150902	47R1 46R1 45R1 43R3 43R1 41R1 41R1 40R2
Control	hdir h7c4 gzhy gsyg gnhb gjjh geuh g4o2	control FC run without DA	20201006-present 20190709-20201006 20180626-20190708 20170926-20180625 20170124-20170926 20160621-20170124 20150901-20160620 20140701-20150902	47R1 46R1 45R1 43R3 43R1 41R1 41R1 40R2
GHG run	hd7v	Tco399L137 NRT CO_2, CH_4 analyses (~25km)	20201101-present	47R1
	he9h	High resolution Tco1279 (~9km) NRT CO_2, CH_4 forecast	20201101-present	47R1
	h72g	Tco399L137 NRT analyses	20191201-20201031	46R1
	h9sp	Tco1279 forecast	20191201-20201031	46R1
	gwx3 gqiq	GHG analysis Tco399 (~25km)	20181201-20191130 20170101-20181130	45R1 43R1
	gznv gqpe	High resolution Tco1279 (~9km) NRT CO_2, CH_4 forecast	20181201-20191130 20170101-20181130	45R1 43R1
	ghqy gf39	High resolution T1279, NRT CO_2 and CH_4 without DA	20160301-20170621 20150101-20160229	

Table 2.2: Satellite retrievals of reactive gases and aerosol optical depth that are actively assimilated in the o-suite in Cy47R1.

Instrument	Satellite	Provider	Version	Type	Status
MLS	AURA	NASA	V4	O3 Profiles	20130107 -
OMI	AURA	NASA	V883	O3 Total column	20090901 -
GOME-2	Metop-A	Eumetsat	GDP 4.8	O3 Total column	20131007 - 20181231
GOME-2	Metop-B	Eumetsat	GDP 4.8	O3 Total column	20140512 -
GOME-2	Metop-C	Eumetsat	GDP 4.9	O3 Total column	20200505 -
SBUV-2	NOAA-19	NOAA	V8	O3 21 layer profiles	20121007 - 20201005
OMPS	Suomi-NPP	NOAA / EUMETSAT		O3 13-layer profiles	20170124 – 20190409 20201006-
OMPS	NOAA-20	NOAA / EUMETSAT		O3 13 layer profiles	20201006-20201215
TROPOMI	Sentinel-5P	ESA		O3 column	20181204-
IASI	MetOp-A	LATMOS/ULB Eumetsat	-	CO Total column	20090901 - 20180621 20180622 - 20191118
IASI	MetOp-B	LATMOS/ULB Eumetsat	-	CO Total column	20140918 - 20180621 20180622 -
IASI	MetOp-C	Eumetsat		CO total column	20191119 -
MOPITT	TERRA	NCAR	V5-TIR V7-TIR V7-TIR Lance V8-TIR	CO Total column	20130129 - 20160124 - 20180626 20180626 20190702
OMI	AURA	KNMI	DOMINO V2.0	NO2 Tropospheric column	20120705 -
GOME-2	MetOp-A	Eumetsat	GDP 4.8	NO2 Tropospheric column	20180626 - 20200504
GOME-2	MetOp-B	Eumetsat	GDP 4.8	NO2 Tropospheric column	20180626 -
GOME-2	MetOp-C	Eumetsat	GDP 4.9	NO2 Tropospheric column	20200505-
GOME-2	MetOp-A	Eumetsat	GDP 4.8	SO2 Total column	20150902 -
GOME-2	MetOp-B	Eumetsat	GDP 4.8	SO2 Total column	20150902-20200414
GOME-2	MetOp-C	Eumetsat	GDP 4.9	SO2 Total column	20200505-
MODIS	AQUA / TERRA	NASA	Col. 5 Deep Blue Col. 6, 6.1	Aerosol total optical depth, fire radiative power	20090901 - 20150902 - 20170124 -
PMAp	METOP-A METOP-B	EUMETSAT		AOD	20170124 - 20170926 -

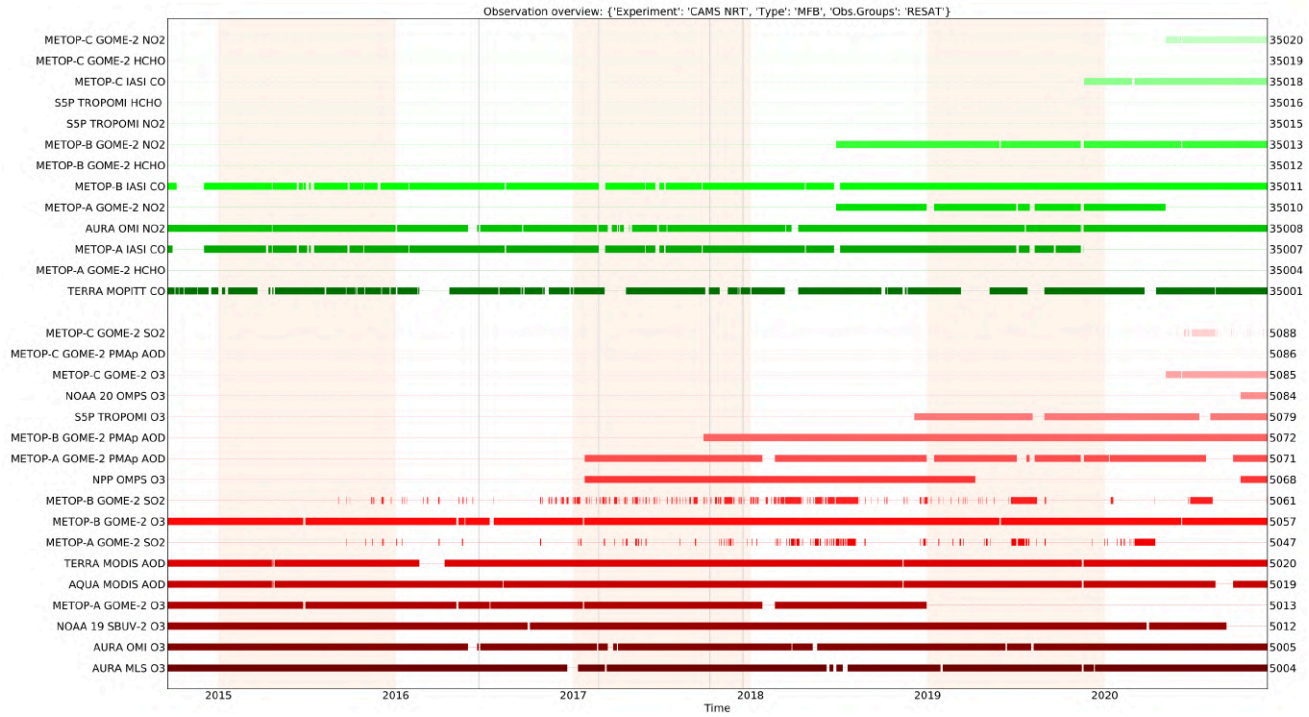

Figure 2.1: Satellite observation usage in the real-time analysis, for ozone, CO, aerosol AOD and NO2, from October 2014 onwards. Top rows (in green): products assimilated using averaging kernels. Sentinel-5P TROPOMI ozone is assimilated since Dec. 2018 and other products from TROPOMI are monitored.

2.1.1 The CAMS o-suite

The o-suite consists of the IFS-CB05 chemistry combined with the CAMS bulk aerosol model. The chemistry is described in Flemming et al. (2015) and Flemming et al. (2017), aerosol is described in Morcrette et al. (2009). The forecast length is 120 h. The o-suite data is stored under **expver '0001'** of **class 'MC'**. On 21 June 2016 the model resolution has seen an upgrade from T255 to T511, and forecasts are produced twice per day.

A short summary of the main model specifications:

- The modified CB05 tropospheric chemistry is used (Williams et al., 2013), originally taken from the TM5 chemistry transport model (Huijnen et al., 2010)
- Stratospheric ozone during the forecast is computed from the Cariolle scheme (Cariolle and Teyssèdre, 2007) as already available in IFS, while stratospheric NOx is constrained through a climatological ratio of HNO_3/O_3 at 10 hPa.
- Monthly mean dry deposition velocities are based on the SUMO model provided by the MOCAGE team.
- Data assimilation is described in Inness et al. (2015) and Benedetti et al. (2009) for chemical trace gases and aerosol, respectively. Satellite data assimilated is listed in Table 2.2 and Fig. 2.1.
- Anthropogenic and biogenic emissions are based on MACCity (Granier et al., 2011) and a climatology of the MEGAN-MACC emission inventories (Sindelarova et al., 2014). Anthropogenic emissions changed to CAMS_GLOB v2.1 with the July 2019 update.
- NRT fire emissions are taken from GFASv1.2 (Kaiser et al. 2012).

The aerosol model includes 14 prognostic variables (Remy et al., 2019).

- 3 size bins each for sea-salt and desert dust
- 2 bins (hydrophibic and hydrophobic) each for organic matter and black carbon
- 1 bin for sulphate
- 2 bins (fine and coarse) for nitrate (New since 46R1)
- 1 bin for ammonium (New since 46R1)

The SO_2 precursor for sulphate aerosol no longer exists as a separate prognostic in the aerosol scheme, which since 46R1 couples directly to the SO_2 in the chemistry scheme instead. Likewise, the precursors for the new nitrate and ammonium aerosol (nitric acid and ammonia) are also part of the chemistry scheme rather than the aerosol scheme.

Aerosol total mass is constrained by the assimilation of MODIS and PMAp AOD (Benedetti et al. 2009). A variational bias correction is currently applied for the PMAp AOD based on the approach used also elsewhere in the IFS (Dee and Uppala, 2009).

A history of updates of the o-suite is given in Table 2.3, and is documented in earlier MACC-VAL and CAMS reports: https://atmosphere.copernicus.eu/node/326. This includes a list with changes concerning the assimilation system.

The CAMS o-suite system is upgraded regularly, following updates to the ECMWF meteorological model as well as CAMS-specific updates such as changes in chemical data assimilation. These changes are documented in e-suite validation reports, as can be found from the link above. Essential model upgrades are also documented in Table 2.3.

The upgrade of the system to Cy45r1 took place on 26 June 2018. This upgrade is also relevant for this report (for the period up to 8 July), and the validation for this upgrade is described in Eskes et al., 2018b/2018c.

Note on the fire emissions between mid-August to 6 October:
Aqua MODIS products were unavailable following an issue with the satellite between 16 August and 8 September. The Aqua MODIS FRP observations were “blacklisted” in GFAS when the data went offline and, unfortunately, a switch in the suite was not set correctly when observations became available again in early September. This means that the fire emissions used in the CY46R1 o-suite were reduced due to the missing Aqua observations. The largest impact is in the tropics. The hourly GFAS suite picked up the Aqua MODIS FRP correctly so the CY47R1 o-suite is not affected.

2.1.2 Short description of the latest CAMS upgrade (47r1) of 6 October 2020

The last major upgrade of the CAMS global system is based on IFS version cy47r1_CAMS. For the aerosol and reactive trace gas components the upgrade took place on 6 October 2020. For the greenhouse gases the upgrade to 47R1 took place on 1 November 2020. see https://atmosphere.copernicus.eu/cycle-47r1 or https://confluence.ecmwf.int/display/COPSRV/Current+global+production+suites.

Table 2.3: Long-term o-suite system updates.

Date	o-suite update
2009.08.01	Start of first NRT experiment f7kn with coupled MOZART chemistry, without aerosol. Also without data assimilation.
2009.09.01	Start of first MACC NRT experiment f93i, based on meteo cy36r1, MOZART v3.0 chemistry, MACC aerosol model, RETRO/REAS and GFEDv2 climatological emissions, T159L60 (IFS) and 1.875°×1.875° (MOZART) resolution.
2012.07.05	Update to experiment fnyp: based on meteo cy37r3, MOZART v3.5 chemistry, where changes mostly affect the stratosphere, MACCity (gas-phase), GFASv1 emissions (gas phase and aerosol), T255L60 (IFS) and 1.125°×1.125° (MOZART) resolution. Rebalancing aerosol model, affecting dust.
2013.10.07	Update of experiment fnyp from e-suite experiment fwu0: based on meteo cy38r2, no changes to chemistry, but significant rebalancing aerosol model. Assimilation of 21 layer SBUV/2 ozone product
2014.02.24	Update of experiment fnyp from e-suite experiment fzpr: based on meteo cy40r1. No significant changes to chemistry and aerosol models.
2014.09.18	Update to experiment g4e2: based on meteo cy40r2. In this model version IFS-CB05 is introduced to model atmospheric chemistry.
2015.09.03	Update to experiment g9rr: based on meteo cy41r1.
2016.06.21	Update to experiment 0067: based on meteo cy41r1, but a resolution increase from T255 to T511, and two production runs per day
2017.01.24	Update to cycle 43R1_CAMS, T511L60
2017.09.26	Update to cycle 43R3_CAMS, T511L60
2018.06.26	Update to cycle 45R1_CAMS, T511L60
2019.07.09	Update to cycle 46R1_CAMS, T511L137
2020.10.06	Update to cycle 47R1_CAMS, T511L137

The validation for this 47r1 upgrade is described in Eskes et al. 2020: https://atmosphere.copernicus.eu/sites/default/files/2020-10/CAMS84_2018SC2_D3.2.1-202009_esuite.pdf

The meteorological changes can be found on the ECMWF-IFS CY47R1 page, https://confluence.ecmwf.int/display/COPSRV/Implementation+of+IFS+cycle+47r1.

The atmospheric composition content of the 47R1 cycle includes the following aspects:

Assimilation:

- No changes compared to 46R1

Observations:

- TROPOMI volcanic SO_2:

- Activation on 6 Oct 2020 (for SO2 > 5DU)

- OMPS O_3 layers from NOAA-20 and NPP activated on 20201006
- SBUV/2 NOAA-19 O_3 layers retired on 20201005
- No other changes compared to the observations used in 46R1.

Emissions:

- Updated emissions inventories: CAMS_GLOB_ANT v4.2 (anthropogenic) and volcanic outgassing (based on Carn et al., 2017).
- Updated to GFASv1.4 biomass-burning emissions.
- Excluded agricultural waste burning from CAMS_GLOB_ANT, avoiding double-counting with GFAS.
- Improved diurnal cycle (CO, NO, SO_2, NH_3) and vertical profile for anthropogenic emissions (SO_2, all over sea).

Other model changes:

- Hybrid Linear Ozone (HLO) scheme (a Cariolle-type linear parameterisation of stratospheric ozone chemistry using the multi-year mean of the CAMS reanalysis as mean state).
- New sea-salt emission scheme based on Albert et al. (2016), providing better agreement with measured sea-salt size distribution.
- Updated dust source function, reducing excess dust in the Sahara, Middle East and other regions, and restoring missing dust over Australia.
- Revised coefficients in UV processor, based on ATLAS3 spectrum.

2.1.3 Control

The control run (relevant expver = **gzhy,** since 26/06/2018; expver = **h7c4** since 09/07/2019; expver = **hdir** since 06/10/2020) applies the same settings as the respective o-suites, based on the coupled IFS-CB05 system with CAMS aerosol, except that data assimilation is not switched on. The meteorology in the control run is initialized with the meteorological fields from the o-suite.

2.1.4 High-resolution CO_2 and CH_4 forecasts and delayed-mode analyses

The pre-operational forecasts of CO_2 and CH_4 use an independent setup of the IFS at a resolution of TL1279, i.e. ~16 km horizontal, and with 137 levels. This system runs in real time and does not apply data assimilation for the greenhouse gases.

The land vegetation fluxes for CO_2 are modelled on-line by the CTESSEL carbon module (Boussetta et al., 2013). A biogenic flux adjustment scheme is used in order to reduce large-scale biases in the net ecosystem fluxes (Agusti-Panareda, 2015). The anthropogenic fluxes are based on the annual mean EDGARv4.2 inventory using the most recent year available (i.e. 2008) with estimated and climatological trends to extrapolate to the current year. The fire fluxes are from GFAS (Kaiser et al.,

2012). Methane fluxes are prescribed in the IFS using inventory and climatological data sets, consistent with those used as prior information in the CH_4 flux inversions from Bergamaschi et al. (2009). The anthropogenic fluxes are from the EDGAR 4.2 database (Janssens-Maenhout et al, 2012) valid for the year 2008. The biomass burning emissions are from GFAS v1.2 (Kaiser et al., 2012). The high-resolution forecast experiments also included a linear CO scheme (Massart et al., 2015).

The experiments analysed in this report are:

- "**hd7v**" NRT CO_2, CH_4 analyses from 1 November 2020, with a resolution Tco399 (~25km) and 137 vertical levels. Cycle 47R1.
- "**he9h**" NRT CO_2, CH_4 forecasts from 1 November 2020, with high resolution Tco1279 (~9km) and 137 vertical levels. Cycle 47R1.
- "**h72g**" NRT CO_2, CH_4 analyses from 1 December 2019, with a resolution Tco399 (~25km) and 137 vertical levels. Cycle 46R1.
- "**h9sp**" NRT CO_2, CH_4 forecasts from 1 December 2019, with high resolution Tco1279 (~9km) and 137 vertical levels. Cycle 46R1.
- "**gqpe**" (43R1) from January 2017, and "**gznv"** (45R1) from 1 December 2018 to present. It runs with a TCO1279 Gaussian cubic octahedral grid (equivalent to approximately 9km horizontal resolution). Note that the CO_2, CH_4 and linear CO tracers are initialized with the GHG analysis (gqiq) for CO_2 and CH_4 and the CAMS operational analysis for CO.
- The greenhouse gas analysis experiment runs on a TCO399 grid (equivalent to around 25km) and 137 vertical levels and is available from January 2017 ("**gqiq**", 43R1) and 1 December 2018 ("**gwx3**", 45R1). This experiment runs in delayed mode (4 days behind real time) and makes use of observations from TANSO-GOSAT (methane and CO_2) and MetOp-IASI (methane).
- "**ghqy**" from March 2016. The initial conditions used in ghqy on 1st of March 2016 are from the GHG analysis (experiment gg5m). Furthermore, the meteorological analysis used to initialize the ghqy forecast changed resolution and model grid in March 2016. Note that the CO_2, CH_4 and linear CO tracers are free-running.

2.2 Other systems

2.2.1 BASCOE

The NRT analyses and forecasts of ozone and related species for the stratosphere, as delivered by the Belgian Assimilation System for Chemical ObsErvations (BASCOE) of BIRA-IASB (Lefever et al., 2014; Errera et al., 2008), are used as an independent model evaluation of the CAMS products. The NRT BASCOE product is the ozone analysis of Aura/MLS-SCI level 2 standard products, run in the following configuration (version 05.07):

- The following species are assimilated: O_3, H_2O, HNO_3, HCl, HOCl, N_2O and ClO.
- It lags by typically 4 days, due to latency time of 4 days for arrival of non-ozone data from Aura/MLS-SCI (i.e. the scientific offline Aura/MLS dataset).

- Global horizontal grid with a 3.75° longitude by 2.5° latitude resolution.
- Vertical grid is hybrid-pressure and consists in 86 levels extending from 0.01 hPa to the surface.
- Winds, temperature and surface pressure are interpolated in the ECMWF operational 6-hourly analyses.
- Time steps of 20 minutes, output every 3 hours

See the stratospheric ozone service at http://www.copernicus-stratosphere.eu/. It delivers graphical products dedicated to stratospheric composition and allows easy comparison between the results of o-suite, BASCOE and TM3DAM. The BASCOE data products (HDF4 files) are also distributed from this webpage. Other details and bibliographic references on BASCOE can be found at http://bascoe.oma.be/. A detailed change log for BASCOE can be found at http://www.copernicus-stratosphere.eu/4_NRT_products/3_Models_changelogs/BASCOE.php.

2.2.2 SDS-WAS multimodel ensemble

The World Meteorological Organization's Sand and Dust Storm Warning Advisory and Assessment System (WMO SDS-WAS) for Northern Africa, Middle East and Europe (NAMEE) Regional Center (http://sds-was.aemet.es/) has established a protocol to routinely exchange products from dust forecast models as the basis for both near-real-time and delayed common model evaluation. Currently, twelve regional and global models (see the complete list in the following link https://sds-was.aemet.es/forecast-products/forecast-evaluation/model-inter-comparison-and-forecast-evaluation/at_download/file) provides daily operational dust forecasts (i.e. dust optical depth, DOD, and dust surface concentration).

Different multi-model products are generated from the different prediction models. Two products describing centrality (multi-model median and mean) and two products describing spread (standard deviation and range of variation) are daily computed. In order to generate them, the model outputs are bi-linearly interpolated to a common grid mesh of 0.5º x 0.5º. The multi-model dust optical depth (DOD at 550 nm) median from nine dust prediction models participating in the SDS-WAS Regional Center is used for the validation of the CAMS NRT streams.

2.3 CAMS products

An extended list of output products from the NRT stream o-suite are available as 3-hourly instantaneous values up to five forecast days. These data are available from the CAMS Atmosphere Data Store (ADS), https://atmosphere.copernicus.eu/data, in netcdf and grib2 format.

2.4 Availability and timing of CAMS products

The o-suite data delivery for the period September-November 2020 (SON-2020) was excellent, with an on-time delivery percentage of 100%. See table 2.6 for detailed statistics from 2014 to SON-2020. The availability statistics provided in Table 2.6 are computed for the end of the 5-day forecast run. The CAMS production KPI is defined as the percentage of cycles in which all the general data dissemination tasks are completed before the deadlines: 10 UTC for the 00:00 and 22 UTC for the 12:00 UTC run. This was in part based on requirements from the regional models. We note that at present most regional models can still provide their forecasts even if the global forecast is available a bit later. Since 21 June 2016 two CAMS forecasts are produced each day.

Table 2.6: Timeliness of the o-suite from December 2014. From June 2016 onwards CAMS has produced two forecasts per day.

Months	On time, 10 & 22 utc	80th perc	90th perc	95th perc
Dec-Feb '14-'15	97%	D+0, 19:43	D+0, 20:28	D+0, 21:13
Mar-May 2015	96%	D+0, 19:38	D+0, 21:03	D+0, 21:40
Jun-Aug 2015	95%	D+0, 20:24	D+0, 20:53	D+0, 21:54
Sept-Nov 2015	95%	D+0, 19:44	D+0, 20:55	D+0, 21:51
Dec-Feb '15-'16	100%	D+0, 18:39	D+0, 18:57	D+0, 19:43
Mar-May 2016	98%	D+0, 19:32	D+0, 19:47	D+0, 20:00
Jun-Aug 2016 (00 and 12 cycle)	100%	D+0, 08:53 D+0, 20:55	D+0, 09:04 D+0, 21:01	D+0, 09:18 D+0, 21:18
Sep-Nov 2016	98.9%	D+0, 08:44 D+0, 20:44	D+0, 08:51 D+0, 20:48	D+0, 08:52 D+0, 20:51
Dec 2016 - Feb 2017	99.4%	D+0, 09:02 D+0, 21:01	D+0, 09:11 D+0, 21:02	D+0, 09:18 D+0, 21:04
Mar-May 2017	100%	D+0, 09:08 D+0, 21:07	D+0, 09:14 D+0, 21:09	D+0, 09:19 D+0, 21:11
Jun-Aug 2017	100%	D+0, 09:05 D+0, 21:05	D+0, 09:07 D+0, 21:08	D+0, 9:09 D+0, 21:10
Sep-Nov 2017	100%	D+0, 09:02 D+0, 21:00	D+0, 09:05 D+0, 21:04	D+0, 9:09 D+0, 21:07
Dec 2017 - Feb 2018	98.33%	D+0, 08:55 D+0, 20:54	D+0, 08:59 D+0, 20:59	D+0, 09:01 D+0, 21:02
Mar-May 2018	98.9%	D+0, 09:00 D+0, 21:00	D+0, 09:06 D+0, 21:03	D+0, 09:08 D+0, 21:06
Jun-Aug 2018	100%	D+0, 09:11 D+0, 21:07	D+0, 09:14 D+0, 21:09	D+0, 09:20 D+0, 21:11
Sep-Nov 2018	100%	D+0, 09:05 D+0, 21:03	D+0, 09:09 D+0, 21:07	D+0, 09:13 D+0, 21:10
Dec 2018 - Feb 2019	98.9%	D+0, 09:03 D+0, 21:04	D+0, 09:06 D+0, 21:06	D+0, 09:08 D+0, 21:10
Mar-May 2019	100%	D+0, 09:07 D+0, 21:05	D+0, 09:10 D+0, 21:09	D+0, 09:12 D+0, 21:11
Jun-Aug 2019	99.5%	D+0, 09:19 D+0, 21:14	D+0, 09:22 D+0, 21:17	D+0, 09:27 D+0, 21:19
Sep-Nov 2019	98.9%	D+0, 09:14 D+0, 21:07	D+0, 09:23 D+0, 21:20	D+0, 09:26 D+0, 21:24
Dec 2019 - Feb 2020	99.4%	D+0, 09:00 D+0, 20:58	D+0, 09:03 D+0, 21:02	D+0, 09:12 D+0, 21:08
Mar-May 2020	100%	D+0, 08:55 D+0, 20:57	D+0, 08:58 D+0, 21:01	D+0, 09:00 D+0, 21:05
Jun-Aug 2020	100%	D+0, 08:58 D+0, 20:55	D+0, 09:03 D+0, 20:59	D+0, 09:05 D+0, 21:02
Sep-Nov 2020	100%	D+0, 08:50 D+0, 20:50	D+0, 08:58 D+0, 20:53	D+0, 09:04 D+0, 21:01

3. Tropospheric Ozone

3.1 Validation with sonde data in the free troposphere

Model profiles of the CAMS runs were compared to free tropospheric balloon sonde measurement data of 38 stations taken from the NDACC, WOUDC, NILU and SHADOZ databases for January 2013 to November 2020 (see Fig. 3.1.1 - 3.1.2). Towards the end of the period, the number of available soundings decreases, which implies that the evaluation results may become less representative. The figures contain the number of profiles in each month that are available for the evaluation. The methodology for model comparison against the observations is described in Douros et al., 2017. The free troposphere is defined as the altitude range between 750 and 200hPa in the tropics and between 750 and 300hPa elsewhere.

Please note that recent scientific findings (Thompson et al., 2017; Witte et al., 2017; 2018, Stauffer, et al. in preparation 2020) show a drop-off in Total Ozone at various global ozone stations in comparison with satellite instruments. This drop-off amounts between 5-10% for stratospheric ozone. Changes in the ECC ozone instrument are associated with the drop-off, but no single factor has been identified as cause yet. For tropospheric ozone (<50 hPa) no alternations are reported, but some systematic effect cannot be ruled out. Data availability is thus recently limited.

MNMBs for the o-suite are mostly within the range ±20%, for all months, in all zonal bands, except for the Tropics and Antarctica, where larger positive MNMBs up to ±45% appear, see Fig. 3.1.4. During the last year (November 2019 to November 2020) MNMBs are within – 2% and 20% over the Arctic, within – 2% and 15% over the northern mid-latitudes and ±18% over Antarctica, see Fig. 3.1.1.-3.1.4.

Over the Arctic, the o-suite mostly shows smaller and partly slightly negative MNMBs during winter and spring season 2020 (MNMBs between -2% and up to 14%) and positive biases during the rest of the period (MNMBs up to 20%) see, Fig. 3.1.1.

Over the NH mid-latitudes the MNMBs for the o-suite is within 10%.

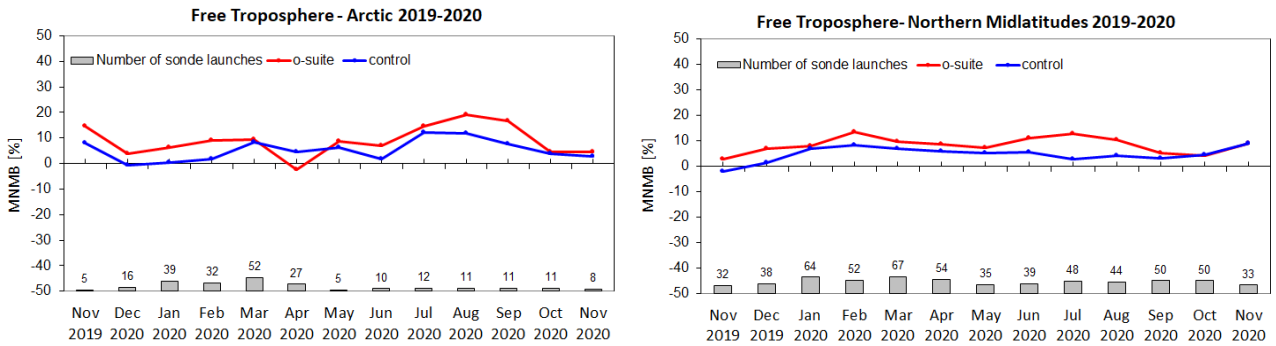

Figure 3.1.1: MNMBs (%) of ozone in the free troposphere (between 750 and 300 hPa) from the IFS model runs against aggregated sonde data over the Arctic (left) and the Northern mid latitudes (right). The numbers indicate the amount of individual number of sondes.

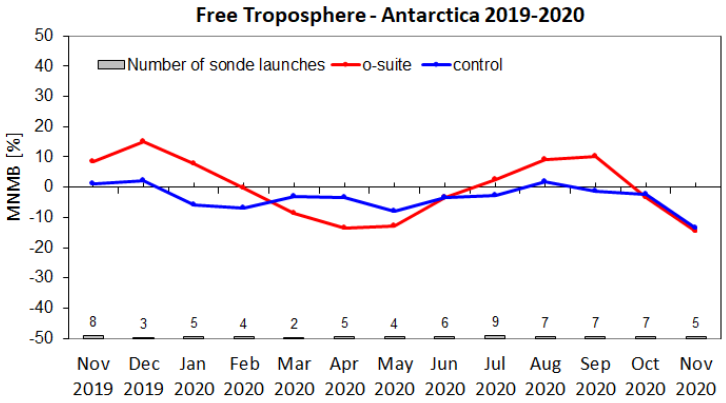

Figure 3.1.2: MNMBs (%) of ozone in the free troposphere (between 750 and 200hPa (Tropics) / 300hPa) from the IFS model runs against aggregated sonde data over Antarctica. The numbers indicate the amount of individual number of sondes.

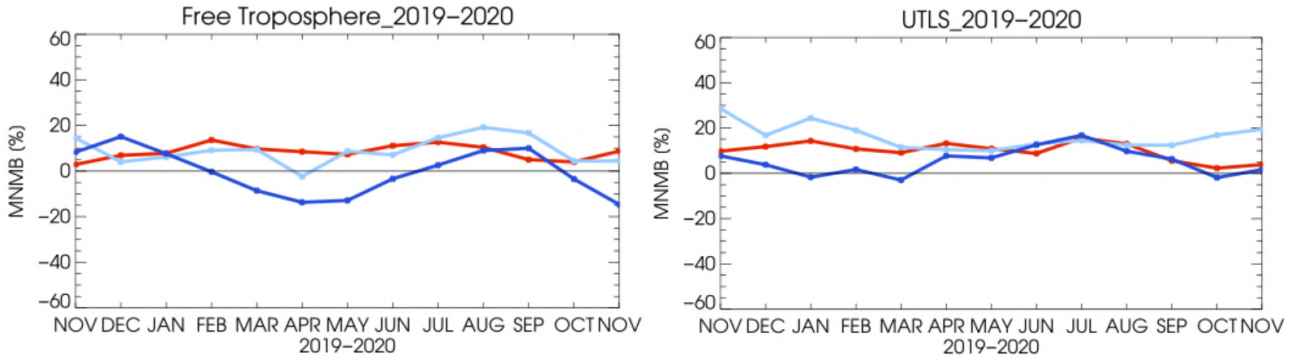

Figure 3.1.3: MNMBs (%) of ozone in the free troposphere (left, between 750 and 200hPa (Tropics) / 300hPa) and UTLS (right, between 300 and 100hPa (Tropics) / 60hPa) from the IFS model runs against aggregated sonde data over Antarctica (blue), Arctic (light blue) and Northern Midlatitudes (red).

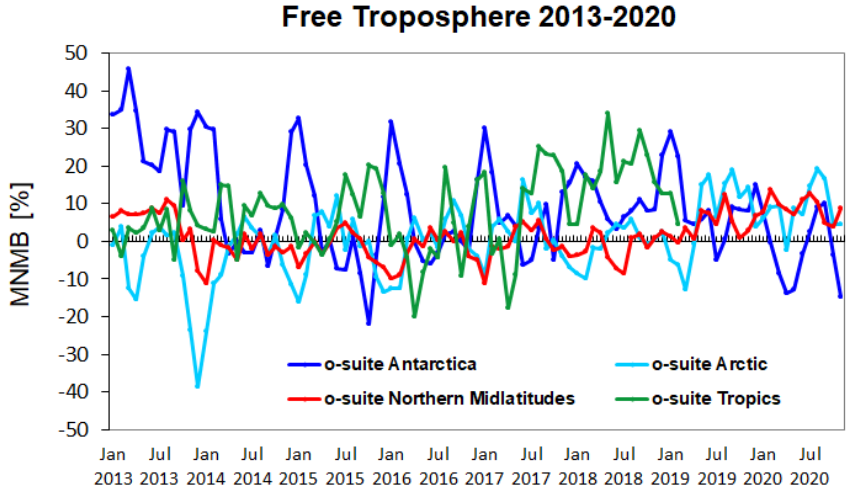

Figure 3.1.4: Time series of MNMB of ozone in the o-suite, compared against ozone sondes, averaged over different latitude bands. The free troposphere is defined as the layer between 750 and 300 hPa. There was a problem with sonde data in the tropics in 2020, see https://tropo.gsfc.nasa.gov/shadoz/.

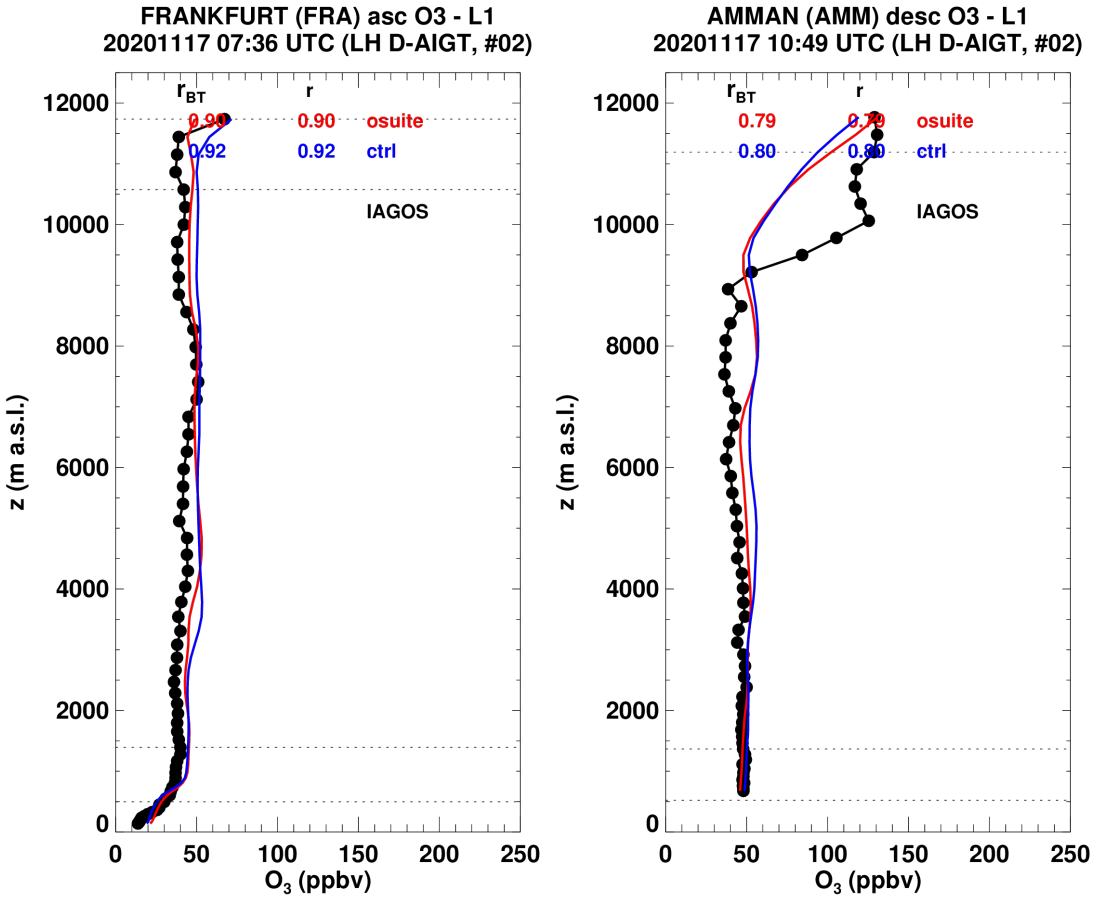

Figure 3.2.1.: Vertical profiles of ozone measured with the IAGOS aircraft over Frankfurt and Amman on 17 November 2020, compared to o-suite (red) and control (blue).

3.2 Ozone validation with IAGOS data

Unfortunately, due the covid-19 crisis and its impact on the airlines operations, only one IAGOS flight have been recorded during this reporting period. This is the first time since the beginning of IAGOS that we have almost no data to provide. The following period (DJF) will provide regular measurements again. For more detailed comparisons against IAGOS we refer to the previous NRT report, period JJA-2020 (Ramonet et al., 2021)

Figure 3.2.1 shows the results for a flight between Frankfurt and Amman on 17 November. The nearly constant mixing ratio over Frankfurt between 1 and 11 km is well reproduced by the CAMS models. The increase of ozone observed over Amman at an altitude of about 10 km is not captured by the CAMS o-suite and control.

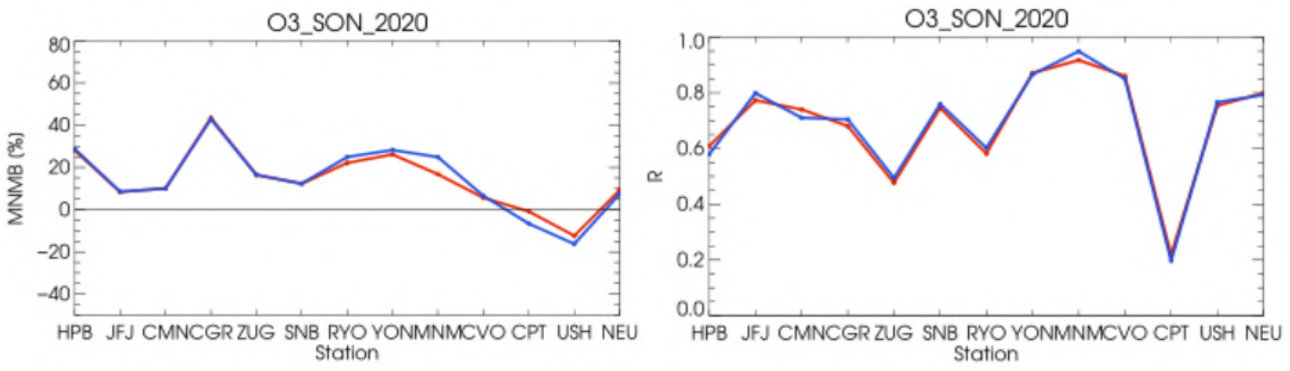

Figure 3.3.1: Modified normalized mean bias in % (left) and correlation coefficient (right) of the NRT forecast runs compared to observational GAW data in the period September-November 2020 (o-suite: red, control: blue).

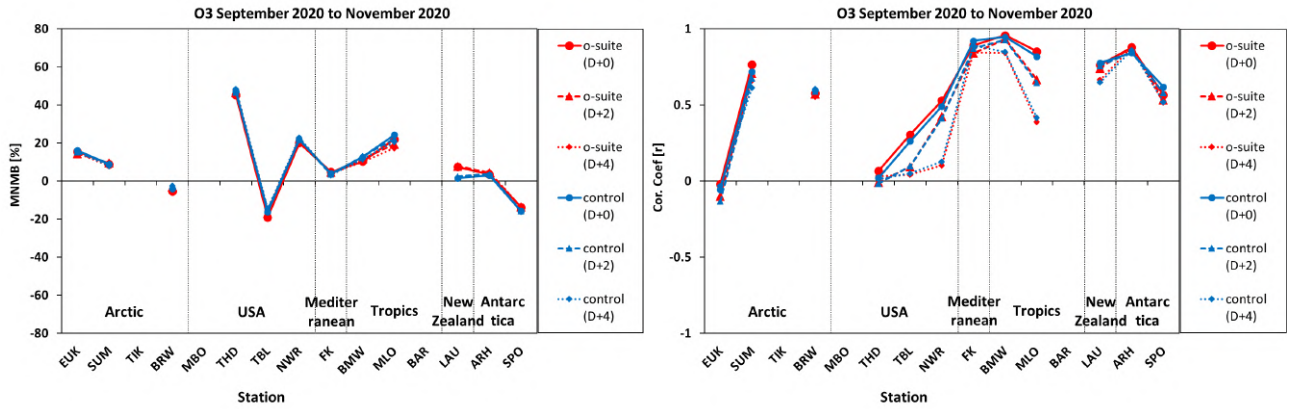

Figure 3.3.2: Modified normalized mean bias in % (left) and correlation coefficient (right) of the NRT forecast runs compared to observational ESRL data in the period September-November 2020. Circles correspond to D+0, triangles to D+2 and rhombs to D+4 metrics respectively.

3.3 Validation with GAW and ESRL-GMD surface observations

For the Near Real Time (NRT) validation, 13 GAW stations and 11 ESRL stations are currently delivering O_3 surface concentrations in NRT, and the data are compared to model results. In the following, a seasonal evaluation of model performance for the 2 NRT runs (o-suite and control) has been carried out for the period from September to November 2020. The latest validation results based on GAW stations and based on ESRL observations can be found on the CAMS website, see section 1, Table 1.2.

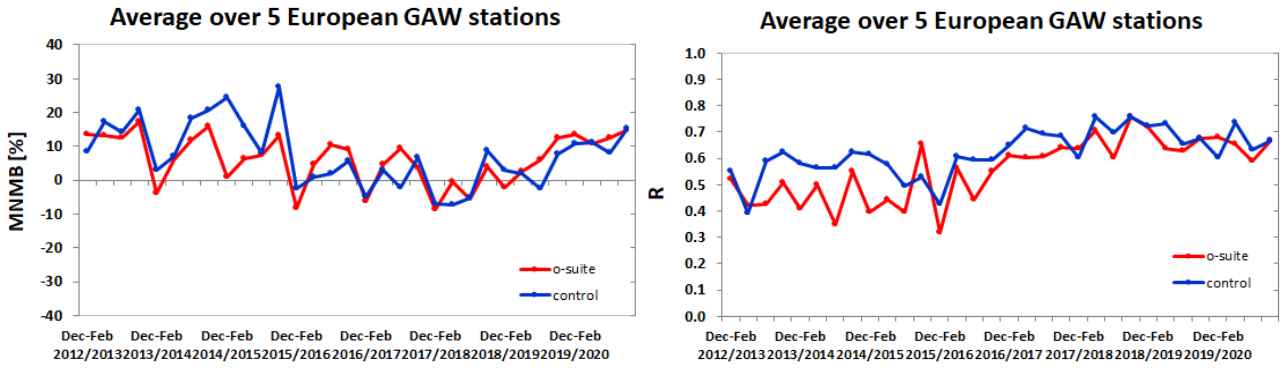

Figure 3.3.3: Long term (December 2012 – November 2020) evolution of seasonal mean MNMB (left) and correlation (right), as averaged over 5 GAW stations in Europe, for o-suite (red) and control (blue).

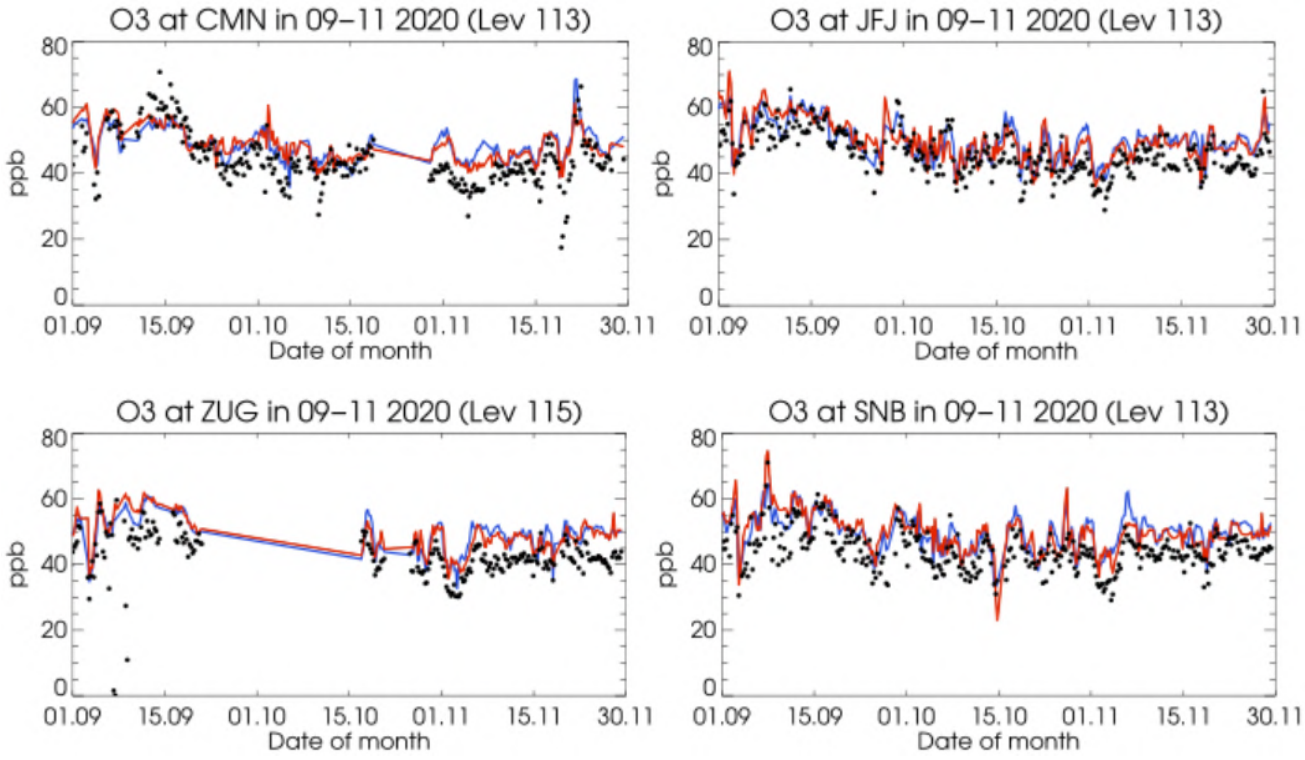

Figure 3.3.4: Time series for the o-suite (red) and control (blue) compared to GAW observations for Monte Cimone (44.18°N, 10.70°E) and Jungfraujoch (46.55°N, 7.99°E) (upper panel), Zugspitze (47.4°N, 10.9°E) and Sonnblick (47.05°N, 12.96°E) (lower panel).

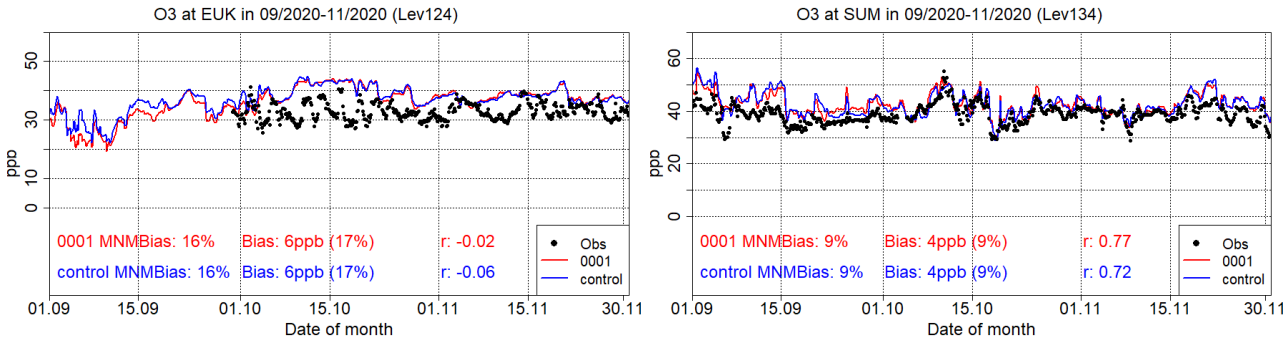

Figure 3.3.5: Time series for the o-suite (red) and control (blue) compared to ESRL observations at Eureka Canada station (80.05°N, 86.42°W, left) and at Summit, Greenland station (72.57°N, 38.48°W, right)

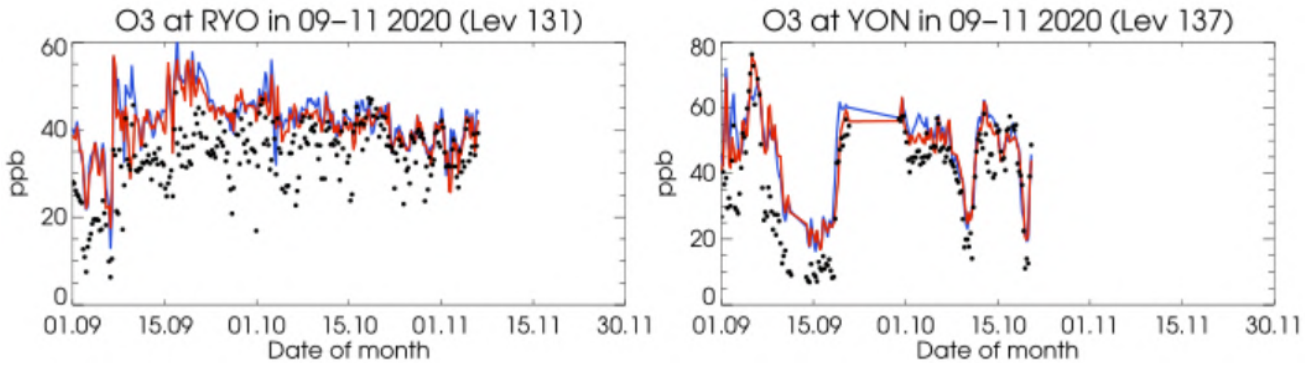

Figure 3.3.6: Time series for the o-suite (red) and control (blue) compared to GAW observations for Ryori (39.03°N, 141.82°E, left panel) and Yonagunijima (24.47°N, 123.02°E, right panel).

A comparison of the seasonal-mean MNMB over Europe (Fig. 3.3.3) from December 2012 to present shows minimal MNMBs during the winter season and larger biases in other months. Also, on average the MNMB for the o-suite and control shows an improvement over the years. The temporal correlation is consistently better for the control run than for the o-suite, but the o-suite shows strong improvements recently. Modified normalized mean biases in % (left panel) and correlation coefficients (right panel) for different forecasts days (D+2, red-dashed and D+4, red- pointed) with respect to GAW and ESRL observations are shown in Figs. 3.3.1 and 3.3.2. It indicates that MNMBs for both o-suite and control run mostly remain stable up to D+4 (forecast run from 96h to 120h). Correlations between simulated and observed surface ozone values remain almost stable up to D+2 (forecast run from 48h to 72h), but then drop especially over Mid-Latitudes and the Tropics (correlations for D+4 are lower than correlations for D+2 and D+0), see Fig. 3.3.1 and 3.3.2, right graph).

Looking at different regions, for European stations (HPB, JFJ, ZUG, SNB, CMN, CGR), observed O_3 surface mixing ratios are overestimated with MNMBs ranging between 8 - 28% (exception: CGR with a bias of 43%). Correlations for European stations are between 0.48 and 0.77 for the o-suite and between 0.49 and 0.79 for the control run, see Fig. 3.3.1.

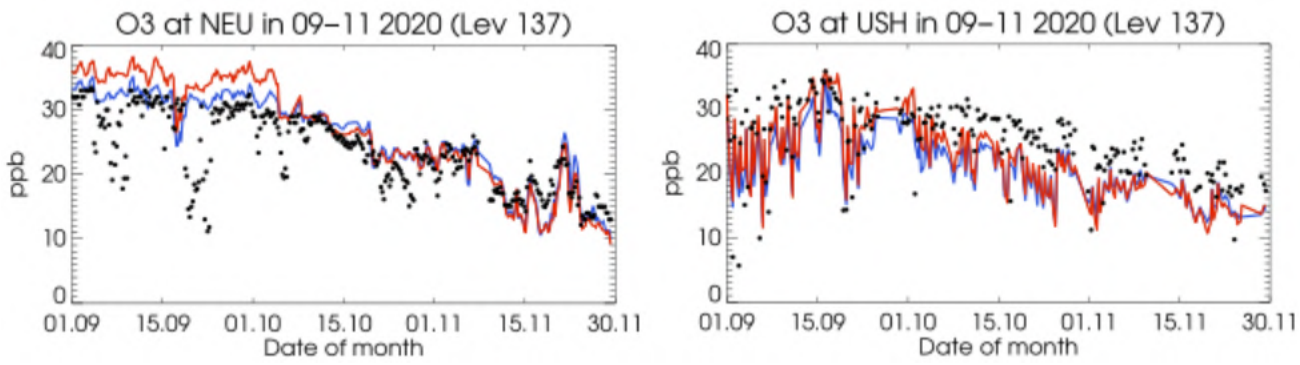

Figure 3.3.7: Time series for the o-suite (red) and control (blue) compared to GAW observations (black dots) at Neumayer (70.65°S, 8.25°W) and Ushuaia (54.85°S, 68.32°W).

Over Eureka (EUK) and Summit (SUM) Arctic stations, both CAMS NRT runs overestimate surface ozone values by 15% and 10% respectively, while at Point Barrow Alaska station sligthly underestimate is by -5%. Correlations between modelled and observed ozone values are highly significant at 0.6 at BRW and SUM stations, 0.6 and 0.7 respectively. On the contrary at Eureka station both CAMS NRT runs cannot reproduce the day to day surface ozone variability resulting to poor correlation (r≈0).

Concerning USA stations (THD, TBL and NWR), the observed ozone mixing ratios are strongly overestimated by both the o-suite and the control run by 45% and 20% at THD and NRW respectively, while in the TBL station both models underestimate surface ozone values by -20%. Correlations between o-suite and observations are 0.31 at TBL, 0.52, at NWR and almost zero at THD for the o-suite and 0.26 at TBL, 0.49, at NWR and almost zero at THD for the control run.

Modelled O_3 mixing ratios for Asian stations (RYO, MNM, YON) show MNMBs between 16 and 26%. Correlation coefficients are high ranging between 0.58 and 0.92 for o-suite and between 0.6 and 0.95 for control run.

At CVO station, the model corresponds well to the observations with MNMB of 5% and correlation of 0.86.

The O_3 mixing ratios of the southern hemispheric stations (CPT, USH) show MNMBs between about 0 and -12% for the o-suite. Correlation coefficient for CPT is 0.22 and for USH is 0.75.

The observed ozone mixing ratios are overestimated by both runs at Mauna Loa (MLO) (MNMBo-suite≈22%, MNMBcontrol≈24%) and Bermuda (BMD) (MNMBo-suite≈10%, MNMBcontrol≈13%) stations in the Tropics. Correlations between simulated and observed surface ozone are high for both the o-suite and the control run (r>0.8).

At Lauder (LDR) station in New Zealand the o-suite overestimates O_3 mixing ratios by 7% while the and control run by 1%. Correlations between simulated and observed surface ozone values for the o-suite and the control run are 0.76 and 0.78, respectively.

Table 3.4.1: Coordinates, elevation, corresponding model level (level 137 is the surface level), as well as validation scores (MNMBs and correlations for the period SON 2020) obtained with the 2 forecast runs (o-suite and control), for each one of the selected Mediterranean stations. MNMBs and correlations with blue denote stations where control run performs better while with red are denoted stations where o-suite performs better.

						Distance from the	MNMB		Cor. Coef	
Station Name	Stat_ID	Lon	Lat	Alt (m)	Level	shore (km)	o-suite	control	o-suite	control
Al Cornocales	ES1648A	-5.66	36.23	189	133	16	32.6	30.9	0.82	0.82
Caravaka	ES1882A	-1.87	38.12	1	137	73	-1.2	-2.5	0.76	0.76
Zarra	ES0012R	-1.10	39.08	885	130	70	16.0	14.9	0.87	0.86
VIillar Del Arzobispo	ES1671A	-0.83	39.71	430	137	48	27.4	26.1	0.84	0.83
Cirat	ES1689A	-0.47	40.05	466	137	37	36.6	35.4	0.83	0.82
Bujaraloz	ES1400A	-0.15	41.51	327	137	60	24.4	24.2	0.87	0.86
Morella	ES1441A	-0.09	40.64	1150	128	51	NA	NA	NA	NA
Bc-La Senia	ES1754A	0.29	40.64	428	137	21	-15.0	-15.4	0.81	0.80
Ay-Gandesa	ES1379A	0.44	41.06	368	136	15	29.1	28.6	0.75	0.75
Ak-Pardines	ES1310A	2.21	42.31	1226	135	81	34.2	33.6	0.58	0.59
Hospital Joan March	ES1827A	2.69	39.68	172	133	3	-1.2	-2.5	0.76	0.76
Al-Agullana	ES1201A	2.84	42.39	214	137	25	10.7	10.8	0.71	0.69
Av-Begur	ES1311A	3.21	41.96	200	132	9	17.7	16.9	0.72	0.75
Plan Aups/Ste Baume	FR03027	5.73	43.34	675	124	21	19.5	19.2	0.79	0.80
Montemonaco	IT1842A	13.34	42.90	1000	127	46	10.1	9.2	0.82	0.79
Gharb	MT00007	14.20	36.07	114	132	31	4.2	4.1	0.66	0.69
Aliartos	GR0001R	23.11	38.37	110	137	18	NA	NA	NA	NA
NEO	-	21.67	37.00	50	137	2	NA	NA	NA	NA
Finokalia	GR0002R	25.67	35.32	250	132	4	4.7	3.9	0.89	0.92
Agia Marina	CY0002R	33.06	35.04	532	133	14	1.6	4.3	0.85	0.85

Both CAMS NRT runs slightly overestimate surface ozone values at Arrival Height (ARH) by 3. At South Pole (SPO) Both CAMS NRT runs underestimate surface ozone values by -13% (o-suite) and -16 (control) respectively. It is interesting to note that till 2019 the control run negative MNMBs are significantly greater than the o-suite MNMbs. Correlation coefficients are 0.84 for the o-suite and 0.88 for the control run at ARH, and 0.56 for the o-suite and 0.62 for the control at SPO.

For Neumayer station (NEU) the MNMB is 9% for the o-suite and 7% for the control run. Correlation coefficient for both runs is 0.8 (Fig. 3.3.7).

3.4 Validation with AirBase observations in Mediterranean

The surface ozone validation analysis over the Mediterranean is based on an evaluation against station observations from the Airbase Network. In addition, 1 station from the Department of Labour Inspection - Ministry of Labour and Social Insurance, of Cyprus () is used in the validation analysis. For the validation analysis, stations in the Mediterranean located within about 100 km from the shoreline of the Mediterranean shore are used. Table 3.4.1 shows the names, coordinates, elevation and the MNMBs and correlations obtained with the 2 forecast runs (o-suite and control). It indicates that the variance explained by each station of both the o-suite and control is high and correlations are highly significant over Western, Central and Eastern Mediterranean. It should be noted that the o-suite run reproduces slightly better than the control run the surface ozone day to day variability over most of the Mediterranean stations (see Table 3.4.1).

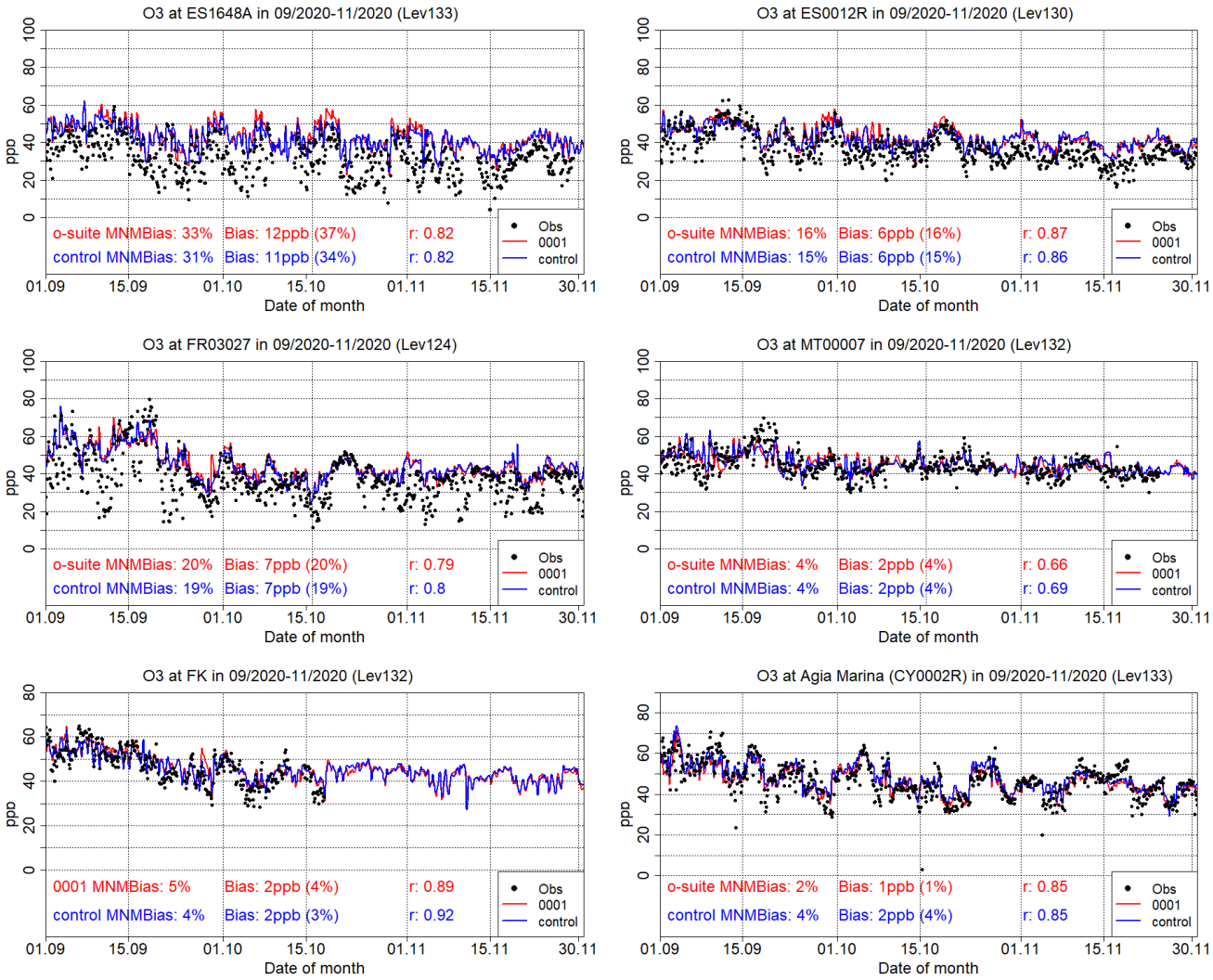

Figure 3.4.1: Time series for the o-suite (red) and Control (blue) compared to Airbase observations at Al Cornocales, Spain station (36.23°N, 5.66 °W, top left), at Zarra, Spain station (39.08°N, 1.10°W, top right), at Plan Aups/Ste Baume, France station (43.34°N, 5.73°E, center left), at Gharb, Malta station (36.07°N, 14.20°E, center right at Finokalia, Crete Greece station (35.32°N, 25.67°E, bottom left) and compared to observations provided by the Department of Labour Inspection - Ministry of Labour and Social Insurance of Cyprus) at Agia Marina, Cyprus station (35.04°N, 33.06 °E, low right).

In terms of biases, o-suite mostly overestimates surface ozone values (with the exception of Caravaka, Hospital Joan March and Bc-La Senia stations) and its MNMBs vary between -15% and 35% depending on the stations over the Mediterranean shore of Spain (average MNMB for the 12 Spain Mediterranean stations is 17.6%). The Control MNMBs are on average 1% lower than those of the o-suite and are closer to zero. Over the stations Plan Aups/Ste Baume in France and Montemonaco in Italy the o-suite overestimates surface ozone concentrations by 20% and 10% respectively. Again, the Control MNMBs are lower by about 1% than the o-suite MNMBs and are closer to zero compared to the o-suite. Over Gharb station in Malta both runs overestimate surface ozone values by 4%.

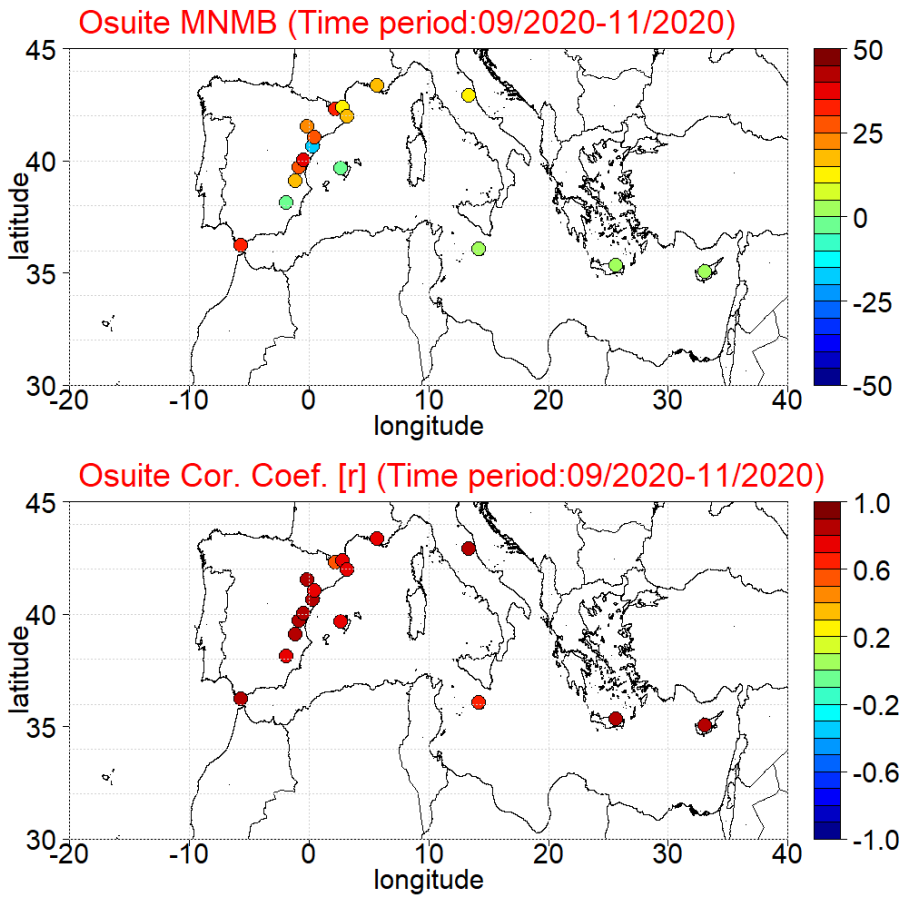

Figure 3.4.2: Spatial distribution of MNMB in % (left) and correlation coefficient (right) of the o-suite run compared to observational data during the period from 1 September to 30 November 2020.

Finally over Finokalia station in Crete the o-suite overestimates surface ozone concentrations by 4% and control run overestimates it by 1% less and over Agia Marina in Cyprus these two percentages for o-suite and control run are 1% and 4%, respectively. It should be noted that over all selected Mediterranean stations the differences between the o-suite and the control run MNMBs are lower compering to those reported in previous CAMS NRT reports.

The spatial distribution of MNMBs and the correlation coefficients of the o-suite over the Mediterranean are shown in Fig. 3.4.2, where it is evident that correlations over the entire Mediterranean from Gibraltar to Cyprus are highly significant. It is also evident that the CAMS NRT run overestimate surface ozone values over the entire Mediterranean from Gibraltar to Cyprus and that CAMS NRT have a better performance over Central and Eastern Mediterranean compared to the Mediterranean shore of Spain in terms of biases.

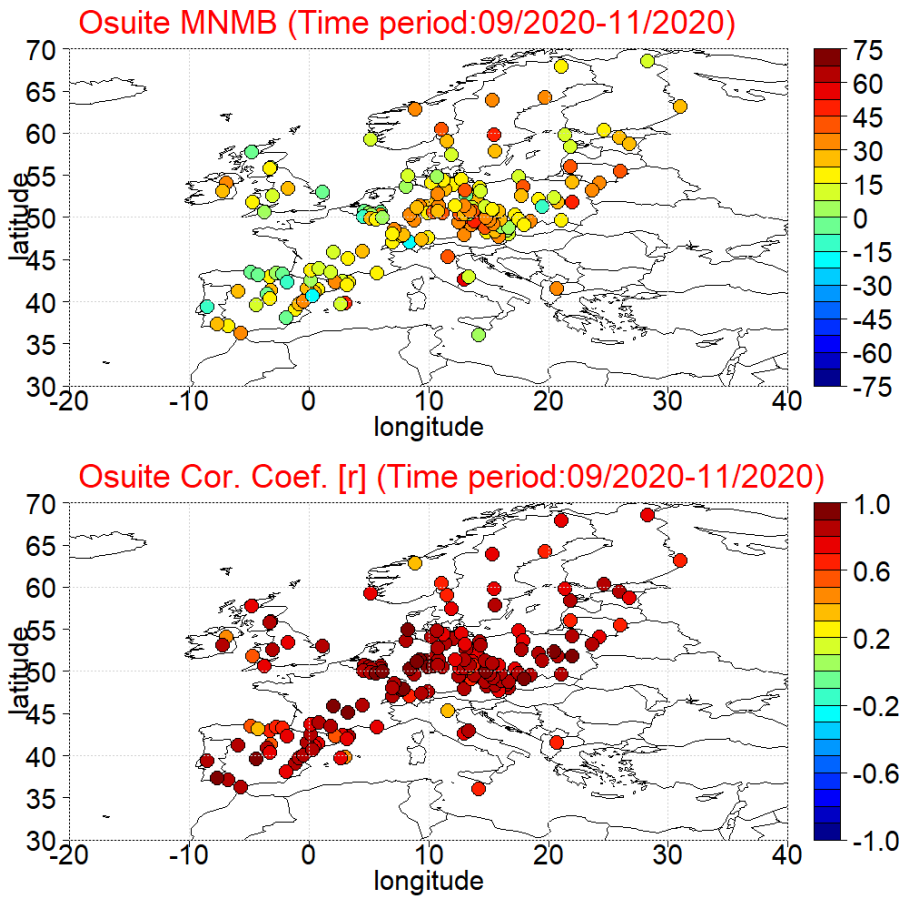

Figure 3.5.1: Spatial distribution of MNMB in % (left) and correlation coefficient (right) of the o-suite run compared to observational data during the period from 1 September 2020 to 30 November 2020.

3.5 Validation with AirBase observations over Europe

The surface ozone validation analysis over Europe is based on an evaluation against Background rural Classes 1-2 O_3 Joly-Peuch classification (Joly and Peuch, 2012) station observations from the Airbase Network. The spatial distribution of MNMBs and the correlation coefficients of the o-suite over Europe are shown in Fig. 3.5.1, where it is evident that correlations over most European AirBase stations in the entire Europe (with a very few exceptions) are highly significant ($0.6<r<0.95$). CAMS NRT runs mostly overestimate surface ozone values with MNMBs varying from -20% to +50% over Europe depending on the station. More specifically, CAMS NRT surface ozone MNMBs over UK, Belgium, the Iberian peninsula and Swiss vary from -15% to +30%. It is also evident that over France, the Czech republic and Finland CAMS NRT overestimate surface ozone up to 30%, and that overestimate it more up to 50% over Ireland, Germany, Poland, Austria, Norway, Sweden and the Baltics. The above-mentioned findings concerning CAMS NRT runs biases and correlations are also observed in individual time series at selected stations plotted in Figure 3.5.2. From these time series and the plotted validation metrics is also evident that the control run surface ozone mean autumn concentrations are almost the same with the o-suite values resulting to almost identical MNMBs.

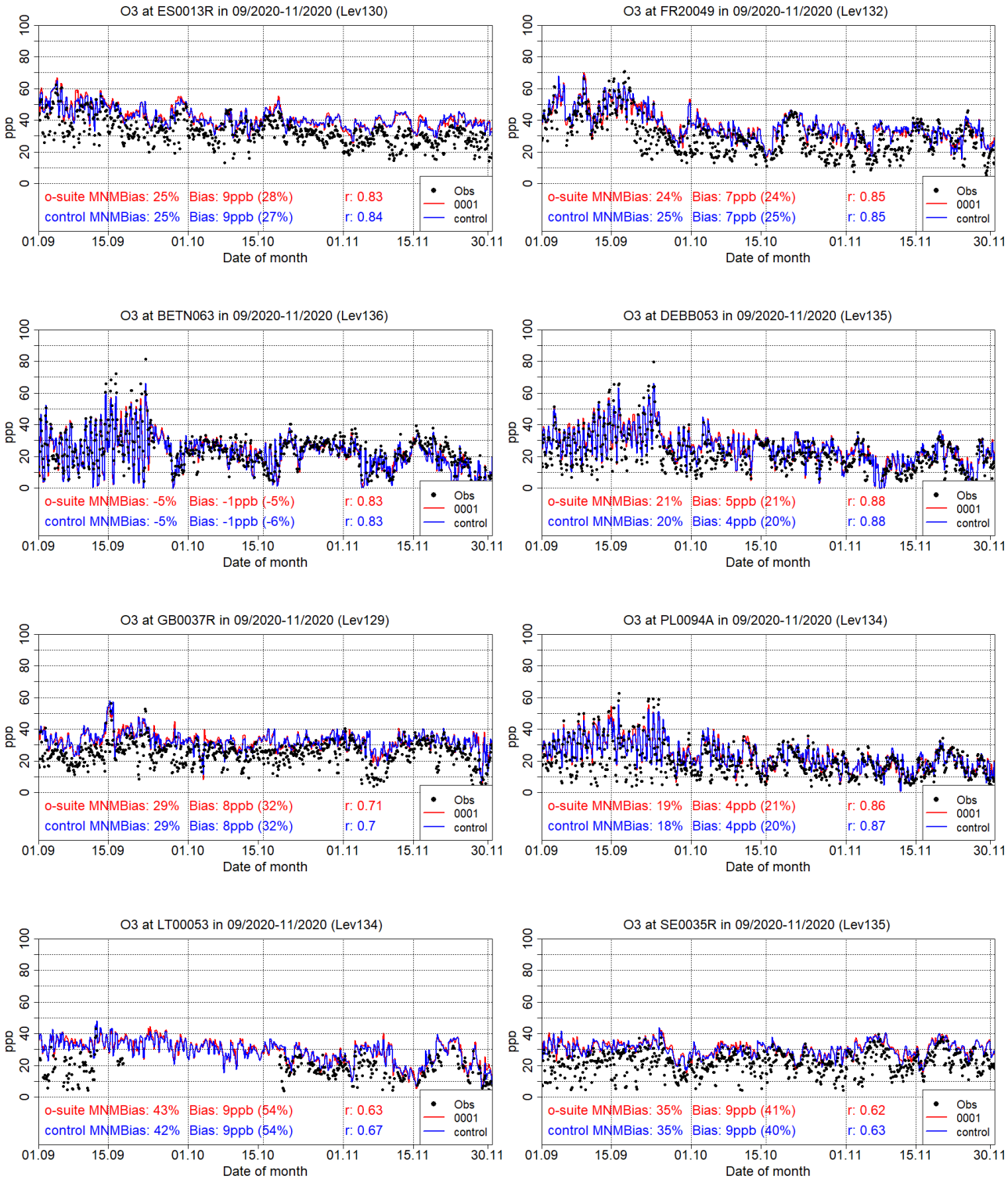

Figure 3.5.2: Time series for the o-suite (red) and Control (blue) compared to Airbase observations at Al Penausende, Spain station (41.24°N, 5.90 °W, 1st row left), at Haut Beaujolais, France station (45.96°N, 4.47°E, 1st row right), at Corroy L.G., Belgium Station (50.67°N, 4.67°E, 2nd row left), at Hasenholz, Germany (52.56°N, 14.02°E, 2nd row right), at Ladybower, Great Britain station (53.40°N, 1.75°W, 3nd row left), at LdGajewWIOSAGajew, Poland station (52.14°N, 19.23°E 3nd row right), at Zemaitija, Lithuania station (56.01°N, 21.89°E, 4nd row left) and at Vindeln, Sweden station (64.25°N, 19.77°E, 4nd row right).

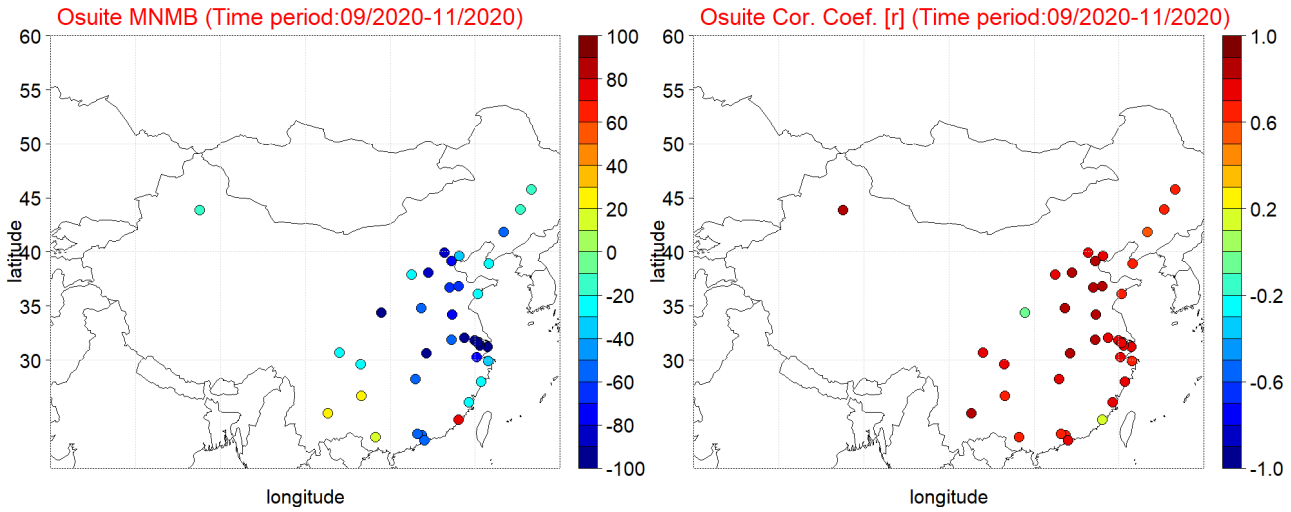

Figure 3.6.1: Spatial distribution of MNMB in % (left) and correlation coefficient (right) of the o-suite run compared to observational data during the period from 1 September 2020 to 30 November 2020

3.6 Validation with surface ozone observations over China

The surface ozone validation over China is based on station observations from more than 1,500 in situ stations covering all major cities in China, operated by the China National Environmental Monitoring Center, reporting the pollutants PM10, PM2.5, O_3, NO_2, SO_2, and CO (e.g. Bai et al., 2020). The measurements were collected within the EU MarcoPolo and Panda projects. Individual station observations were clustered for 37 megacities (e.g. 10-20 stations per city) and the observed surface ozone values are compared with the model ozone values for the corresponding grid point.

Table 3.6.1 shows the names, coordinates, observed and simulated ozone values as well as validation metrics namely the MNMBs and correlations obtained with the o-suite run. The spatial distribution of MNMBs and the correlation coefficients of the o-suite over China are shown in Fig. 3.6.1, where it is evident that correlations over most stations in the entire China (with the exceptions of Xiamen and Xian Megacities) are highly significant ($0.6<r<0.9$). In terms of biases, o-suite mostly underestimate surface ozone values. More specific o-suite MNMBs vary between -10% and -20% depending on the station over North-eastern and North-western China. For stations in the latitudinal belt 30°N-40°N o-suite strongly underestimate surface ozone values with MNMBs varying between -20% and -120%. For stations in the latitudinal belt 20°N-30°N o-suite surface ozone MNMBs vary between -20% and 20% (exceptions are Changsha, Guangzhou and Dongguan with MNMBs≈-50%).

The above-mentioned findings concerning CAMS o-suite biases and correlations are also observed in individual time series at selected cities plotted in Figure 3.6.2. From all the time series it is also evident that the o-suite run reproduced well the observed downward surface ozone trend during SON 2020 period.

Table 3.6.1: Names, coordinates, observed and simulated ozone values as well as o-suite validation metrics for each one from 37 China Megacities under study.

MegaCity	Lat	Lon	O3_OBS (ppb)	O3_o_suite (ppb)	MNMB	Cor. Coef.
Beijing	39.92	116.38	39.47	16.95	-83.1	0.76
Changchun	43.89	125.33	34.65	30.64	-11.8	0.61
Changsha	28.20	112.97	59.44	36.26	-57.6	0.73
Changzhou	31.81	119.97	65.65	22.90	-99.5	0.75
Chengdu	30.66	104.07	37.26	28.59	-26.6	0.73
Chongqing	29.56	106.55	28.81	23.83	-22.0	0.79
Dalian	38.91	121.60	67.19	54.11	-22.9	0.61
Dongguan	23.02	113.75	69.41	42.15	-52.2	0.60
Fuzhou	26.08	119.31	78.16	64.89	-20.7	0.77
Guangzhou	23.13	113.25	64.93	39.03	-54.7	0.67
Guiyang	26.65	106.63	48.73	58.09	20.2	0.63
Hangzhou	30.25	120.17	56.30	27.12	-75.5	0.75
Harbin	45.75	126.63	37.56	31.51	-18.1	0.64
Hefei	31.85	117.27	55.19	34.16	-50.8	0.82
Jinan	36.67	116.98	59.48	31.76	-61.3	0.81
Kunming	25.04	102.71	39.21	49.99	25.6	0.83
Nanjing	32.05	118.77	62.20	22.25	-100.0	0.76
Nanning	22.82	108.32	49.62	60.02	18.0	0.65
Ningbo	29.87	121.54	65.84	46.07	-34.3	0.62
Qingdao	36.07	120.38	68.58	54.34	-23.4	0.69
Shanghai	31.22	121.47	66.38	15.62	-127.1	0.73
Shenyang	41.80	123.40	37.80	21.73	-53.4	0.58
Shenzhen	22.54	114.06	71.96	43.24	-51.6	0.71
Shijiazhuang	38.04	114.51	47.98	20.43	-84.8	0.89
Suzhou	31.30	120.60	63.83	20.70	-106.8	0.71
Taiyuan	37.87	112.55	44.30	35.05	-23.2	0.77
Tangshan	39.63	118.18	40.60	28.51	-39.8	0.72
Tianjin	39.13	117.25	44.27	21.89	-73.4	0.81
Urumqi	43.83	87.62	38.08	33.90	-15.2	0.88
Wenzhou	27.99	120.70	64.30	48.63	-27.1	0.76
Wuhan	30.58	114.30	58.55	19.90	-107.9	0.82
Wuxi	31.57	120.33	61.63	20.26	-103.4	0.72
Xiamen	24.48	118.09	34.95	73.01	73.8	0.17
Xi'an	34.34	108.94	83.04	26.58	-106.3	-0.05
Xuzhou	34.21	117.28	55.67	28.36	-71.1	0.87
Zhengzhou	34.76	113.65	52.34	31.77	-56.7	0.89
Zibo	36.78	118.05	55.80	28.85	-67.7	0.85

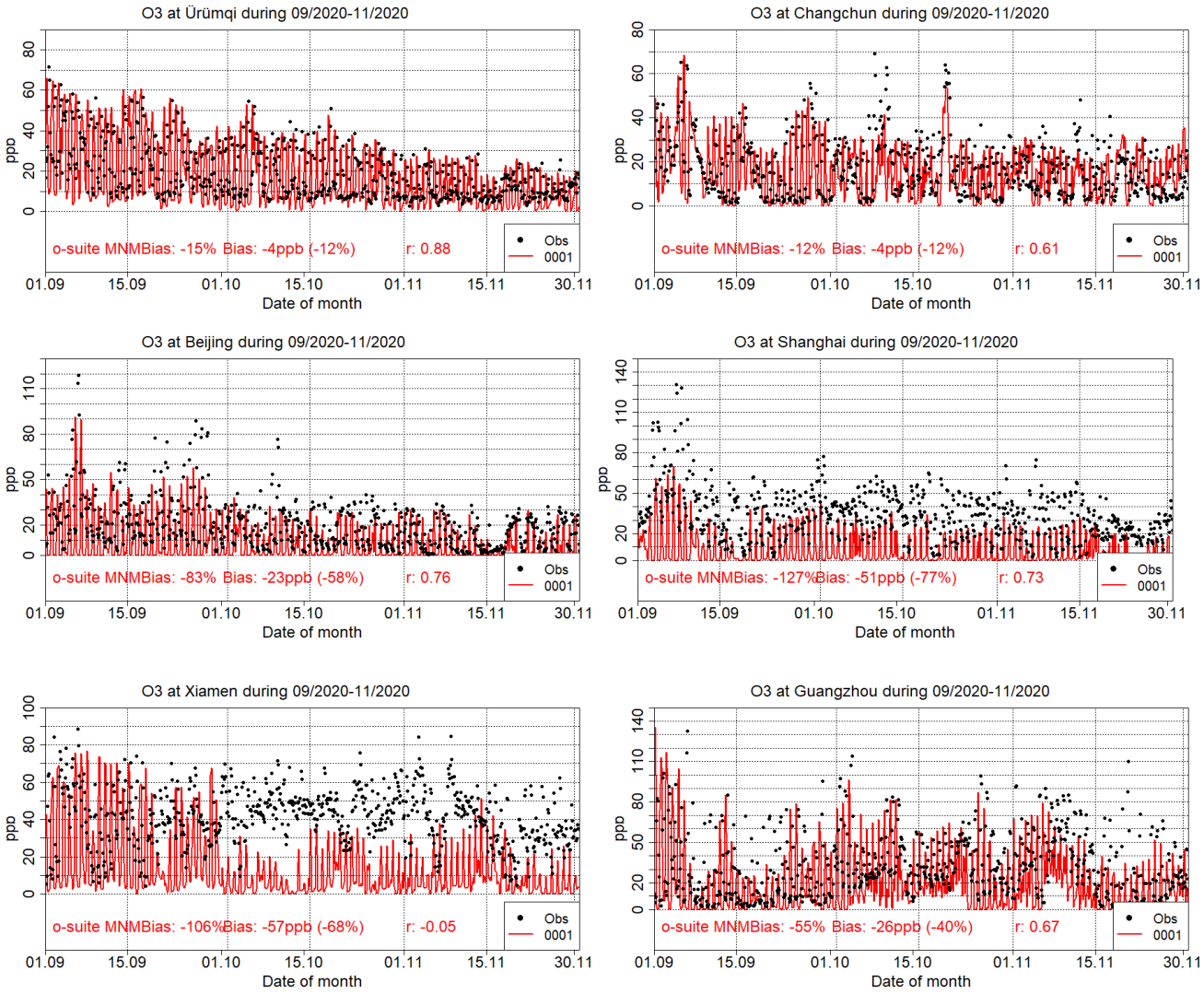

Figure 3.6.2: Surface ozone time series for the o-suite (red) compared to MarcoPolo-Panda project observations at Urumqi (43.83°N, 87.62°E, 1st row left), at Changchun (43.89°N, 125.33°E, 1st row right), at Beijing (39.92°N, 116.38°E, 2nd row left), at Shanghai (31.22°N, 121.47°E, 2nd row right), at Xiamen (24.48°N, 118.09°E, 3rd row left), and at Guangzhou (23.13°N, 113.25°E, 3rd row right).

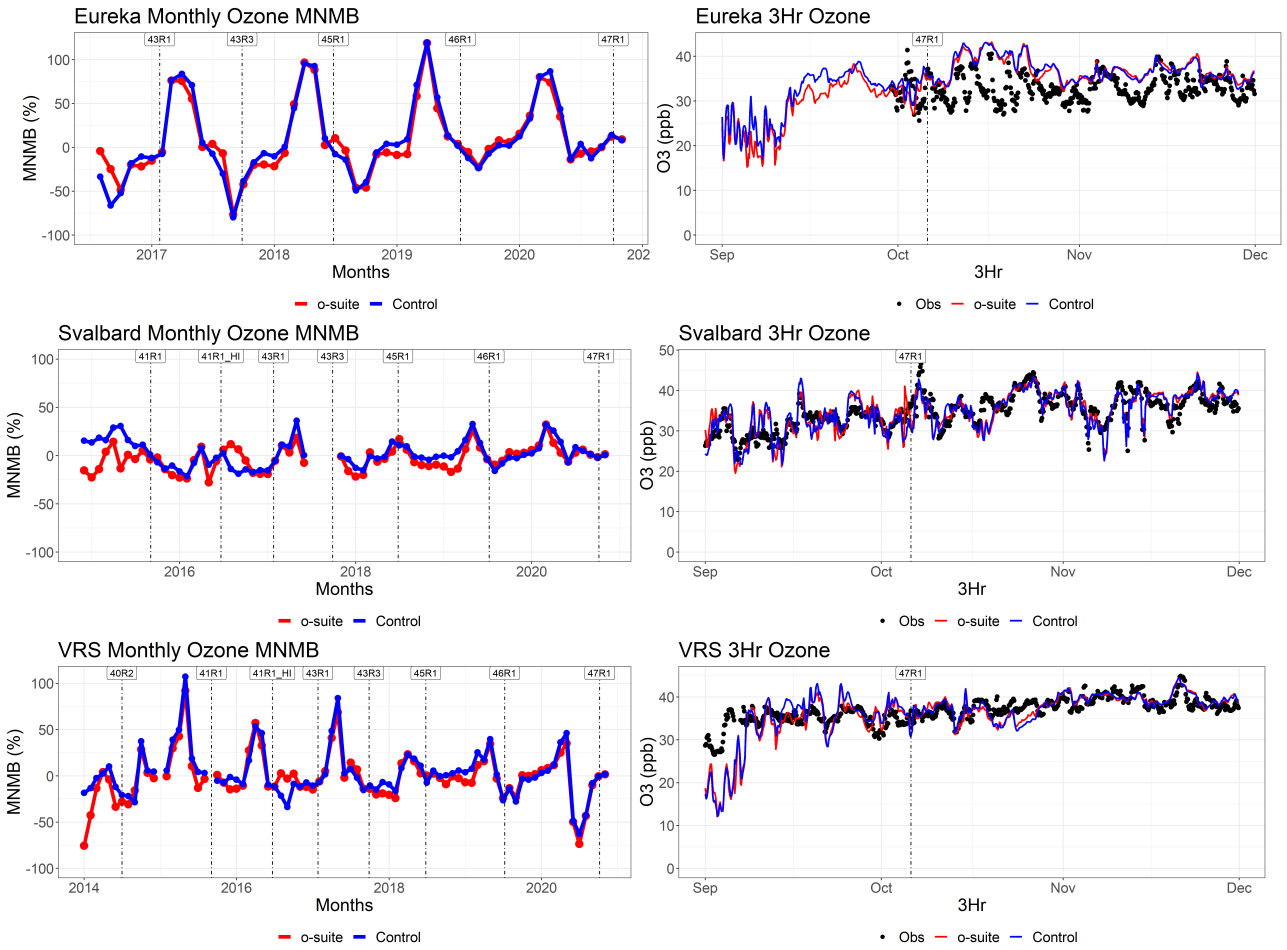

Figure 3.7.1: Time series for o-suite (red) and control (blue) compared to observations (black dots) at Eureka (top row), Svalbard (middle row) and the Villum Research Station, Station Nord, Greenland (bottom row) MNMB for the full period (left) and concentrations for September-November (right).

3.7 Validation with IASOA surface observations

CAMS results were compared to surface O_3 observations from the Villum Research Station, Station Nord in north Greenland (81.6°N 16.7°W) Eureka, Nunavut, Canada (80.1°N 86.4°W), and Zeppelin Mountain, Svalbard (78.9°N 11.9°E) from the IASOA network (Fig. 3.6.1).

The data from Svalbard and VRS are covering the period from December 2014 to November 2020. Data from Eureka covers the period August 2016 – November 2020. The CAMS simulations do not capture ozone depletion events in March – June in 2015 – 2020 at any of the sites. These events are related to halogen chemistry reactions that are not represented in the CAMS simulations. The simulations are on average in good agreement with the observations apart from the spring depletion events.

For the period September – November 2020 the measurements are not quality controlled. The CAMS simulations are capturing the surface O_3 levels very well at Svalbard and VRS. At Eureka, there is a gap in measurements for September and on average a small overestimation for the rest of the period (MNMB= 7% – 8%; Table 3.7.1). The o-suite and the control simulations are very similar in performance for all three sites (Table 3.7.1).

Table 3.7.1. Modified Normalised Mean Bias (MNMB) and correlation coefficient (r) of the CAMS o-suite and control simulations for the sites Eureka, Svalbard and Villum Research Station (VRS) for the period June – August 2020.

		MNMB	R
Eureka*	o-suite	0.07	0.26
	control	0.08	0.24
Svalbard	o-suite	0.00	0.78
	control	0.00	0.78
VRS	o-suite	-0.03	0.70
	control	-0.02	0.68

* Only data for October-November

3.8 Validation with IASI satellite data

Ozone total columns from the o-suite and control run are compared with IASI Metop-B version V6.5.0 daytime only satellite observations (Clerbaux et al., 2009). For the comparison with the IASI data, the vertically integrated model O_3 data were transformed using IASI averaging kernels (Rodgers, 2000).

The global distribution of the O_3 total column obtained from IASI, as well as the relative difference between the model runs and IASI, are shown in Fig. 3.8.1 for November 2020. Satellite data shows relatively high O_3 over the northern/southern mid- and high-latitudes, especially over the east of Russia and Canada and very low values over Antarctica. The o-suite run shows good agreement with observations with bias within 10%. The underestimation of ozone over cold areas in the Northern Hemisphere and over Antarctica is up to 20%. This is probably due to low IASI sensitivity over the cold surfaces. The IASI sensitivity is the lowest over the cold surfaces of Antarctica and Greenland (especially during March-April-May season) where IASI O_3 values are positively biased by up to 20%. The control run shows underestimation over the cold areas in the Northern Hemisphere (up to 20%) and overestimation over Antarctica and adjoined Southern Ocean (up to 30%). The forecast day 4 shows growing negative bias over the cold northern areas in Russia and Canada and growing positive bias over high southern latitudes.

Figure 3.8.2. shows data as a function of latitude and time from January till November 2020. IASI data show record-low ozone values over the Arctic in March and over Antarctic during September-November. O-suite run shows good agreement with observations with bias within 10% with some regional and temporal exceptions (e.g. bias about 20% over Southern high latitudes in October). Control run have distinct difference before September and after September with new control run. New control run shows relatively good results with bias within 10%. The overestimation of about 20% can be seen over southern high latitudes in October and November. The forecast day 4 shows smaller negative bias for both runs and growing positive bias over high southern latitudes in control run.

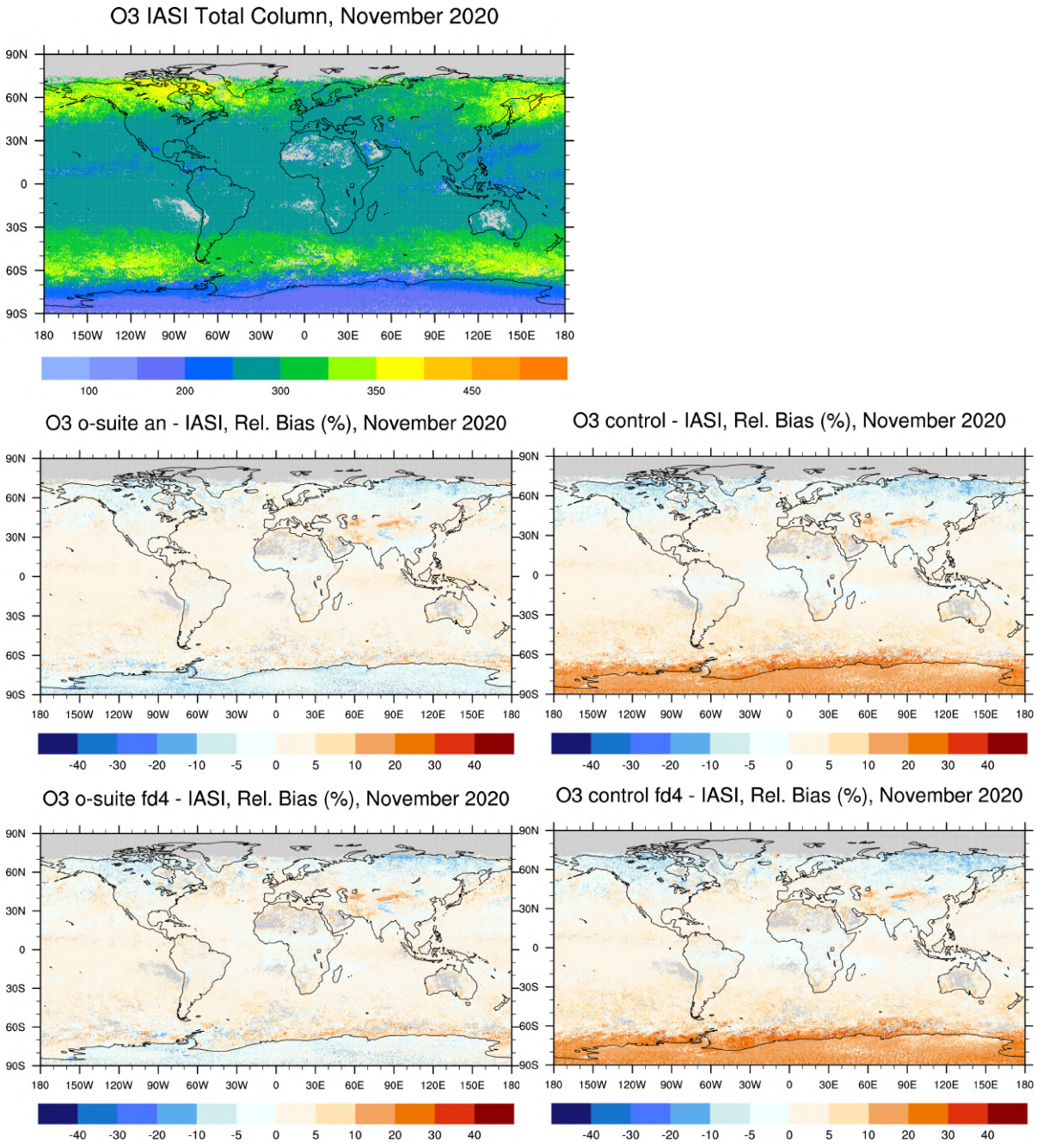

Figure 3.8.1: O_3 total column for IASI satellite observations (top) and relative difference between the model runs and IASI for November 2020: o-suite analysis and forecast day 4 (left), control run and control run forecast day 4 (right). Grey colour indicates missing values.

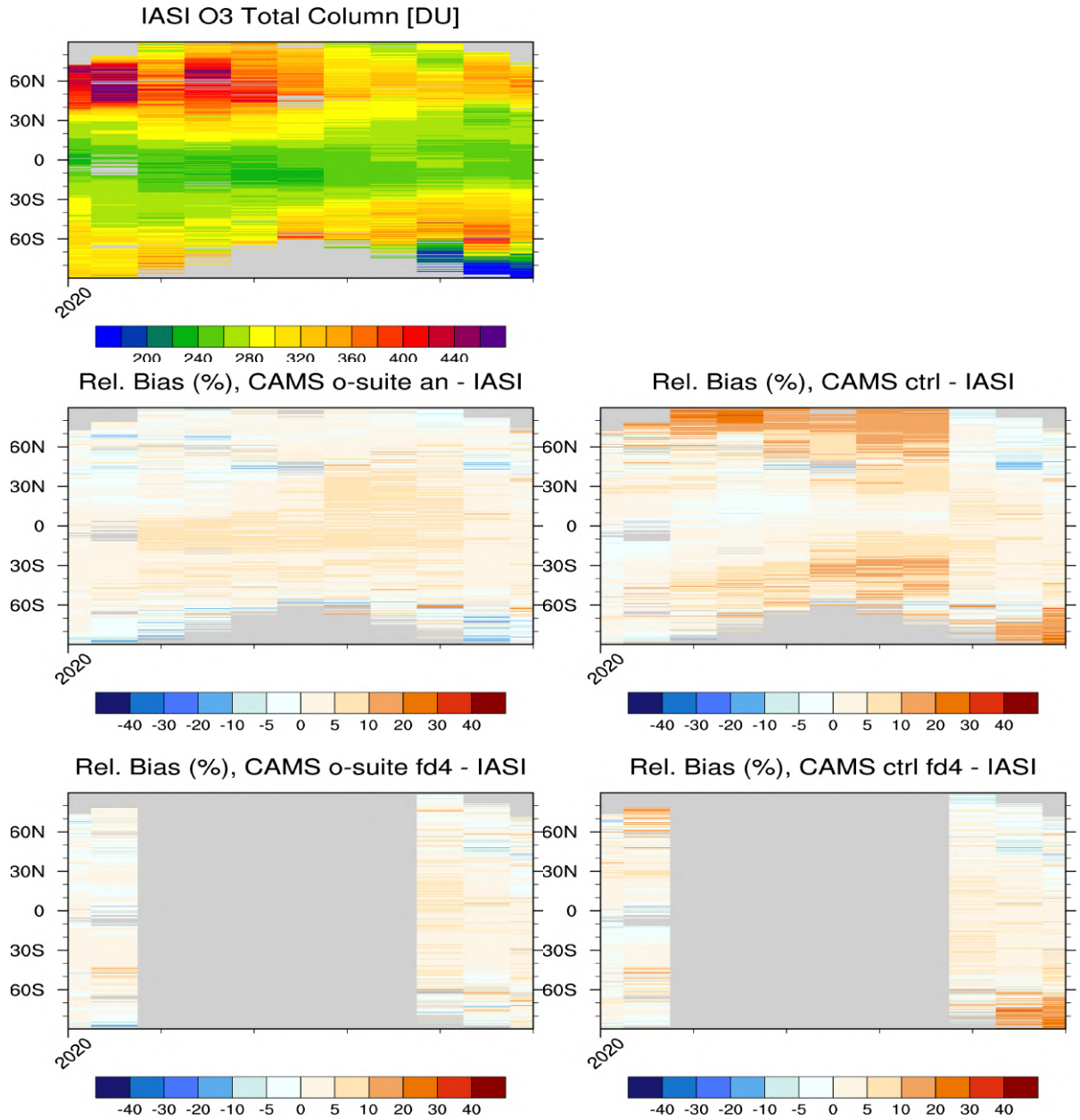

Figure 3.8.2: IASI Metop-A O_3 total column (top) as function of latitude and time from January to November 2020. Relative difference between the model runs and IASI: o-suite analysis and forecast day 4 (left), control run and control forecast day 4 (right). Grey colour indicates missing values.

4. Carbon monoxide

4.1 Validation with Global Atmosphere Watch (GAW) Surface Observations

For the Near-Real-Time (NRT) validation, 10 GAW stations have delivered CO surface mixing ratios in NRT and data is compared to model results as described in Eskes et al. (2021) and is used for CAMS model evaluation for September to November 2020. The latest validation results can be found on the CAMS website, see section 1.

Both runs mostly show negative MNMBs for stations in the Northern Hemisphere (Fig. 4.1.1).

A comparison of the seasonal-mean MNMB over Europe (Fig. 4.1.2) from December 2012 to present shows an improving MNMB from about -20% in 2013 to less than -10% for more recent periods. Temporal correlation remains relatively constant at r=0.6 on average, except for the quarter JJA in 2018, where the correlation of the control run drops to 0.24.

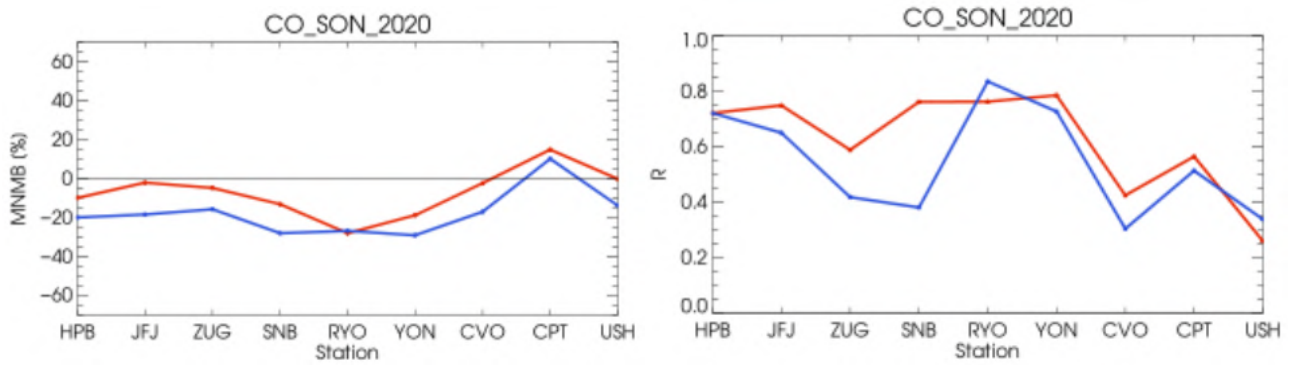

Figure 4.1.1: Modified normalized mean bias in % (left) and correlation coefficient (bottom right) of the NRT model runs compared to observational GAW data in the period September-November 2020 (o-suite: solid red, and control: blue).

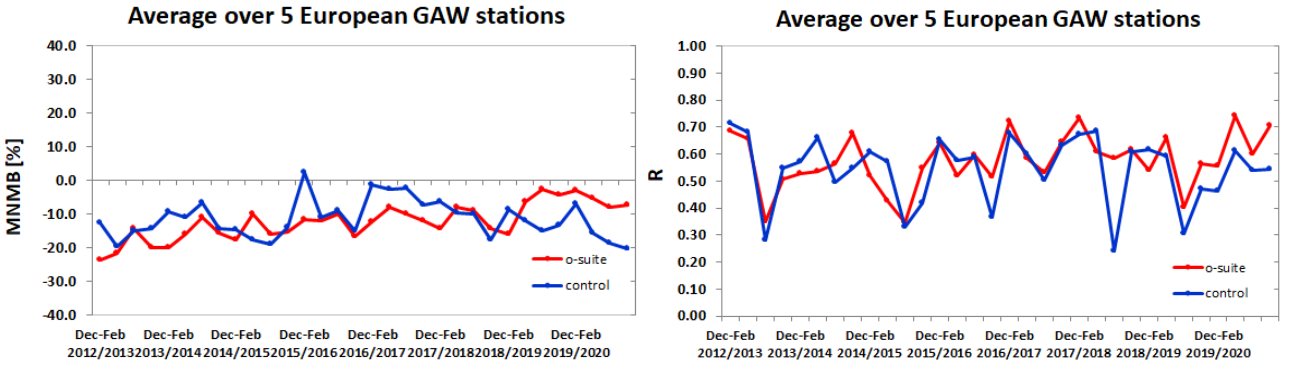

Figure 4.1.2: Long term (Dec. 2012 – November 2020) evolution of seasonal mean MNMB (left) and correlation (right), as averaged over 5 GAW stations in Europe, for o-suite (red) and control (blue).

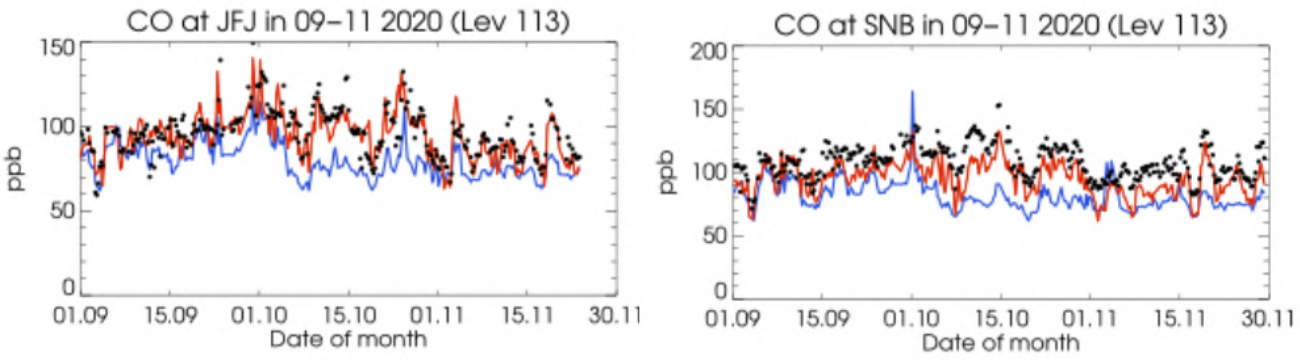

Figure 4.1.3: Time series for the o-suite (red) and control (blue) compared to GAW observations for and Jungfraujoch (46.55°N, 7.99°E) and Sonnblick (47.05°N, 12.96°E).

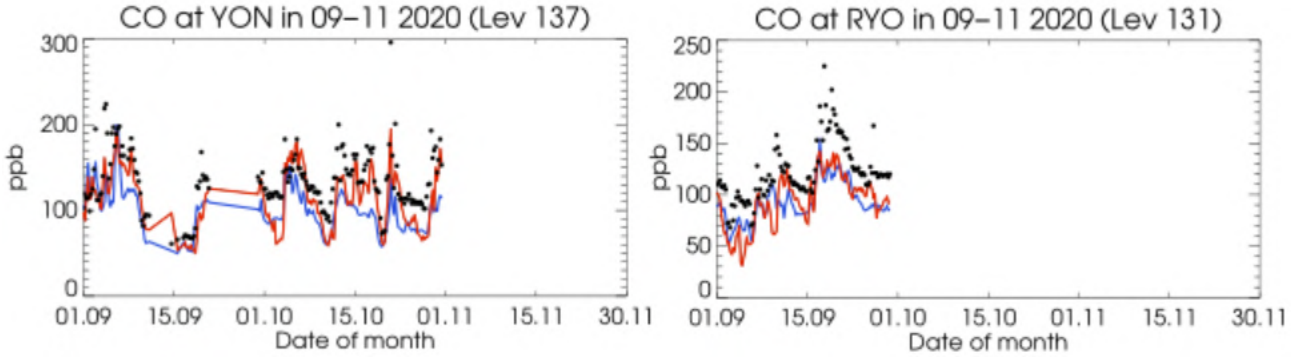

Figure 4.1.4: Time series for the o-suite (red) and control (blue) compared to GAW observations at Yonagunijima (24.47°N, 123.02°E) and Ryori (39.03°N, 141.82°E).

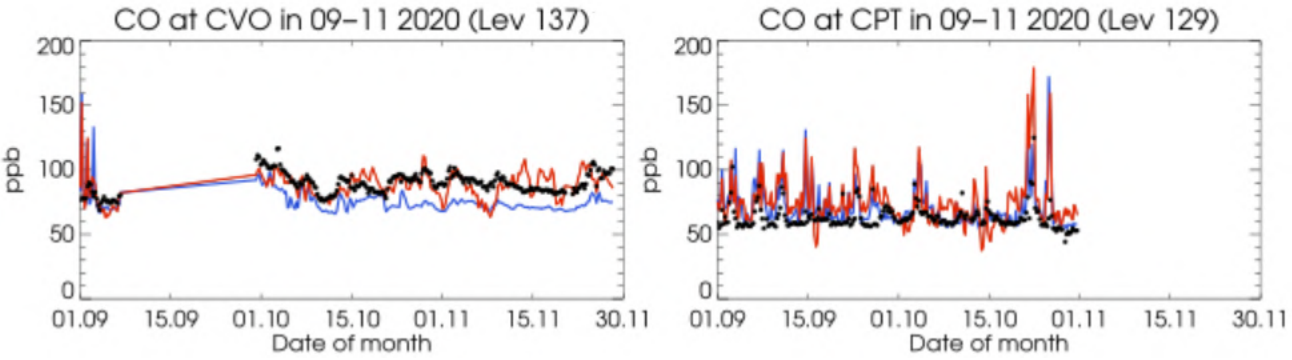

Figure 4.1.5: Time series for the o-suite (red) and control (blue) compared to GAW observations at Cape verde (16.85°N, -24.87°W) and Cape Point (34.35°S, 18.5°E).

For European stations (Fig. 4.1.3), the o-suite shows only a slight underestimation of CO with MNMBs mostly within 13%, whereas the control run underestimates the observations with MNMBs up to -28%. Correlation coefficients are between 0.59 and 0.76 for the o-suite and between 0.38 and 0.72 for the control run.

For Asian stations, CO mixing ratios are underestimated by up to -28% by both runs. Correlation coefficients range between 0.76 and 0.79 for the o-suite and between 0.73 and 0.84 for the control run (Fig. 4.1.4).

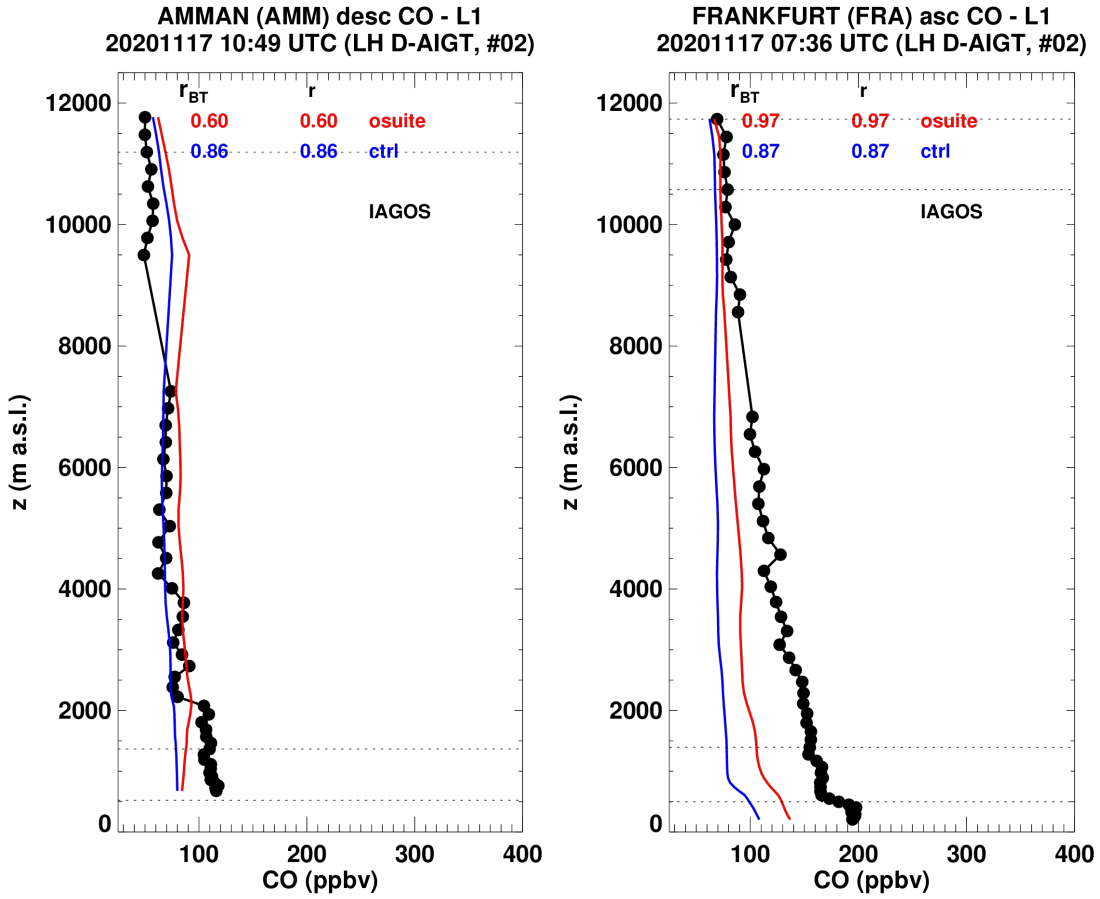

Figure 4.2.1.: Vertical profiles of CO measured with the IAGOS aircraft over Frankfurt and Amman on 17 November 2020, compared to o-suite (red) and control (blue).

For CVO, MNMBs is -2 for o-suite with a correlation of 0.42 and MNMBs is -17 for control run with a correlation of 0.3 (Fig.4.1.5).

For the two stations in the Southern mid-latitudes (CPT and USH), MNMBs vary between almost 0% and -14% for the o-suite and between 10% and -13% for the control run. Correlation coefficients are relatively low for both runs (for the o-suite 0.26 (USH) and 0.56 (CPT) and for the control 0.34 (USH) and 0.51 (CPT).

4.2 Validation with IAGOS Data

Unfortunately, due the covid-19 crisis and its impact on the airlines operations, only one IAGOS flight have been recorded during this reporting period. This is the first time since the beginning of IAGOS that we have almost no data to provide. The following period (DJF) will provide regular measurements again. For more detailed comparisons against IAGOS we refer to the previous NRT report, period JJA-2020 (Ramonet et al., 2021)

Figure 4.2.1 shows the results for a flight between Frankfurt and Amman on 17 November. CO over Frankfurt is underestimated by CAMS, with the analysis performing better than the control run. The CO concentrations observed over Amman are well captured by the CAMS o-suite and control, with a bit of underestimation near the surface, and overestimation at around 9 km altitude.

4.3 Validation against FTIR observations from the NDACC network

In this section, we compare the CO profiles of the CAMS products with FTIR measurements at 21 FTIR stations within the NDACC network. These ground-based, remote-sensing instruments are sensitive to the CO abundance in the troposphere and lower stratosphere, i.e. between the surface and up to 20 km altitude. Tropospheric and stratospheric CO partial columns are validated. A description of the instruments and applied methodologies can be found at .

Figure 4.3.1 show that the o-suite tropospheric columns of CO agree well. The model upgrade (60 to 137 levels) implemented in July 2019 changes the overall biases in both the troposphere and stratosphere. The negative bias for the tropospheric columns increased from -2% before July 2019 to -7% in the most recent quarterly and is larger than the reported measurement uncertainty. The stratospheric column bias also changed to -7% in SON 2020 compared to values well above +10% before July 2019. There are no large differences between the o-suite AN and 1d FC, except at Boulder and Jungfraujoch where the o-suite AN performs significantly worse than the o-suite 1d forecast.

Figure 4.3.2 shows a negative trend in the tropospheric CO column at Jungfraujoch (4km – TP) of about 2% per year. A similar trend is observed at Zugspitze (3km above sea level), but not at other non-mountain sites like St Petersburg. The trend at the o-suite 1dFC at both mountain stations is much lower (around -0.5%/y), which suggests the trend is located in the upper tropospheric column and is related to the assimilation.

The Taylor diagrams in Figure 4.3.3 provide information on the correlation of all three CAMS products under consideration with the FTIR time series. Leaving out the sites with few measurements, the assimilation has a positive effect on the correlation coefficient. Looking at the correlation values for the period 2020 SON, the o-suite 1d FC (averaged correlation for all sites is 0.84) is slightly worse to the o-suite AN (averaged correlation for all sites is 0.9).

Table 4.3.1: Detailed statistics for tropospheric CO column comparisons for FTIR measurements during SON 2020. Both analysis and 1d FC o-suite behave similar, except at Boulder and Jungfraujoch where the bias is significantly lower for the o-suite AN.

	o-suite AN tropospheric column					o-suite 1d FC tropospheric column					
FTIR site	#	rel. std	corr	rel diff (%)	rel diff std(%)	#	rel. std	corr	rel diff (%)	rel diff std(%)	lat
THULE	30	0.9	0.96	-14.31	4.12	30	0.8	0.96	-13.72	4.37	76.5
ST.PETERSBURG	10	1.3	0.95	-5.9	2.98	10	1	0.97	-4.62	2.4	59.9
BREMEN	7	1.1	0.63	-5.34	5.74	7	1.3	0.25	-8.33	7.12	53.1
JUNGFRAUJOCH	26	1.1	0.96	-13.82	3.51	26	1.2	0.91	-5.79	5.09	46.6
TORONTO	35	0.8	0.92	-1.91	8.76	35	1	0.89	-5.26	7.67	43.6
BOULDER.CO	42	0.9	0.79	-15.1	11.04	42	0.8	0.61	-7.23	15.26	40
MAUNA.LOA.HI	45	1	0.95	-11.84	2.92	45	0.9	0.94	-11.09	3.49	19.5
ALTZOMONI	3	0.8	0.97	-8.87	5.07	3	1.1	0.96	-4.82	3.22	19.1
WOLLONGONG	42	1.2	0.81	-8.11	9.28	42	1.2	0.8	-5.76	9.58	-34.4
LAUDER	62	1.1	0.96	-4.18	3.51	62	1.1	0.96	-3.81	3.57	-45
ARRIVAL.HEIGHTS	25	1	0.96	2.09	1.92	25	0.9	0.96	2.26	2.02	-77.8
		1	0.9	-7.93	5.35		1	0.84	-6.2	5.8	

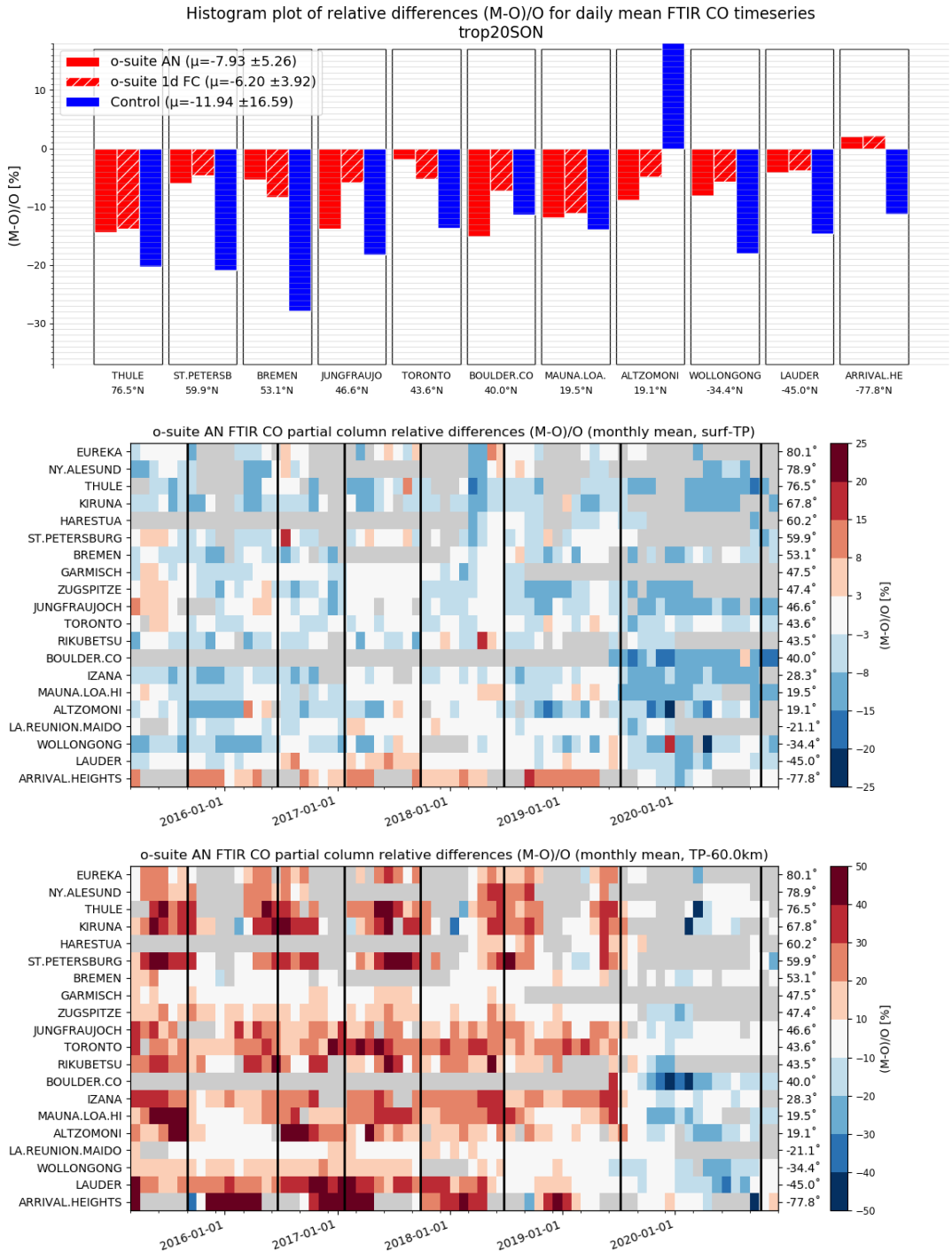

Figure 4.3.1: Seasonal relative mean bias for tropospheric CO columns (MB, %) for the considered period SON 2020 (top) and monthly mean biases for a longer time period for the tropospheric CO columns (middle) and stratospheric CO columns (bottom) (o-suite upgrades are indicated in black vertical lines, stations are sorted by latitude).The overall uncertainty for the CO measurements is approximately 3% on the tropospheric columns and 10% for the stratospheric columns. The o-suite analysis averaged bias in tropospheric columns increased to -6% for SON compared to -2% bias before the model update in July 2019. The bias in the stratosphere reduced to -8.5% compare to +18% before July 2019 and is comparable to the measurement's uncertainty.

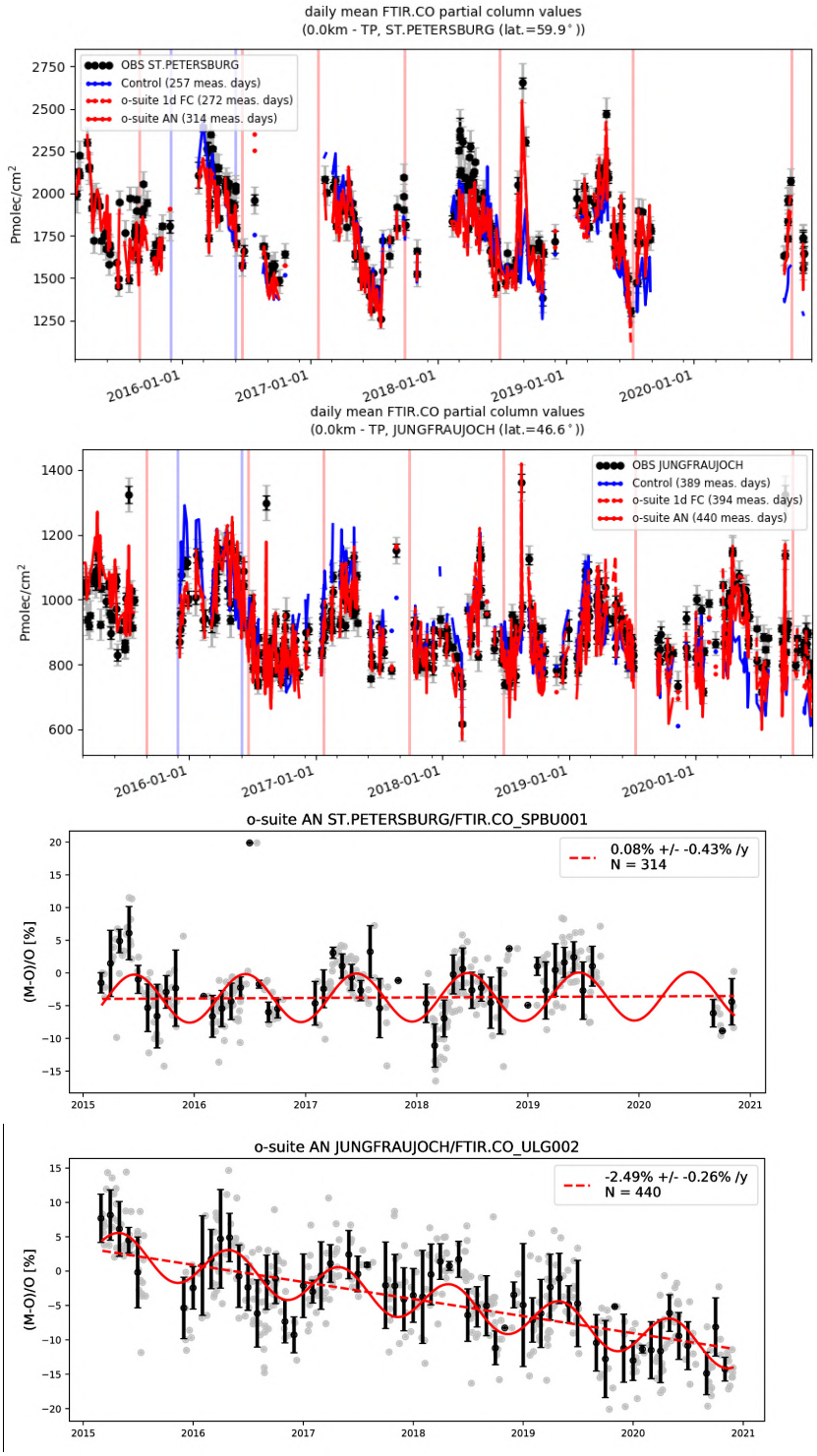

Figure 4.3.2: Top: daily mean values of tropospheric CO columns by the o-suite (AN and 1d FC, red) and the control run (blue) compared to NDACC FTIR data at St Petersburg and Jungfraujoch for the period March 2015-November 2020. During March 2018 the o-suite underestimated the CO columns at St. Petersburg. The bottom two rows contain a linear fit and seasonal cycle fit through the relative differences for the o-suite AN. An underestimation is observed during the local autumn/winter months. The negative trend at Jungfraujoch is -1%/y in the o-suite 1dFC and 2.5% in the o-suite AN.

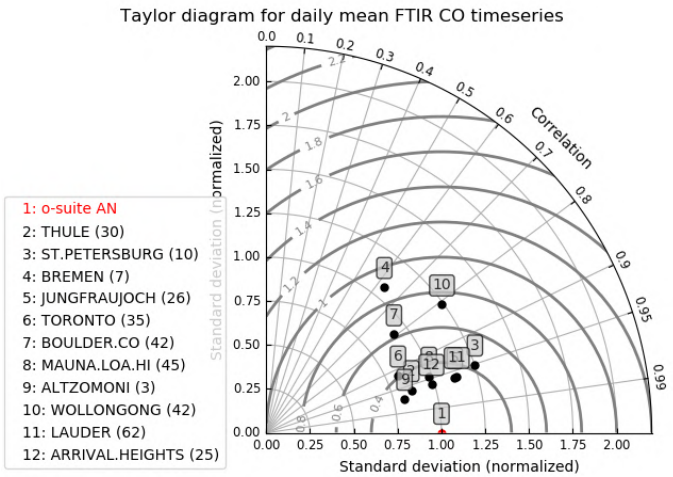

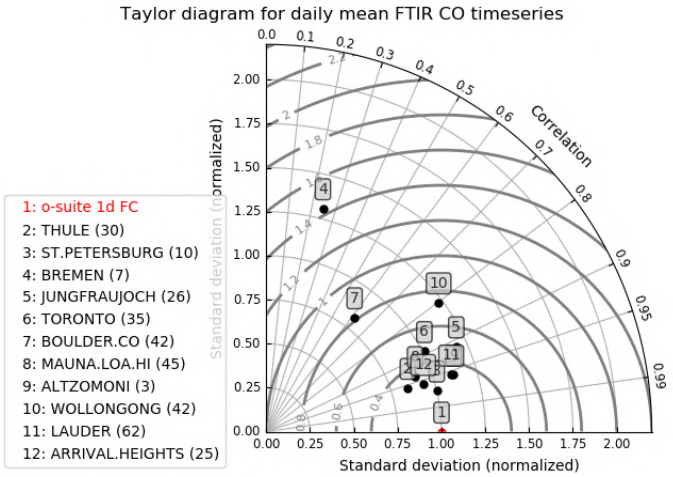

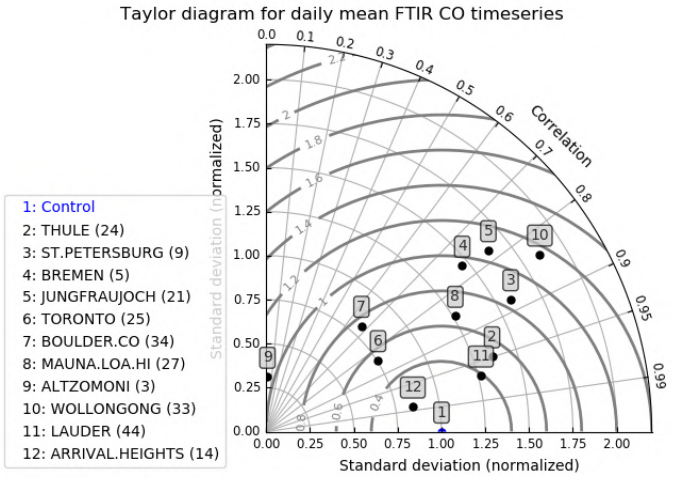

Figure 4.3.3: Taylor diagrams relating the standard deviations for the model /GB time series of tropospheric CO column data and their correlation. All time-series are normalised such that the std of the model is 1. Wollongong has low correlation in this quarter because the number of measurements is low and because background values are measured.

4.4 Validation against FTIR observations from the TCCON network

CO column averaged mole fractions of the CAMS models are compared with data from the Total Carbon Column Observing Network (TCCON). Column averaged mole fractions provide different information content than the in situ measurements and are therefore complementary to the in situ data. In this section, we compare column averaged mole fractions of CO of the CAMS models with TCCON retrievals. Data from the following TCCON sites has been used:

Izana (Blumenstock et al., 2017), Reunion (De Mazière et al., 2017), Bialystok (Deutscher et al., 2019), Manaus (Dubey et al., 2017), Four Corners (Dubey et al., 2017), Ascension (Feist et al., 2014), Anmeyondo (Goo et al., 2017), Darwin (Griffith et al., 2017), Wollongong (Griffith et al., 2017), Karlsruhe (Hase et al., 2017), Edwards (Iraci et al., 2017), Indianapolis (Iraci et al., 2017), Saga (Kawakami et al., 2017), Sodankyla (Kivi et al., 2017), Hefei (Liu et al., 2018), Tsukuba (Morino et al., 2017), Burgos (Morino et al., 2018), Rikubetsu (Morino et al., 2017), Bremen (Notholt et al., 2017), Spitsbergen (Notholt et al., 2017), Lauder (Sherlock et al., 2017, Pollard et al., 2019), Eureka (Strong et al., 2018), Garmisch (Sussmann et al., 2017), Zugspitze (Sussmann et al., 2018), Paris (Te et al., 2017), Orleans (Warneke et al., 2017), Park Falls (Wennberg et al., 2017), Caltech (Wennberg et al., 2017), Lamont (Wennberg et al., 2017), Jet Propulsion Laboratory (Wennberg et al., 2017), East Trout Lake (Wunch et al., 2017), Nicosia (Petri et al., 2020)

For the validation of the models in September, October and November the only site that made data available for the whole comparison period was Nicosia.

For the comparison period the osuite AN- and the osuite FC- model simulations compare very well with the measurements (Fig 4.4.1). These two models slightly underestimate the CO for all sites except Pasadena (Fig. 4.4.1 and Fig. 4.4.3). For the control model the underestimation is significantly higher(Fig. 4.4.1 and Fig. 4.4.3).

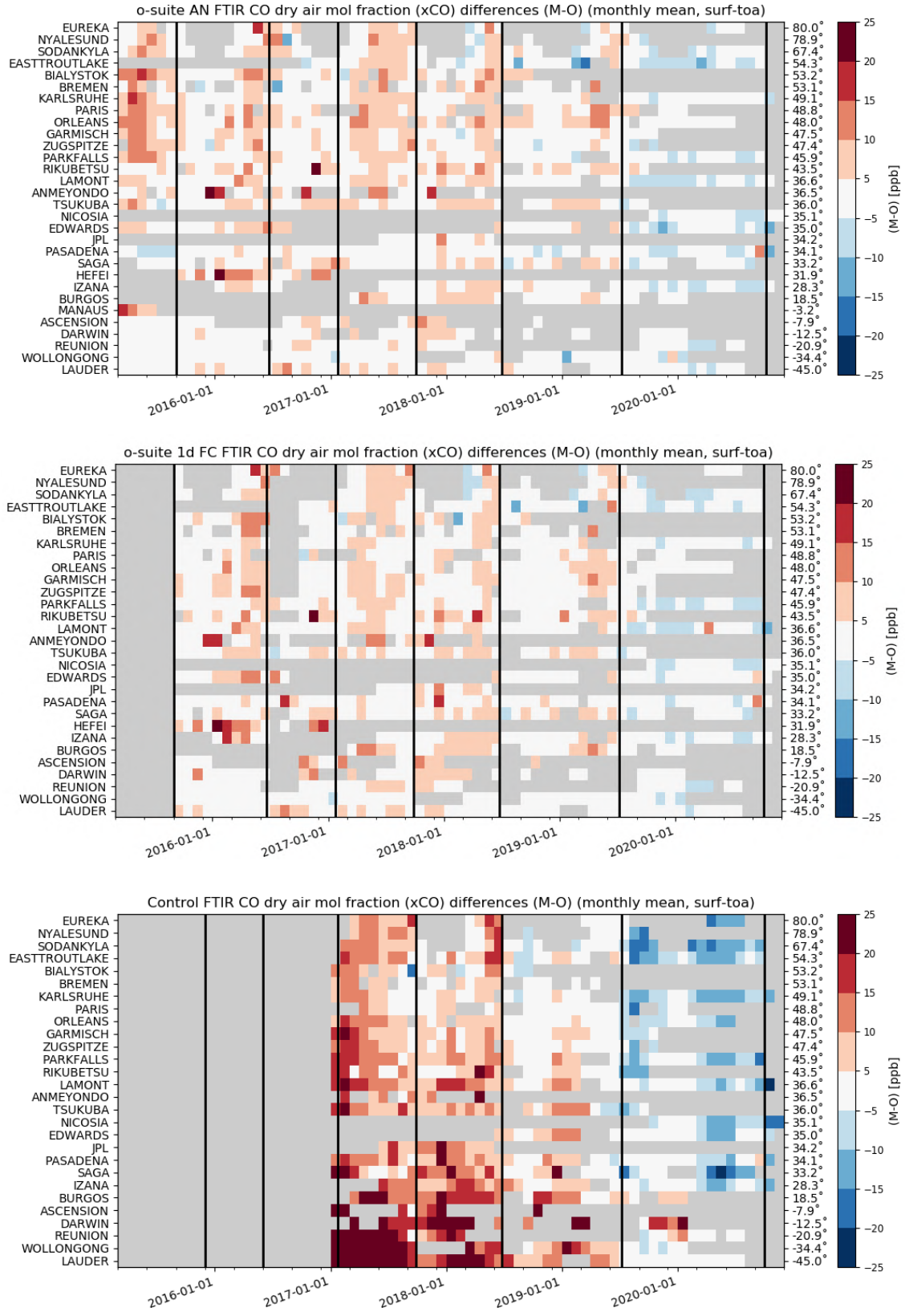

Figure 4.4.1: Monthly differences since March 2017. The stations are sorted by latitude (northern to southern hemisphere).

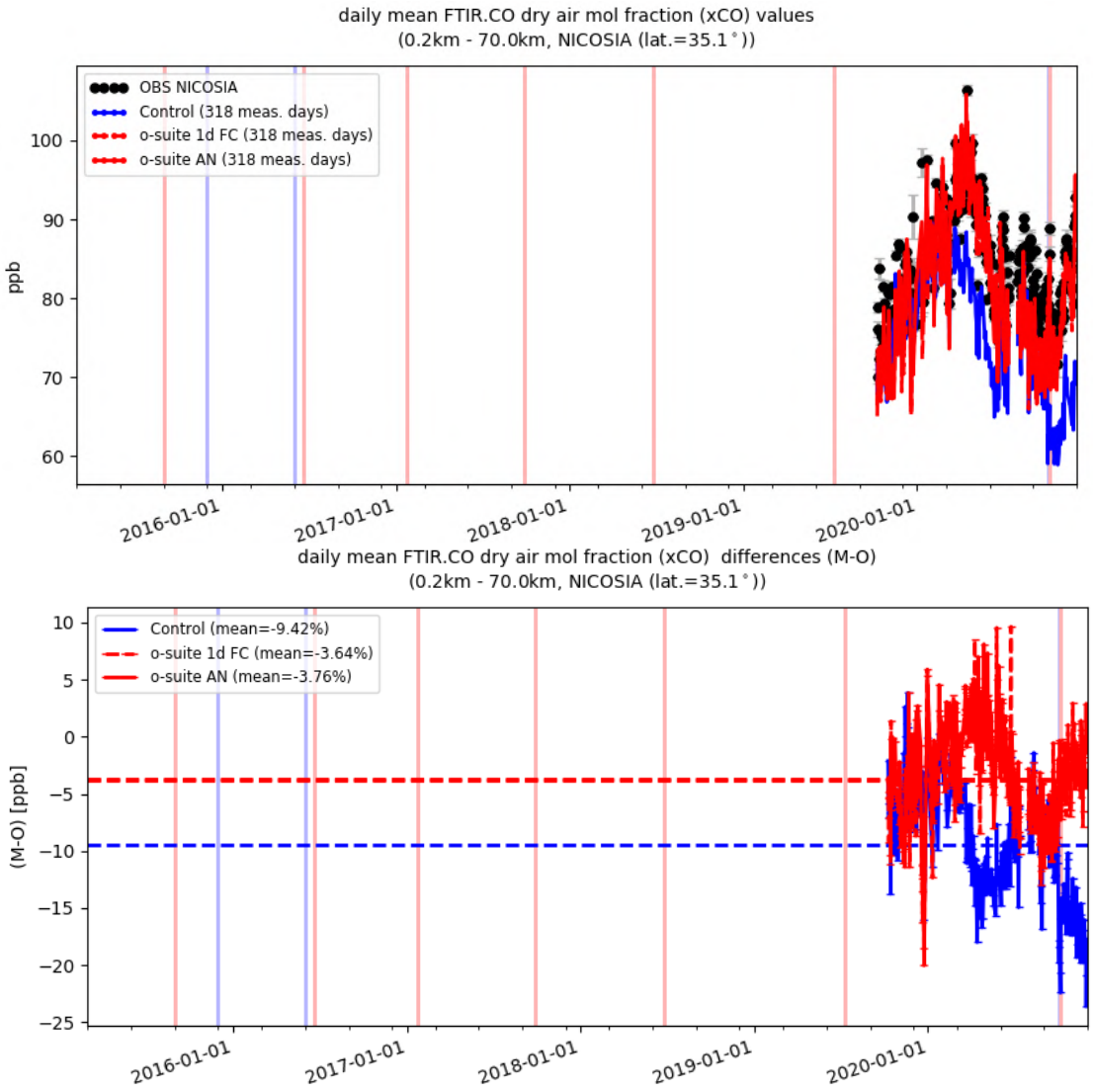

Figure 4.4.2: Comparison of the CO model data with TCCON CO at Nicosia.

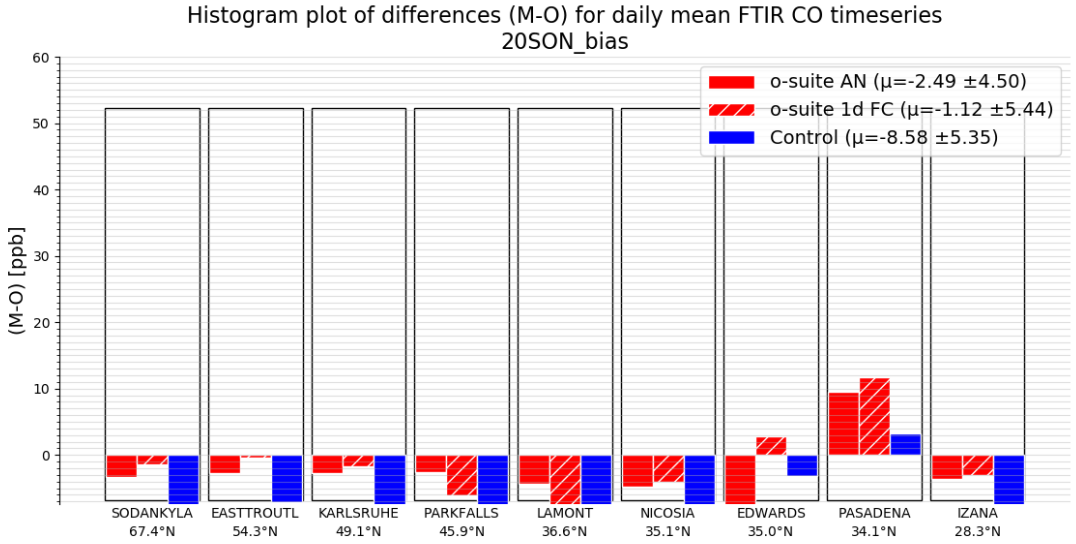

Figure 4.4.3: Differences during the reporting period. The different sites cover different periods of the comparison period.

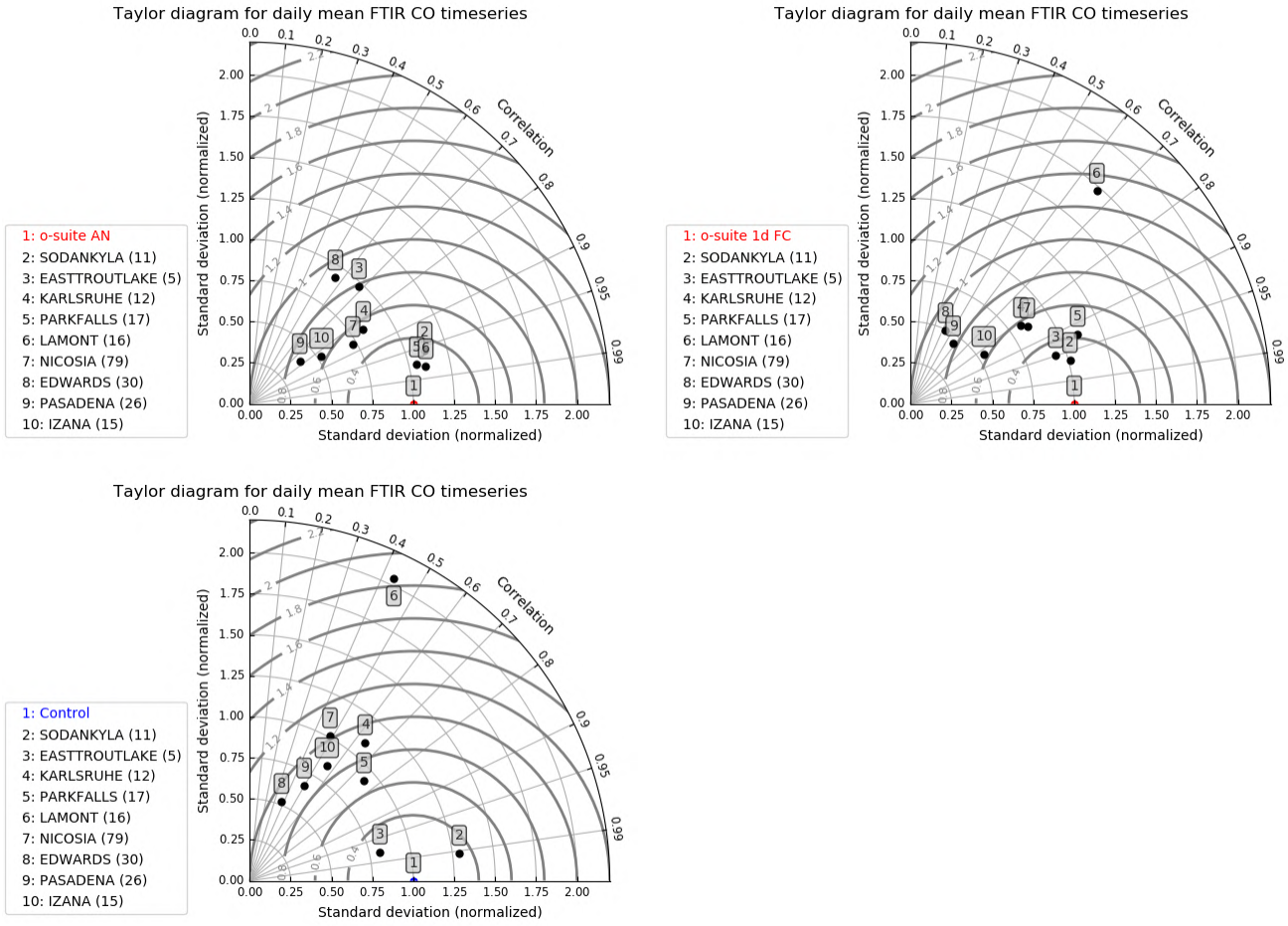

Figure 4.4.4: Taylor diagrams for the comparison period.

4.5 Evaluation with MOPITT and IASI data

In this section, modeled CO total columns are compared to MOPITT version 8 (thermal infrared radiances) (Emmons et. al., 2009, Deeter et al., 2010) and IASI satellite retrievals (Clerbaux et al., 2009). Figure 4.5.1 shows the global distribution of CO total columns retrieved from MOPITT V8 (top left) and IASI (top right) and the relative biases of the model runs with respect to MOPITT V8 (analysis and forecast day4)(middle). MOPITT shows high values over the biomass burning area in South America, over south Africa, India and East of China. IASI shows higher values over the above-mentioned regions.

The modeled CO geographical distribution and magnitude of values show that the model performs reasonably well. The relative difference between the model runs and MOPITT shows that the o-suite performs better than the control run without data assimilation. The o-suite underestimates the satellite data by about 10% with some regional exceptions where the negative bias reaches 20% (mostly over the land). The model shows overestimation over the areas with high CO values mentioned above (up to 20%). The control run shows an overestimation of the satellite data by about 30%, except biomass burning area in North Africa, China and Indonesia, where model has a positive bias (up to 20%). The o-suite run shows a growing positive bias on the 4th forecast day over the areas with high CO values, as well as a growing negative bias over Sahara and biomass burning area in South Africa, over Australia and other areas.

In comparison to IASI data (Fig. 4.5.2), the o-suite run has a positive bias over the low latitudes and middle northern latitudes of about 20% and a negative bias over the high southern latitudes up to 30%. The control run shows in generally underestimation by about 30% and in some areas up to 50% (over the biomass burning areas in South America and Southern Africa).

Figure 4.5.3 shows time series of CO total column for MOPITT V8, IASI and the model runs over the eight selected regions. For the comparison with MOPITT, the modelled CO concentrations were transformed using MOPITT V8 averaging kernels (Deeter, 2004). Both, MOPITT and IASI CO total columns are assimilated in the o-suite run, while a bias correction scheme is applied to IASI data to bring it in line with MOPITT. MOPITT and IASI CO total columns show a relatively similar variability over different regions. IASI CO values are lower than MOPITT over most regions with some seasonal exceptions till the year 2016. Since then IASI and MOPITT are more consistent with each other over Europe, the US and East Asia. Significant difference between MOPITT and IASI are observed over the Alaskan and Siberian fire regions in winter seasons, with IASI CO total column values being lower up to 30%. In North and South Africa, deviations become larger since 2016 with IASI values being higher than MOPITT by up to 20%. The modelled seasonality of CO total columns is in relatively good agreement with the retrievals. In general, the comparison between the o-suite and control run shows that the assimilation of satellite CO has a more positive, pronounced impact on model results over East and South Asia, South Africa, and since the end of 2016, over the US in winter and spring seasons, and smaller impact over the other regions. Since June 2016, the o-suite shows very good agreement with the satellite retrievals over Europe and the US with biases less than 5%. In late summer and early autumn of 2018 over Europe, the control run has larger negative biases compared to the satellite data then early in 2018 and the two previous autumn seasons.

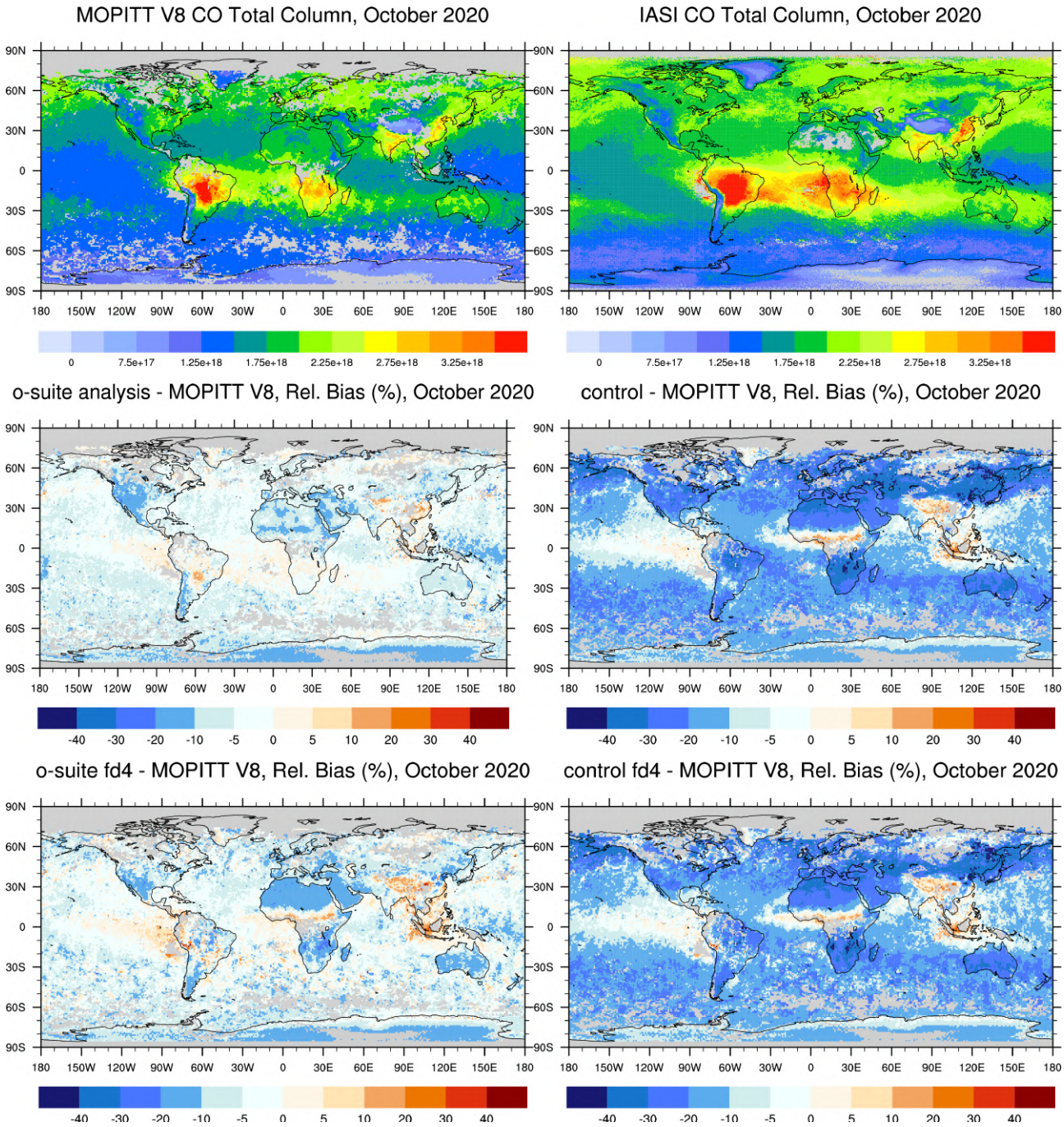

Fig. 4.5.1: CO total columns for MOPITT V8 (top left) and IASI (top right) satellite retrievals and relative difference between the model runs and MOPITT for January 2020: o-suite analysis (middle left), control run (middle right), o-suite 4th forecast day (middle left), o-suite 4th forecast day (midle right). Grey colour indicates missing values.

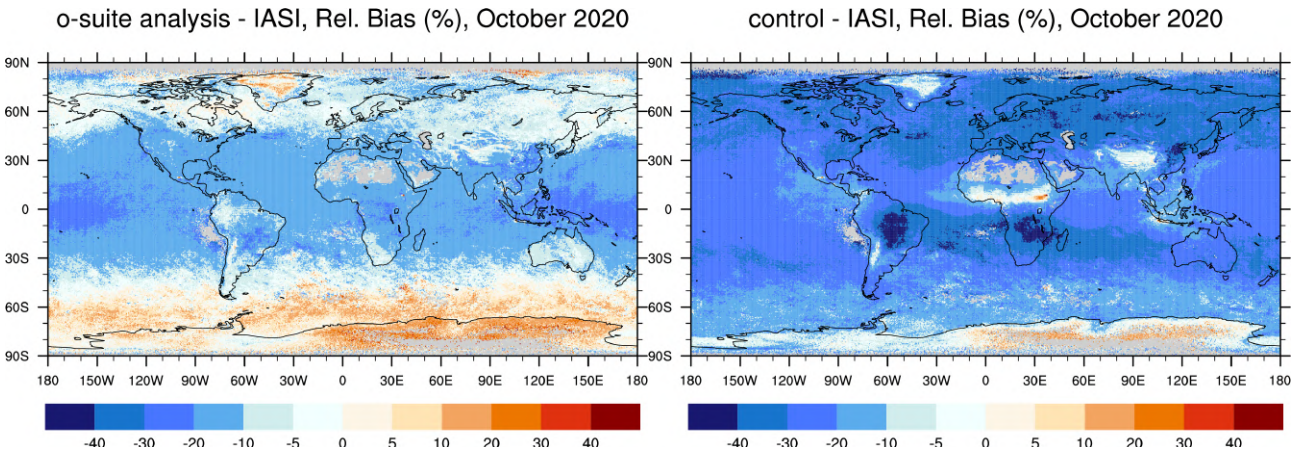

Fig. 4.5.2: Relative difference between the model runs and IASI: o-suite analysis (bottom left), control run (bottom right). Grey colour indicates missing values.

A general reduction of CO values from the year 2015 to the year 2018 can be seen over Europe, the US and East Asian regions. The South African region shows a slight increase of the seasonal minimum compared to previous springs. Summer 2019 was characterised by a strong fire events in Siberia. This can be seen in IASI data (peak in August), but it is not reflected in the MOPITT data partly due to only few days of observations available in August.

In SON 2020, the CO concentration over Europe, US, Siberian fire region and African regions are increased compared to previous year. The CO peak in September over South Africa reached maximal values for the last three years and is captured by the o-suite very well, while the 4th day forecast is underestimated by about 20%. The control run didn't capture the peak.

The modified normalized mean bias (MNMB) of the model runs compared to MOPITT V8 (Fig. 4.5.4) allows quantifying the impact of the assimilation on the model performance. In year 2020, the o-suite model run shows negative biases over all selected regions within 10%. The better agreement can be seen over Europe and East and South Asian regions with bias within 5%.

The control run shows a systematic positive bias up to 20% over South Asia in November-December 2014, 2015, 2016, and 2017. Over southern Africa the control run overestimates satellite retrieved values by up to 25% in winter and spring 2015, 2016, and 2017. In general, the o-suite is within +/- 10% in all regions, while the control run shows larger biases over East and South Asia and North and South Africa, as well as stronger seasonal cycles.

Starting from the second half of the year 2019, the negative biases over Europe and US increase for both runs (from about 5% to about 10% for o-suite). The o-suite results over Asian regions improved and are very close to the observations, especially over East Asia. The control run shows reduction of biases over South Asia. Change of bias sign from positive to negative and/or increase of the negative bias can be seen over all selected regions for both runs. For the control run, the strong increase of negative bias in September-October can be seen over Europe, US, Siberian and Alaskan fire regions and over South African region.

In general, the increase of underestimation in both runs can be seen over the selected regions.

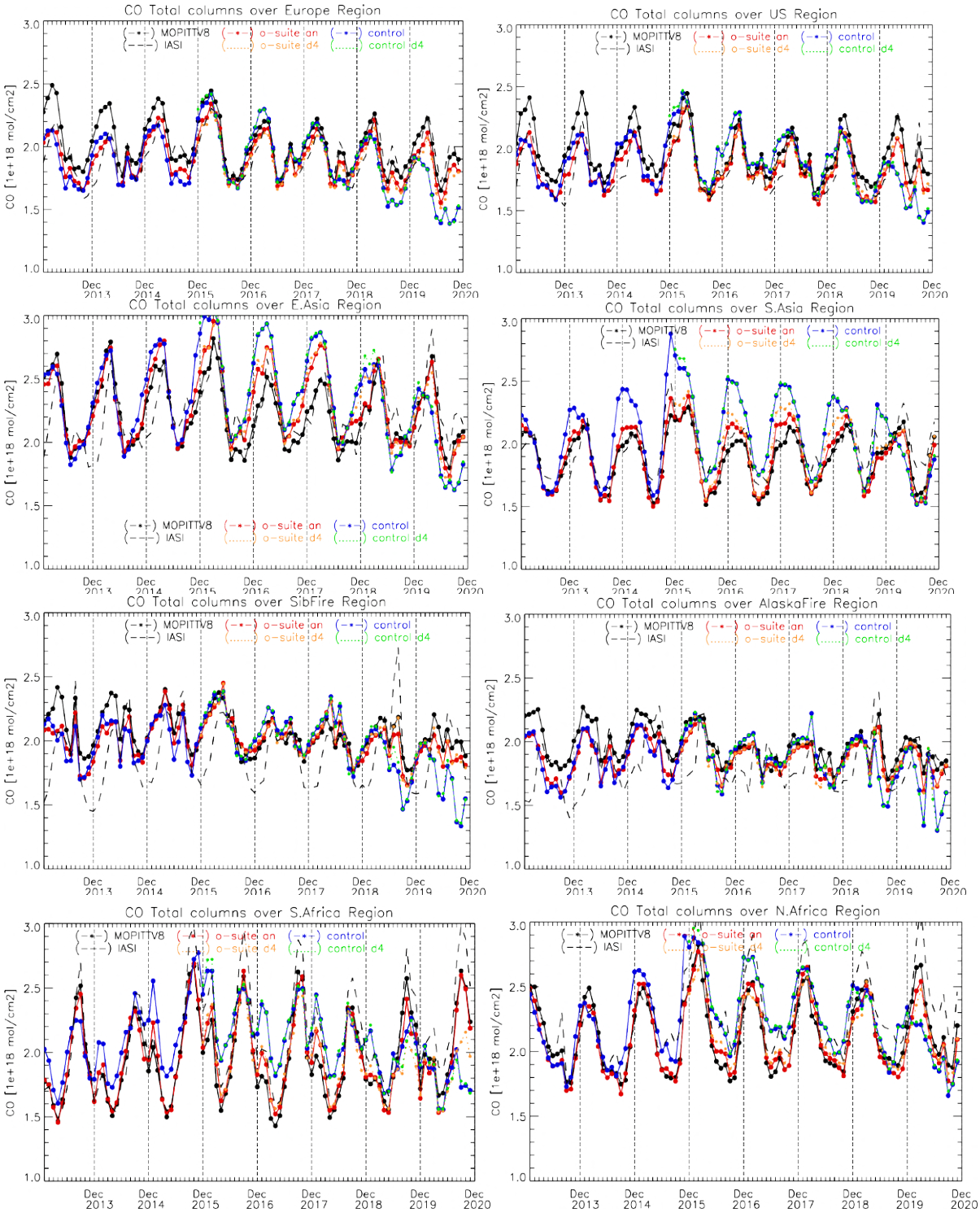

Fig. 4.5.3: Time series of CO total columns for satellite retrievals MOPITT V8, IASI (black) and the model runs over the selected regions: o-suite analysis (red, solid), control (blue, solid), o-suite 4th forecast day (orange, dotted), control 4th forecast day (green, dotted). Period: January 2013 to November 2020.

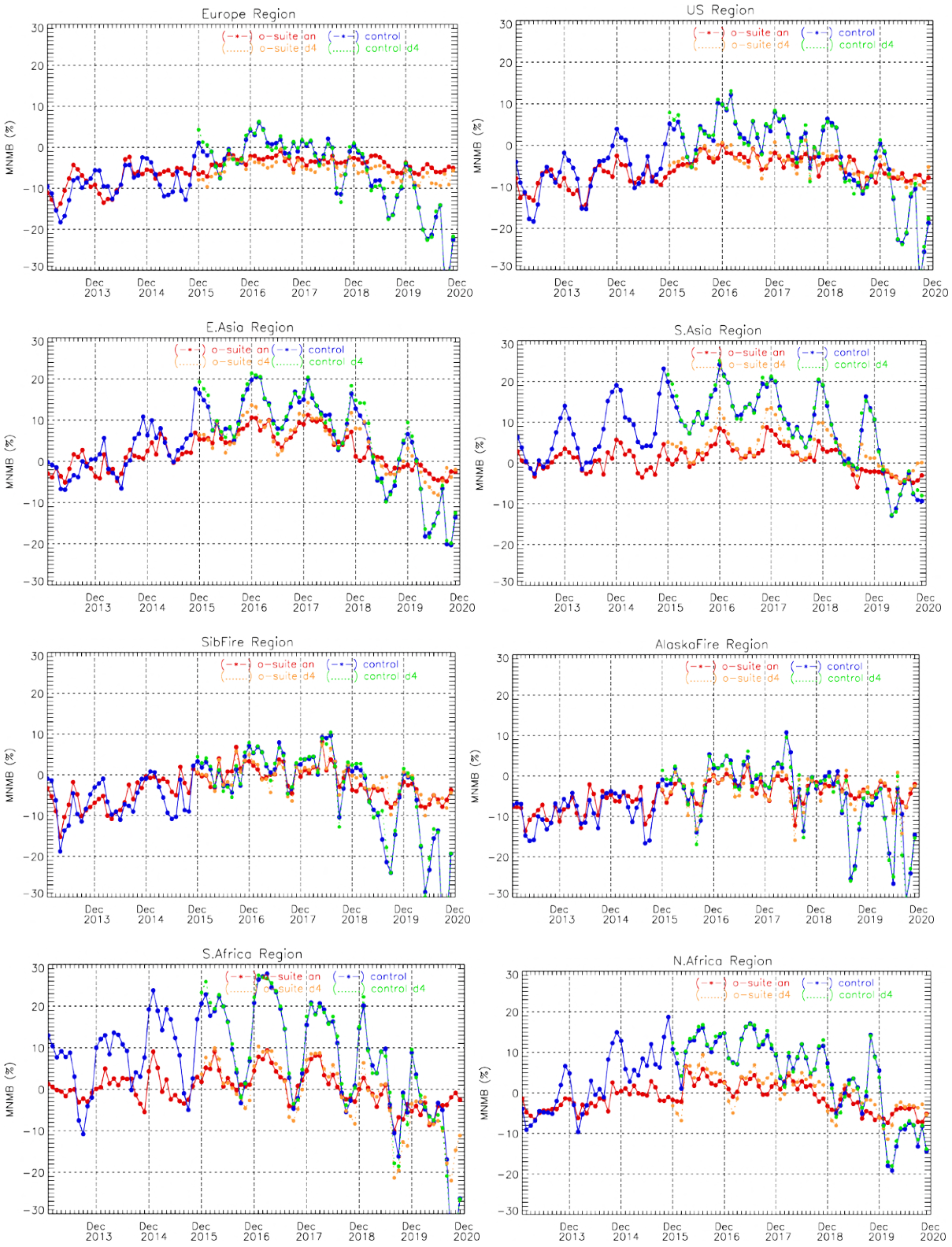

Fig. 4.5.4: Timeseries of modified normalized mean bias (%) for CO total columns from the model simulations vs MOPITT V8 retrievals over selected regions. O-suite analysis (red, solid), control run (blue, solid), o-suite 4th forecast day (orange, dotted), control 4th forecast day (green, dotted). Period: January 2013 to November 2020.

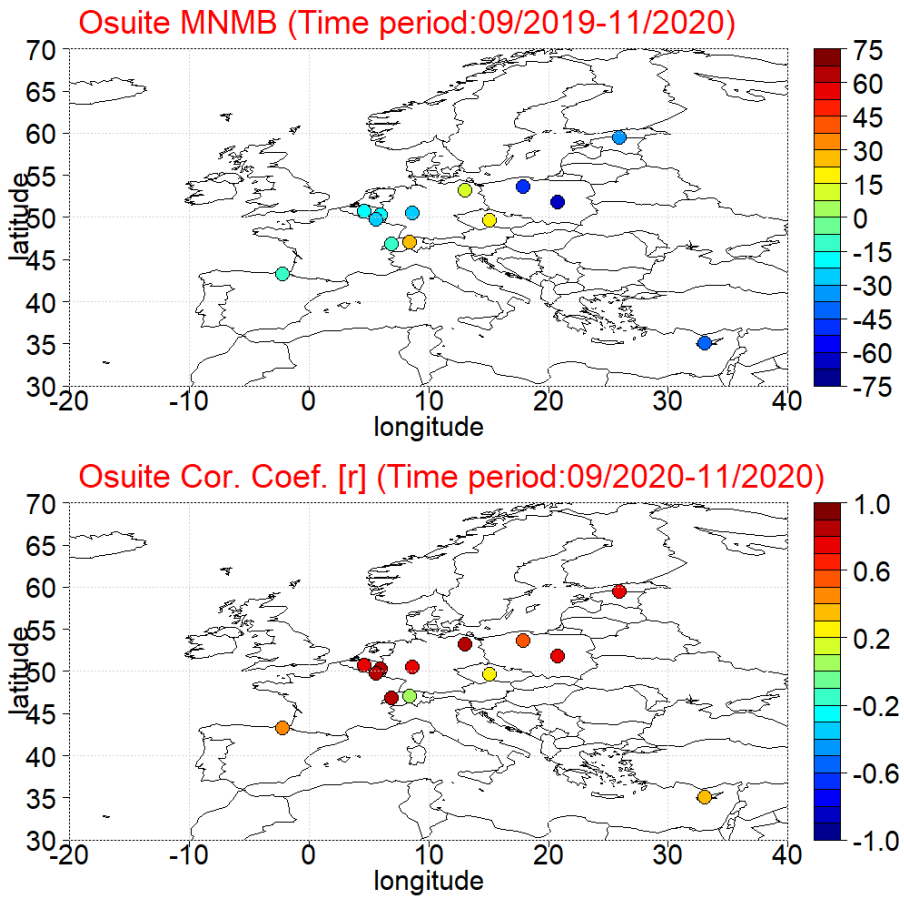

Figure 4.6.1: Spatial distribution of MNMB in % (left) and correlation coefficient (right) of the o-suite run compared to observational data during the period from 1 September to 30 November 2020.

4.6 Evaluation with CO surface observations over Europe

The surface carbon monoxide validation analysis over Europe is based on an evaluation against background rural classes 1 to 5 of the Joly-Peuch classification (Joly and Peuch, 2012). The station observations are taken from the Airbase Network database at EEA (http://acm.eionet.europa.eu/databases/airbase/). In addition, 1 station from the Department of Labour Inspection - Ministry of Labour and Social Insurance, of Cyprus (http://www.airquality.dli.mlsi.gov.cy/) is used in the validation analysis. The spatial distribution of bias and correlation coefficients of the o-suite over Europe are shown in Fig. 4.6.1. The results show that correlations over almost all CO European AirBase stations are highly significant (0.3<r<0.9) with the exceptions of Rigi (Swiss) and Kosetice (Czech Republic) where correlations drop close to zero. Concerning biases CAMS o-suite underestimate surface carbon monoxide mean concentrations over Spain, Belgium and Western Switzerland and Germany (depending on the station MNMBs vary from -25% to -10%), and underestimate more over Estonia (-35%), Cyprus (-40%) and Poland (-60%). On the contrary CAMS o-suite overestimate surface carbon monoxide mean concentrations over Neuglobsow in Germany (10%) Kosetice in Czech Republic (20%) and Rigi in Switzerland (22%). These findings are further illustrated in time series at selected stations plotted in Figure 4.6.2. The control run surface carbon monoxide concentrations are 15-20 ppb (10%-20%) lower than the o-suite, resulting in a stronger negative bias in all stations (exception is Rigi station in Switzerland).

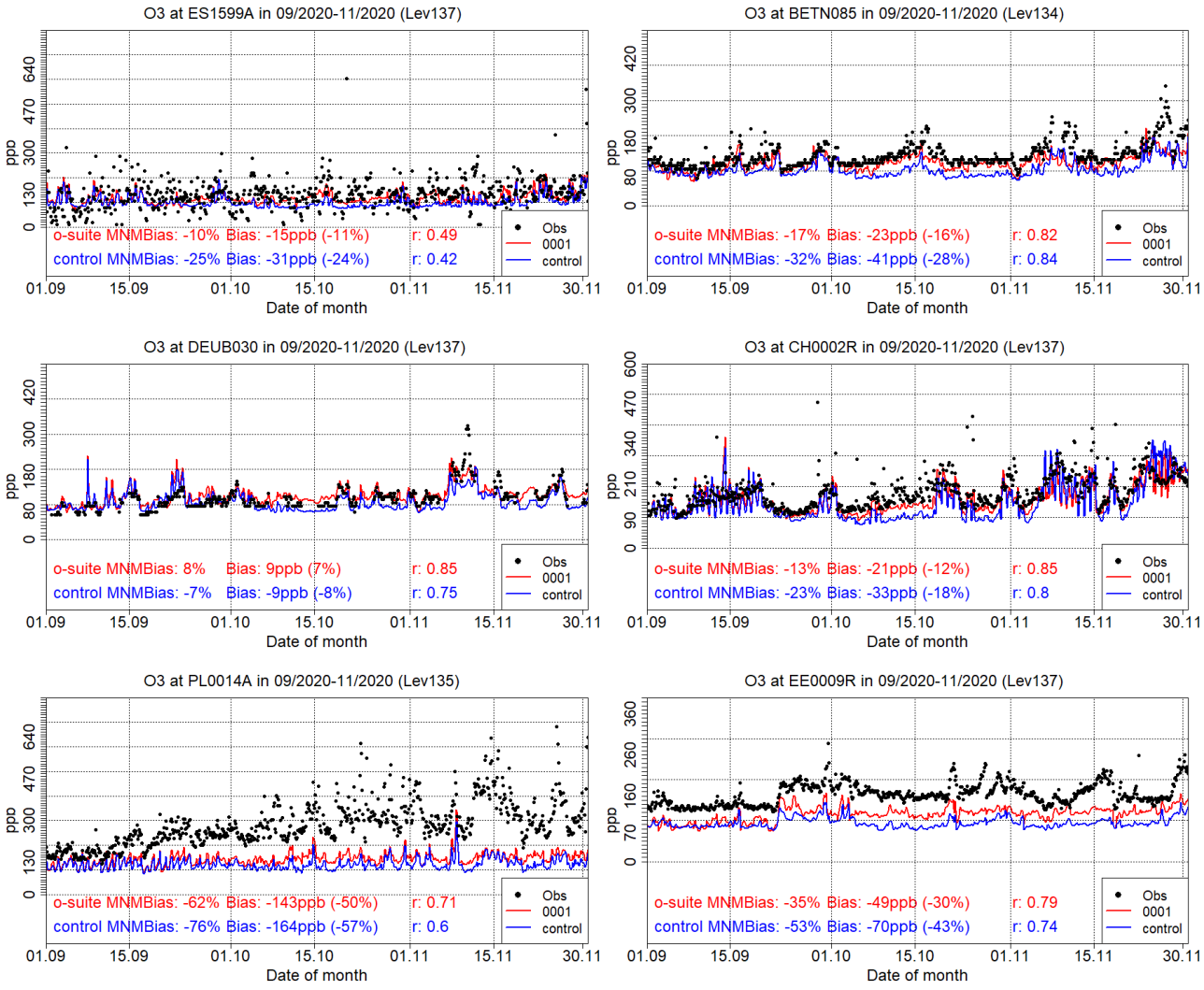

Figure 4.6.2: Time series for the o-suite (red) and control run (blue) compared to Airbase observations at Pagoeta, Spain station (43.25°N, 2.15 °W, 1st row left), at Vielsalm, Belgium station (50.30°N, 6.02°E, 1st row right), at Neuglobsow, Germany (53.14°N, 14.02°E, 2nd row left), at Payerne, Swiss station (46.81°N, 6.94°E, 2nd row right), at Belsk, Poland station (51.84°N, 20.79°E 3rd row left), and at Lahemaa, Esthonia (59.49°N, 25.93°E, 3rd row right)

5. Tropospheric nitrogen dioxide

5.1 Evaluation against GOME-2 and TROPOMI retrievals

In this section, model columns of tropospheric NO_2 are compared to SCIAMACHY/Envisat NO_2 satellite retrievals (IUP-UB v0.7) [Richter et al., 2005] for model data before April 2012, and to GOME-2/MetOp-A NO_2 satellite retrievals (IUP-UB v1.0) [Richter et al., 2011] for simulations after April 2012. First comparisons (for model data from Jan 2019 onwards) to TROPOMI/Sentinel-5P data (IUP-UB v0.9, preliminary) and to GOME-2/MetOp-C (IUP v0.9, preliminary) are provided, using the CAMS o-suite as a-priori in these retrievals only. The satellite data provides excellent coverage in space and time and very good statistics. However, only integrated tropospheric columns are available, and the satellite data is always taken at the same local time, roughly 09:30 LT for the GOME-2 instruments, 10:00 LT for SCIAMACHY and 13:30 LT for TROPOMI and at clear sky only. Therefore, model data are vertically integrated, interpolated in time and then sampled to match the satellite data. The satellite data were gridded to model resolution (currently 0.4° x 0.4° degree). Model data were treated with the same reference sector subtraction approach as the satellite data for all SCIAMACHY/GOME-2A comparisons. For all comparisons to TROPOMI and GOME-2C satellite data, the stratospheric contribution has been removed from the measurements using STREAM-B which is an IUP-Bremen version of the STREAM algorithm by Beirle et al. (2016). In the current version of STREAM-B, the free tropospheric contribution is not yet well accounted for, which leads to a negative offset in the current preliminary TROPOMI and GOME-2C data versions and will be improved by addition of tropospheric background values in the near future. Uncertainties in NO_2 satellite retrievals are large and depend on the region and season. Winter values in mid and high latitudes are usually associated with larger error margins. Systematic uncertainties in regions with significant pollution are on the order of 20% – 30%.

Figure 5.1.1 shows global maps of GOME-2A and model monthly mean tropospheric NO_2 columns as well as differences between retrievals and simulations for October 2020 as an example for the last autumn. The overall spatial distribution and magnitude of tropospheric NO_2 is well reproduced by both CAMS runs, indicating that emission patterns and NO_x photochemistry are reasonably well represented. Some differences are apparent between observations and simulations, with generally larger shipping signals simulated by the models. For example, shipping signals are much more pronounced in model simulations to the south of India.

Emissions over Europe and especially the pollution hotspots around the Benelux countries are regularly underestimated, especially during winter. However, other local maxima of tropospheric NO_2 observed over anthropogenic emission hotspots in East Asia (e.g., over the heavily populated Sichuan Basin; 30°N, 105°E), India and others such as Teheran, Mecca and Moscow and over boreal forest fires (mainly during summer) are regularly overestimated. Values over the Persian Gulf and the Red Sea (mainly summer and autumn) as well as near Lake Balkash and the Casian Sea are regularly overestimated. A systematic overestimation over anthropogenic pollution is visible in the TROPOMI and GOME-2C based map comparisons (Figure 5.1.2).

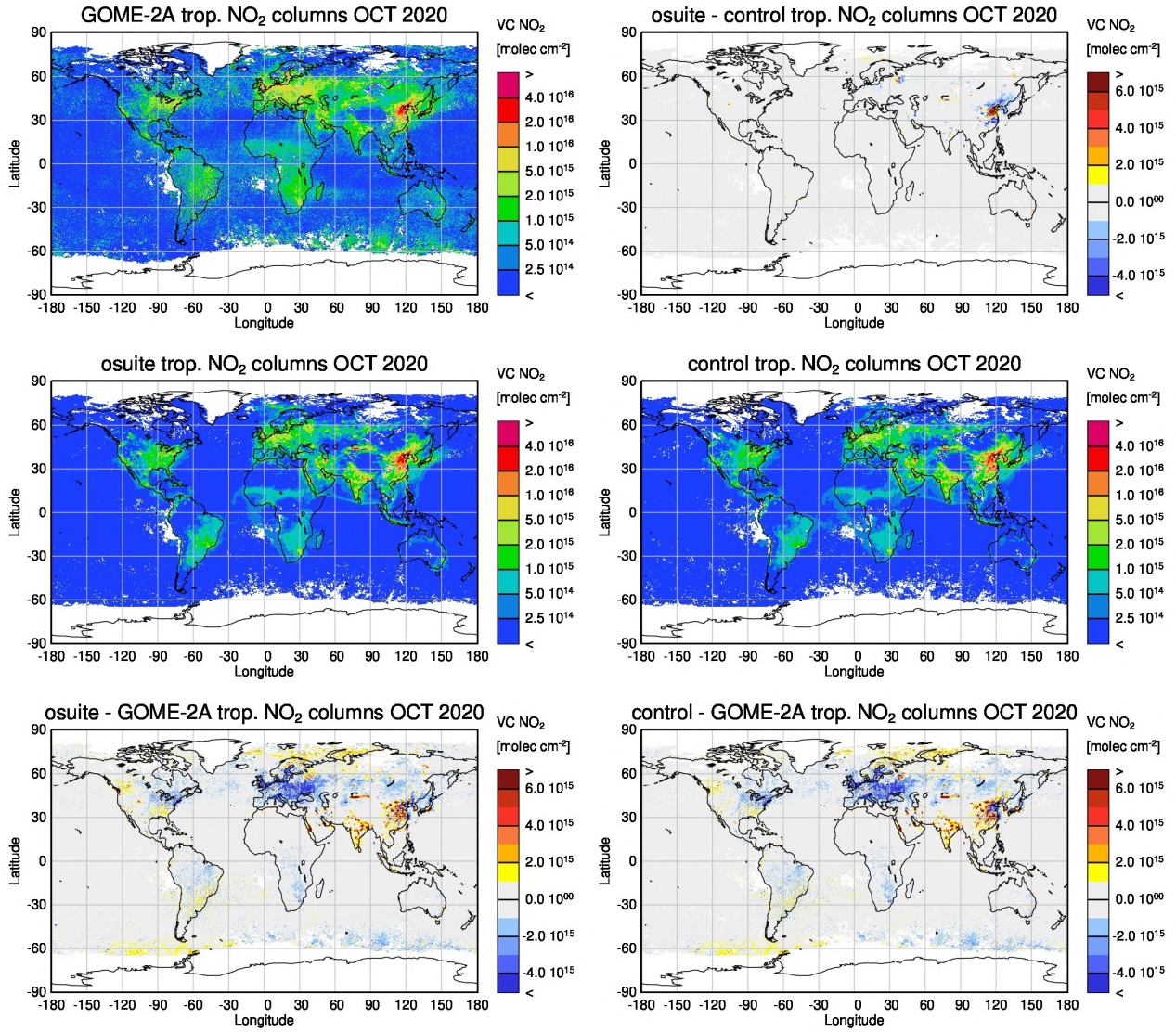

Figure 5.1.1: Global map comparisons of satellite retrieved and model simulated tropospheric NO2 columns [molecules cm-2] for October 2020. The top row shows monthly mean tropospheric NO2 columns retrieved from GOME-2A as well as the difference between o-suite and control, the second row shows the corresponding tropospheric NO2 columns for model simulated averages. The third row shows differences of monthly means between models and GOME-2A. GOME-2A data were gridded to model resolution (i.e. 0.4° x 0.4° degree). Model data were treated using the same stratospheric correction method as for the satellite data.

The TROPOMI IUP Bremen data product shows lower background values compared to the operational offline product, this is expected to be reduced with the next data version of the Bremen product (see data description above). Differences in comparison results between the sensors are in principle due to differences in observation time and the retrieval products. Note that the standard IUP-UB GOME-2A retrievals use different a priori profiles, different Air Mass Factors (AMFs) and a different stratospheric correction method compared to the GOME-2C product.

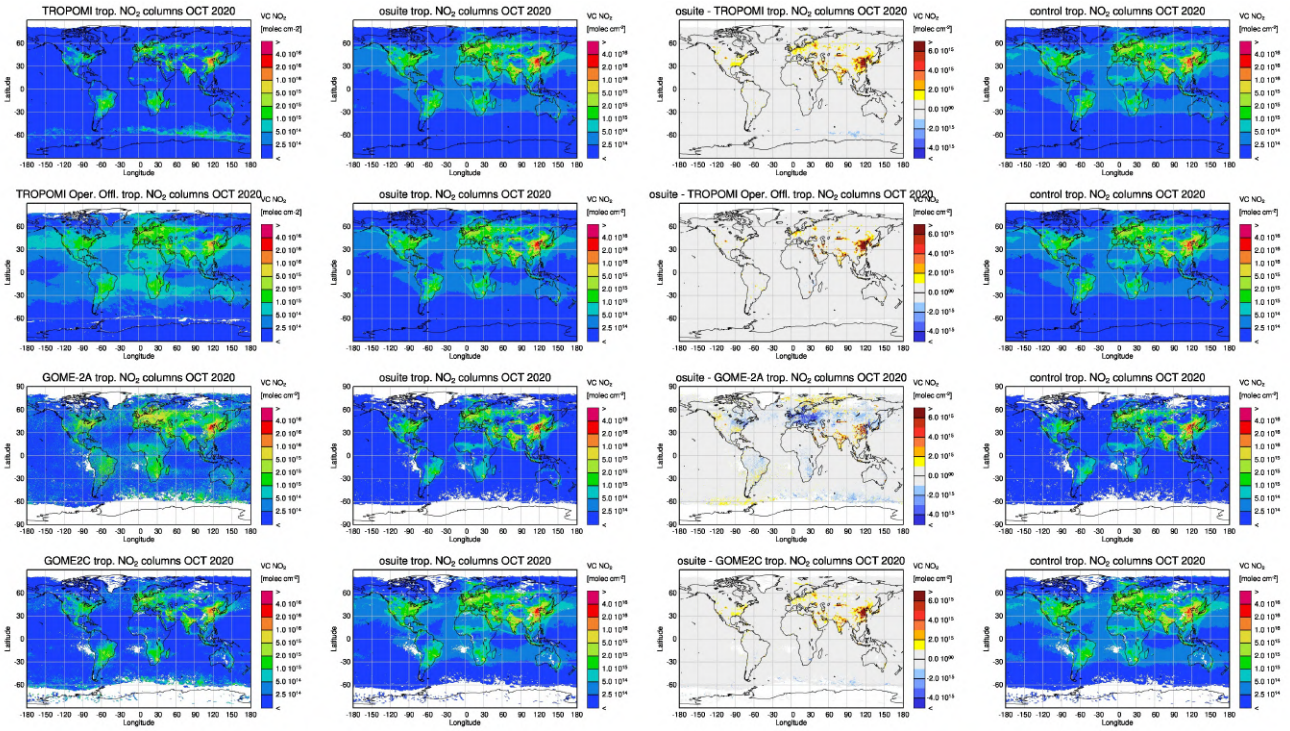

Figure 5.1.2: Global map comparisons of satellite retrieved and model simulated tropospheric NO_2 columns [molecules cm-2] for October 2020 based on (from top to bottom) TROPOMI, TROPOMI operational offline, GOME-2A and GOME-2C. The columns show (from left to right) satellite observations, o-suite, the difference between o-suite and satellite observations, control. The satellite data were gridded to model resolution (i.e. 0.4° x 0.4° degree) and the CAMS o-suite was used as a-priori in the GOME-2C and TROPOMI IUP-Bremen retrievals only.

Closer inspection of the seasonal variation of tropospheric NO_2 in some selected regions (Fig. 5.1.3) reveals significant differences between GOME-2A measurements and model results and points to some simulation problems. Over regions where anthropogenic emissions are major contributors to NOx emissions, models correctly simulate the occurrence of maxima and minima in seasonality in time, but fail to reproduce the inter-annual variability observed by GOME-2A. Over East-Asia, absolute values and seasonality were strongly underestimated before 2014 by all model runs (most likely due to an underestimation of anthropogenic emissions) for all seasons apart from summertime minima, with the o-suite showing improved results since an upgrade in July 2012. As wintertime NO2 column retrievals decreased significantly in 2014, model simulated wintertime maxima previously have been in better agreement with the satellite retrieved ones for recent years.

However, the observed NO_2 decrease was not reproduced by the simulations and therefore the better agreement for more recent years could not be attributed to model improvements. Moreover, summertime model minima increased in 2015 compared to previous years, which is in contrast to the satellite retrievals, so that the simulated values for the summers since 2015 are about 50% larger than satellite retrieved ones. For the first time in the time series, model results for the latest winter season (DJF 2019/2020) overestimate the peak in seasonality, with the control showing a significantly larger overestimation compared to the o-suite. Note that the overestimation occurs already for Dec 2019, in advance of the COVID-19 pandemic in China. The long-term

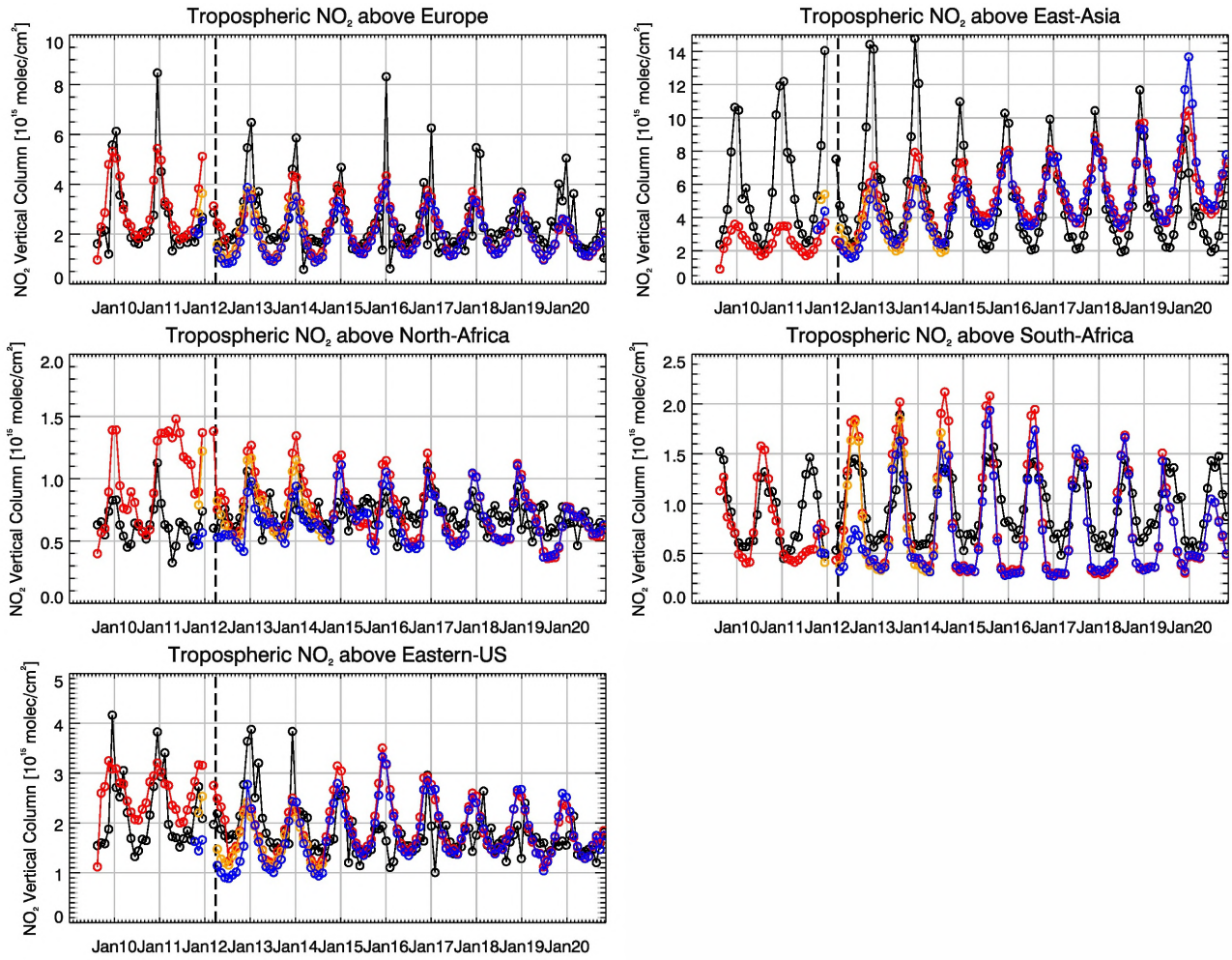

Figure 5.1.3: Time series of average tropospheric NO_2 columns [10^{15} molec cm^{-2}] from SCIAMACHY (up to March 2012, black) and GOME-2A (from April 2012 onwards, black) compared to model results (red: o-suite; blue: MACC-TM5 forecast, MACC-CIFS forecast or control; orange: MACC-MOZART forecasts) for different regions (see Annex 2). The upper panels and lower panel represent regions dominated by anthropogenic emissions, and the panels for Africa represent those dominated by biomass burning. Vertical dashed black lines mark the change from SCIAMACHY to GOME-2A based comparisons in April 2012.

development of model simulated tropospheric NO_2 columns over East-Asia points to inadequate scenarios of emission development.

As for East-Asia, a decrease in satellite retrieved values also occurred in 2015 over Europe where a peak is usually found around January, which was, as a result, only slightly underestimated by the models for January 2015. The underestimation of tropospheric NO_2 columns over Europe may be caused to some extent by a change of emission inventories in 2012. However, the situation changed for the three winter periods between 2015 and 2017, for which GOME-2A shows (compared to previous years) a strong increase in January peak values, combined with a decrease in values for December and February that is not reproduced by the models. It is not clear if the GOME-2A observations are realistic here, although an inspection of daily GOME-2A satellite images did not point to problems regarding the retrieval. The simulations show the same pattern as the retrievals

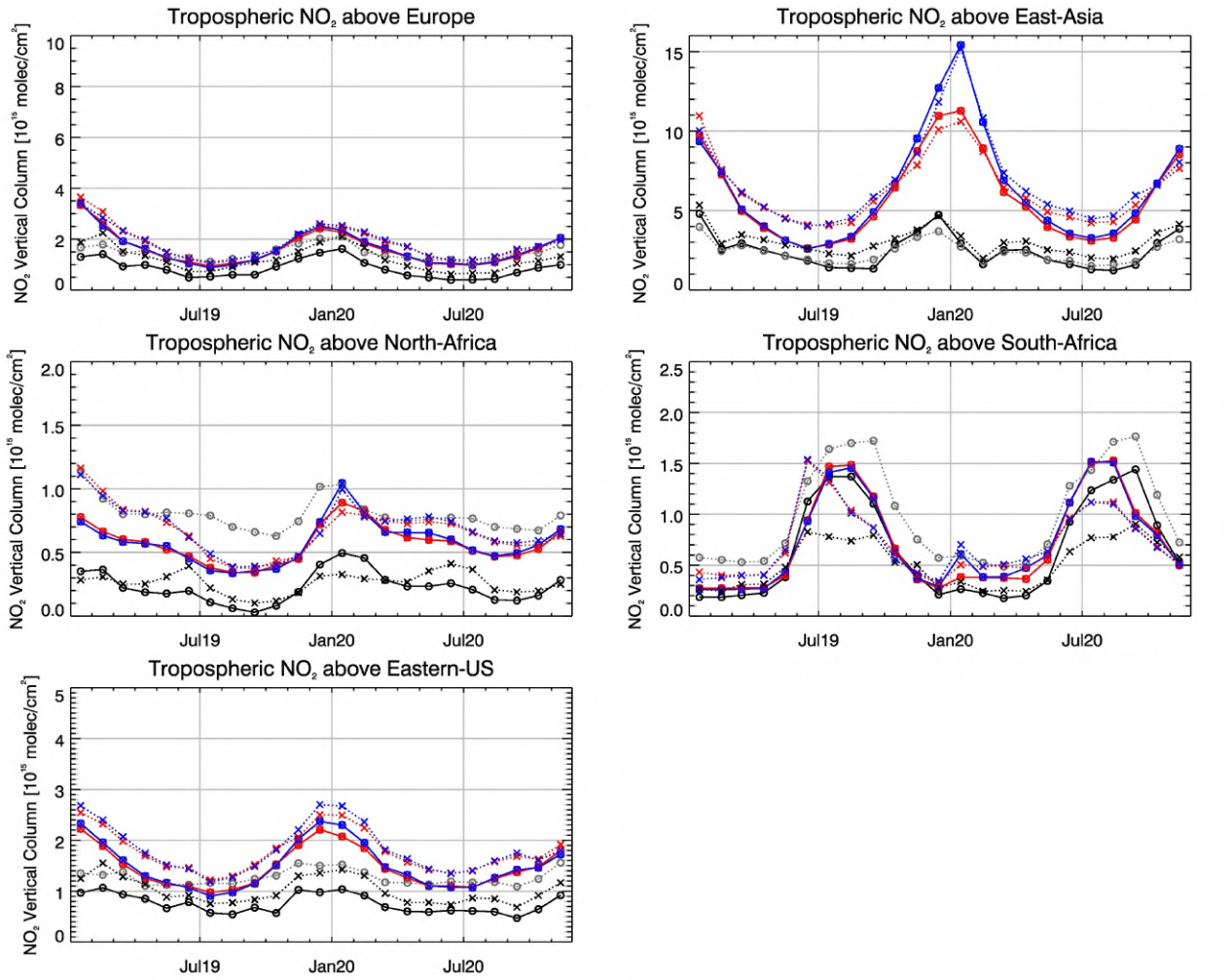

Figure 5.1.4: Time series of average tropospheric NO_2 columns [10^{15} molec cm^{-2}] from (black and grey) satellite retrievals, (blue) control and (red) o-suite model results since Jan 2019 (see Annex 2 for definition of regions). The solid lines with circles show comparisons based on TROPOMI (in black the IUP-Bremen product and in grey the operational offline product), the dotted lines with crosses show comparisons for GOME-2C. The upper panels represent regions dominated by anthropogenic emissions, and the lower panels represent those dominated by biomass burning.

however for winter 2018/2019 but strongly underestimate the retrievals again for the last winter (DJF 2019/2020).

Over regions where biomass burning is the major contributor to NO_x emissions, seasonality and amplitude of model columns are determined by fire emissions. The seasonality for the two regions in Africa was simulated reasonably well for 2010 and after October 2011. In the time period in between, a bug in reading fire emissions lead to simulation errors for all MOZART runs. Over North-Africa, the o-suite shows improved results since an update in July 2012 and the change to IFS-CB05 in September 2014. However, tropospheric NO_2 columns around December are still overestimated by the models. Summer to autumn NO_2 columns over North-Africa are underestimated compared to the satellite data from 2015 onwards and especially for 2019. The models (especially the o-suite) generally overestimate the seasonal cycle for South-Africa, particularly for 2014-2016 with an overestimation of the seasonal maximum, which usually occurs around August (e.g. by a factor of

1.4 larger compared to GOME-2A retrievals in 2016). However, August maxima were in better agreement with the upgrade of the o-suite in 2017 (though minima during SH summer remain underestimated), but are now underestimated for JJA 2020.

Time series comparisons between the o-suite and TROPOMI as well as GOME-2C are shown in Figure 5.1.4 for data since January 2019. They show differences with respect to the GOME-2A based ones: the o-suite is in general positively biased compared to the TROPOMI and GOME-2C retrievals, only over North- and South-Africa the o-suite shows smaller values than the TROPOMI operational offline product. For 2020, the TROPOMI observations show the peak in the time series over South-Africa for September, while the o-suite and control run simulate the peak for July/August. As described above, differences in comparison results are in principal due to differences in observation time or differences in the retrieval products.

With respect to months affected by COVID-19 lockdown time periods, the o-suite generally fails to reproduce observed reductions in tropospheric NO_2 for large areas over China and South Asia, but performs better for Europe (see section 11.3).

More NO_2 evaluation plots can be found on the CAMS website, see table 1.2.

5.2 Evaluation against ground-based DOAS observations

In this section, we compare the NO_2 columns of the CAMS products with UVVIS DOAS profile measurements at Xianghe and column data from the other stations.[1] This ground-based, remote-sensing instrument is sensitive to the NO_2 abundance in the lower troposphere, up to 1km altitude with an estimated uncertainty of 8%. Tropospheric NO_2 profiles and columns are validated (up to 3.5km or 10km). A description of the instruments and applied methodologies is the same for all DOAS OFFAXIS measurements, see . It is important to mention here that the model partial column values are calculated from the smoothed model profiles. This guarantees that the model levels where the measurement is not sensitive do not contribute to the observed bias. We should mention that the measurement data is still catalogued as rapid delivery and not in the consolidated NDACC database.

Figure 5.2.1 shows the biases for the latest validation periods June-August 2020 and Sept-Nov 2020 at the different sites. The corresponding time series are shown in Fig. 5.2.2. The o-suite is able to capture only few of the high pollution events for Bremen, De Bilt and Cabauw. In Athens no high pollution events are captured by the o-suite.

[1] No contribution from Uccle, Reunion and OHP due to instrument failure.

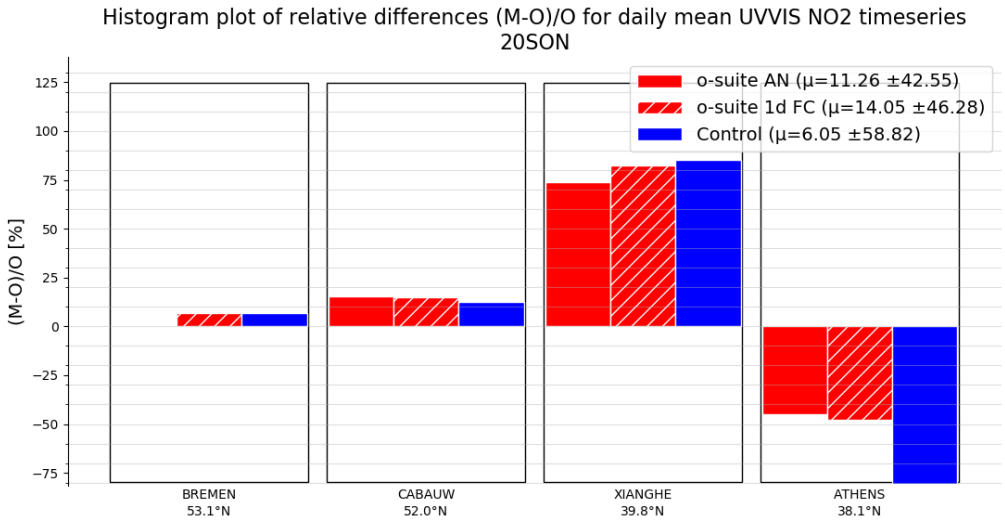

Figure 5.2.1: Table diagram showing the seasonal bias June-August 2020 (top) and September-November (bottom) for five stations, sorted by latitude. Xianghe data, with many hight pollution events, was recently updated on NDACC.

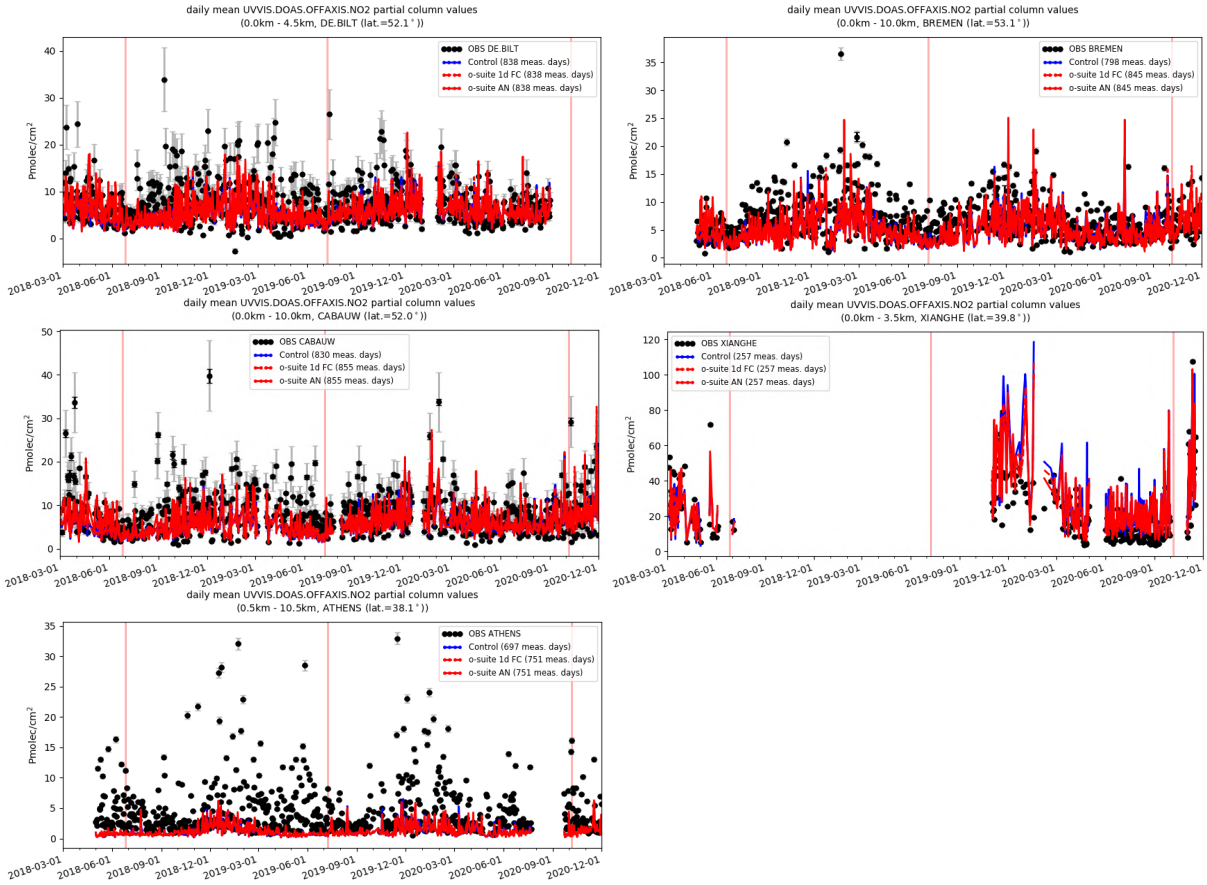

Figure 5.2.2: Time series of NO_2 partial columns at the five different sites. For all sites except Athens, background concentrations are well captured by the CAMS products. The o-suite and control runs show little difference.

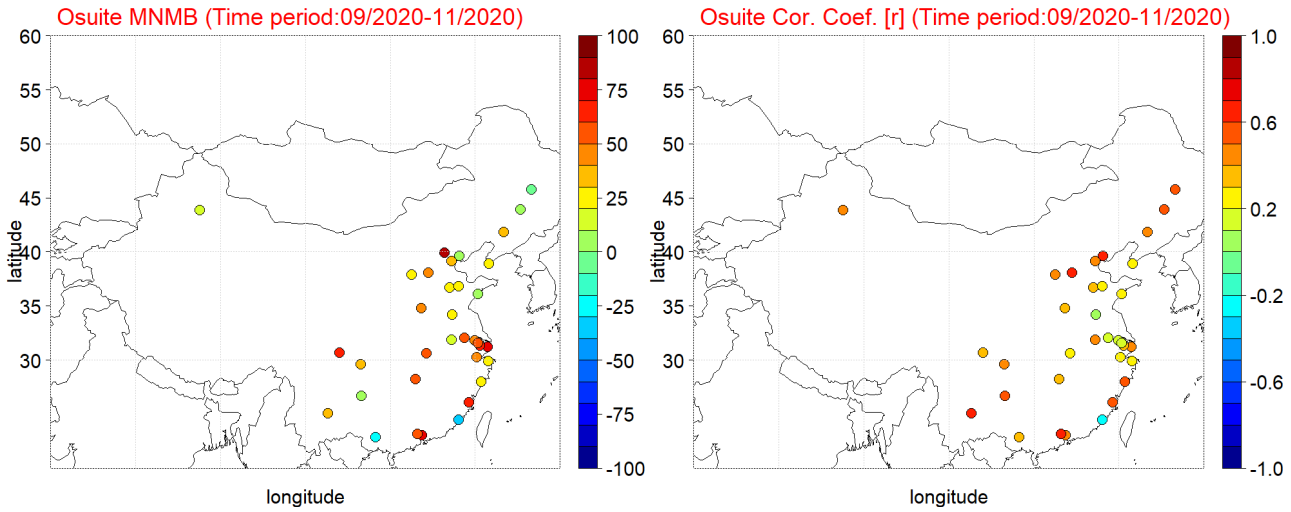

Figure 5.3.1: Spatial distribution of MNMB in % (left) and correlation coefficient (right) of the o-suite run compared to observational data during the period from 1 September 2020 to 30 November 2020.

5.3 Evaluation against surface nitrogen dioxide observations over China

The surface NO_2 validation over China is based on station observations from more than 1,500 in situ stations covering all major cities in China, operated by the China National Environmental Monitoring Center, reporting the pollutants PM10, PM2.5, O_3, NO_2, SO_2, and CO (e.g. Bai et al., 2020). The measurements were collected within the EU MarcoPolo and Panda projects. Individual station data was clustered for 37 megacities (e.g. 10-20 stations per city) and the observed surface NO_2 values are compared with the simulated NO_2 values calculated for the corresponding o-suite grid point.

Table 5.3.1 shows the names, coordinates, observed and simulated ozone values as well as validation metrics namely the MNMBs and correlations obtained for the o-suite run. The spatial distribution of MNMBs and the correlation coefficients of the o-suite over China are shown in Fig. 5.3.1, where it is evident that correlations over most megacities in the entire China (with few exceptions namely Changzhou, Dalian, Wuxi, Xiamen and Xian, Xuzhou and Zibo) are highly significant ($0.25<r<0.65$). The o-suite mostly overestimate surface NO_2 values, particularly in cities northern than 30° N. More specific o-suite MNMBs for NO_2 vary between -5% and 30% depending on the station over North-eastern and North-western China. For stations in the latitudinal belt 30°N-40°N o-suite strongly overestimate surface NO_2 values with MNMBs varying between 25% and 100% (exceptions are Tangshan, Hefei and Qingdao cities where o-suite MNMBs are close to zero). For the Megacities southern of the 30° N parallel, o-suite MNMBs varying between 25% and 130% (exceptions are Nanning and Xiamen cities where o-suite underestimate surface NO_2 values by -28% and -36% respectively and Guiyang city where o-suite MNMB is almost zero).

The above-mentioned findings concerning CAMS o-suite biases and correlations are also observed in individual time series at selected cities plotted in Figure 5.3.2.

Table 5.3.1: Names, coordinates, observed and simulated ozone values as well as o-suite validation metrics for each one from 37 China Megacities under study.

MegaCity	Lat	Lon	O3_OBS (ppb)	O3_o_suite (ppb)	MNMB	Cor. Coef.
Beijing	39.92	116.38	34.98	89.97	89.3	0.62
Changchun	43.89	125.33	30.02	31.81	5.1	0.54
Changsha	28.20	112.97	27.91	46.05	52.0	0.32
Changzhou	31.81	119.97	42.80	67.51	46.1	0.19
Chengdu	30.66	104.07	36.55	65.94	60.3	0.35
Chongqing	29.56	106.55	41.27	60.01	39.2	0.43
Dalian	38.91	121.60	26.95	37.39	27.9	0.21
Dongguan	23.02	113.75	28.48	62.13	71.3	0.48
Fuzhou	26.08	119.31	16.42	33.38	62.4	0.56
Guangzhou	23.13	113.25	36.66	67.14	56.9	0.63
Guiyang	26.65	106.63	17.93	17.75	0.2	0.59
Hangzhou	30.25	120.17	41.60	64.36	43.9	0.25
Harbin	45.75	126.63	31.80	28.34	-8.8	0.55
Hefei	31.85	117.27	46.25	51.01	12.8	0.45
Jinan	36.67	116.98	47.06	59.94	26.2	0.30
Kunming	25.04	102.71	26.04	36.87	35.9	0.65
Nanjing	32.05	118.77	38.99	66.63	54.1	0.18
Nanning	22.82	108.32	26.61	19.78	-28.0	0.33
Ningbo	29.87	121.54	36.91	50.52	28.6	0.27
Qingdao	36.07	120.38	37.66	40.31	2.9	0.25
Shanghai	31.22	121.47	40.16	86.03	74.0	0.41
Shenyang	41.80	123.40	36.41	50.06	32.1	0.43
Shenzhen	22.54	114.06	22.17	70.68	102.8	0.58
Shijiazhuang	38.04	114.51	45.92	74.70	49.1	0.64
Suzhou	31.30	120.60	38.08	73.06	63.7	0.31
Taiyuan	37.87	112.55	48.63	60.96	22.9	0.48
Tangshan	39.63	118.18	52.80	52.51	1.1	0.60
Tianjin	39.13	117.25	46.34	67.75	39.5	0.45
Urumqi	43.83	87.62	39.56	45.73	16.6	0.43
Wenzhou	27.99	120.70	33.31	43.09	24.6	0.60
Wuhan	30.58	114.30	43.55	73.68	53.3	0.25
Wuxi	31.57	120.33	40.64	70.23	53.8	0.11
Xiamen	24.48	118.09	47.37	33.86	-35.9	-0.24
Xi'an	34.34	108.94	14.45	71.44	131.6	-0.15
Xuzhou	34.21	117.28	45.05	59.62	29.2	0.00
Zhengzhou	34.76	113.65	45.97	71.95	46.1	0.34
Zibo	36.78	118.05	47.21	60.14	24.6	0.29

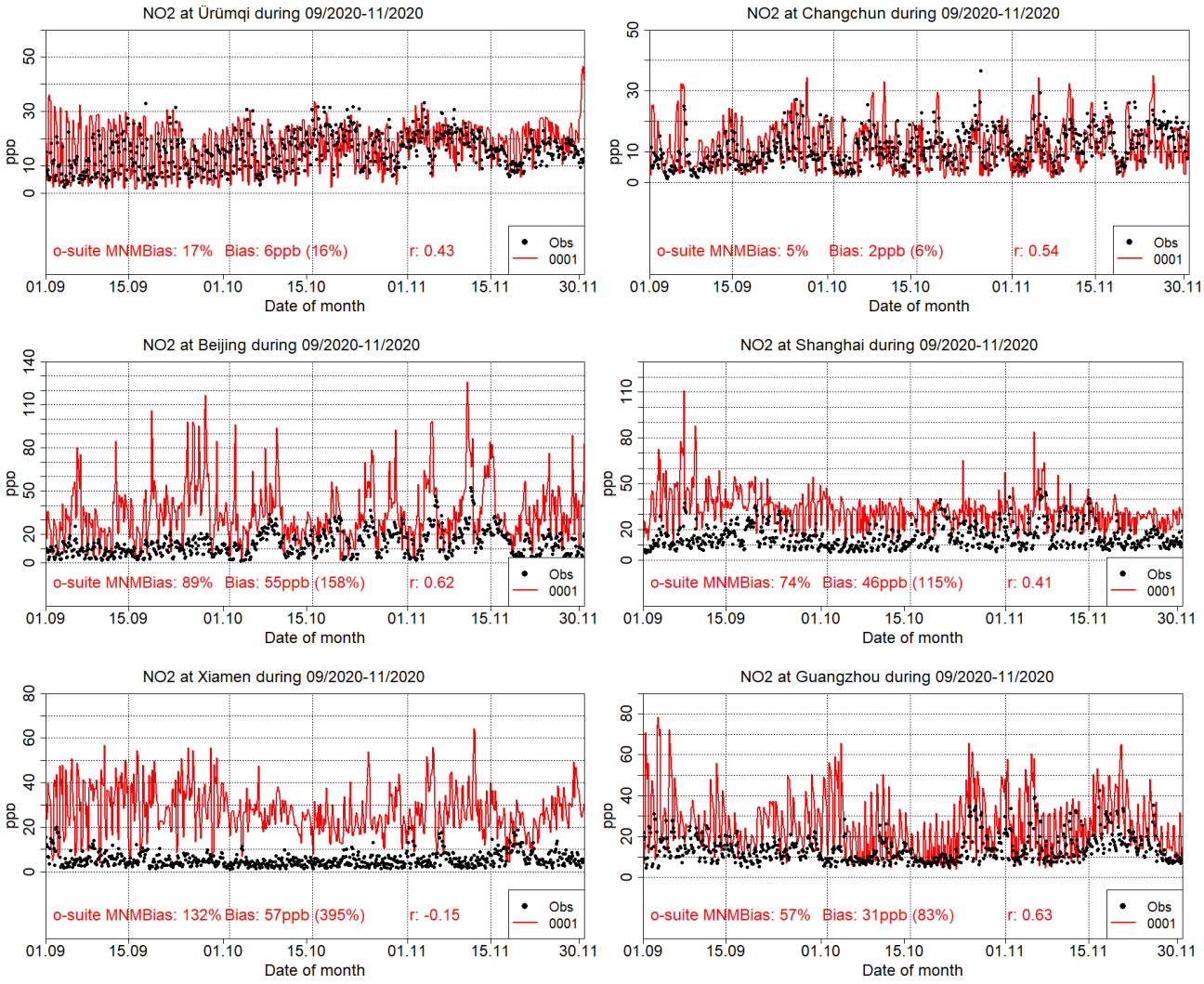

Figure 5.3.2: Surface NO_2 time series for the o-suite (red) compared to MarcoPolo-Panda project observations at Urumqi (43.83°N, 87.62°E, 1st row left), at Changchun (43.89°N, 125.33°E, 1st row right), at Beijing (39.92°N, 116.38°E, 2nd row left), at Shanghai (31.22°N, 121.47°E, 2nd row right), at Xiamen (24.48°N, 118.09°E, 3rd row left), and at Guangzhou (23.13°N, 113.25°E, 3rd row right).

6. Formaldehyde

6.1 Validation against satellite data

In this section, simulations of tropospheric formaldehyde are compared to SCIAMACHY/Envisat HCHO satellite retrievals (IUP-UB v1.0) [Wittrock et al., 2006] for model data before April 2012 and to GOME-2/MetOp-A HCHO data (IUP-UB v1.0) [Vrekoussis et al., 2010] afterwards. First comparisons to TROPOMI/Sentinel-5P data (IUP-UB v1.0) and to GOME-2/MetOp-B (IUP v0.9, preliminary) are provided, using the CAMS o-suite as a-priori in the TROPOMI retrievals. The HCHO retrievals are described in Alvarado et al. (2019). The satellite data (tropospheric columns only) are always taken at approximately the same local time, roughly 09:30 LT for the GOME-2 instruments, 10:00 LT for SCIAMACHY and 13:30 LT for TROPOMI and at clear sky only. The satellite data were gridded to model resolution (currently 0.4° x 0.4° degree). As the retrieval is performed in the UV part of the spectrum where less light is available and the HCHO absorption signal is smaller than that of NO_2, the uncertainty of monthly mean HCHO columns is relatively large (20% – 40%) and both noise and systematic offsets have an influence on the results. However, absolute values and seasonality are retrieved more accurately over HCHO hotspots.

In Figure 6.1.1, monthly mean satellite HCHO columns from GOME-2A are compared to model results for October 2020 as an example for the last autumn. The magnitude of oceanic and continental background values and the overall spatial distribution are well represented by the o-suite and control. The models regularly overestimate values over regions in Central Africa, which could be due to fire or biogenic emissions. This appears less pronounced since autumn 2019. Moreover, HCHO columns over regions with fire and biogenic emissions in Northern Australia were regularly overestimated mainly during SON and DJF, but this appears much less pronounced since 2019. The TROPOMI based map comparisons (see Figure 6.1.2 for July 2020) show a very good agreement for July 2020, while the comparison to GOME-2B shows a positive bias over main emission regions of HCHO and over the ocean at a higher southern latitudes. Differences in comparison results between the sensors are in principal due to differences in observation time and the retrieval products. Note that the standard IUP-UB GOME-2A retrievals use different a priori profiles and Air-Mass Factors (AMF) compared to the GOME-2B product.

Time series comparisons based on GOME-2A in Fig. 6.1.3 highlight three cases:

- East-Asia and the Eastern US, where HCHO is dominated by biogenic emissions. Model results and GOME-2A retrievals generally agree rather well. However, all model runs underestimate the yearly cycle over East-Asia since 2012. In contrast to MOZART runs, MACC_CIFS_TM5 overestimated satellite values for the Eastern US since the middle of 2013. However, the newer IFS-CB05 runs perform well for Eastern US since 2015. For recent years and both regions, there is virtually no difference between the most recent o-suite run with IFS-CB05 chemistry and the corresponding control run without data assimilation. The variability or “ups and downs” in HCHO columns observed by GOME-2A since December 2014 is due to the lack of data (caused by instrument degradation) for these regions during winter in the Northern Hemisphere, leading to e.g. the negative values in the GOME-2A time

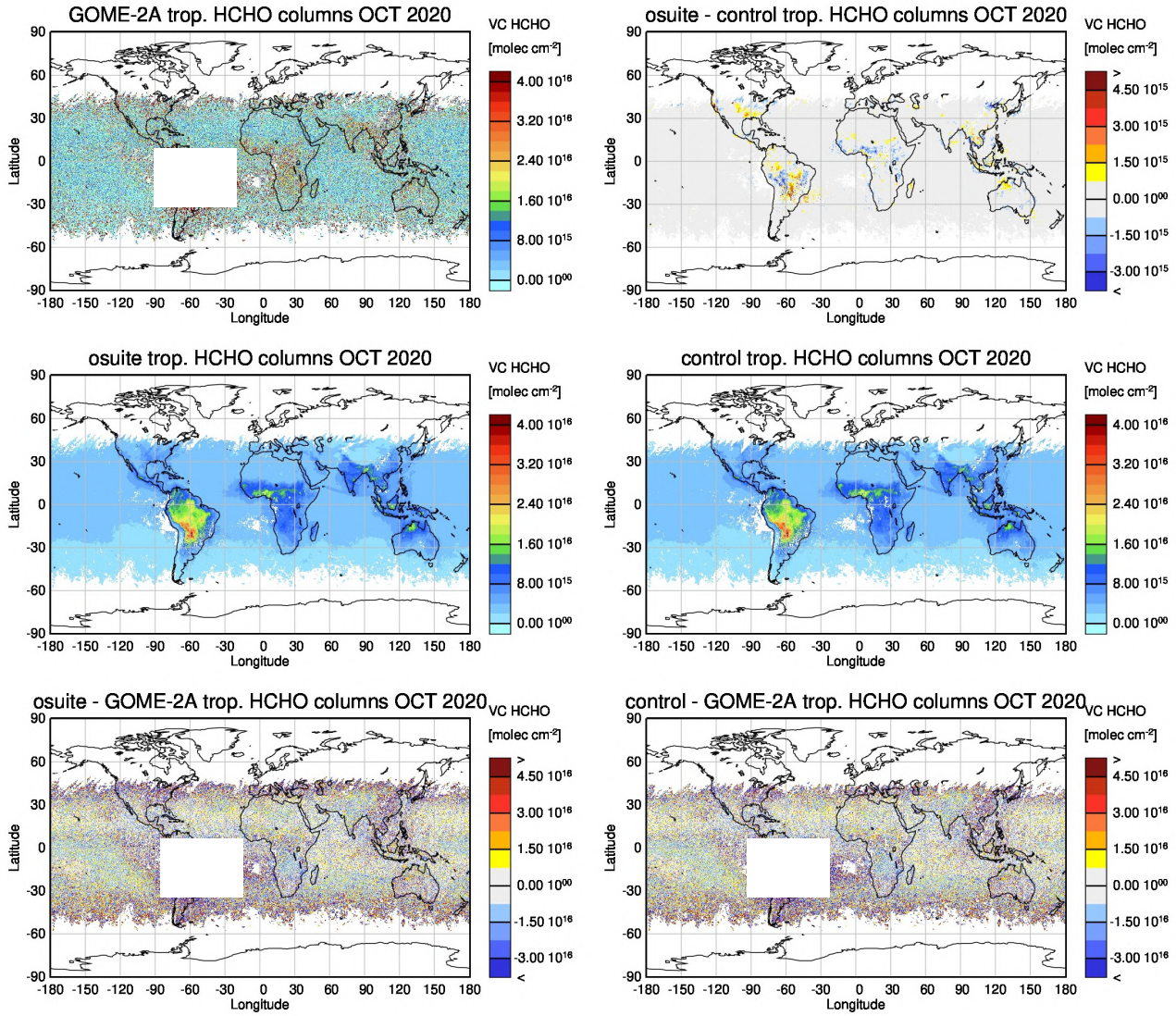

Figure 6.1.1: Global map comparisons of satellite-retrieved and model-simulated tropospheric HCHO columns [molec cm-2] for October 2020. The top row shows monthly mean tropospheric HCHO columns retrieved by GOME-2A, the second row shows the same but for model simulated averages. The third row shows differences of monthly means between models and GOME-2A. GOME-2A data were gridded to model resolution (i.e. 0.4° deg x 0.4° deg). Satellite retrieved values in the region of the South Atlantic anomaly are not valid and therefore masked out (white boxes in all images except those which show model results only).

series for Eastern US since December 2015. Summertime maxima are still underestimated over East-Asia despite of the higher resolution of the model runs since 2019. The observed increase for November 2020 over East-Asia is not reproduced by the models. The JJA peak observed by GOME-2A over Eastern-US is more pronounced in 2020 compared to the last years, this is not reproduced by the simulations.

- North-Africa, where biomass burning as well as biogenic sources largely contribute to HCHO and its precursors. GOME-2A satellite observations over North-Africa tend to be slightly overestimated by IFS-CB05 chemistry model runs since 2014 and also the latest higher

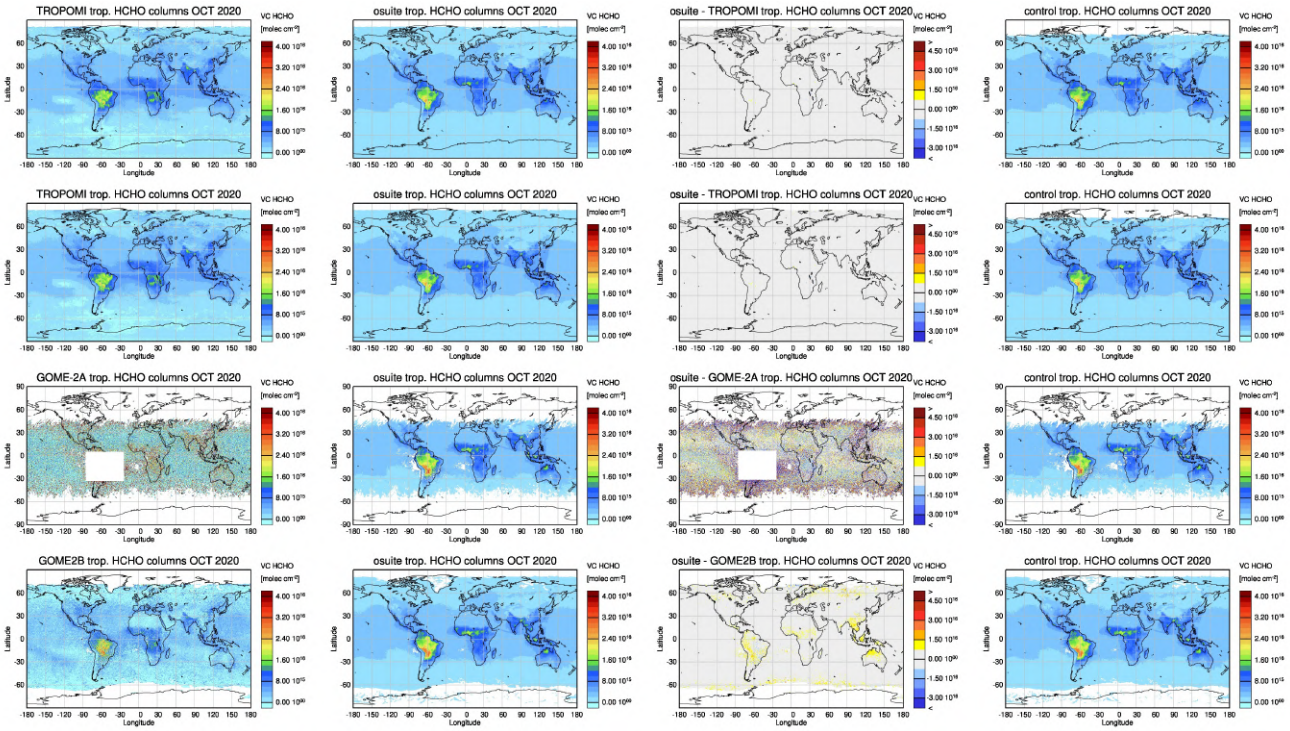

Figure 6.1.2: Global map comparisons of satellite retrieved, and model simulated tropospheric HCHO columns [molec cm^{-2}] for October 2020 based on (from top to bottom) TROPOMI, GOME-2A and GOME-2B. The columns show (from left to right) satellite observations, o-suite, the difference between o-suite and satellite observations, control. The satellite data were gridded to model resolution (i.e. 0.4° x 0.4° degree) and the CAMS o-suite was used as a-priori in the TROPOMI IUP-Bremen retrievals only and not in the TROPOMI operational offline product.

resolution model versions since July 2016. However, GOME-2A values are higher, and model values a bit lower for summer 2019 compared to previous years, resulting in a pronounced underestimation with respect to the satellite observations. Moreover, the model simulated HCHO columns increase from summer 2019 to May 2020, though the satellite observed columns show seasonality (a decrease followed by an increase for this period). For 2020, models show a pronounced underestimation compared to GOME-2A, the satellite observed values are unusually high over North-Africa for last year.

- Indonesia, where HCHO is also dominated by biogenic sources and biomass burning. Old MOZART based model versions generally overestimated satellite values here (by a factor of 3 – 4 in the second half of 2010) and failed to reproduce the observed seasonality. This may be due to the use of fire emissions including El Nino years, which experience much larger fire activities. MOZART simulations and observations agreed much better since late 2012. IFS-CB05 runs agree very well with satellite retrieved ones for December 2014 to August 2015. For September and October 2015, satellite retrieved HCHO columns show a pronounced maximum. 2015 was a strong El Nino year, which caused droughts and higher fire activity in Indonesia. Another pronounced, but by the models overestimated, increase in satellite observed values associated with comparatively weaker El Nino conditions occurs for Sep 2019. As for previous El Nino years, fire emissions used by IFS-CB05 seem to be largely

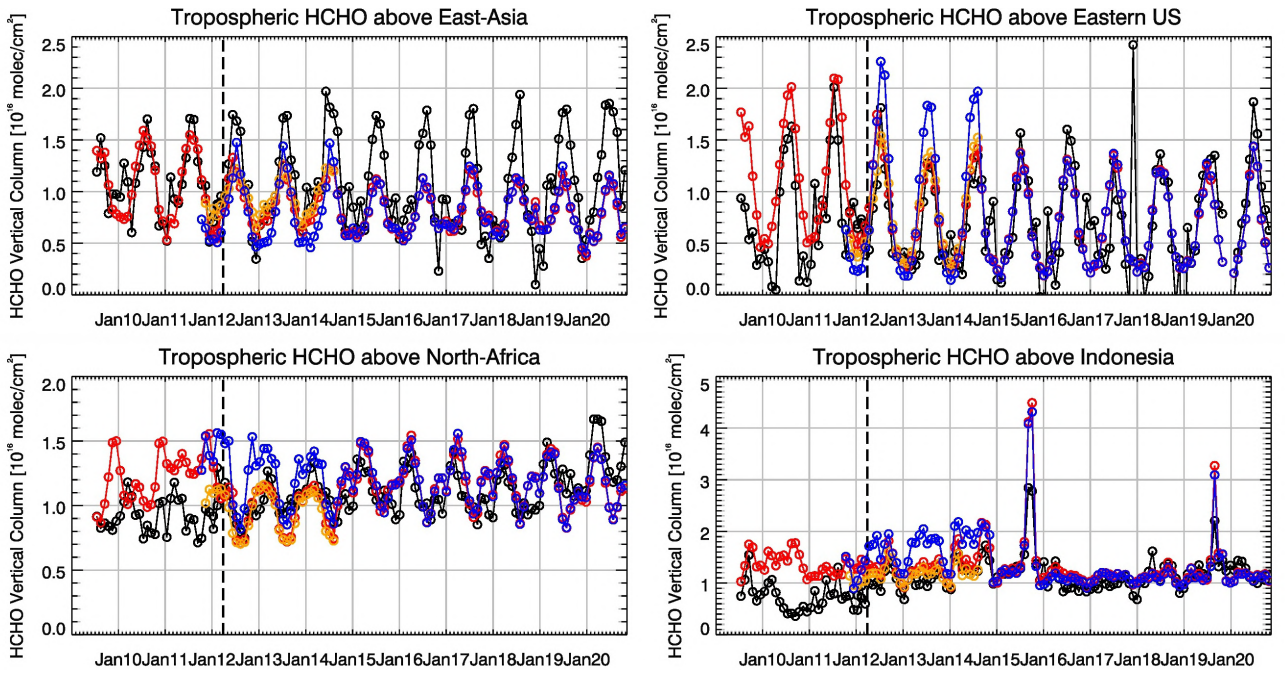

Figure 6.1.3: Time series of average tropospheric HCHO columns [10^{16} molec cm^{-2}] from SCIAMACHY (up to March 2012, black) and GOME-2 (from April 2012 onwards, black) compared to model results (red – o-suite, blue - MACC_fncrt_TM5/MACC_CIFS_TM5/control, orange - MACC_fcnrt_MOZ) for different regions. The blue line shows MACC_fcnrt_TM5 from November 2011 to November 2012, MACC_CIFS_TM5 results from December 2012 to August 2014 and control results from September 2014 onwards (the model run without data assimilation is termed control since Sep 2014). The regions differ from those used for NO_2 to better focus on HCHO hotspots: East-Asia (25-40°N, 110-125°E), Eastern US (30-40°N, 75-90°W), Northern Africa (0-15°N, 15°W-25°E) and Indonesia (5°S-5°N, 100-120°E). Negative satellite retrieved values over Eastern US are due to a lack of data (caused by instrument degradation) during Northern Hemisphere winter months for this region. Vertical dashed black lines mark the change from SCIAMACHY to GOME-2A in April 2012.

overestimated, resulting in model-simulated HCHO columns, which are up to twice as large as those retrieved by GOME-2A. Further investigations (see previous reports) show that this is not caused by cloud flagging applied to the satellite and model data. Between the middle of 2016 and Sep 2019 there was mainly little variation from one month to another in both, satellite observations and model simulations and the magnitude of model and satellite values agreed overall well.

Time series comparisons between the o-suite and TROPOMI as well as GOME-2B are shown in Figure 6.1.4 for data since Jan 2019. They show differences with respect to the GOME-2A based ones: the peak over Indonesia for Sep 2019 is much less pronounced for both the o-suite and satellite observations (the agreement is better for the control), for North-Africa the development of values in time for Jan 2019 to May 2020 is in agreement and there is no pronounced underestimation for last spring, for East-Asia the seasonality is in good agreement between the satellite sensors and the model runs, for Eastern-US the observed JJA peak is less pronounced and the agreement to the simulations is hence better. Apart from GOME-2B for North-Africa and Indonesia, differences between the satellite sensors and the o-suite are generally less pronounced. Differences in comparison results are in principal due to differences in observation time or differences in the retrieval products.

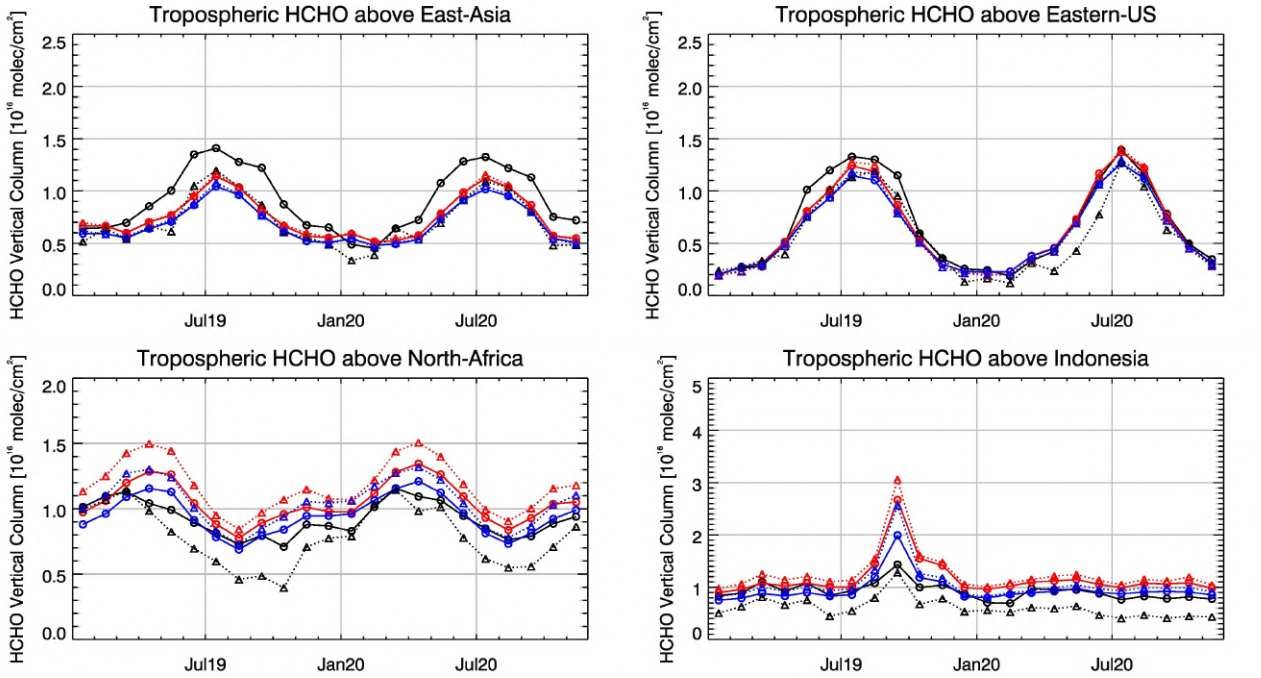

Figure 6.1.4: Time series of average tropospheric HCHO columns [10^{16} molec cm^{-2}] from (black and grey) satellite retrievals, (blue) control and (red) o-suite model results since Jan 2019. The solid lines with circles show comparisons based on TROPOMI, the dotted lines with triangles show comparisons for GOME-2B. The regions differ from those used for NO_2 to better focus on HCHO hotspots: East-Asia (25-40°N, 110-125°E), Eastern US (30-40°N, 75-90°W), Northern Africa (0-15°N, 15°W-25°E) and Indonesia (5°S-5°N, 100-120°E).

For details on the HCHO evaluation:

6.2 Evaluation against ground-based DOAS observations

In this section, we compare the HCHO columns of the CAMS products with UVVIS DOAS measurements at Xianghe, Cabauw and De Bilt.[2] These ground-based, remote-sensing instruments are sensitive to the HCHO abundance in the lower troposphere. Tropospheric HCHO profiles and columns are validated (up to 3.5km (Xianghe) or 10km (Cabauw and De Bilt)). The validation methodology is the same as for the MWR O_3 and FTIR O_3 and CO validations see . It is important to mention here that the CAMS partial column values are calculated for the smoothed model profiles. This guarantees that the model levels where the measurement is not sensitive do not contribute to the observed bias. We should mention that the measurement data is catalogued as rapid delivery and not in the consolidated NDACC database.

Figure 6.2.1 shows the absolute biases Sept – November 2020 at the different sites and indicates strongly reduced biases for the different sites. At all three sites high pollution events are not captured by the CAMS runs and leads to a higher overall underestimation (Fig 6.2.2). From Fig. 6.2.1 and 6.2.2 we see little difference between the o-suite and the control run. Although the background column values are well captured by the products, the high emission events are not. A longer time

[2] No contribution from Reunion, Uccle and OHP due to instrument failure.

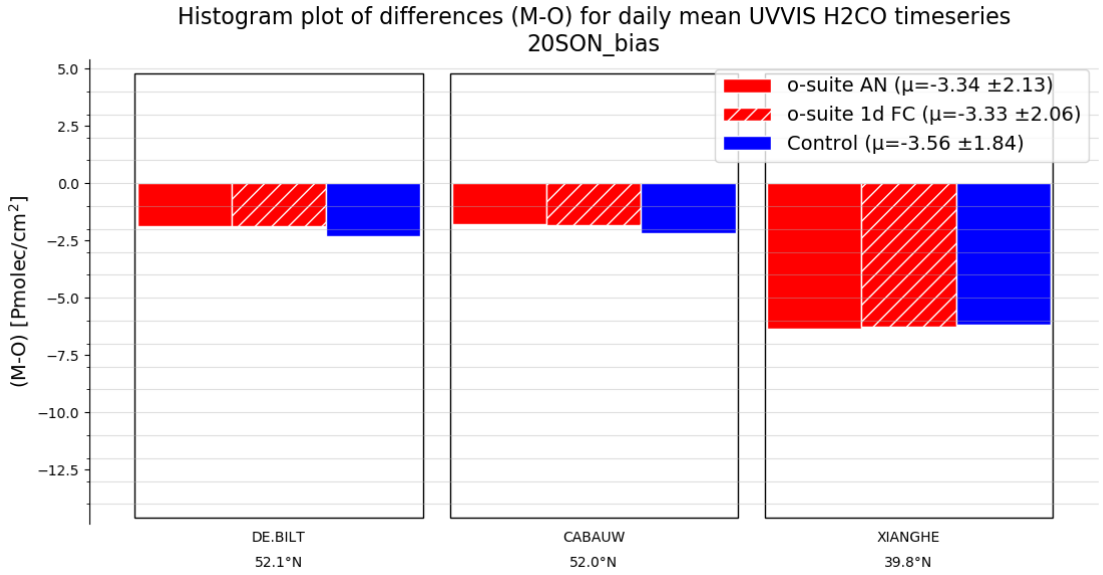

Figure 6.2.1: Table diagram showing the seasonal absolute bias in SON 2020 for three stations, sorted by latitude

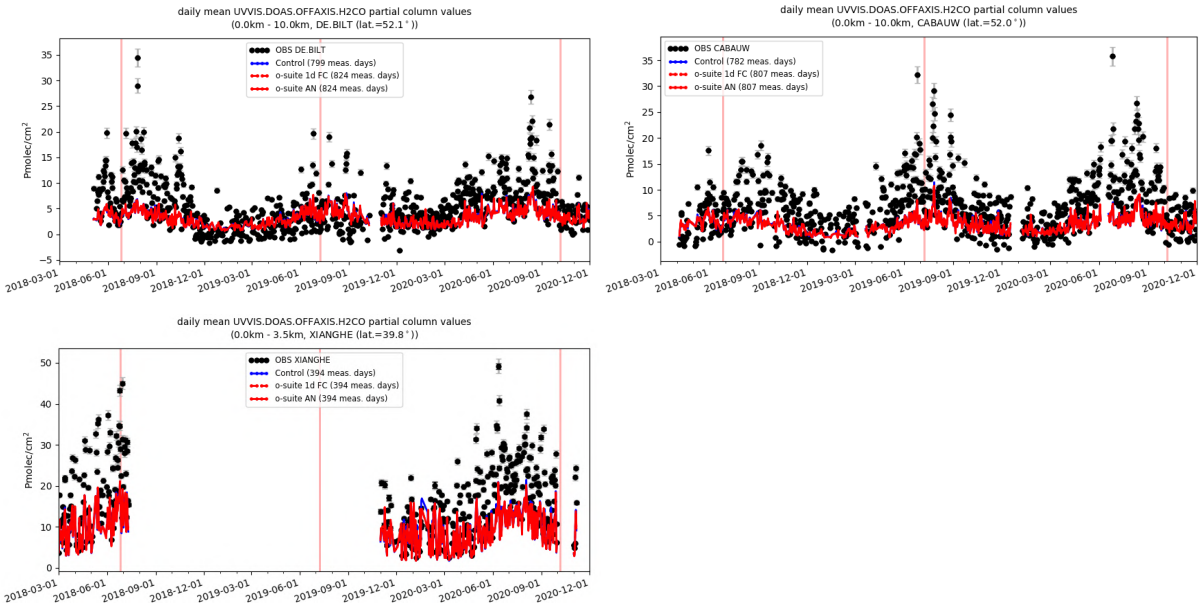

Figure 6.2.2: Time series of HCHO partial columns at the three different sites. All CAMS products underestimate the high peak HCHO concentrations. At Cabauw and De Bilt a seasonal dependence in the bias can be seen.

series is required to analyse a seasonal dependence in the bias, at Cabauw and De Bilt, however a seasonal dependence may be observed with an underestimation during summer and overestimation during winter months.

7. Water vapour

Unfortunately, due the covid-19 crisis and its impact on the airlines operations, only one IAGOS flight have been recorded during this reporting period. This is the first time since the beginning of IAGOS that we have almost no data to provide. The following period (DJF) will provide regular measurements again. For more detailed comparisons against IAGOS we refer to the previous NRT report, period JJA-2020 (Ramonet et al., 2021)

Figure 7.1 shows the results for a flight between Frankfurt and Amman on 17 November. The smooth drop in mixing ratio over Frankfurt is well reproduced by the CAMS models. The variability over Amman is largely captured by the CAMS o-suite and control, apart from the finer-scale features. As expected the o-suite and control run show only minor differences.

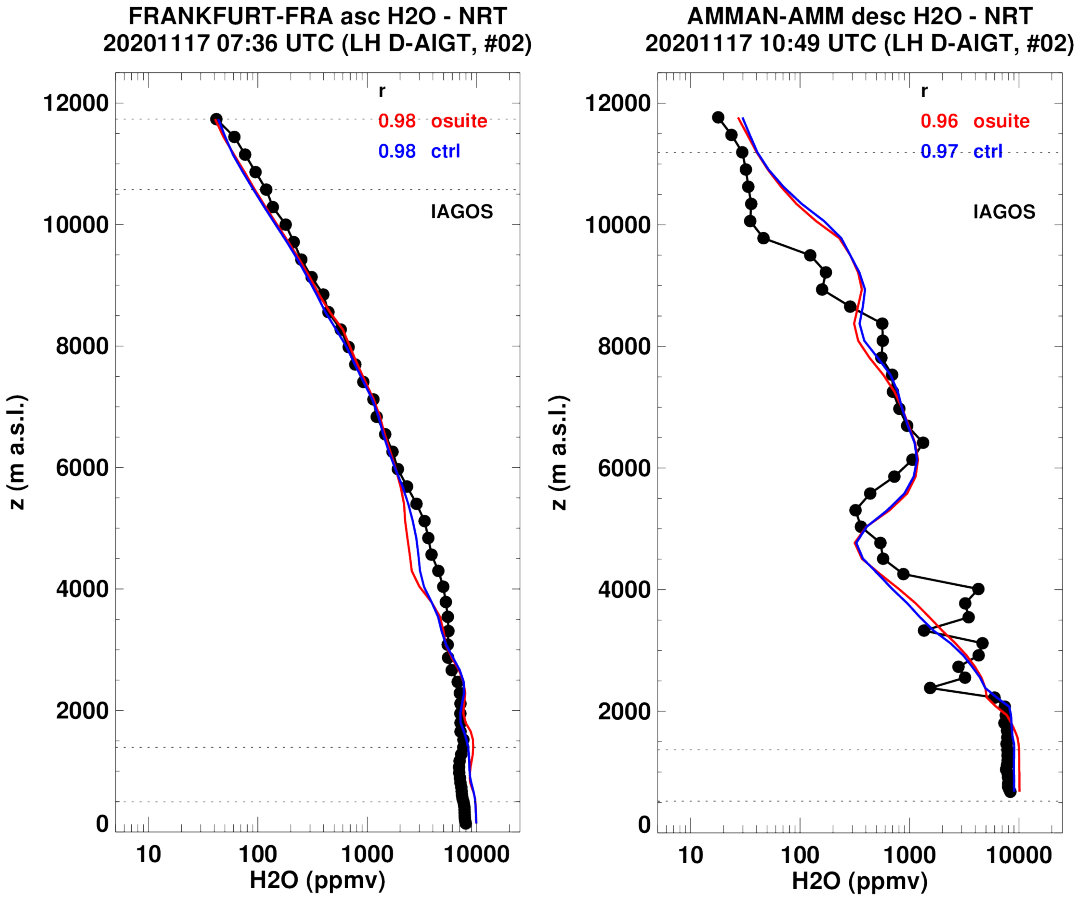

Figure 7.1. Vertical profiles of water vapour measured with the IAGOS aircraft over Frankfurt and Amman on 17 November 2020, compared to o-suite (red) and control (blue).

8. Aerosol

8.1 Global comparisons with Aeronet and EMEP

The comparison of the CAMS simulation of time series of aerosol optical depth can be found for all Aeronet stations at: http://aerocom.met.no/cams-aerocom-evaluation/

More detailed evaluation including scores, maps, scatterplots, bias maps and histograms illustrating the performance of the aerosol simulation in the IFS system are made available through the AeroCom web interface. The model run can be compared here to e.g. the CAMS interim reanalysis and other models, such as the AeroCom Median model.

A second web interface integrates NRT global surface observations of PM10, PM25, NO2, ozone and Aeronet AOD and AE, available since January 2020 (https://policy.atmosphere.copernicus.eu/aeroval.php#) .

Correlation, based on daily aerosol optical depth and NRT Aeronet observations, has been rather stable recently. The o-suite forecast at +3 days shows only slightly lower correlation. See figure S3.

Part of the month-to-month variation in correlation is due to the varying quality and coverage of the Aeronet network. This has been improved by the version 3 from Aeronet. We use therefore version 3 level 1.5 for all global comparison to Aeronet.

The performance of the o-suite model exhibits some seasonal variation in AOD depending on region (Fig. 8.1.1). Noteworthy is the persistent AOD overestimation over North America (Fig. 8.1.1-bottom), but also a long-term trend to overestimation in East Asia. The latitudinal display of model and Aeronet AOD in the period investigated here (Fig. 8.1.2) shows a small positive bias against Aeronet in the Southern Hemisphere.

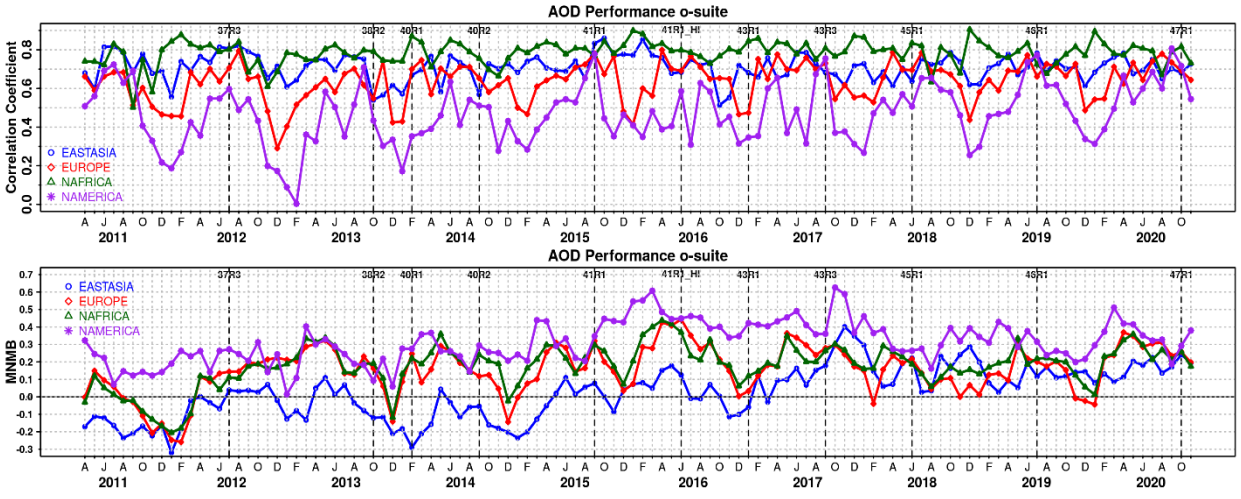

Figure 8.1.1. (top) Correlation coefficient and (bottom) modified normalized mean bias (MNMB) in AOD, since 2011, based on daily AOD comparison (Aeronet V3 level 1.5 data) in four world regions [East-Asia (blue); Europe (red); North Africa (green); North America (purple)] for the o-suite.

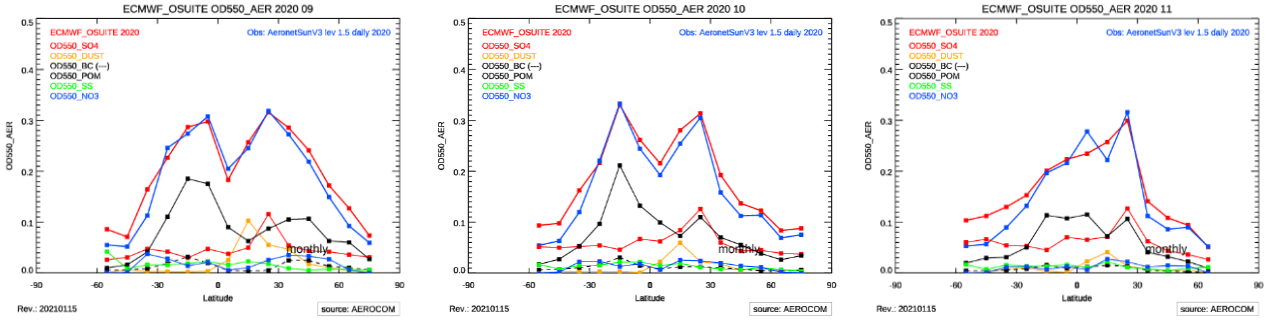

Figure 8.1.2. Aerosol optical depth of o-suite (red) compared to latitudinally aggregated Aeronet V3 level 1.5 data (blue) for the three months covered by this report.

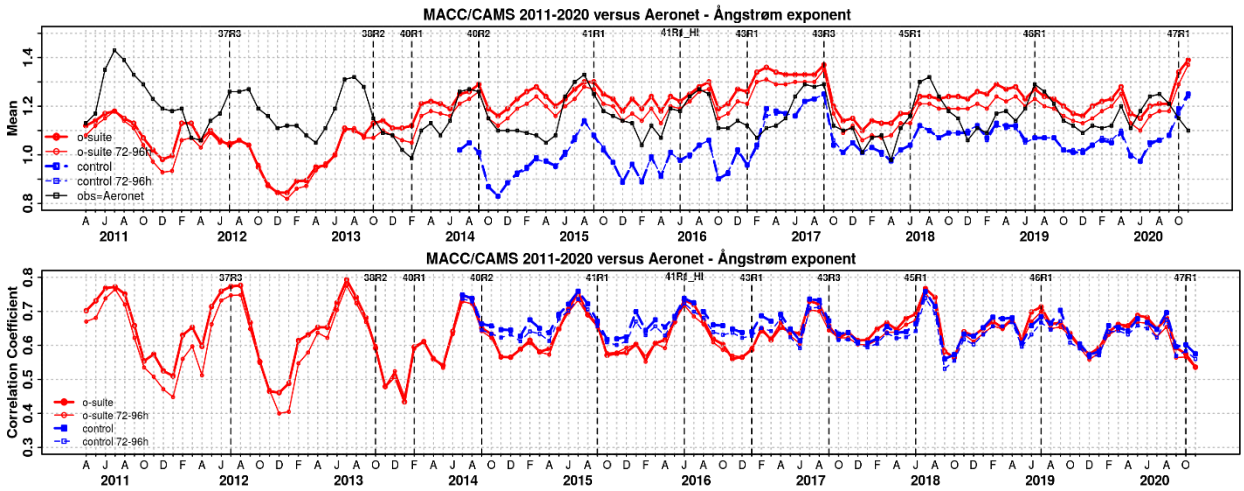

Figure 8.1.3. a) (top) Evolution of mean Ångström exponent in o-suite and control at Aeronet sites (Aeronet V3 level 1.5 data), based on matching monthly mean values. O-suite (thick red curve); o-suite at last forecast day (light red curve); control (blue dashed curve); control at last forecast day (light blue dashed curve). B) (bottom) Correlation using daily matching Ångström exponent.

The simulated aerosol size distribution may be validated to first order using the wavelength-dependent variation in AOD, computed as Ångström exponent, with higher Ångström exponents indicative of smaller particles. We find in SON 2020 a larger bias (Figure 8.1.3-a) particularly since latest model update in October 2020. Temporal and spatial variability is difficult to capture, but correlation from all daily data is lower than for AOD (Figure 8.1.3-b and S3).

Figure 8.1.4 shows that the Sep 2017 and Jun 2018 model changes are responsible for a shift in Ångström exponent. More organic matter seems to shift the size distribution to smaller sizes. The model upgrade in Feb 2017 with a bugfix for sea salt and improved parameterisations for SO4 led to that sea salt increased with 45%, while sulphate further decreased a bit. Sea salt has increased further due to a new sea salt emission scheme implemented in the Jun 2018 model upgrade and is back to earlier 2011-2013 levels. Since the Jul 2019 model upgrade with the improvement to the sulphur cycle, the SO4 seem to have increased to same levels as before the Sep 2017 upgrade. With the latest model upgrade a new sea salt emissions scheme appears to change sea salt.

Table 8.1.1. Mean global total and speciated AOD in the o-suite for the last two periods covered by the VAL report and change after 3 forecast days.

o-suite				
	Mean JJA 2020 0-24h	Change wrt to first day on day 4	Mean SON 2020 0-24h	Change wrt to first day on day 4
AOD@550	0.171	-10%	0.164	-15%
BC-OD@550	0.0065	-21%	0.0072	-20%
Dust-OD@550	0.032	10%	0.014	13%
OA-OD@550	0.039	-22%	0.045	-24%
SO4-OD@550	0.039	-21%	0.049	-25%
SS-OD@550	0.049	-3%	0.043	-6%
NO3-OD@550	0.0043	-1%	0.0038	7%

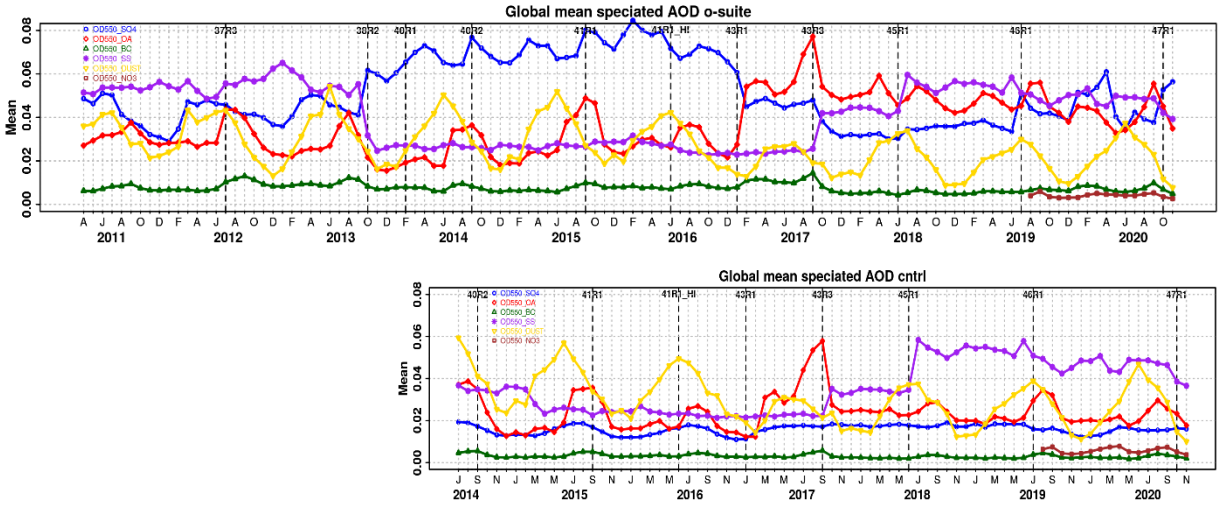

Figure 8.1.4. Evolution of the aerosol components of total AOD@550nm [OD550_SO4 = sulphate(blue); OD550_OA = organics(red); OD550_BC = black carbon(green); OD550_SS = sea salt(purple); OD550_DUST = dust(yellow); OD550_NO3 = nitrate(brown)] in o-suite and control simulation.

The o-suite uses data assimilation to obtain an analysis of the aerosol field. In the forecast period, however, a-priori model parameterisations and emissions (except fire emissions, which are kept in the forecast equal to the latest GFAS emission values) determine increasingly the aerosol fields. The performance of the day three forecasted AOD fields as compared to the first guess is shown in Figure S3 in the summary of this report. Table 8.1.1 shows an average global decrease in total aerosol optical depth during the first four forecast days, dominated by sulphate and organics. The control run with no assimilation shows somewhat less AOD (-35% compared to o-suite, see figure S3). All this supports the conclusion that either a-priori IFS aerosol and aerosol precursor sources are too small, or sinks are too effective in the IFS model.

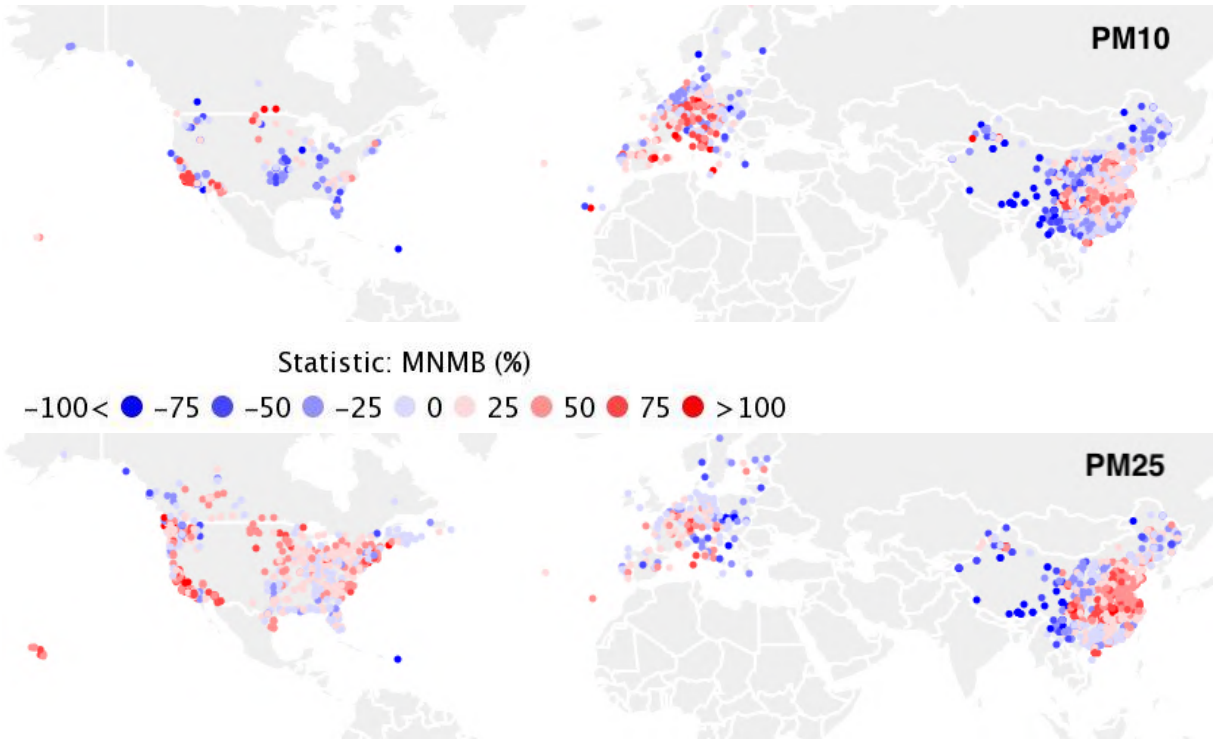

Figure 8.1.5. MNMB Bias [%]of average 2020 values of PM10 and PM2.5 for the IFS o-suite.

Global PM10 and PM25 NRT from surface observations (Airnow, EEA and Marco Polo) have been compared to the IFS aerosol model. NRT data for 2020 suggest on average for North America, Europe and China a PM10 MNMB bias of -5%, +13%, -2% respectively and for PM2.5 a MNMB bias of +14%, -3% and +13% respectively. Local variations of the bias are large. A detailed web interface integrates NRT global surface observations of PM10, PM25, NO2, ozone and Aeronet AOD and AE, available since January 2020 (https://policy.atmosphere.copernicus.eu/aeroval.php#) . Figure 8.1.5 shows exemplary the MNMB bias for PM10 and PM25.

Surface concentration of particulate matter below 10 µm (PM10) and below 2.5 µm (PM25) from the o-suite experiment have been validated against data from 160 background IMPROVE and EMEP stations. A climatological average has been constructed from data in the period 2000-2009 as available in the EBAS database hold at NILU. The data availability is not the same at all stations, and sometimes covers only a few years.

A negative MNMB bias of PM10 in Europe and an overestimate in North America PM2.5 appears (Fig. 8.1.6), consistent with the AOD bias in the two regions. Figure 8.1.7 shows the evolution of mean observed and simulated PM10 and PM2.5. The biggest change appeared in July 2017 with the bias of o-suite now becoming positive almost overall. Shown is also the statistics of being within factor 2, a more robust metrics for a comparison to climatological data. This statistical indicator has clearly improved over time, indicating best PM10 and PM25 performance in summer months for the o-suite. O-suite is also better than the control simulation most of the times for PM10. For PM2.5 the difference is less clear, but since September 2017 (upgrade to 43R3) the control is performing better than the o-suite. With the July 2019 model upgrade the PM2.5 performance of the o-suite is very similar to the control. The time series for the October 2020 upgrade (Cy47R1) is too short to draw conclusions.

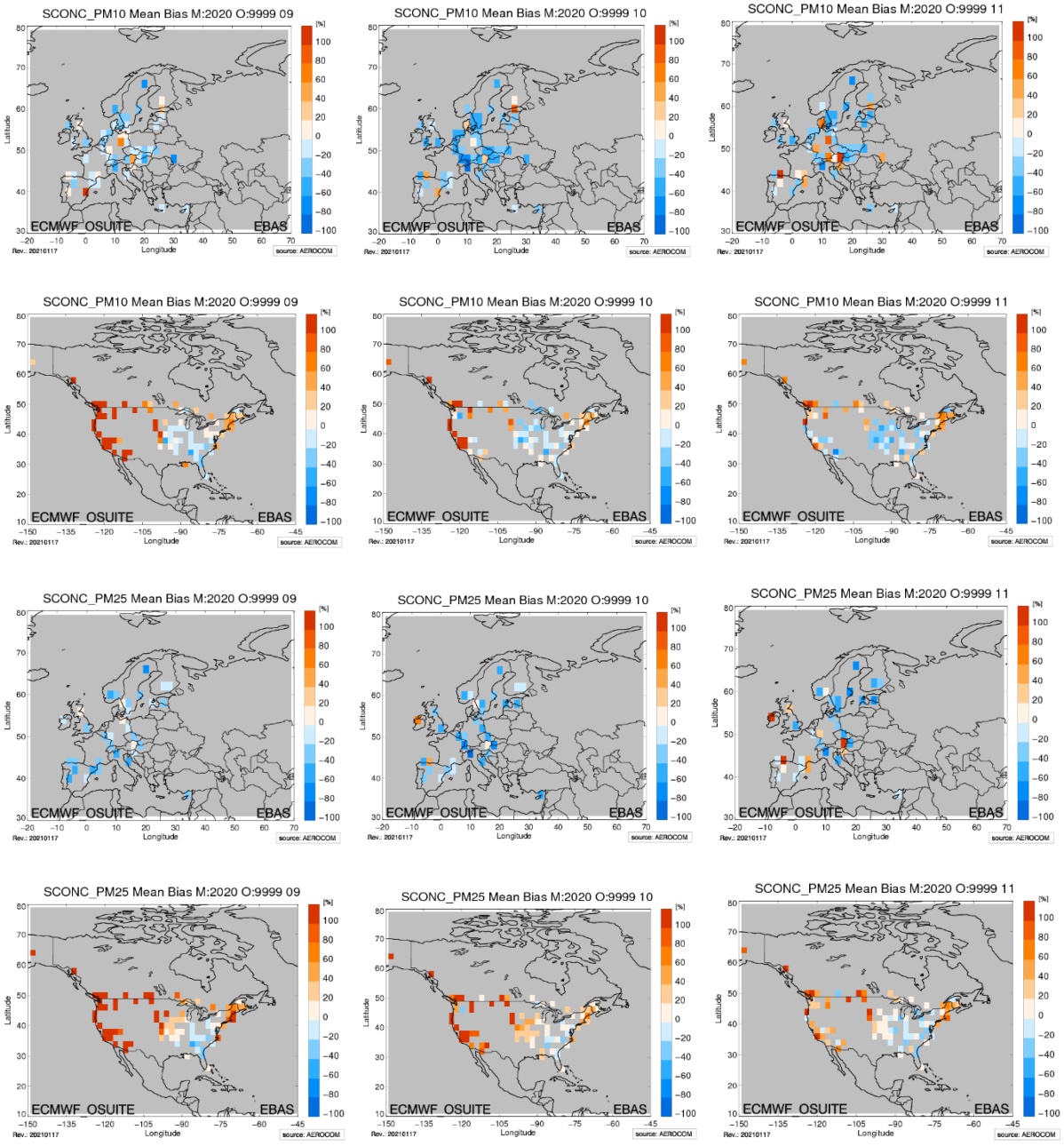

Figure 8.1.6. Bias [%] map of monthly mean PM10 and PM2.5 concentrations at EMEP (Europe, first and third row) and IMPROVE sites (North America, second and fourth row) for August (left column), September (middle) and November 2020 (right); simulated o-suite versus EMEP/IMPROVE derived climatological average (2000-2009).

Anthropogenic black carbon (BC) and organic aerosol (OA) emissions were found to be shifted by 180 degrees in longitude from Jan 2020 to Oct 2020. This resulted in particular in erroneous, shifted black carbon fields, possibly also BC absorption fields (see figure 8.1.8). An analysis of the speciated surface concentration bias shows that the BC bias in Europe is becoming more negative from January 2020 onwards, because due the shift “pacific” BC emissions are effective over Europe (see figure 8.1.9). Since latest Oct 2020 model upgrade the concentrations fields of BC and OA are shifted back to emissions source.

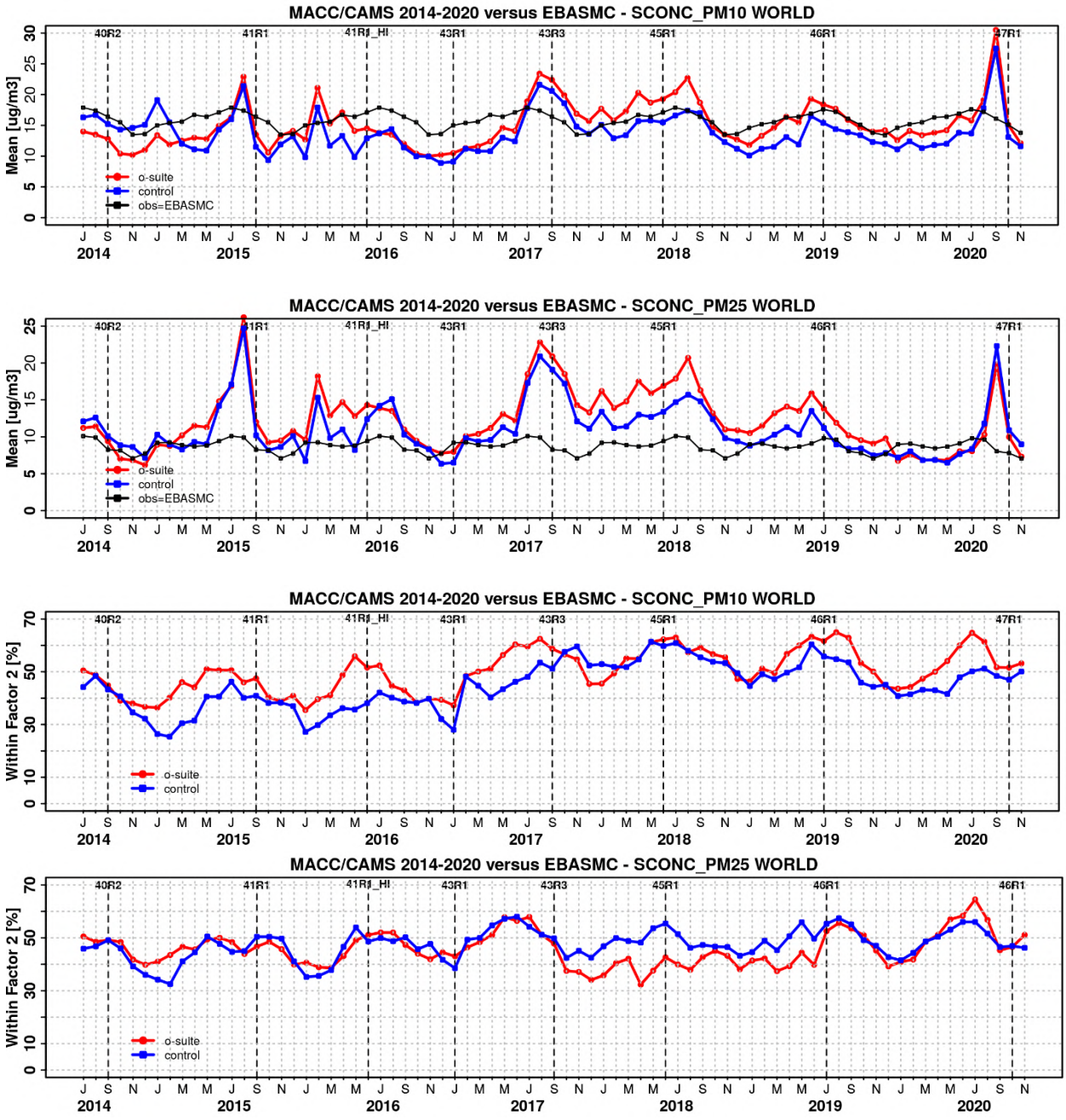

Figure 8.1.7. Temporal evolution of monthly mean average PM10 and PM2.5 concentrations at EMEP (Europe) and IMPROVE sites (North America) and data fraction within a factor 2 of observed; ca 160 sites, observed data averaged from data available in EBAS from 2000-2009.

Organic aerosol results are less affected, since secondary aerosol formation and biomass burning sources are more important for OA fields. PM and Optical depth is also not impacted to a large extent, mainly because BC is a very small fraction of these parameters.

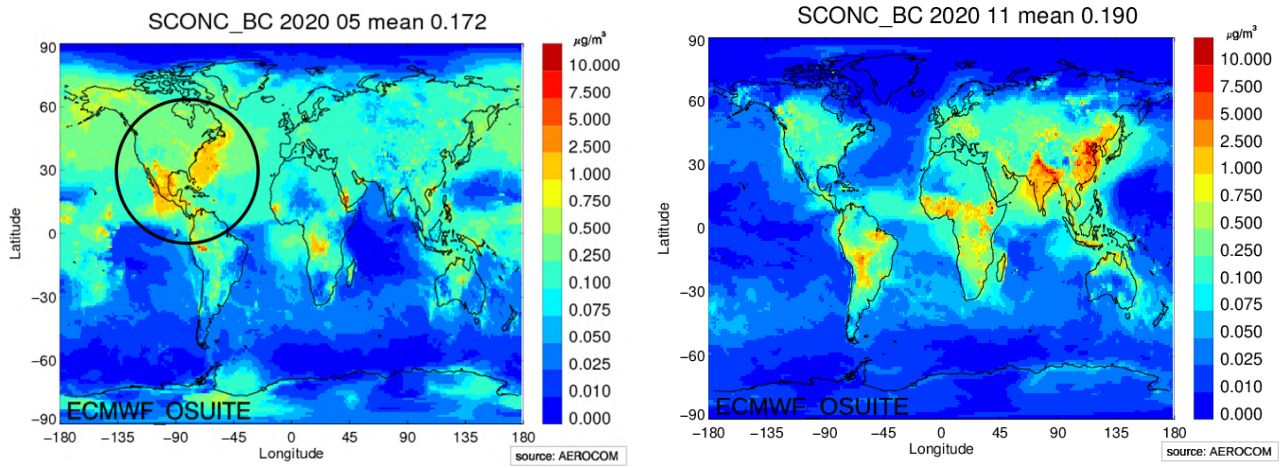

Figure 8.1.8. Surface concentration of black carbon in o-suite for May 2020 (left, 46R1) and November 2020 (right, 47R1). Anthropogenic black carbon (BC) and organic aerosol (OA) emissions were shifted by 180 degree longitude (see circle), a feature which was repaired in Cy47R1.

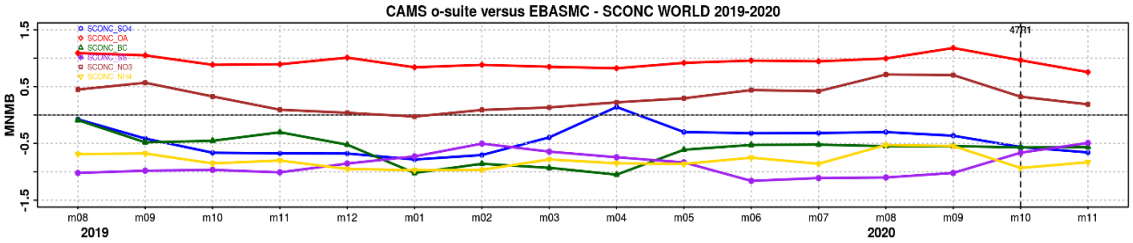

Figure 8.1.9. Evolution of MNMB Bias of simulated surface concentrations in o-suite against a climatology of speciated aerosol concentrations, mainly over Europe and North America.

8.2 Validation of dust optical depth against AERONET, and comparisons with the Multi-model Median from SDS-WAS

The 72-hour forecasts (on a 3-hourly basis) of dust aerosol optical depth (DOD) from CAMS o-suite and control have been validated for the period 1 September 2020 – 30 November 2020 against the AERONET Spectral Deconvolution Algorithm (SDA) cloud-screened observations, MODIS/Terra and Aqua Collection 6.1 Level 3 (1º x 1º) and SDS-WAS Multi-model Median DOD. The SDS-WAS Multi-model Median DOD is obtained from (currently) twelve dust prediction models participating in the Sand and Dust Storm Warning Advisory and Assessment System (SDS-WAS) Regional Center for Northern Africa, Middle East and Europe (http://sds-was.aemet.es/). At those sites where the SDA products are available, the dust AOD evaluation will be complemented with AOD-coarse, which is fundamentally associated with maritime/oceanic aerosols and desert dust. Since sea-salt is related to low AOD (< 0.03; Dubovik et al., 2002) and mainly affects coastal stations, high AOD-coarse values are mostly related to mineral dust.

During this season, satellites (see MODIS in Figure 8.2.1) show that significant dust activity in Northern Africa (seasonal AOD above 0.5) is concentrated in latitudes between 15N and 25N with maximum seasonal AOD values over 0.7 in Mali and Chad. Meanwhile, in the Middle East, high AOD values up to 0.5 are observed in Iraq. Overall, o-suite shows lower SON-2020 values than the control

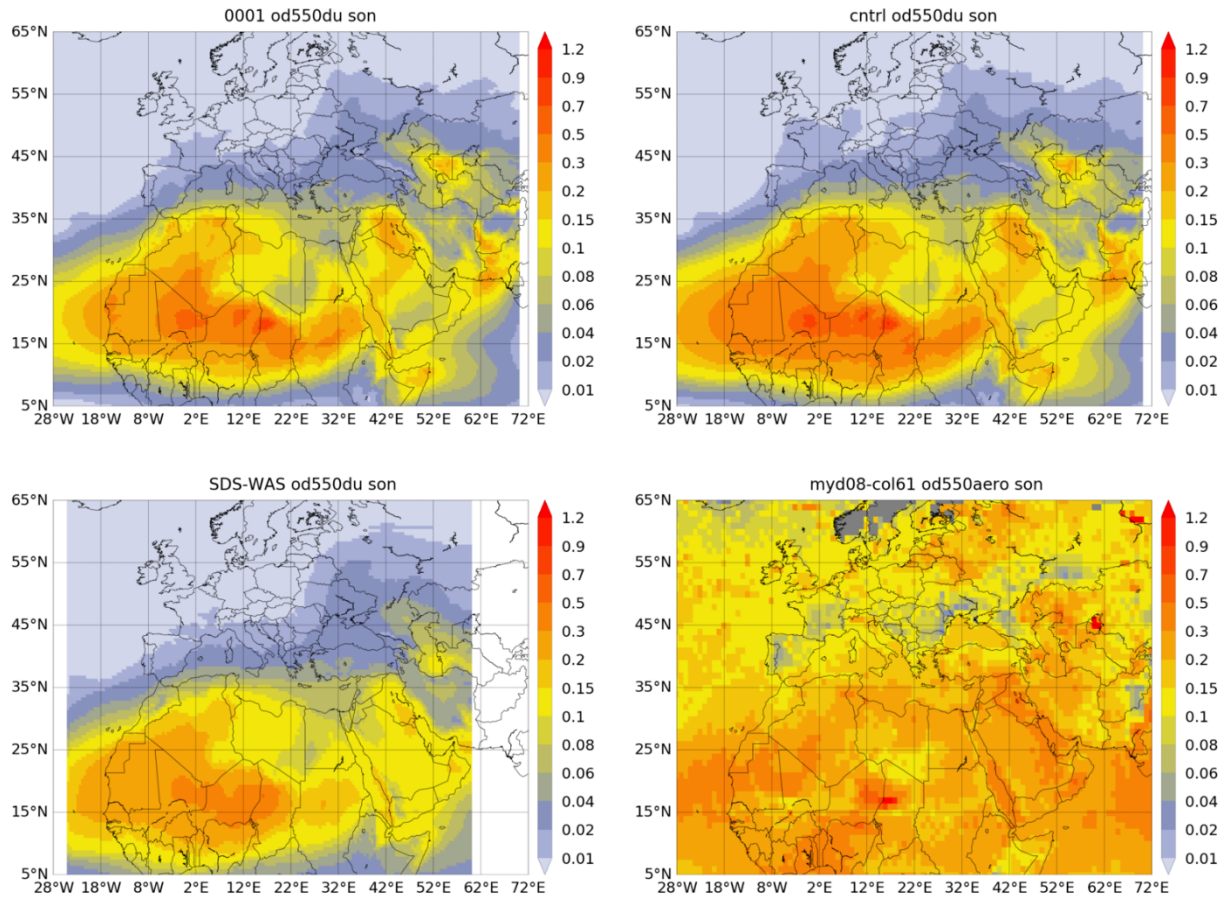

Figure 8.2.1: Averaged DOD 24h forecast from o-suite (top left) and control (top right), DOD of the multi-model SDS-WAS Median product (bottom left) as well as AOD from MODIS/Aqua Collection 6.1 Level 3 combined Dark Target and Deep Blue product (bottom right) for the study period.

run, similar to previous seasons, and both are generally higher than the SDS-WAS multi-median product, in particular in Iraq and over the Eastern Sahara, as well as in regions around the Caspian Sea and the Afghanistan/Pakistan border. Both CAMS runs reproduce the high DOD dust activity in the region of Mali, Mauritania, and Algeria, but they overestimate DOD in Iraq, the Eastern Sahara, the Caspian Sea and the Afghanistan/Pakistan border region in comparison with MODIS. Seasonal DOD over Central Saudi Arabia, Iran and Afghanistan /Pakistan border appears overestimated in comparison with MODIS and the SDS-WAS multi-model ensemble (see Figure 8.2.1). However, both CAMS runs can reproduce the dust transport over the North Atlantic region. On 6th October 2020, the upgrade of the CAMS models is affecting the desert dust module. This upgrade revised the desert dust source mapping and dust emissions. From this date, dust emissions are lower in comparison with the previous model version as is highlighted in the AERONET comparison at sites in desert dust regions (see Figure 8.2.3a).

From September to November, o-suite (control) reproduce the daily variability of AERONET dust-filtered observations (see Figure 8.2.2), with a correlation coefficient of 0.70 (0.70) averaged over all AERONET sites, which is lower than the SDS-WAS multi-model product which has a correlation

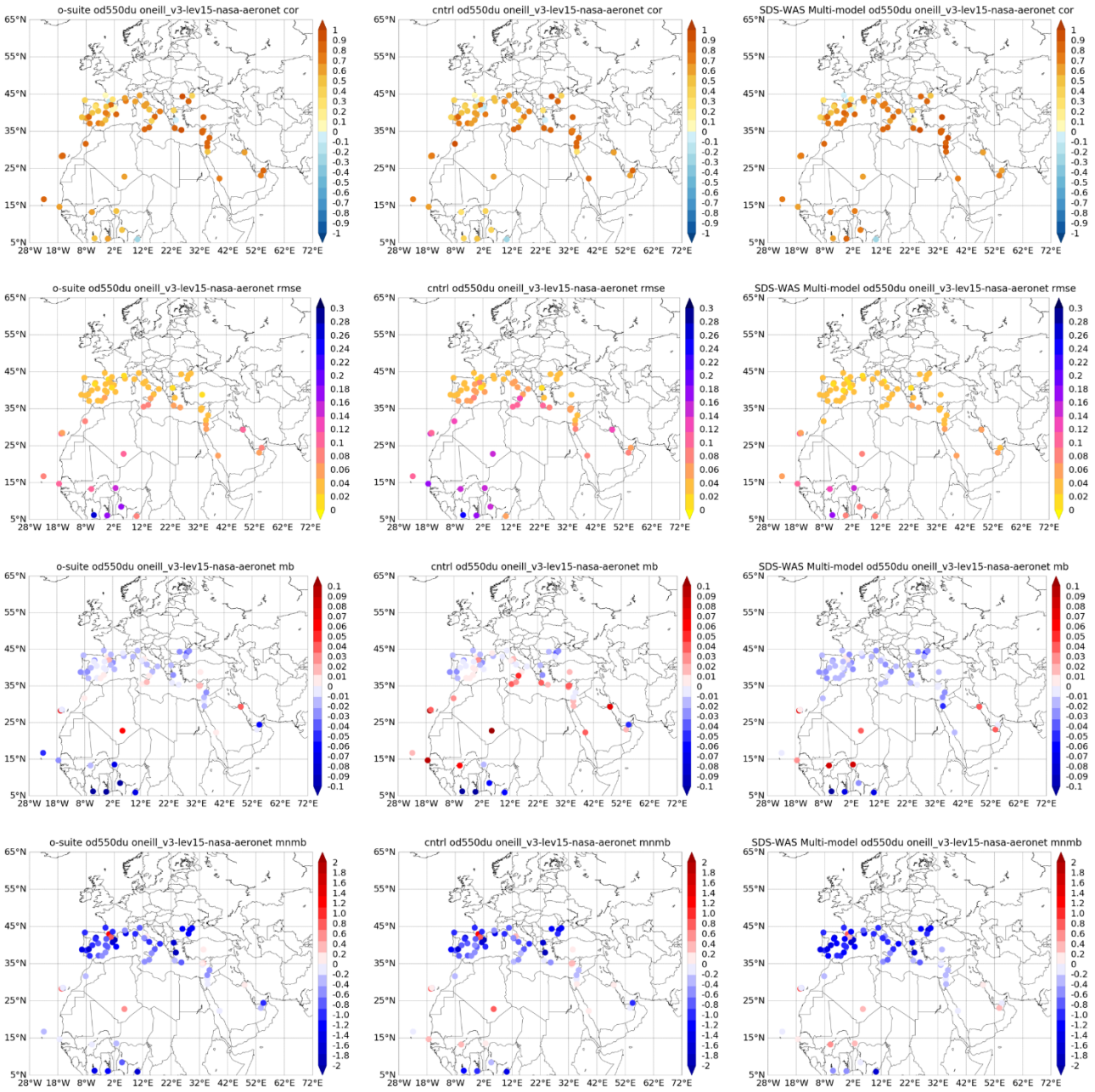

Figure 8.2.2: Skill scores (correlation coefficient, RMSE, MB and MNMB) for 24-hour forecasts of CAMS o-suite (left column), control (central column) and DOD Multi-model SDS-WAS Median (right column) for the study period. AOD-coarse from AERONET SDA is the reference.

coefficient of 0.82. Regarding mean bias (MB), o-suite tends to slightly underestimate the AERONET observations with an MB of -0.01 while the control slightly overestimates it (MB of 0.01). The SDS-WAS multi-model underestimates the AERONET values (MB of -0.01).

Over desert dust sources in the Sahara (see Table 8.2.1 as well as Tamanrasset INM AERONET site in Figure 8.2.3a), CAMS runs do reproduce the daily variability with correlation coefficients 0.64 for o-suite and 0.65 for control. However, DOD is overestimated (MB of 0.06 for o-suite and 0.10 for

Table 8.2.1: Skill scores (MB, MNMB, RMSE and r) of 24h forecasts (on 3hourly basis) for CAMS o-suite, CAMS control and SDS-WAS Multi-model Median for the study period, and the number of data (NDATA) used. DOD (SDA AOD coarse product) from AERONET is the reference.

		Control				o-suite DOD				SDS-WAS Median DOD			
	NDATA	MB	MNMB	RMSE	r	MB	MNMB	RMSE	r	MB	MNMB	RMSE	r
Sahara	324	0.10	0.69	0.15	0.65	0.06	0.50	0.11	0.64	0.04	0.41	0.09	0.66
Sahel	439	-0.04	-0.12	0.16	0.26	-0.10	-0.53	0.17	0.44	0.02	0.15	0.12	0.61
Tropical North Atlantic	71	0.02	-0.08	0.11	0.70	-0.05	-0.44	0.09	0.78	-0.01	-0.05	0.07	0.77
Subtropical North Atlantic	439	0.04	0.26	0.10	0.66	0.01	0.08	0.06	0.74	0.02	0.15	0.07	0.67
North Western Maghreb	198	0.03	-0.41	0.11	0.89	0.00	-0.57	0.07	0.88	-0.02	-0.57	0.04	0.88
Western Iberian Peninsula	732	-0.01	-0.87	0.05	0.57	-0.01	-0.93	0.04	0.58	-0.02	-1.09	0.03	0.65
Iberian Peninsula	1297	-0.01	-0.88	0.05	0.62	-0.01	-0.92	0.03	0.68	-0.02	-1.17	0.03	0.69
Western Mediterranean	1197	0.00	-0.74	0.05	0.59	-0.01	-0.79	0.03	0.62	-0.01	-1.03	0.02	0.66
Central Mediterranean	1564	0.01	-0.66	0.07	0.74	-0.01	-0.79	0.05	0.74	-0.02	-0.91	0.04	0.78
Eastern Mediterranean	2515	0.01	-0.22	0.06	0.79	-0.01	-0.36	0.04	0.82	-0.01	-0.46	0.04	0.85
Eastern Sahara													
Middle East	1244	0.03	-0.07	0.10	0.71	0.00	-0.24	0.08	0.69	0.02	0.13	0.06	0.66
All sites	11615	0.01	-0.39	0.08	0.70	-0.01	-0.53	0.06	0.70	-0.01	-0.57	0.05	0.82

control). As shown in Tamanrasset INM (Figure 8.2.3a), the overestimations observed in control are reduced in the o-suite experiment. The SDS-WAS Multi-model results for Sahara shows better skills for this season (with a seasonal correlation of 0.66 and MB of 0.04). In the Middle East (see Kuwait University in Figure 8.2.3a), the comparison with AERONET observations shows similar correlation coefficients (0.69 for o-suite and 0.71 for control) and smaller MB (MB of 0 for o-suite and 0.03 for control, see Table 8.2.1). These results in the Middle East are slightly better than those obtained by the SDS-WAS Multi-model (with a seasonal correlation of 0.02 and MB of 0.66). After 6th October 2020, all the AERONET sites located in desert dust regions show a clear change in the model behaviour. As mentioned before, on 6th October 2020, there were an upgrade of the CAMS models that it is affecting the desert dust module. After the upgrade, CAMS DOD show a sharp decrease for both o-suite and control.

In the Sahel (see Table 8.2.1), the o-suite enhances the underestimations observed in the control run (MB of -0.04 for control and -0.10 for o-suite) despite o-suite better reproduces the observed daily variability (with a correlation of 0.44 for o-suite in comparison to 0.26 for control). The underestimations observed in o-suite in the Sahel are also spread to the Tropical North Atlantic (MB of -0.05 for o-suite and -0.08 for control, see Table 8.2.1 and Dakar in Figure 8.2.3a). Although, the daily variability is better capture by CAMS in this region with correlation coefficients of 0.70 for control and 0.78 for o-suite.

In the case of the North-Western Maghreb (see Table 8.2.1 and Saada in Figure 8.2.3b), o-suite and control show higher correlation coefficient (0.89 for control and 0.88 for o-suite) and o-suite also reduces overestimations observed in control (MB of 0.03 for control and 0.01 for o-suite). Over the

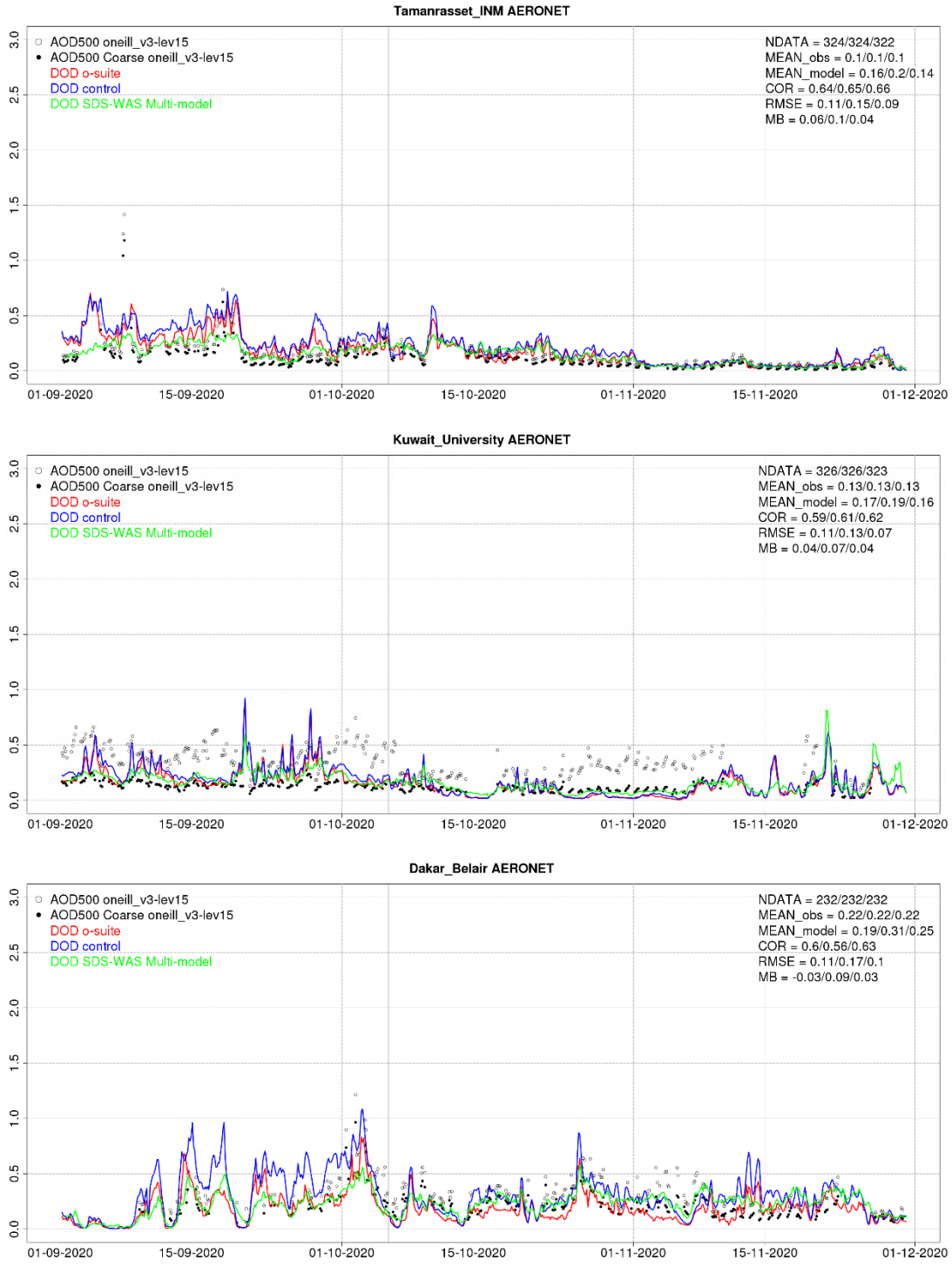

Figure 8.2.3a: AOD and coarse AOD from AERONET Direct-sun (black dots), DOD o-suite (red line), DOD control (blue line) and DOD Multi-model SDS-WAS Median (green line) for the study period over Tamanrasset INM (Sahara), Kuwait University (Middle East) and Dakar (Tropical North Atlantic). Skill scores per each site and model (o—suite/control/ SDS-WAS Multi-model) are shown in the upper right corner (NDATA: available 3-hourly values used for the calculations, MEAN observations, MEAN model, COR, RMSE, MB).

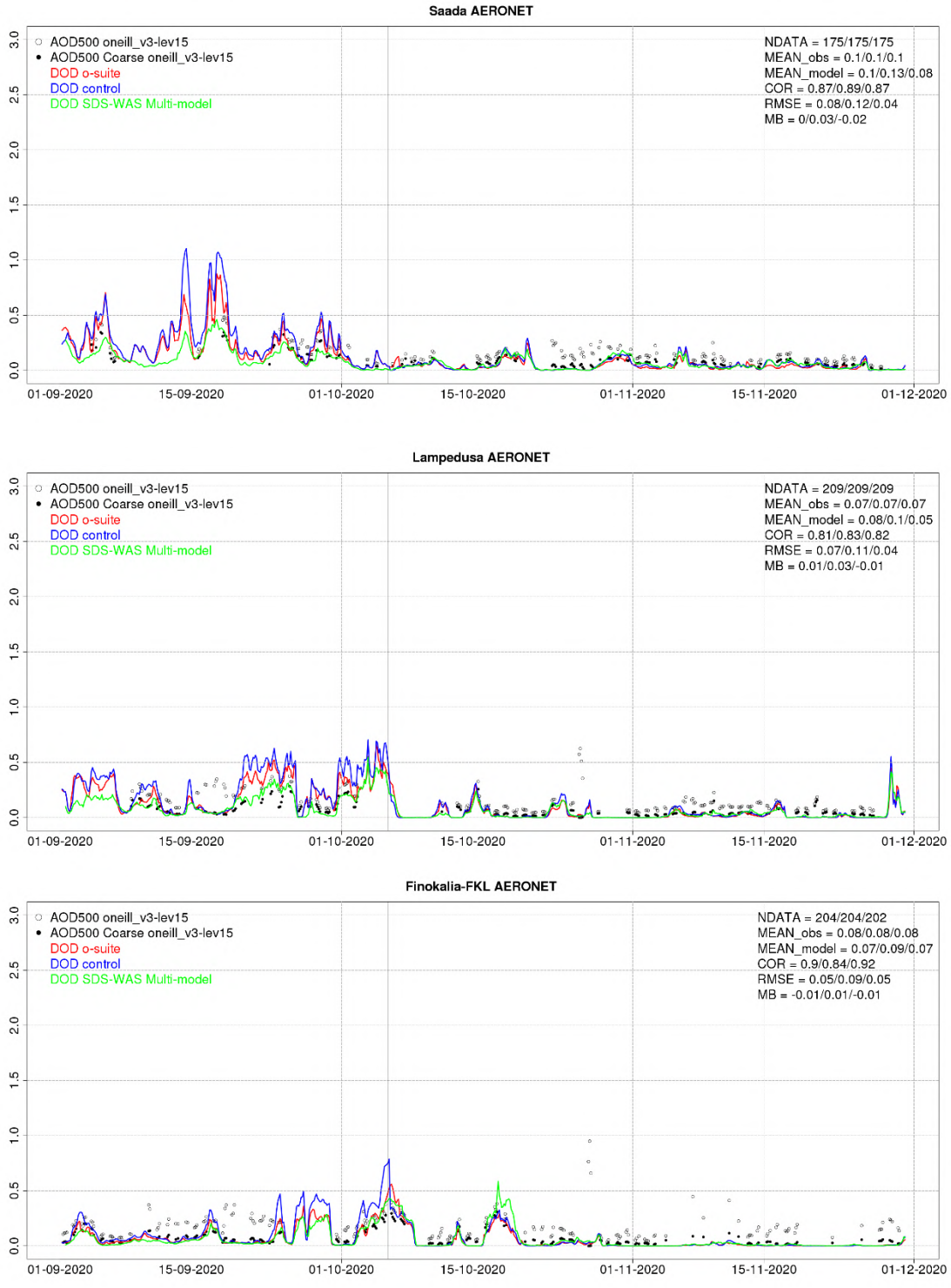

Figure 8.2.3b: AOD and AOD-coarse from AERONET SDA (black dots), DOD o-suite (red line), DOD control (blue line) and DOD Multi-model SDS-WAS Median (green line) for the study period over, Saada (NW Maghreb), Lampedusa (Central Mediterranean) and Finokalia-FKL (Eastern Mediterranean) Skill scores per each site and model (o—suite/control/SDS-WAS Multi-model) are shown in the upper right corner (NDATA: available 3-hourly values used for the calculations, MEAN observations, MEAN model, COR, RMSE, MB).

Iberian Peninsula and the Mediterranean, both CAMS runs show correlations between 0.59 and 0.82 and slightly overestimations in o-suite (MB between 0.03 and 0.05) than control (MB between -0.01 and 0.01). During this season, dust transport is concentrated in Central Mediterranean (see Lampedusa in Figure 8.2.3b) with lower DOD observations in the Western Mediterranean (see Saada in Figure 8.2.3b).

The comparison of the 1- to 3-day forecasts shows that the prediction is stable during the forecasts in comparison with AERONET dust-filtered observations with correlation coefficients of 0.70 (0.70), 0.65 (0.64), and 0.64 (0.63) respectively for 24, 48 and 72h forecasts for all the sites, for o-suite (control).

8.3 Aerosol validation over Europe and the Mediterranean

Three-hourly aerosol optical depth (AOD) and surface concentration (PM10 and PM2.5) from the o-suite and control run have been validated against AERONET AOD direct-sun cloud-screened and EEA PM10 and PM2.5 observations.

Aerosol optical depth over the Mediterranean

During autumn, both CAMS runs do reproduce the daily variability of AERONET AOD observations, although present general overestimation in the whole Mediterranean Basin (see Figure 8.3.1). The correlation coefficient decreases from (0.20, 0.53 and 0.41) for control to (0.14, 0.43 and 0.32) and MB slightly increases from (0.08, 0.10 and 0.12) for control to (0.12, 0.14 and 0.15) for the o-suite respectively for Western, Central and Eastern Mediterranean. Overestimations are linked to an enhanced background aerosols that are not directly linked to natural contributions. This is shown in the Barcelona (Spain, Western Mediterranean), Lecce (Italy, Central Mediterranean) and Sede Boker (Israel, Eastern Mediterranean) from September to November at AERONET sites (see Figure 8.3.2). Since the CAMS model upgrade on 6th October 2020, there is a reduction of the desert dust contribution over the Mediterranean. This decrease in the Saharan dust transport towards Europe is associated with a lower correlation at AERONET sites in the Iberian Peninsula and South Frances (see Figure 8.3.1).

Surface aerosol concentrations in Europe

At surface levels, both CAMS runs show a higher correlation coefficient in north-western Europe (above 0.7) in comparison with the 3-hourly EEA PM10 and PM2.5 observations (see Figure 8.3.3 and 8.3.4). For PM10, both CAMS runs show underestimations (MB under -4 µg/m^3) except in Central Europe and Eastern Iberian Peninsula which appear overestimated (MB above 4 µg/m^3). However the PM2.5 comparison shows lower difference, the overestimations observed in PM10 o-suite in Central Europe are also detected in the PM2.5 o-suite comparison (MB above 4 µg/m^3, see Figure 8.3.4). During September, both CAMS runs predict peaks above 50 µg/m^3 for PM10 (see Figure 8.3.5) and is overall overestimated compared to the EEA observations(see Figure 8.3.5). But since the model upgrade on 6th October, the surface concentrations PM10 and PM2.5 levels are lower. PM10 levels are reduced more than 60% in some sites (see IT2061A and MT00007 in Figure 8.3.5a and ES1569A in Figure 8.3.5b). This reduces the number of predicted PM10 daily exceedances. Coarse aerosol contributions (coming from desert dust and sea-salt) were predicted in Southern Europe during this season as indicated by the low observed PM2.5/PM10 ratio.

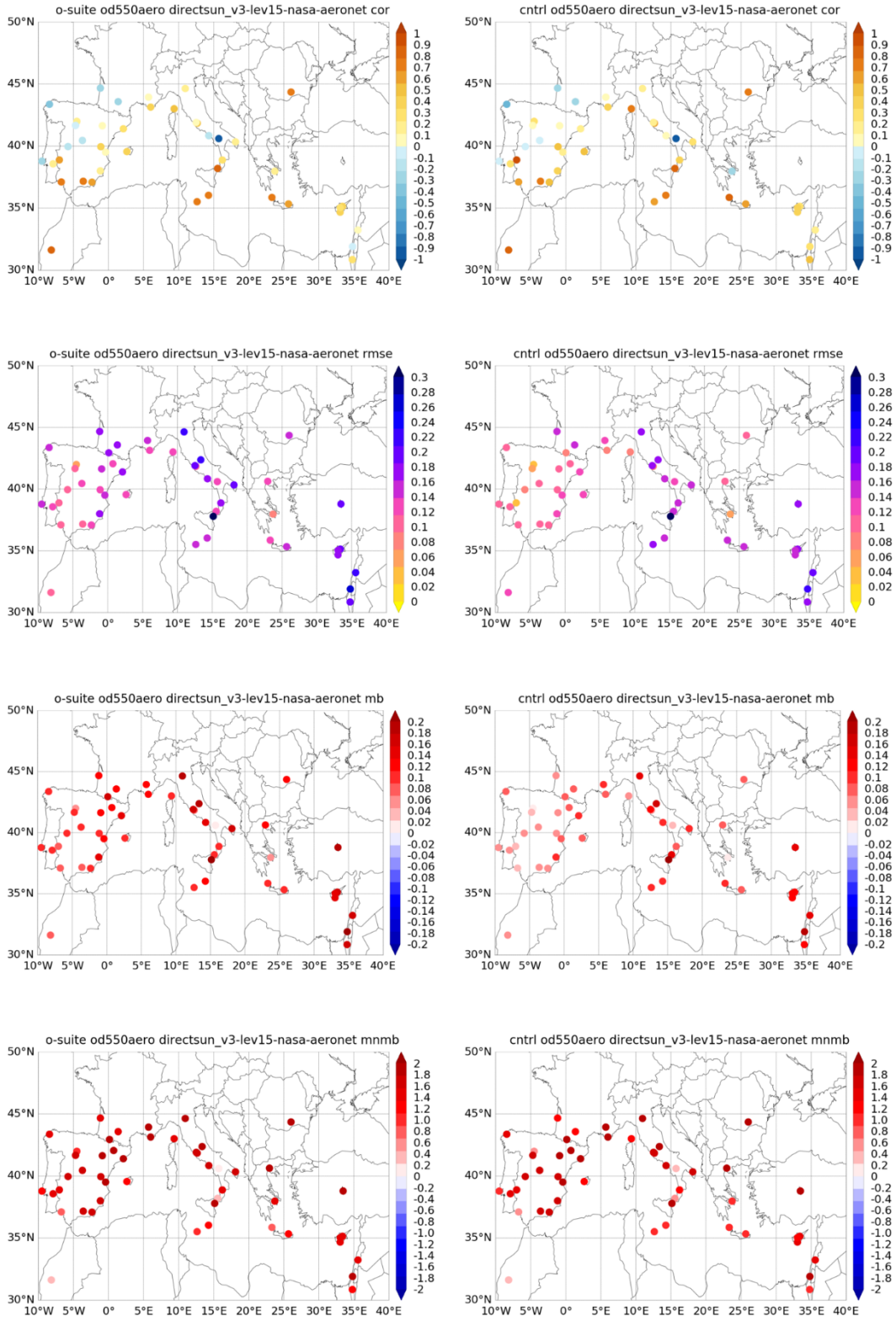

Figure 8.3.1: Skill scores (correlation coefficient, RMSE, MB and MNMB) for 24-hour forecasts of CAMS o-suite and control for the study period. AOD from AERONET direct-sun is the reference.

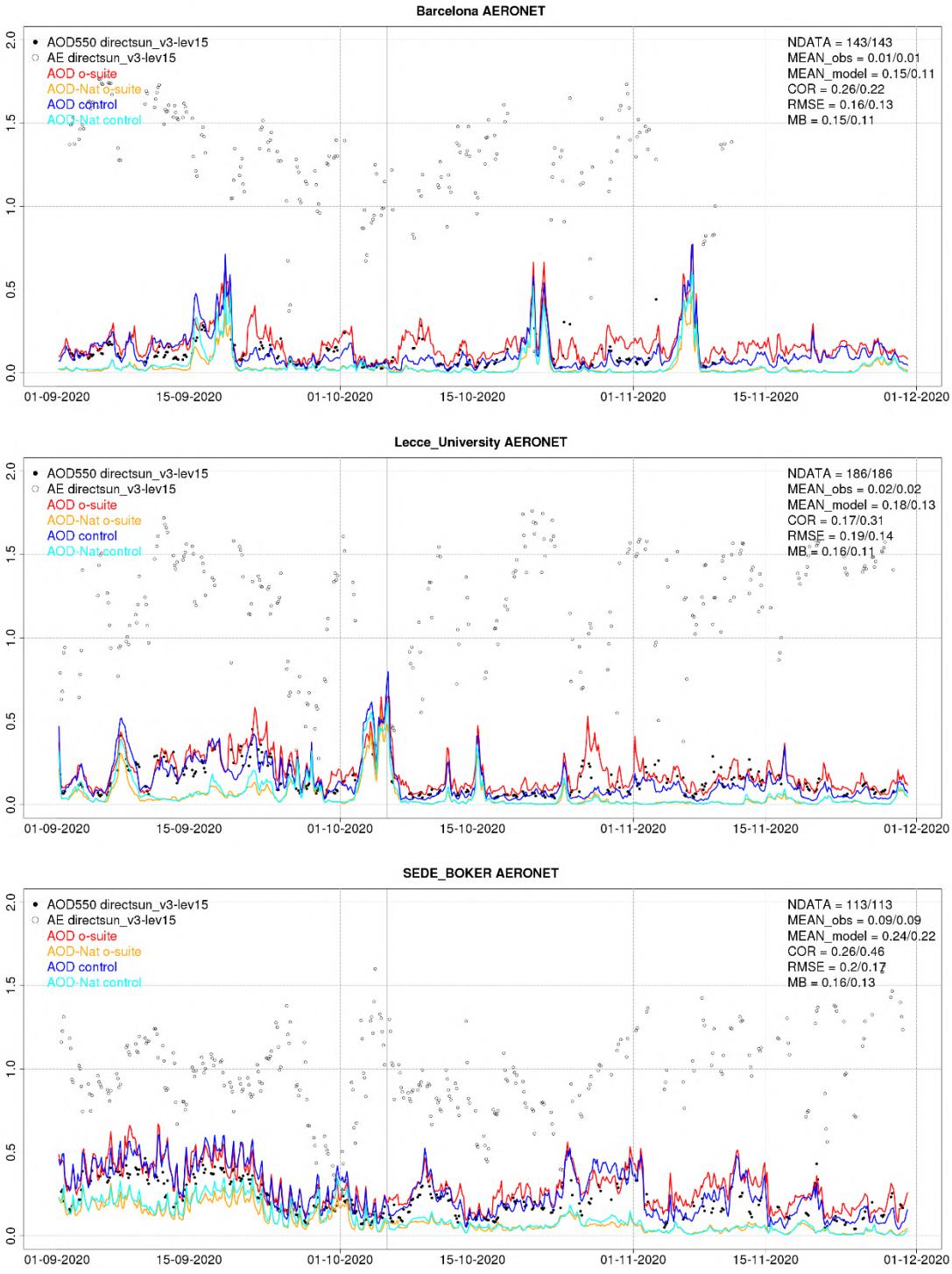

Figure 8.3.2: AOD from AERONET (black dot), AOD o-suite (red line), AOD control (blue line), AOD-Nat o-suite (orange line), AOD-Nat control (cyan line), for the study period over Barcelona (Spain), Lecce University (Italy) and SEDE BOKER (Israel). AOD-Nat corresponds to the natural aerosol optical depth that includes dust and sea-salt. Skill scores per each site and model (o—suite/control) are shown in the upper right corner (NDATA: available 3-hourly values used for the calculations, MEAN observations, MEAN model, COR, RMSE, MB).

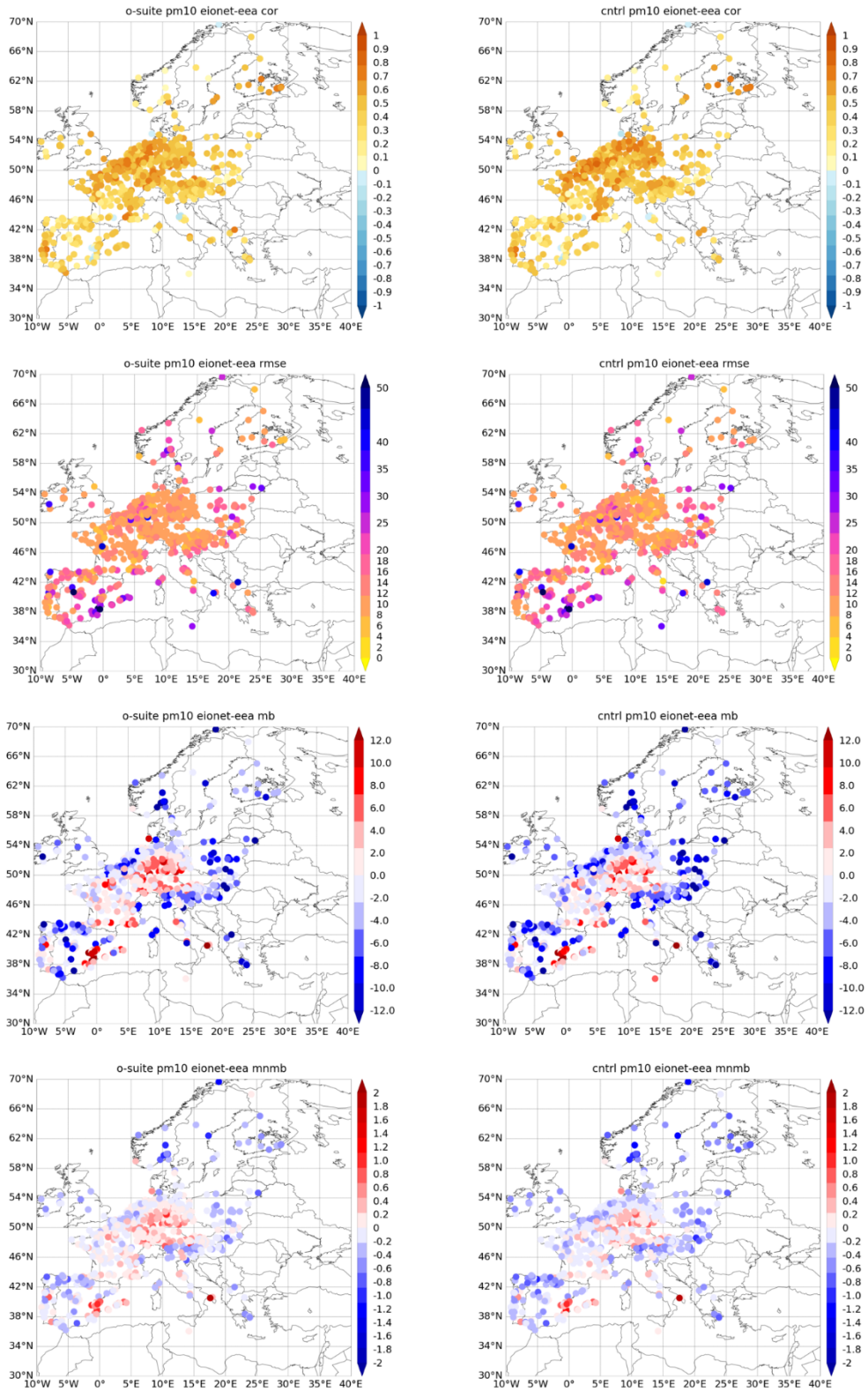

Figure 8.3.3: Skill scores (correlation coefficient, RMSE, MB and MNMB) for 24-hour forecasts (at 3hourly basis) of CAMS o-suite and control for the study period. 3hourly PM10 from EIONET is the reference. Only global scale representative available stations are displayed.

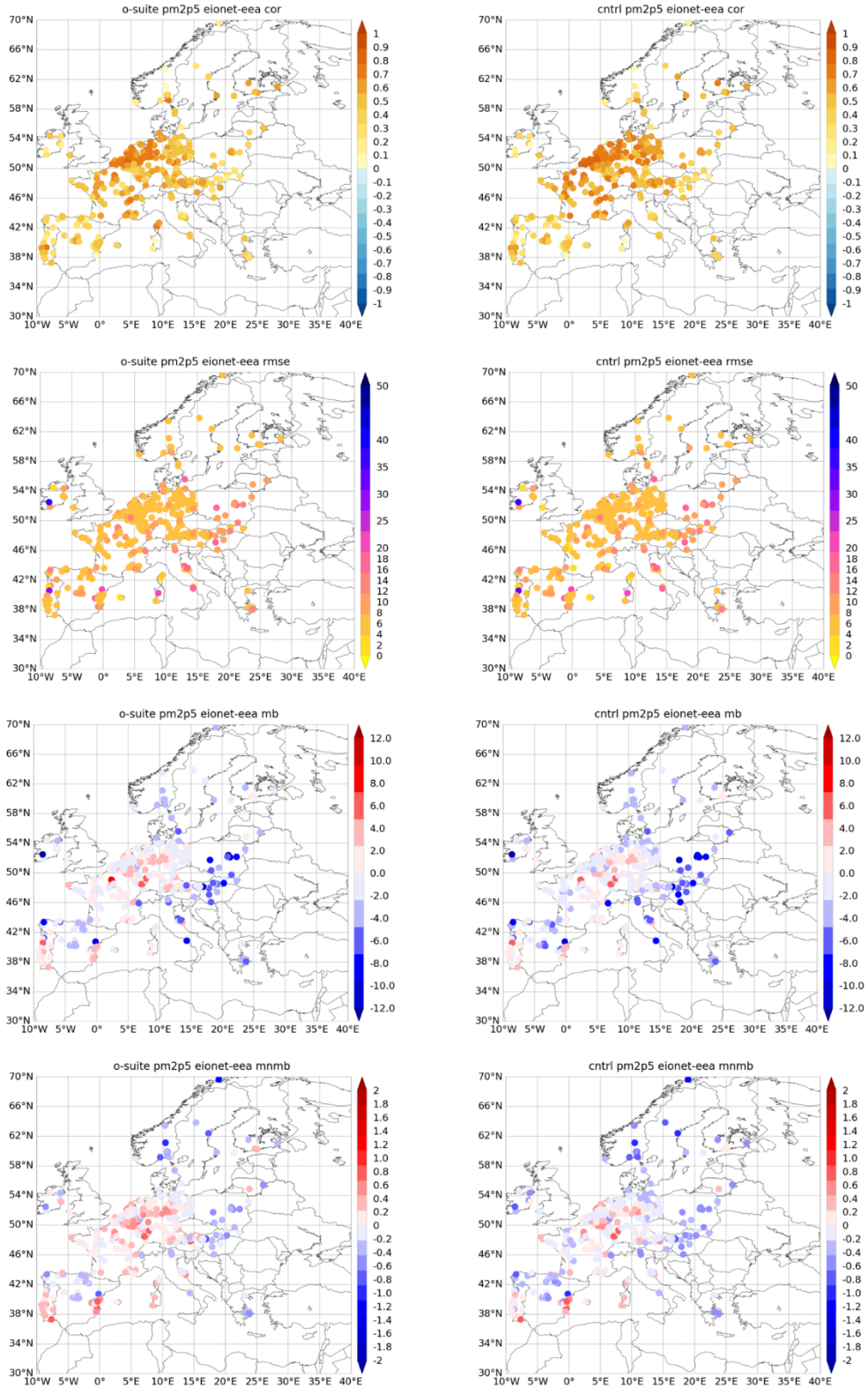

Figure 8.3.4: Skill scores (correlation coefficient, RMSE, MB and MNMB) for 24-hour forecasts (at 3hourly basis) of CAMS o-suite and control for the study period. 3hourly PM2.5 from EIONET is the reference. Only global scale representative available stations are displayed.

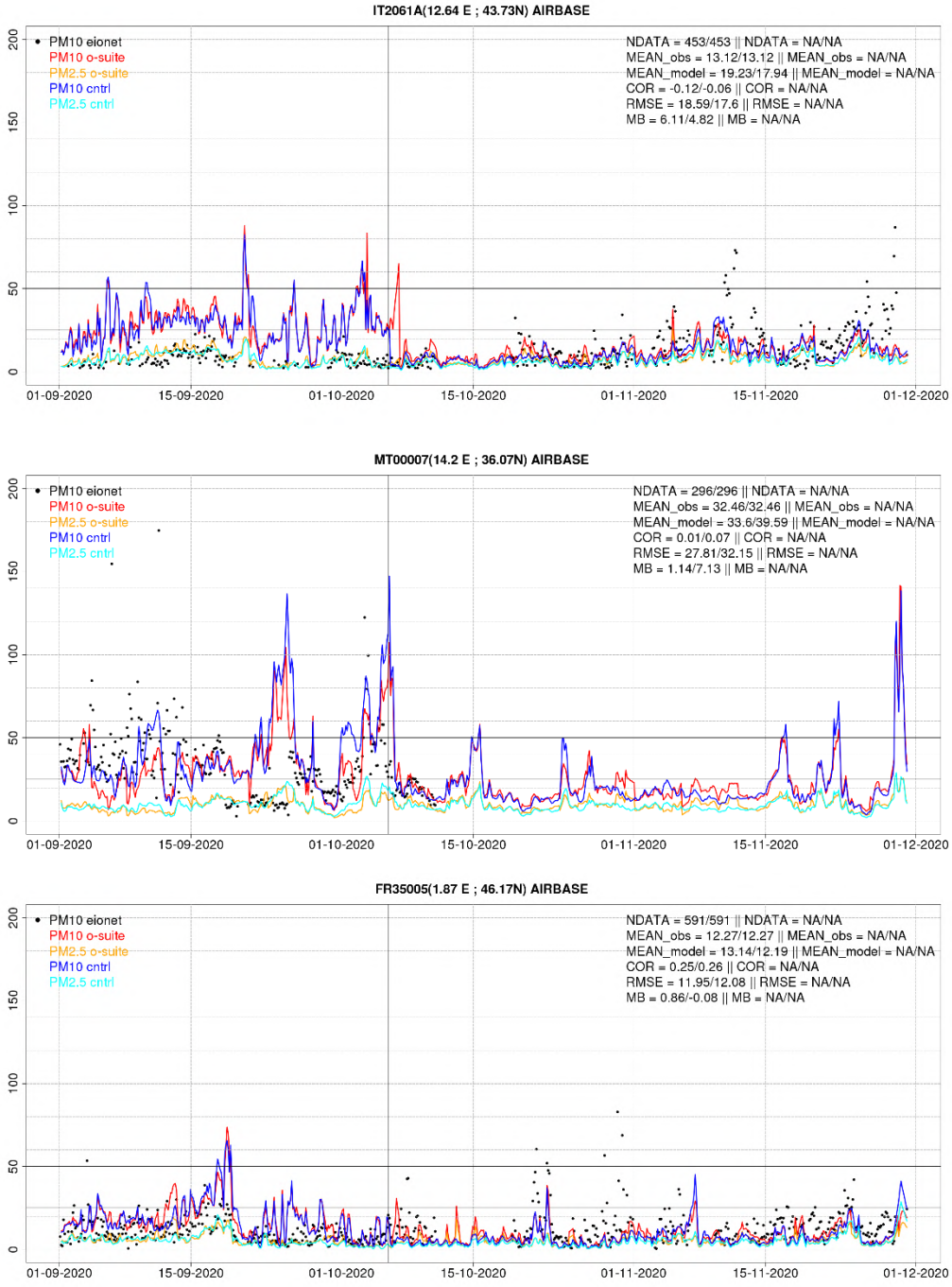

Figure 8.3.5a: PM10 and PM2.5 Airbase observations (black and grey dots, respectively), PM10 and PM2.5 o-suite (red and orange lines, respectively) and PM10 and PM2.5 control (blue and cyan lines, respectively) for the study period over IT2061A (Italy), MT00007 (Malta) and FR35005 (Central France). Skill scores per each site and model (o—suite/control) are shown in the upper right corner (NDATA: available 3-hourly values used for the calculations, MEAN observations, MEAN model, COR, RMSE, MB).

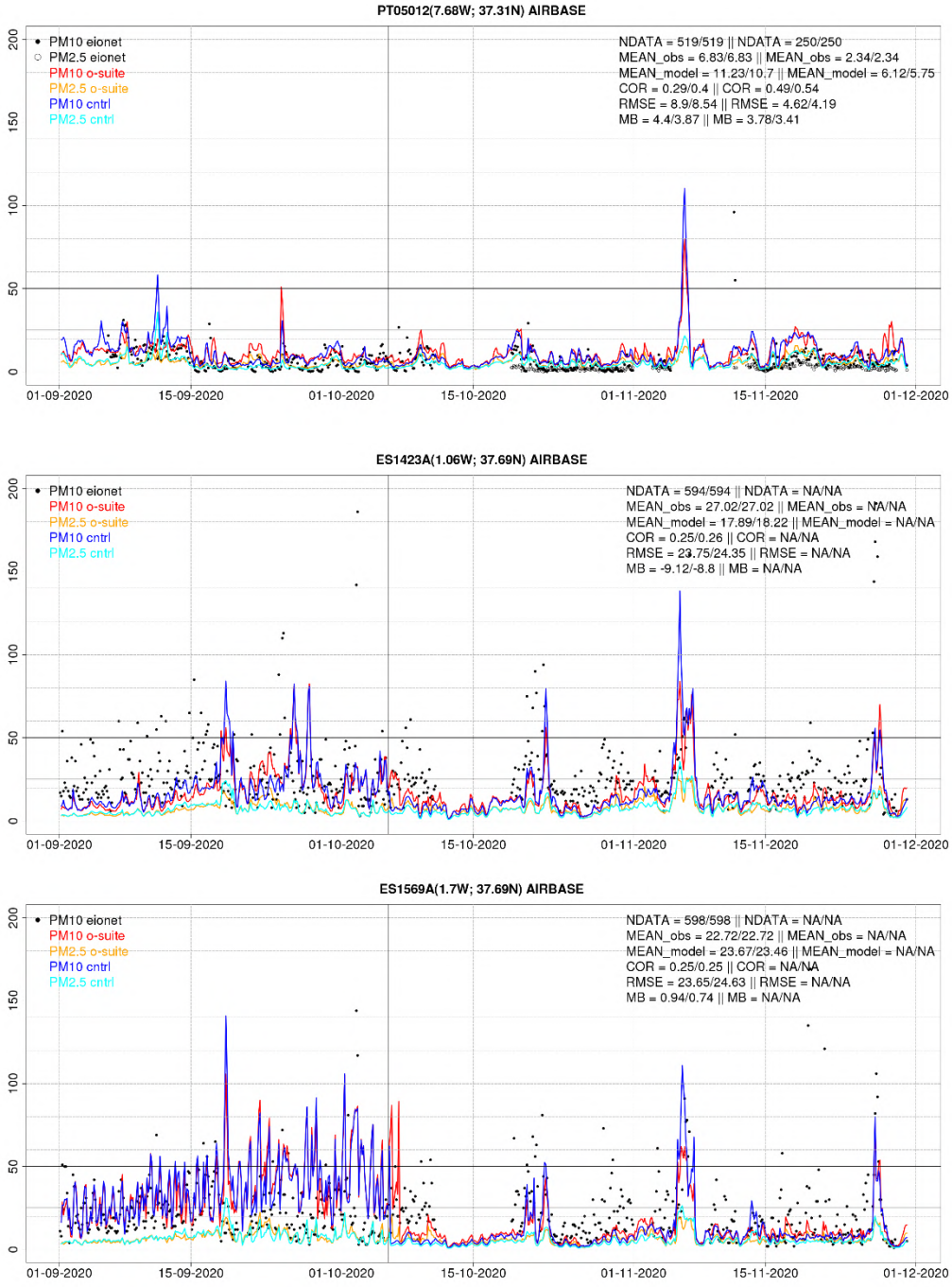

Figure 8.3.5b: PM10 and PM2.5 Airbase observations (black and grey dots, respectively), PM10 and PM2.5 o-suite (red and orange lines, respectively) and PM10 and PM2.5 control (blue and cyan lines, respectively) for the study period over PT05012 (Portugal), ES1423A and ES1569A (Spain, SE Iberian Peninsula). Skill scores per each site and model (o—suite/control) are shown in the upper right corner (NDATA: available 3-hourly values used for the calculations, MEAN observations, MEAN model, COR, RMSE, MB).

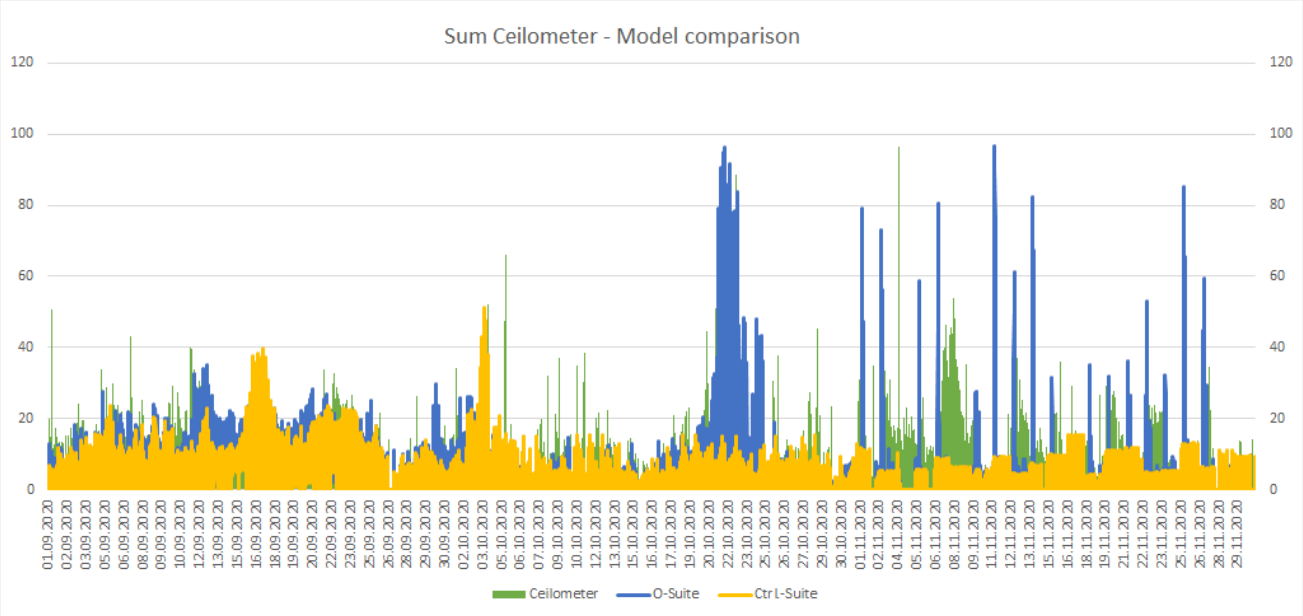

Figure 8.4.1: Hourly Sum of Ceilometer (blue) and Model (red) backscatter comparison over Germany during SON 2020.

8.4 Ceilometer backscatter profiles

Technical specifications of data sources, evaluated parameters and methods are described in Eskes et al (2021). In this section, the temporal and vertical variation of the attenuated backscatter coefficient profiles are evaluated, statistically as bias, correlation, and standard deviation of o-suite and control run vs ceilometers, and summarized in Taylor plots.

Period Overview:
The model aerosol optical depth (AOD) and ceilometer overviews are used to select periods with significant aerosol plumes over Germany. The CAMS-AOD inherits contributions of mineral dust (SD), sea salt (SS), carbonaceous matter (CM), black (BC) and organic carbon (OC), as well as sulfate (SU). During the time covered (see Figure 8.4.1) one mayor Saharan dust events between 7th and 9th of November measured by Ceilometer. The event around 21.10.2020 was masked by bad weather and only low backscatter was measured. With respect to AOD, all aerosol components follow their usual seasonality.

Mean and Median profiles:
In the new IFS cycle 46r1, implemented on 10th July 2019, nitrate NO_3 and ammonia NH_4 have been added and, likewise sulfate SO_4, have been coupled w.r.t homogeneous (gas-phase) and heterogeneous (particle phase) chemical processes. They contribute roughly 10-30% of aerosol mass in the rural central European PBL, as neutralized forms NO_3NH_4 or $(NH_4)_2SO_4$. Simultaneously, emissions of most aerosol components were significantly upgraded. With the next cycle, an upgrade in Dust AOD and surface PM10 and PM2.5 is expected.

The median for the backscatter coefficient show a bias in the lower part of the atmosphere in June to August 2020, increasing in September to November 2020. In October to November 2020, the median profiles have a very good match (see Figure 8.4.2).

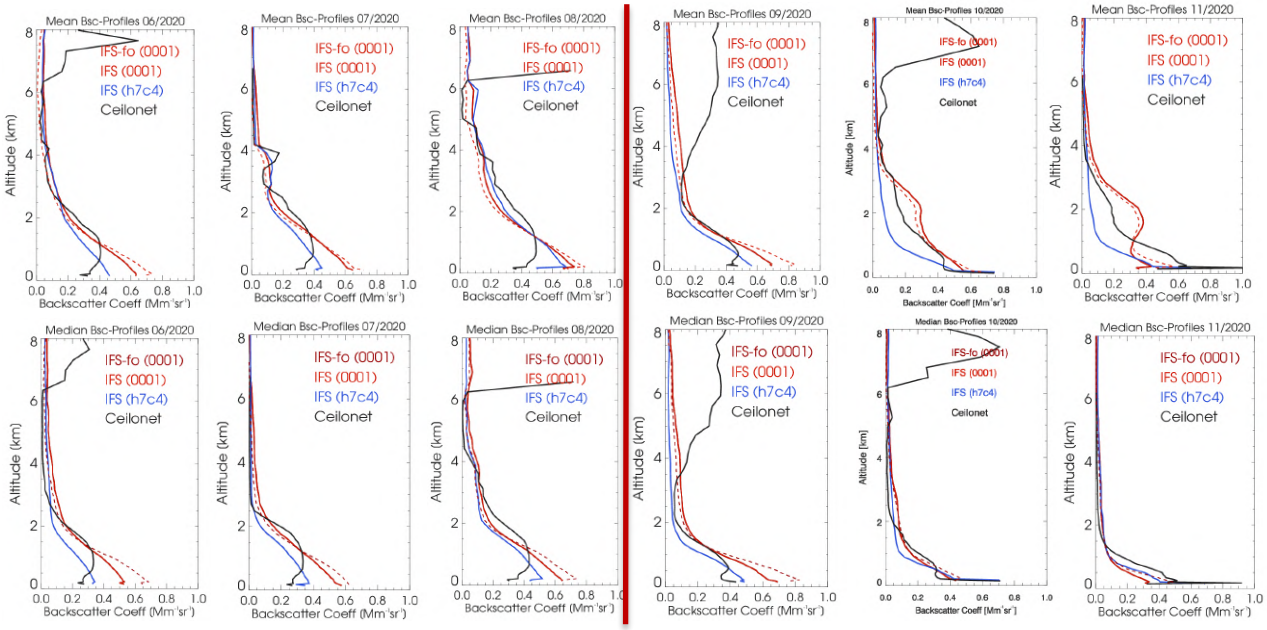

Figure 8.4.2: Left JJA 2020, right SON 2020 Monthly mean profiles (upper panel) and median profiles (lower panel) of backscatter coefficients from o-suite (red), control run (blue), and ceilometers (black) combined from 21 German stations.

The mean and median offset during JJA 2020 could be explained by warm and dry weather situation during summer times, a more uplift of ground particles due to convection and generally more dry air. During SON 2020 the model predictions and measured the median profiles have a relative good match due to the mean values. As shown in Figure 8.4.1 very few events heavily influence the monthly profile.

By comparing SON 2019 to SON 2020, the bias of the model has significantly decreased. The gap between Model and Ceilometer is closing, in comparison to last year (see Figure 8.4.3), especially in the middle troposphere, with the exception of September 2020.

Taylor Plots:

The average coefficient of correlation between modelled and observed vertical backscatter profiles ranges between r = 0.1 – 0.7 in SON 2020 (Fig. 8.4.4). As shown in Figure 8.4.3 the September 2020 plot is heavily influenced by the bias in the middle to upper troposphere. One can also notice that the October and November plots cluster well with a few outlines in the standard deviation. The absolute standard deviation (SD) are normalized to the SD of observations per day, as reference value at SD ≡ 1.0.

During SON 2019 the coefficient ranges between r = 0.2 – 0.8 with the observation, but a lower standard deviation. The lower clustering, in comparison to SON 2020, shows an overall improvement in matching and a lower bias for the SON 2020 period.

The o-suite and control run shows similar correlation. There is a large day-to-day and a seasonal variation of the performance. It must be noted that small vertical displacements decrease the correlation coefficient, although the SD are mostly reproduced at geographically truthful positions.

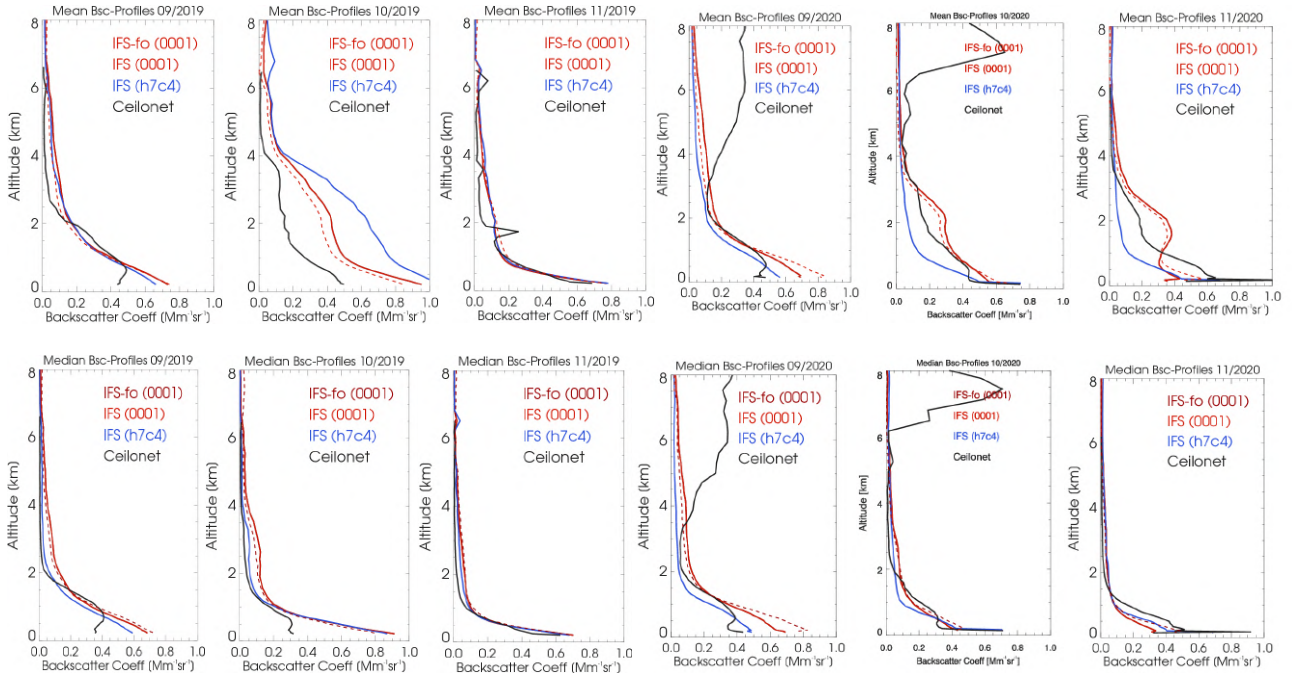

Figure 8.4.3: Comparison of monthly mean (top) and median (bottom) of backscatter coefficients from o-suite (red), control run (blue), and ceilometers (black) combined from 21 German stations for SON 2019 (left) and SON 2020 (right).

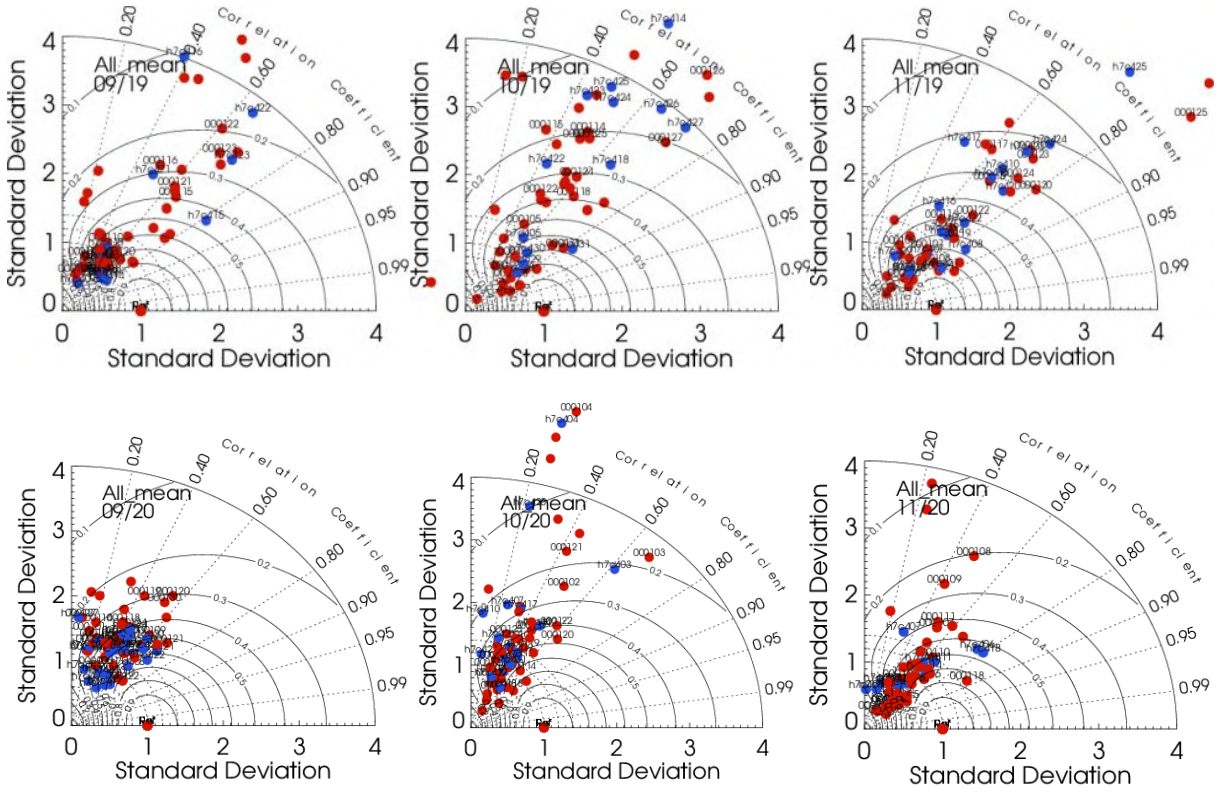

Fig. 8.4.4: Taylor polar plots with daily average standard deviation of vertical profiles versus correlation coefficient, averaged over 21 German ceilometer sites for Sep-Nov 2019 (top) and Sep-Oct 2020 (bottom). The o-suite is shown in red, the control run in blue.

9. Stratosphere

9.1 Validation against ozone sondes

In this section, we present the results of the stratospheric ozone evaluation against ozone soundings from the NDACC, WOUDC, NILU and SHADOZ databases. The sondes have a precision of 3-5% (~10% in the troposphere for Brewer Mast) and an uncertainty of 5-10%. For further details see Cammas et al. (2009), Deshler et al. (2008) and Smit et al (2007). Model profiles of the o-suite are compared to balloon sondes measurement data of 44 stations for the period January 2013 to August 2020 (please note that towards the end of the validation period fewer soundings are available). As C-IFS-CB05 stratospheric composition products beyond O_3 in the o-suite is not useful we provide only a very limited evaluation of the control experiment. A description of the applied methodologies and a map with the sounding stations can be found in Eskes et al. (2019). Please note that recent scientific findings (https://tropo.gsfc.nasa.gov/shadoz/Archive.html, Thompson et al., 2017; Witte et al., 2017; 2018, Stauffer, et al. in preparation 2020) show a drop-off in Total Ozone at various global ozone stations in comparison with satellite instruments. This drop-off amounts between 5-10% for stratospheric ozone. Changes in the ECC ozone instrument are associated with the drop-off, but no single factor has been identified as cause yet.

The o-suite shows MNMBs within the range ±14%, for all regions and months (some exceptions with MNMBs of up to ±18% for single months in the high latitude regions). Figure 9.1.1 shows the results for the past year.

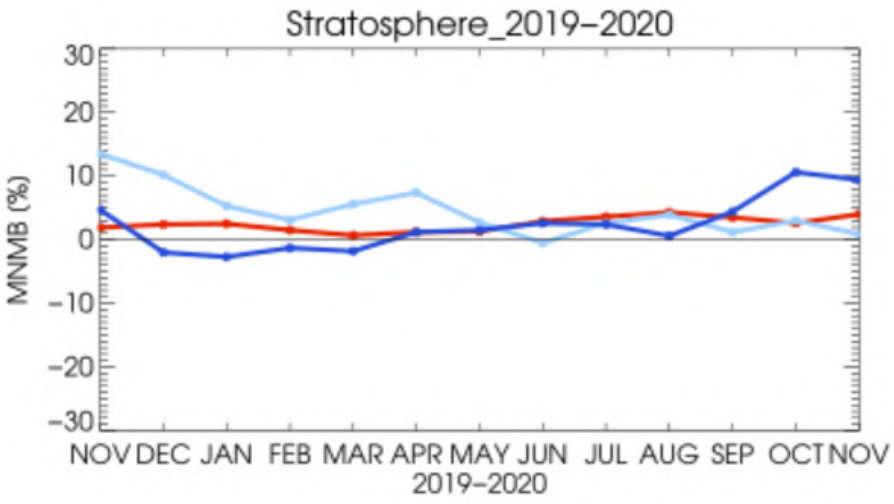

Figure 9.1.1: MNMBs (%) against lower stratospheric ozonesonde column (between 10 and 90 hPa) for the o-suite in the Arctic (light blue), Antarctic (dark blue) and northern midlatitudes (red). Period November 2019 to November 2020.

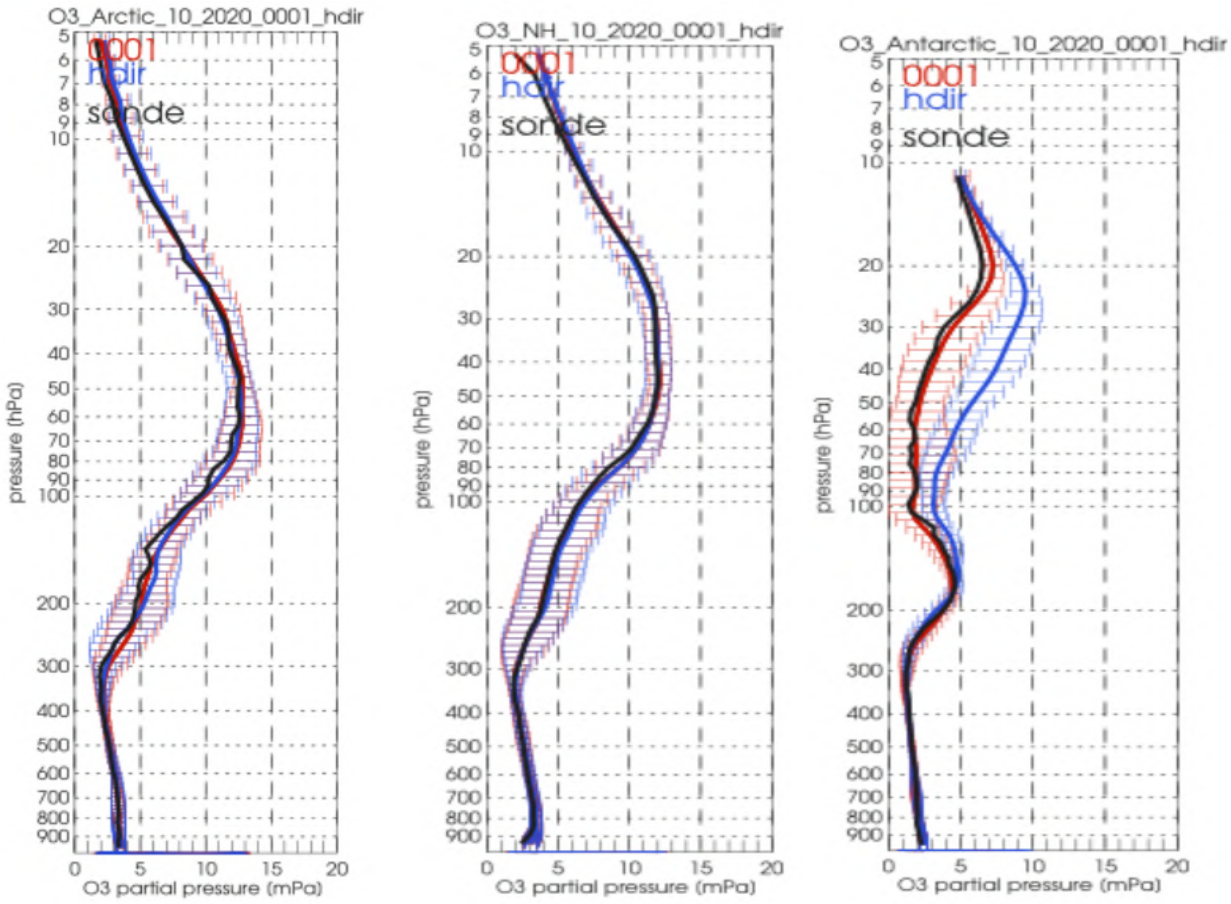

Figure 9.1.2: Comparison between mean O_3 profiles (units: mPa) of o-suite (red), and control (blue) in comparison with observed O_3 sonde profiles (black) for July 2020 for the various latitude bands: Arctic, NH-mid latitudes and Antarctic.

Fig. 9.1.2 compares the averaged profiles in each region during October 2020. The vertical distribution of stratospheric ozone is quite well represented for all regions by the o-suite (MNMBs between ~1 to 11 % for SON 2020). The control run (hdir) shows strong improvement for the Arctic and Northern Midlatitudes especially in the UTLS and stratosphere. The ozone hole over Antarctica is well captured with the o-suite but not by the control run which shows an overestimation of ozone mostly between 20 and 100 hPa.

9.2 Validation against observations from the NDACC network

UVVIS column and FTIR stratospheric columns

Since the start of the CAMS27 project, the number of UVVIS Zenith ozone measurements have increased on NDACC. Currently 15 sites provided data in the recent quarter allowing for a representative picture on the latitude dependence of the CAMS data. Since 2019 also DOBSON measurements are supported by CAMS27 and delivered to NDACC more rapidly.

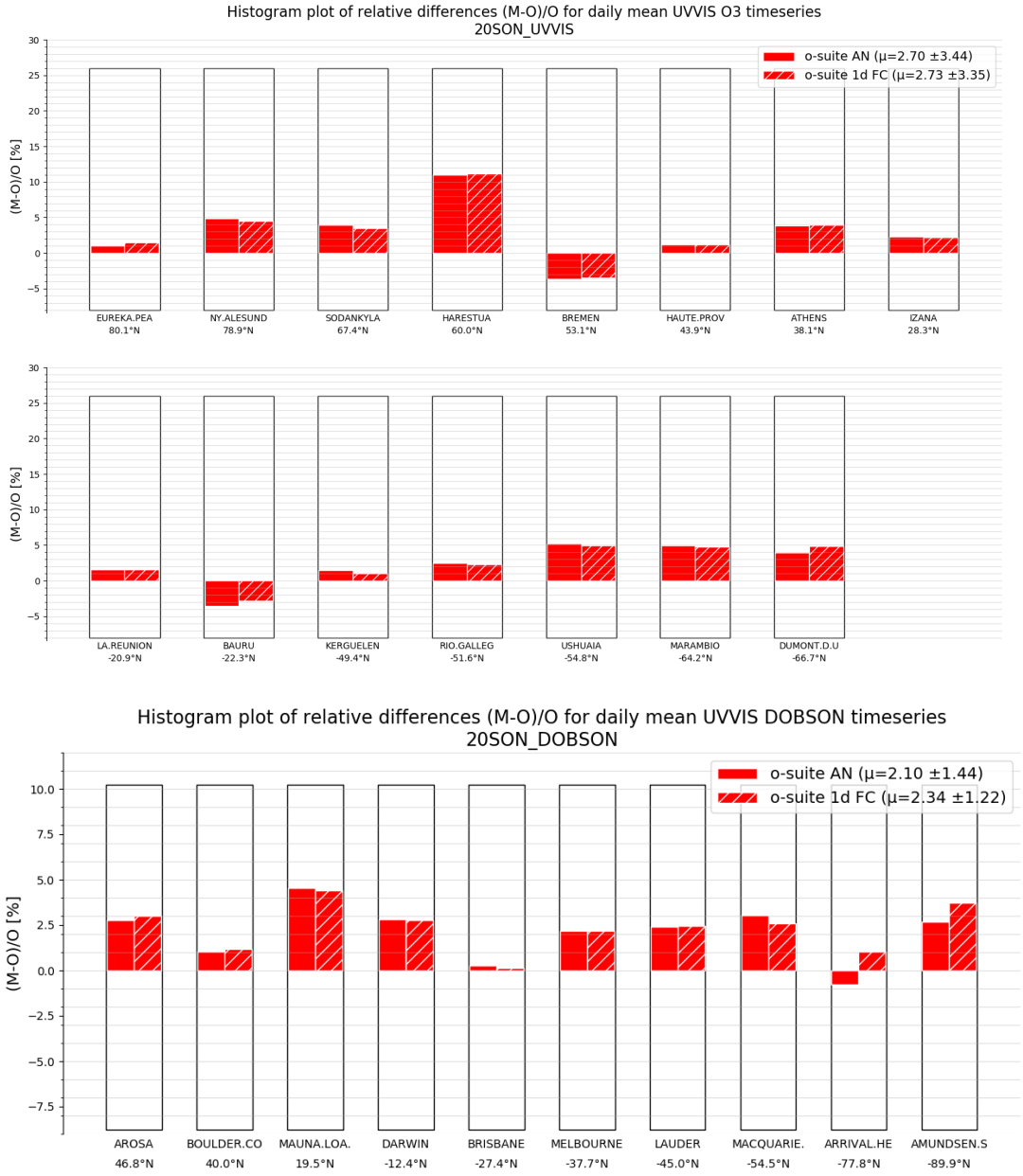

Figure 9.2.1 Relative biases during quarter SON 2020 for 15 UVVIS DOAS stations measuring stratospheric ozone columns with ZENITH measurement geometry and 10 DOBSON instruments (stations sorted with decreasing latitude). The overall relative bias is positive for all latitudes and comparable to the typical measurement uncertainty of 5% for UVVIS ZENITH and 2.5% for DOBSON for most of the sites.

The systematic uncertainty of the UVVIS measurements is typically 5%, hence the relative biases for most sites for both the AN and 1d FC of the o-suite are very close to each other and within the uncertainty ranges, see Figure 9.2.1. The averaged bias for the 15 UVVIS sites is 2.7% and within the reported measurement uncertainty of 5%, the averaged correlation is 0.78 during this quarter and did not change compared to the previous quarter. A similar conclusion holds for the DOBSON comparisons: biases are comparable to the measurement uncertainty which typically lies between 2% and 3%.

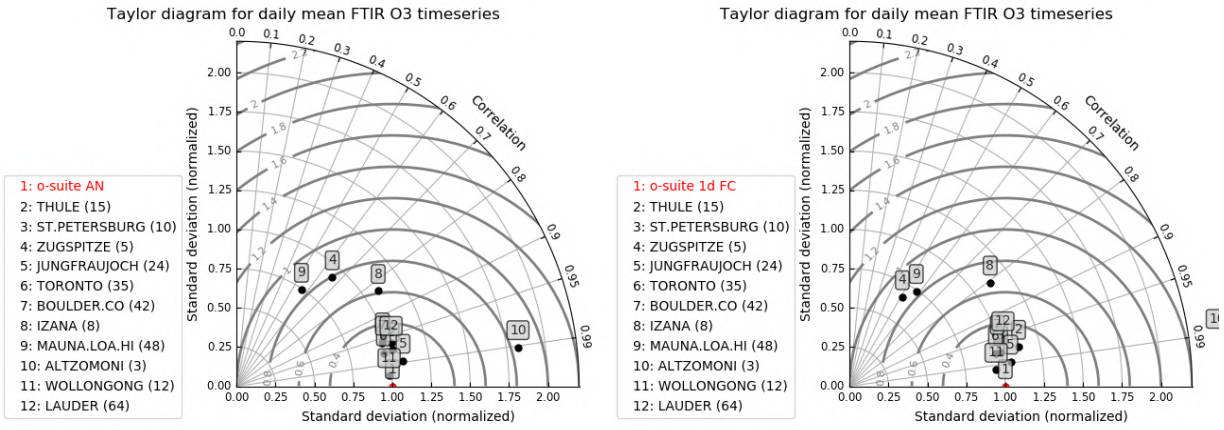

Figure 9.2.2. Taylor diagrams relating the standard deviations for the model and GB stratospheric column time series and their correlation for the time period SON 2020. All time-series are normalized such that the standard deviation of the model is 1. The performance for the o-suite is slightly better (averaged correlation is 0.94 for FTIR and 0.78 for UVVIS) compared to the 1-day forecast (averaged correlation is 0.9 for FTIR and 0.77 for UVVIS).

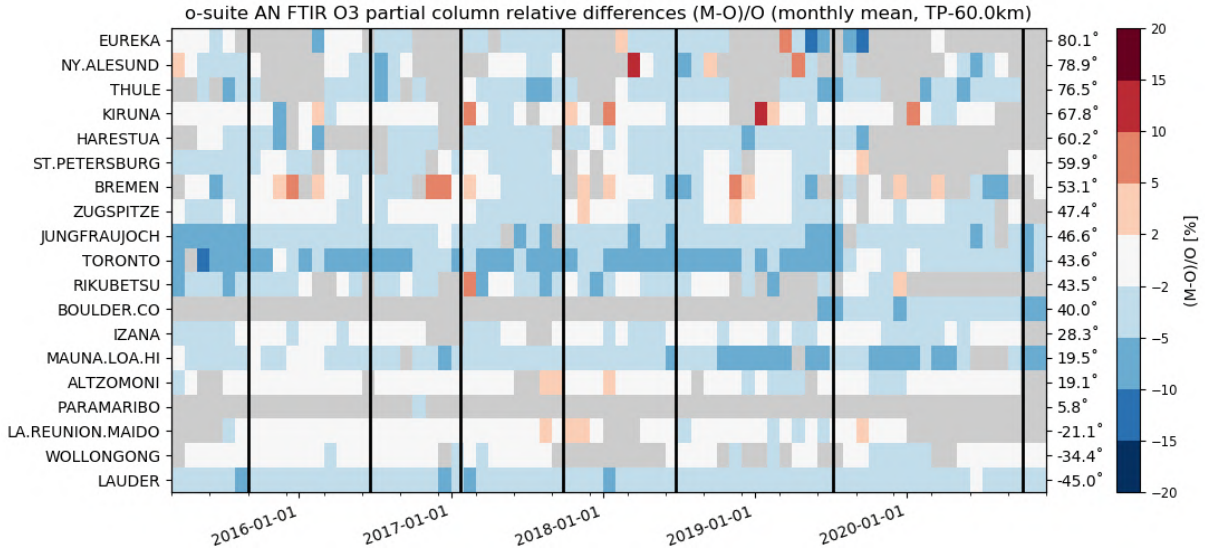

Figure 9.2.3 Time series of monthly mean relative differences for stratospheric FTIR columns along with CAMS cycle updates (black vertical lines show o-suite AN updates).

The correlations between the individual sites and the CAMS runs are presented in the Taylor diagrams in Figure 9.2.2. Again, the o-suite AN and 1d FC perform very similarly in correlation coefficients. Figure 9.2.3 shows the evolution of the relative bias of the stratospheric columns against FTIR data since 2015.

Table 9.2.1: Detailed statistics for stratospheric ozone column comparisons for UVVIS (zenith and Dobson) and FTIR measurements during SON 2020. Standard deviations (std) are relative to the std of the o-suite.

	o-suite AN					o-suite 1d FC					
UVVIS ZENITH site	#	rel. std	corr	rel diff (%)	rel diff std(%)	#	rel. std	corr	rel diff (%)	rel diff std(%)	lat
EUREKA.PEARL	23	0.9	0.78	1.02	4.81	23	0.9	0.76	1.43	4.87	80.1
NY.ALESUND	51	0.9	0.99	4.82	1.52	51	0.9	0.99	4.5	1.83	78.9
SODANKYLA	91	0.9	0.52	3.92	6.9	91	0.9	0.52	3.45	6.9	67.4
HARESTUA	43	0.8	0.93	11.01	2.62	43	0.8	0.93	11.19	2.6	60
BREMEN	91	0.9	0.94	-3.65	1.74	91	0.9	0.93	-3.47	1.84	53.1
HAUTE.PROVENCE	91	1	0.58	1.19	6.17	91	1	0.59	1.18	6.11	43.9
ATHENS	69	1.1	0.94	3.87	1.69	69	1.1	0.94	3.93	1.77	38.1
IZANA	86	1.3	0.55	2.28	2.95	86	1.3	0.55	2.17	2.97	28.3
LA.REUNION.STDENIS	88	1.1	0.76	1.52	1.65	88	1.2	0.73	1.55	1.72	-20.9
BAURU	88	0.9	0.63	-3.58	1.88	88	1	0.61	-2.86	1.88	-22.3
KERGUELEN	91	0.9	0.73	1.45	6.92	91	0.9	0.72	0.99	6.96	-49.4
RIO.GALLEGOS	75	0.9	0.64	2.5	7.43	75	0.9	0.64	2.31	7.41	-51.6
USHUAIA	91	1	0.94	5.22	4.4	91	0.9	0.94	4.93	4.26	-54.8
MARAMBIO	46	0.9	0.98	4.97	6.8	46	0.9	0.98	4.78	7.09	-64.2
DUMONT.D.URVILLE	91	1	0.73	3.91	17.03	91	1	0.73	4.85	17.22	-66.7
		1	0.78	2.7	4.97		1	0.77	2.73	5.03	

	o-suite AN					o-suite 1d FC					
UVVIS DOBSON site	#	rel. std	corr	rel diff (%)	rel diff std(%)	#	rel. std	corr	rel diff (%)	rel diff std(%)	lat
AROSA	71	1	0.99	2.77	1.16	71	1	0.98	3.01	1.39	46.8
BOULDER.CO	81	0.9	0.95	1.07	1.94	81	0.9	0.94	1.16	2.04	40
MAUNA.LOA.HI	90	1	0.78	4.54	1.69	90	1	0.76	4.41	1.8	19.5
DARWIN	92	1.4	0.75	2.83	1.93	92	1.5	0.77	2.76	1.86	-12.4
BRISBANE	92	1	0.9	0.28	1.56	92	1	0.89	0.12	1.61	-27.4
MELBOURNE	80	0.8	0.87	2.17	3.3	80	0.8	0.87	2.19	3.23	-37.7
LAUDER	91	0.9	0.96	2.4	1.73	91	0.9	0.96	2.44	1.76	-45
MACQUARIE.ISLAND	88	1	0.96	3.03	2.21	88	0.9	0.96	2.57	2.33	-54.5
ARRIVAL.HEIGHTS	59	1.1	0.97	-0.76	3.6	59	1.1	0.97	1.04	4.21	-77.8
AMUNDSEN.SCOTT	60	1	0.97	2.69	4.79	60	1	0.97	3.73	5.03	-89.9
		1	0.91	2.1	2.39		1	0.91	2.34	2.53	

	o-suite AN					o-suite 1d FC					
FTIR site	#	rel. std	corr	rel diff (%)	rel diff std(%)	#	rel. std	corr	rel diff (%)	rel diff std(%)	lat
THULE	15	1	0.97	-1.31	1.49	15	1.1	0.97	-1.38	1.53	76.5
ST.PETERSBURG	10	1.1	0.93	-0.81	1.39	10	1.1	0.93	0.02	1.45	59.9
ZUGSPITZE	5	1.1	0.94	-0.58	0.53	5	1	0.49	0.25	1.62	47.4
JUNGFRAUJOCH	24	1.1	0.98	-3.91	1.1	24	1	0.98	-3.55	1.19	46.6
TORONTO	35	0.9	0.97	-3.98	1.52	35	0.9	0.97	-3.95	1.62	43.6
BOULDER.CO	42	0.9	0.96	-3.93	1.79	42	0.9	0.95	-3.75	1.77	40
IZANA	8	1.2	0.91	-0.82	1.06	8	1.1	0.91	-0.84	1.03	28.3
MAUNA.LOA.HI	48	1	0.68	-4.32	1.92	48	1	0.68	-4.34	1.9	19.5
ALTZOMONI	3	1.3	0.98	0.59	0.23	3	1	0.98	0.76	0.14	19.1
WOLLONGONG	12	0.9	0.96	-1.29	1.16	12	0.9	0.95	-1.3	1.31	-34.4
LAUDER	64	1	0.96	-2.69	1.6	64	1	0.95	-2.71	1.78	-45
ARRIVAL.HEIGHTS	24	1	1	-1.91	1.94	24	1	0.99	-0.58	2.19	-77.8
		1	0.94	-2.08	1.31		1	0.9	-1.78	1.46	

Profile comparison using LIDAR and MWR

In this section we present a comparison between the CAMS o-suite and control runs against MWR and LIDAR observations from the NDACC network. A detailed description of the instruments and applied methodologies for all NDACC instruments can be found at http://nors.aeronomie.be. MWR (microwave) at Ny Alesund (79°N, 12°E, Arctic station) and Bern (47°N, 7°E, northern midlatitude station). LIDAR at Observatoire Haute Provence (OHP), France (43°N, 5.7°E, altitude 650m),

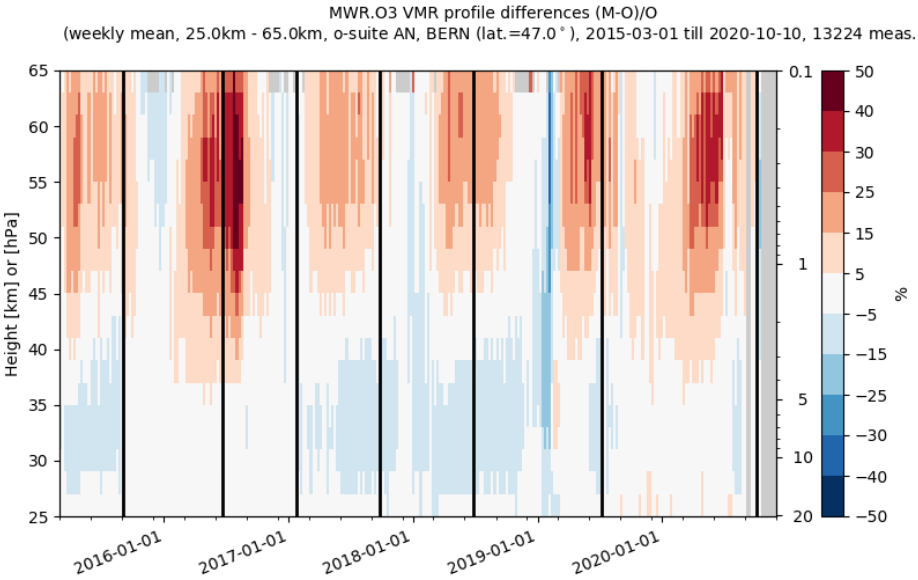
MWR.O3 VMR profile differences (M-O)/O
(weekly mean, 25.0km - 65.0km, o-suite AN, BERN (lat.=47.0°), 2015-03-01 till 2020-10-10, 13224 meas.)
Height [km] or [hPa]
%
2016-01-01
2017-01-01
2018-01-01
2019-01-01
2020-01-01

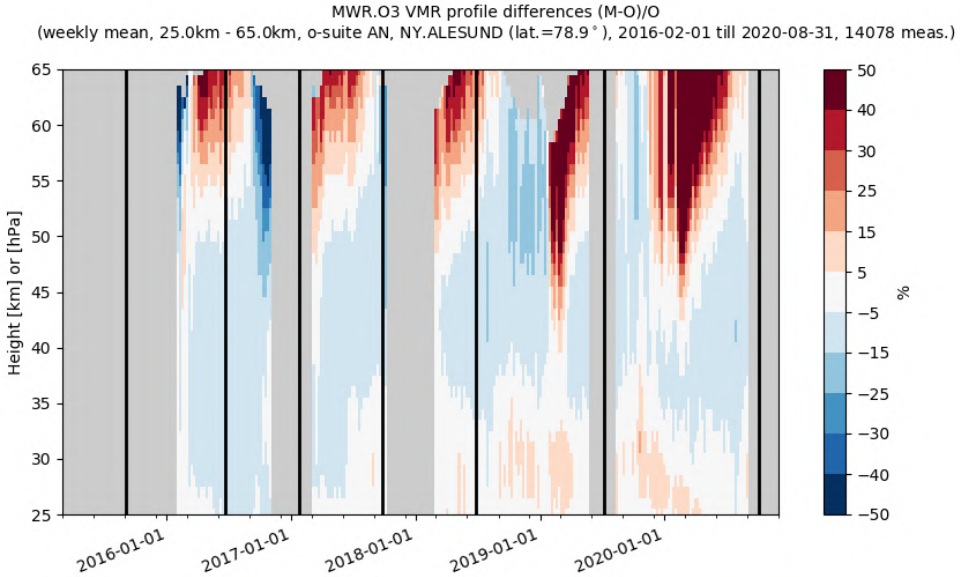
MWR.O3 VMR profile differences (M-O)/O
(weekly mean, 25.0km - 65.0km, o-suite AN, NY.ALESUND (lat.=78.9°), 2016-02-01 till 2020-08-31, 14078 meas.)
Height [km] or [hPa]
%
2016-01-01
2017-01-01
2018-01-01
2019-01-01
2020-01-01

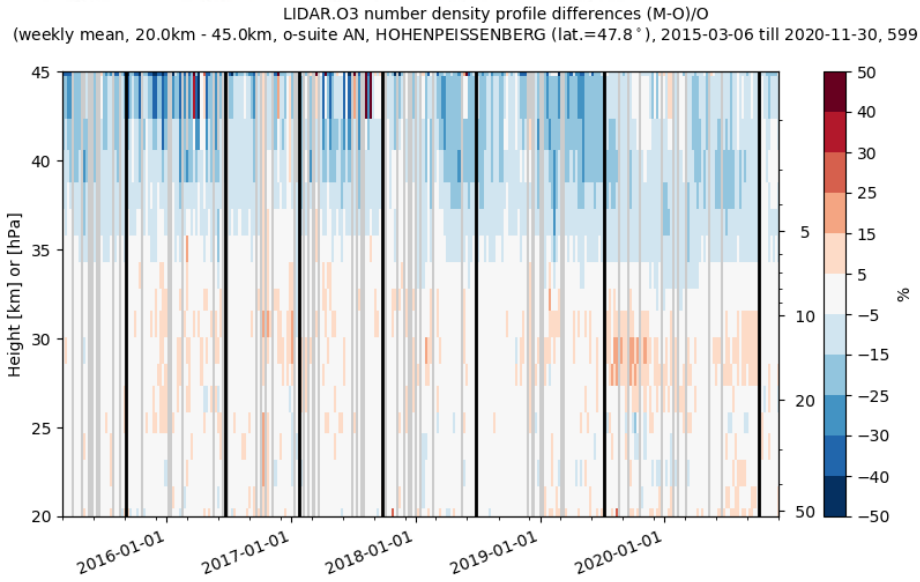
LIDAR.O3 number density profile differences (M-O)/O
(weekly mean, 20.0km - 45.0km, o-suite AN, HOHENPEISSENBERG (lat.=47.8°), 2015-03-06 till 2020-11-30, 599 meas.)
Height [km] or [hPa]
%
2016-01-01
2017-01-01
2018-01-01
2019-01-01
2020-01-01

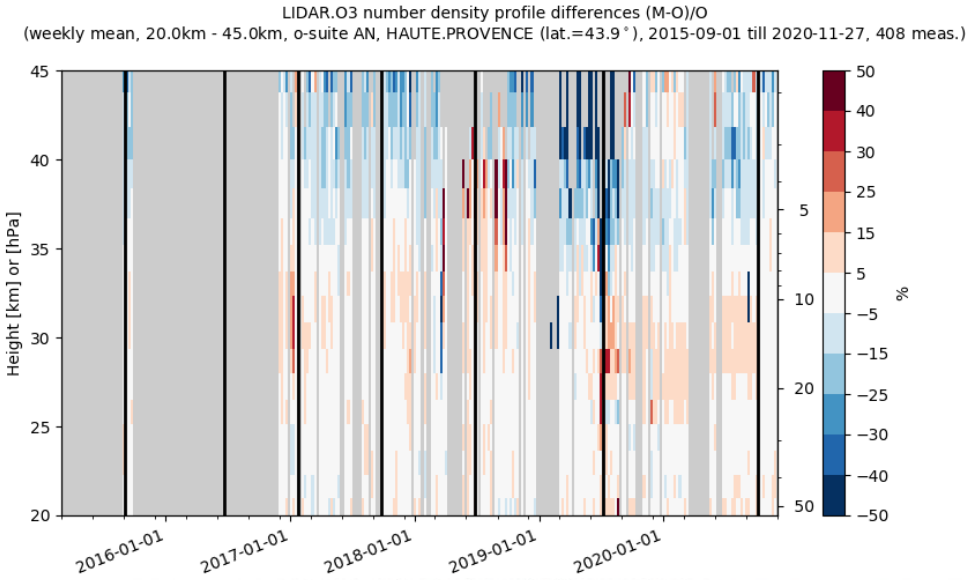
LIDAR.O3 number density profile differences (M-O)/O
(weekly mean, 20.0km - 45.0km, o-suite AN, HAUTE.PROVENCE (lat.=43.9°), 2015-09-01 till 2020-11-27, 408 meas.)
Height [km] or [hPa]
%
2016-01-01
2017-01-01
2018-01-01
2019-01-01
2020-01-01

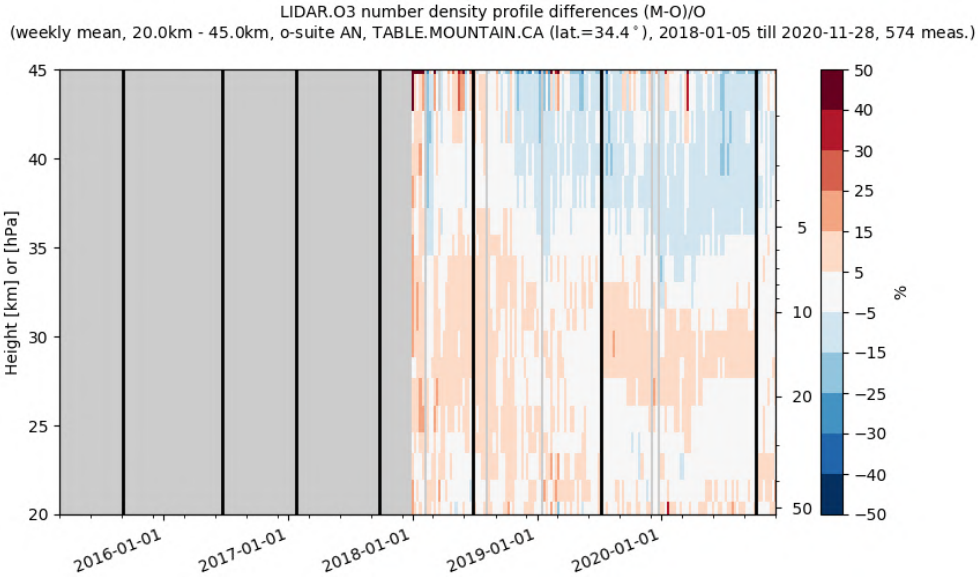
LIDAR.O3 number density profile differences (M-O)/O
(weekly mean, 20.0km - 45.0km, o-suite AN, TABLE.MOUNTAIN.CA (lat.=34.4°), 2018-01-05 till 2020-11-28, 574 meas.)
Height [km] or [hPa]
%
2016-01-01
2017-01-01
2018-01-01
2019-01-01
2020-01-01

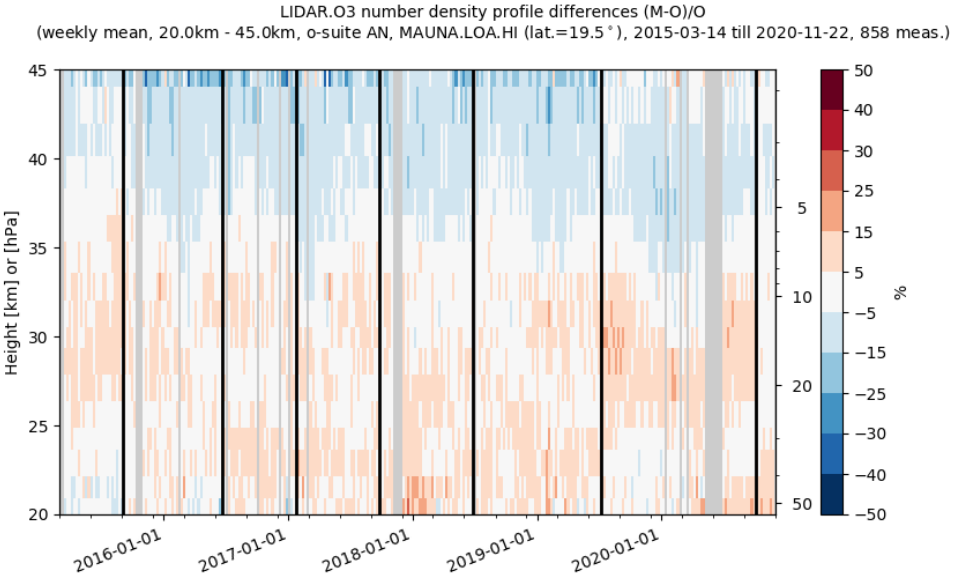
LIDAR.O3 number density profile differences (M-O)/O
(weekly mean, 20.0km - 45.0km, o-suite AN, MAUNA.LOA.HI (lat.=19.5°), 2015-03-14 till 2020-11-22, 858 meas.)
Height [km] or [hPa]
%
2016-01-01
2017-01-01
2018-01-01
2019-01-01
2020-01-01

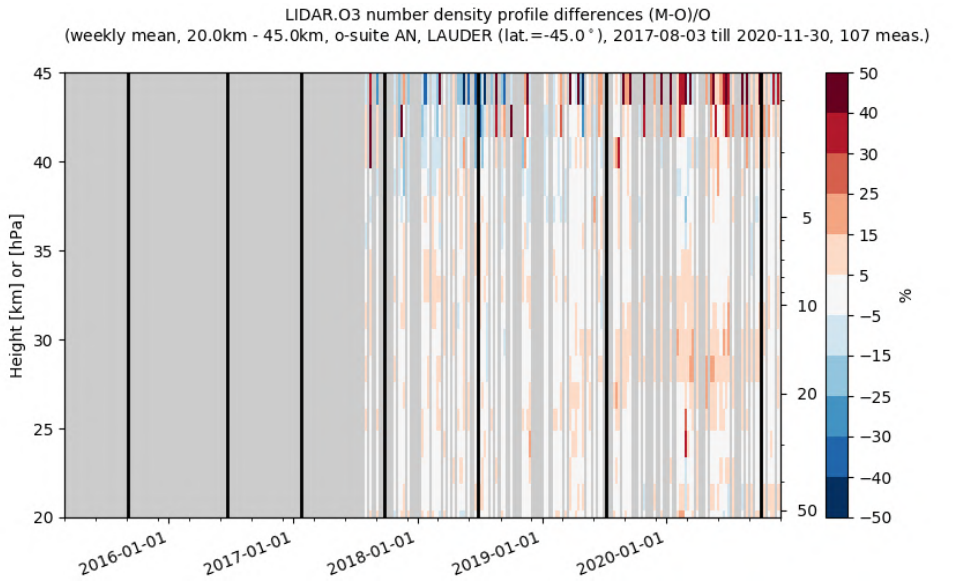

Figure 9.2.4: Comparison of the weekly mean profile bias between the O3 mixing ratios of o-suite AN and the NDACC station at Ny Alesund, Bern, Hohenpeissenberg, OHP, Mauna Loa, Table Mountain and Lauder. For the LIDAR stations, the measurement uncertainty above 35km is comparable to the observed profile bias. The latest model update changed the positive bias observed in the stratosphere (around 30km in the LIDAR comparisons)

Hohenpeissenberg, Germany (47°N, 11°E, altitude 1km), Table Mountain (34°N, 117.7°W, altitude 2.3km), Mauna Loa, Hawaii (19.5°N, 204°E, altitude 3.4km) and Lauder (45°S, 169.7°E),

For all LIDAR sites (see Figure 9.2.4) the o-suite slightly overestimated the observed ozone (<10%) between 25km and 35km. Since the latest osuite update, which introduced a different stratospheric ozone paramatrisation, this overestimation vanishes. The uncertainty on the LIDAR concentration increases with altitude and above 35km the observed differences are comparable to the measurement uncertainty (>10%, see http://nors.aeronomie.be/projectdir/PDF/NORS_D4.2_DUG.pdf).

9.3 Comparison with dedicated systems and with observations by limb-scanning satellites

This section compares the output of the o-suite for the JJA 2020 period with observations by limb-sounding satellite instruments, using the methodology described by Lefever et al. (2015). We also include the comparisons for the o-suite 4th day forecasts (96h to 120h) of stratospheric ozone.

All datasets are averaged over all longitudes and over the three most interesting latitude bands for stratospheric ozone: Antarctic (90°S-60°S), Tropics (30°S-30°N) and Arctic (60°N-90°N). In order to provide global coverage, the two mid-latitude bands (60°S-90°S and 60°N-90°N) are also included in some comparisons with satellite observations.

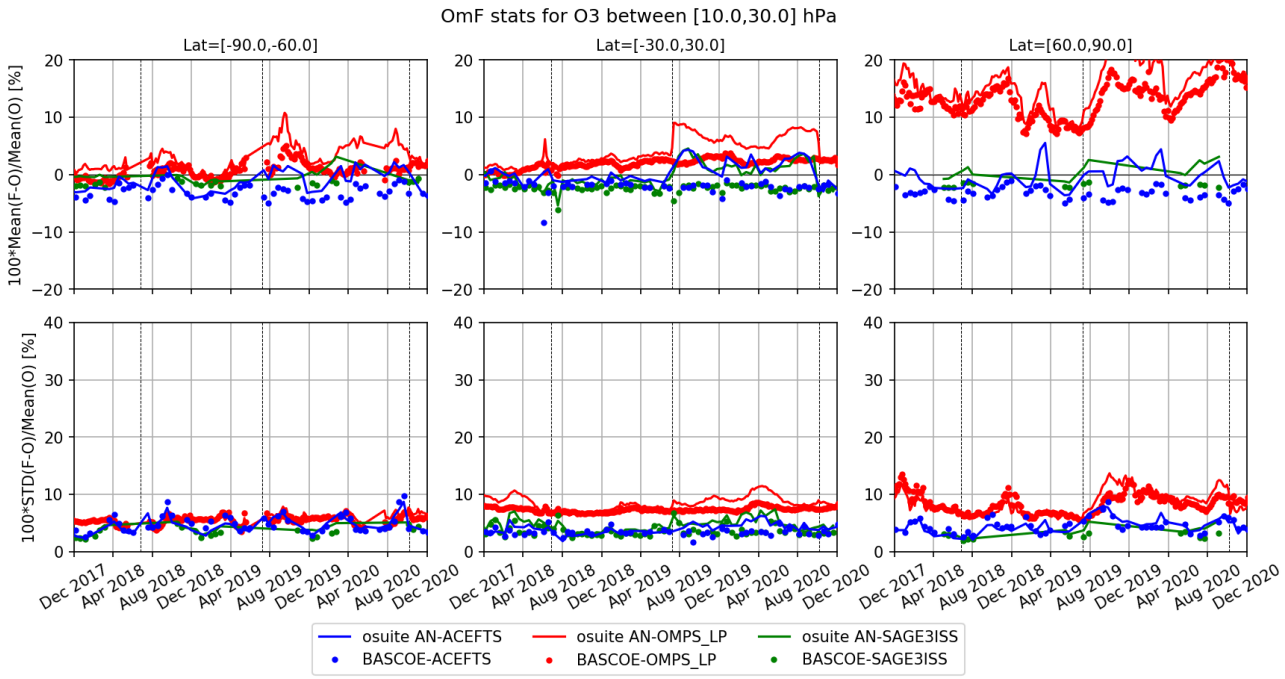

Figure 9.3.1: Time series comparing model runs to observations for the period 01-Dec-2017 to 01-Dec-2020 in the pressure range between 10 and 30 hPa: o-suite analyses (solid lines) and BASCOE (dotted lines) vs OMPS-LP (red), ACE-FTS (blue) and SAGE-III (green). Top row, normalized mean bias (model-obs)/obs (%); bottom row, standard deviation of relative differences (%). Vertical dashed lines indicate the date of CAMS model updates: CY45r1 (26 Jun 2018), CY46r1 (9 Jul 2019) and CY47r1 (6 Oct 2020).

The level-2 data from limb sounding instrument used in this section are:

- ACE-FTS version 3.6, on board SCISAT-1.
- SAGE-III version 5.1, on board the International Space Station (ISS); among the 3 different ozone profiles delivered by the solar occultation (denoted Mesospheric, MLR and AO3), we use the AO3 retrieval which is recommended by the mission science team.
- OMPS-LP version 2.5, on board NPP

For reference, we also compare these observations with BASCOE analyses which are constrained by the Aura MLS v4.2 offline profiles.

Figure 9.3.1 to 9.3.3 present, in the upper row, the time series over the last 36 months of the bias of the o-suite against the three satellite measurements for respectively three layers of the stratosphere (10-30hPa, 30-70hPa, and 70-100hPa); the bottom row of the figures shows the standard deviation of the differences and can be used to evaluate the random error in the analyses.

Against ACE-FTS, the agreement of the o-suite and BASCOE is good, the bias is generally within ±5% except in the tropical lower stratosphere (TLS, between 70 and 100 hPa) where the bias is around ±10%.

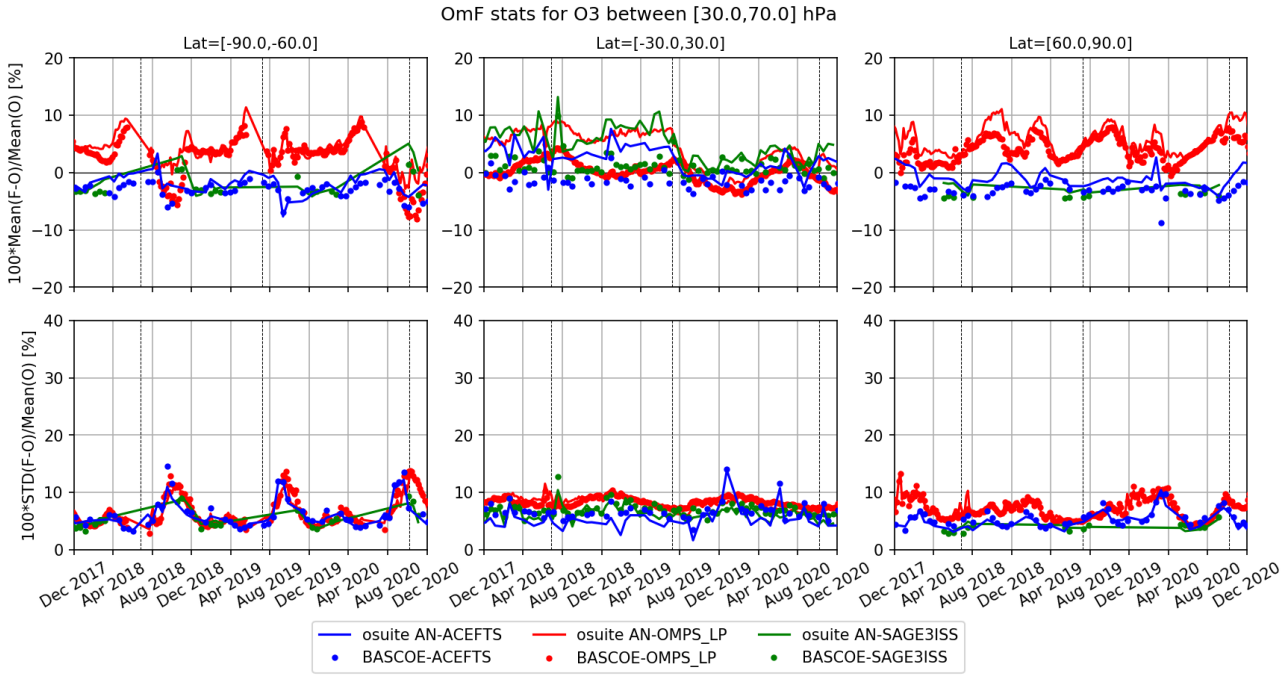

Figure 9.3.2: As Fig. 9.3.1 but in the pressure range between 30 and 70hPa.

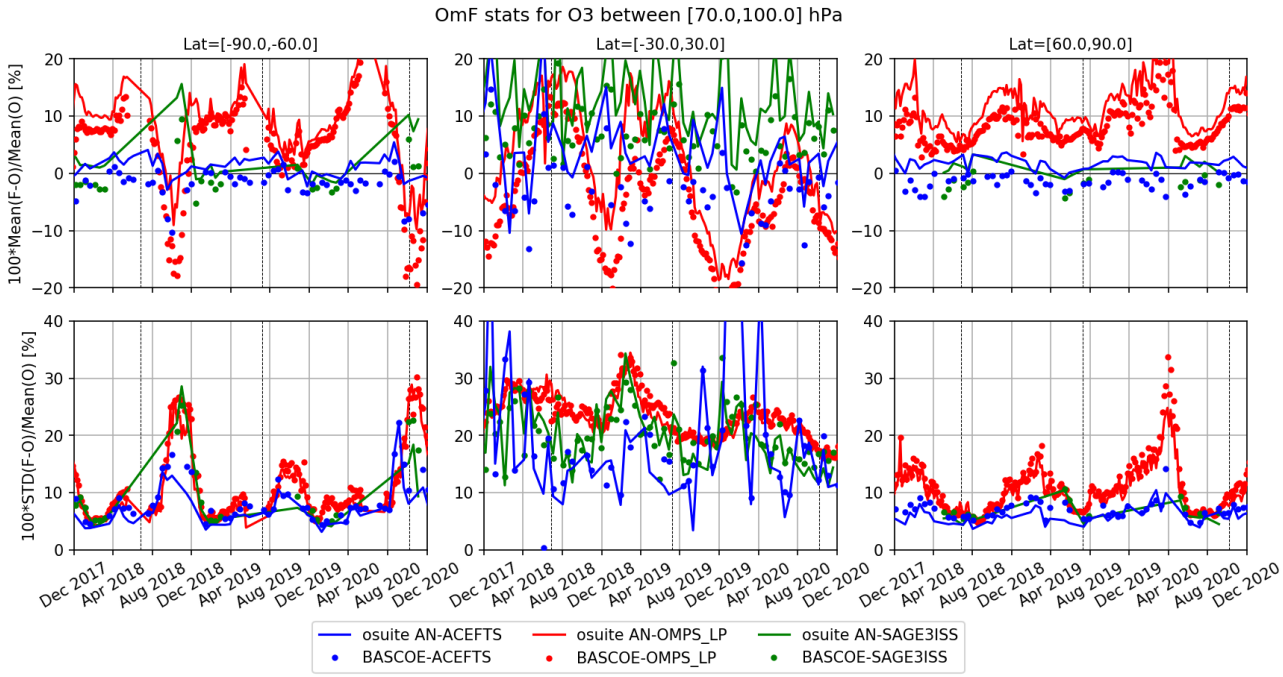

Figure 9.3.3: As Fig. 9.3.1 but in the pressure range between 70 and 100 hPa.

The SAGE-III onboard ISS provide observations since June 2017. The latitudinal coverage is more limited than ACE-FTS; the polar regions are only covered during the polar summer. Where available, the agreement of the o-suite with SAGE-III is good, with biases similar to those observed against ACE-FTS, except in the TLS where they are more positive (3-13%).

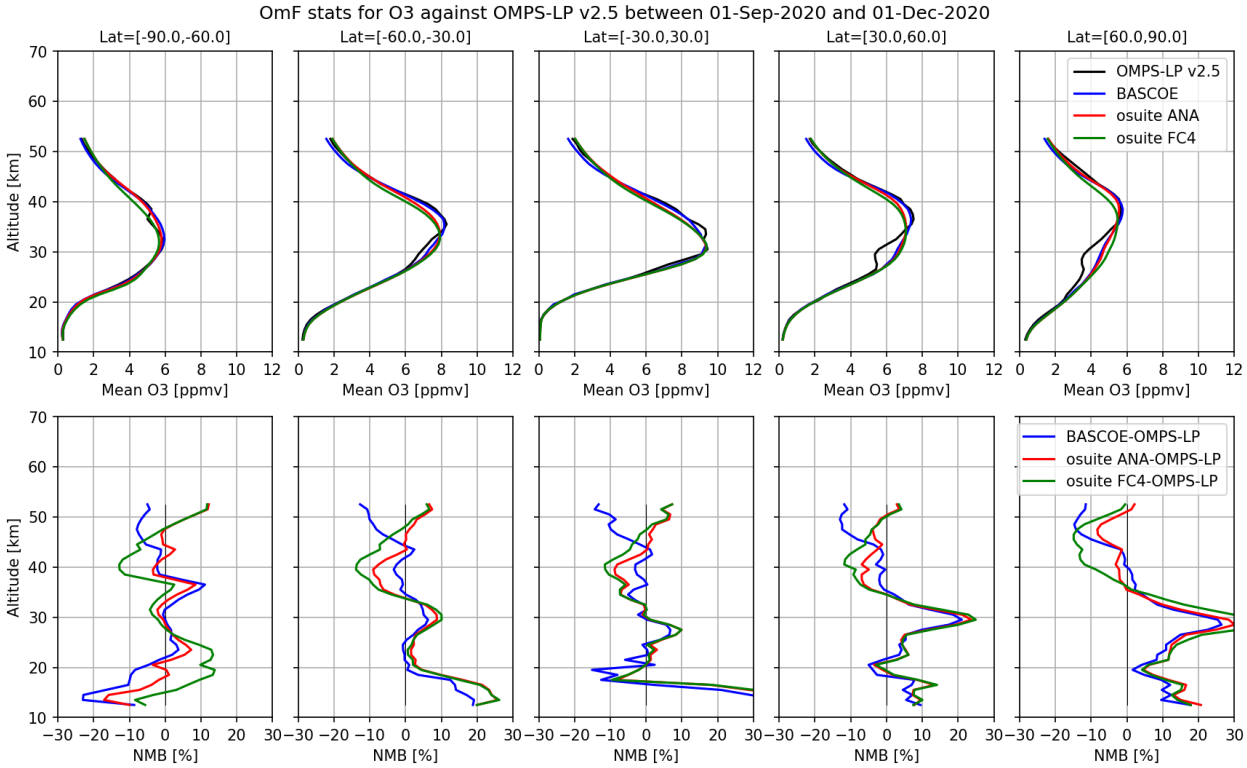

Figure 9.3.4: Mean value (top) and normalized mean bias (bottom) of the ozone profile between o-suite analyses (red), o-suite forecasts 4th day (green) and BASCOE (blue) with OMPS-LP v2.5 observations for the period SON 2020.

Compared to OMPS-LP, there is an almost systematic overestimation by the o-suite; the biases are more variable and more marked than for the other instruments (10% to 15% in the north polar at 10-30hPa region, up to 10% at 30-70hPa and up to 20% at 70-100hPa).

However, the recent implementation of CY47r1 in early Octobre 2020 show an overall improvement of the o-suite, in particular in the tropics between 10-30 hPa. Also, the o-suite ozone bias against these independent observations in this region is now similar to the one of BASCOE.

Figure 9.3.4 to 9.3.7 display vertical profiles of the relative biases between the o-suite or BASCOE and the satellite measurements. The difference is averaged over the most recent 3-month period considered in this validation report, i.e. JJA 2020.

All o-suite profiles present a common feature of a slight overestimation at around 30km, followed by a stronger underestimation at around 40km, which is evidenced in the 4th day forecast.

The profiles of OMPS-LP in the northern hemisphere present irregularities (mainly in the part contributed by the sensor in the visible), which are not found in the other instruments nor in the o-suite or the BASCOE models; hence they should be disregarded for this validation.

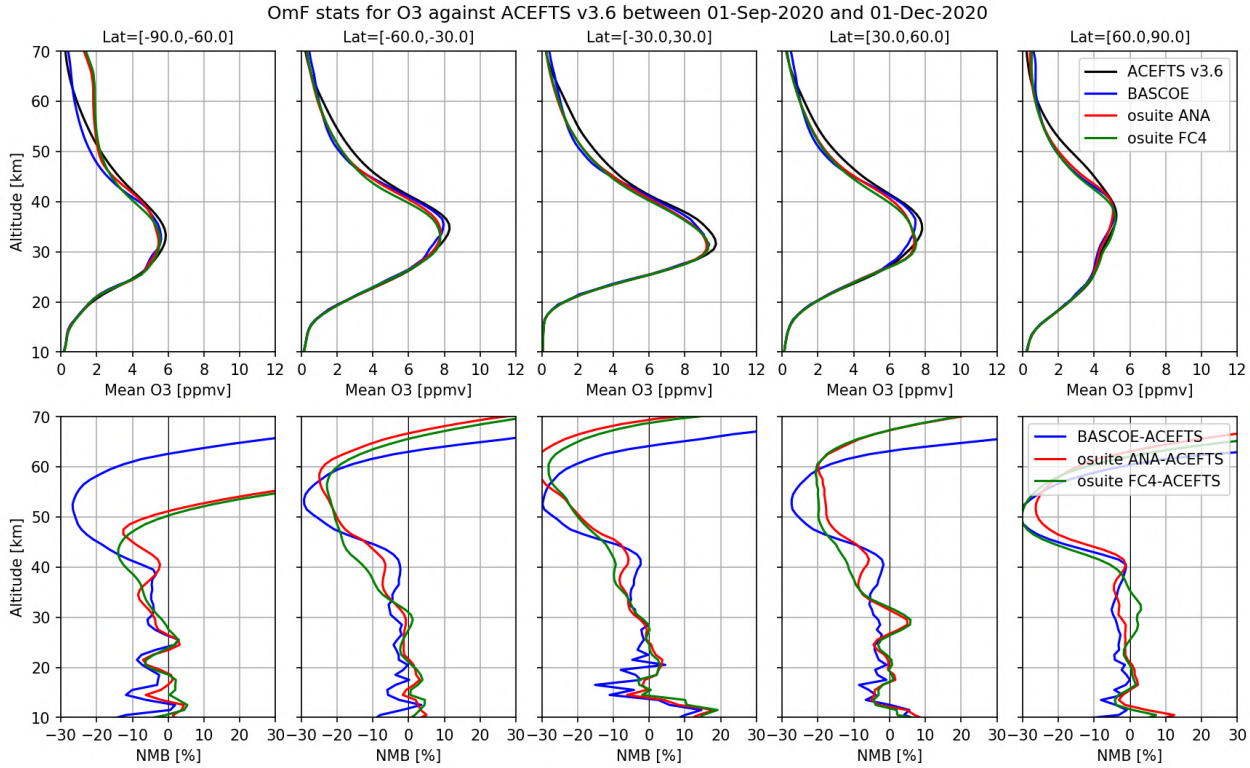

Figure 9.3.5: As Fig. 9.3.4 but for comparison against ACE-FTS observations..

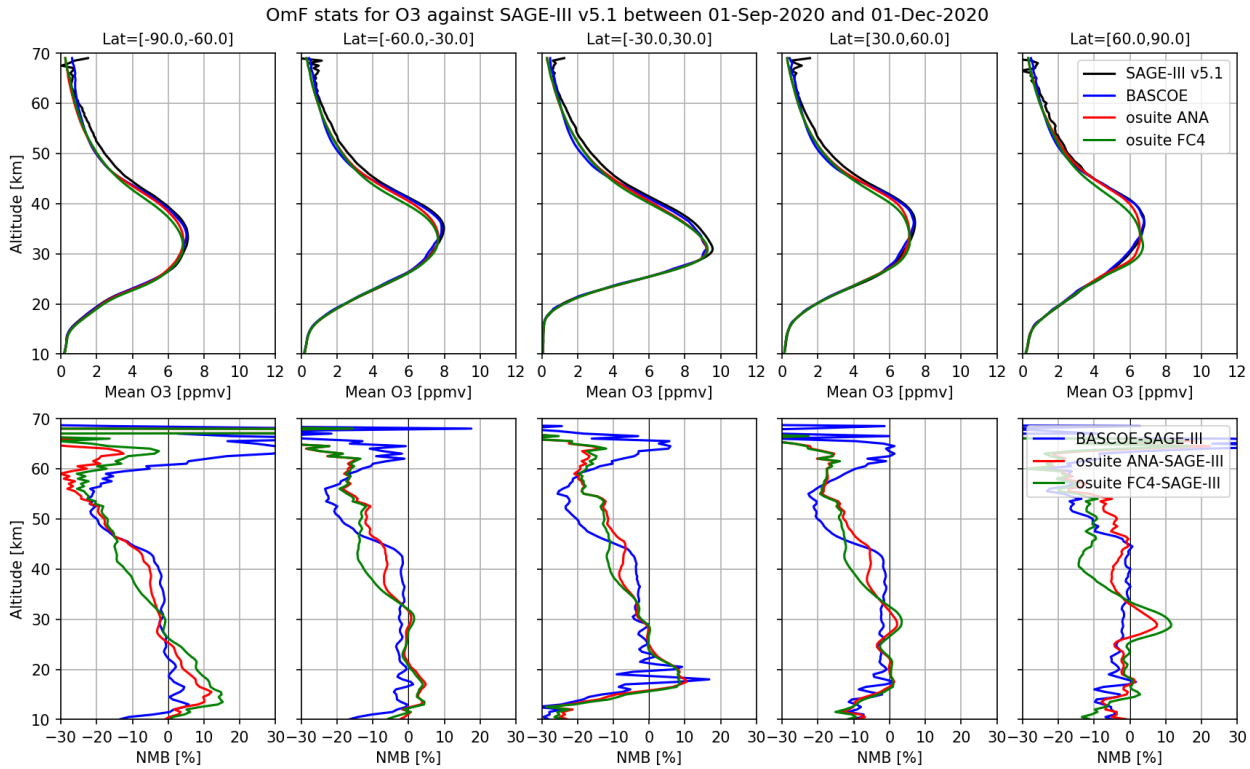

Figure 9.3.6: As Fig. 9.3.4 but for comparison against SAGE-III observations.

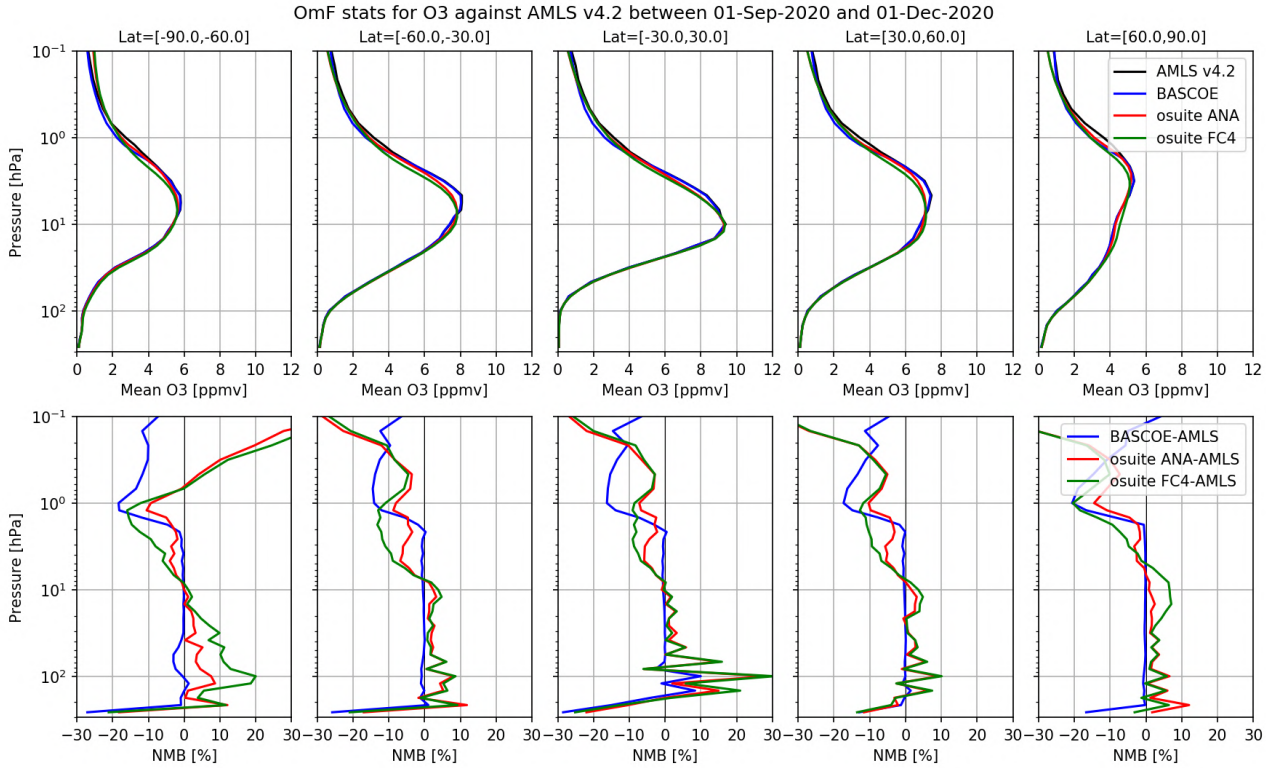

Figure 9.3.7: As Fig 9.3.4 but for comparison against MLS offline observations.

It must be noted that the different instruments have a variety of spatial and temporal coverage: for a 3 month period and over the latitude bands considered, OMPS-LP and Aura MLS provide daily data with more than 40000 valid profiles (while OMPS-LP being blind in the polar night), while ACE-FTS provides around 700 profiles in the polar region and 200 profiles in the tropics, and SAGE-III around 800 profiles in each latitude band except the south polar region (none).

9.4 Stratospheric NO_2

The CAMS model uses a tropospheric chemistry scheme in combination with a parameterization for stratospheric ozone. Stratospheric ozone is also well constrained by satellite observations. Therefore, the only useful product in the stratosphere is ozone, and all other compounds, including NO_2, should not be used, as demonstrated by the validation results presented here.

In this section, nitrogen dioxide from SCIAMACHY/Envisat satellite retrievals (IUP-UB v0.7) and GOME-2/MetOp-A satellite retrievals (IUP-UB v1.0) are compared to modelled stratospheric NO_2 columns. Monthly mean stratospheric NO_2 columns from SCIAMACHY and GOME-2 have relatively small errors on the order of 20% in the tropics and in mid-latitudes in summer and even lower errors at mid-latitudes in winter. As the time resolution of the saved model files is rather coarse and NO_x photochemistry in the stratosphere has a large impact on the NO_2 columns at low sun, some uncertainty is introduced by the time interpolation at high latitudes in winter.

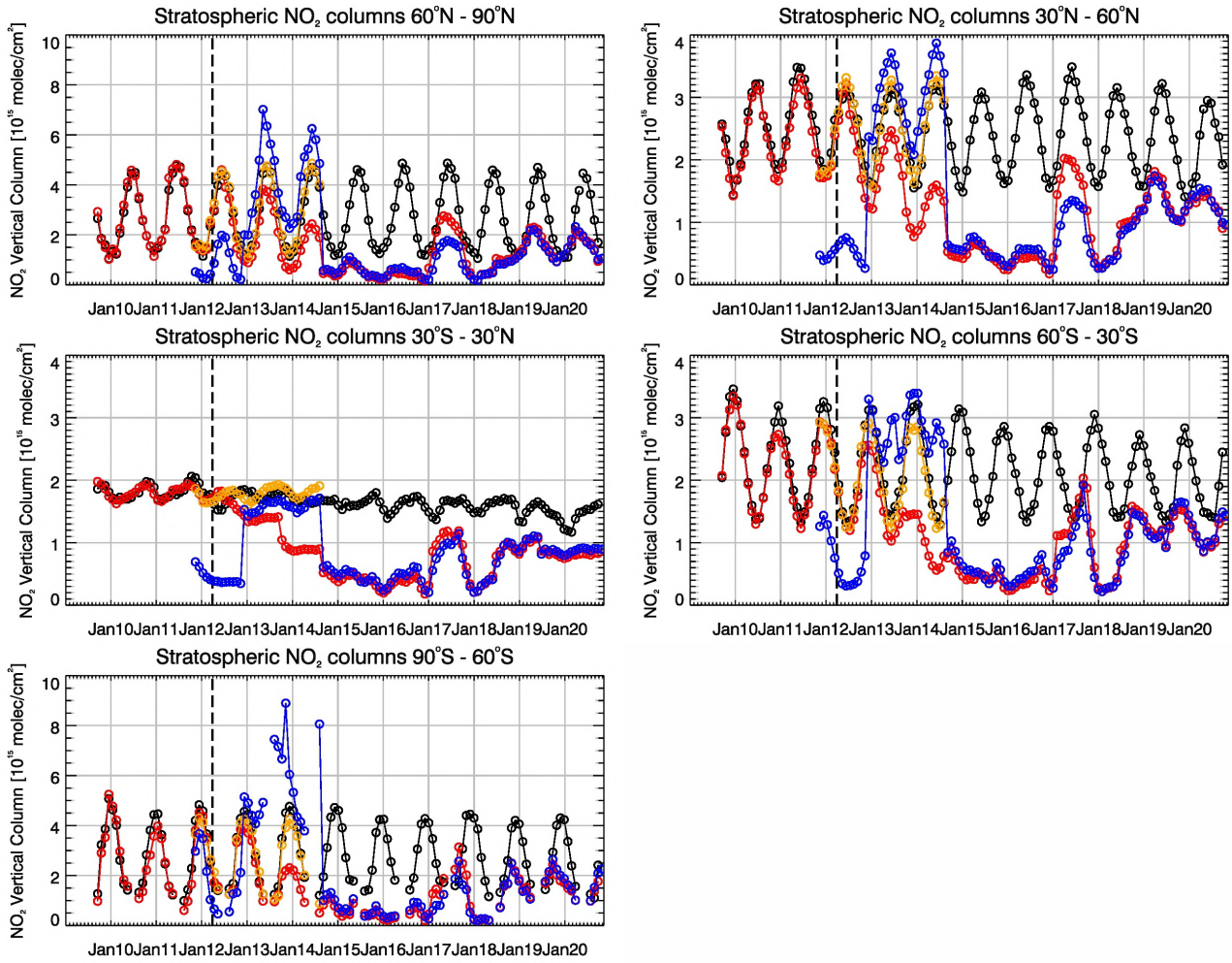

Figure 9.4.1: Time series of average stratospheric NO2 columns [1015 molec cm-2] from SCIAMACHY (up to March 2012) and GOME-2 (from April 2012, black) compared to model results (red: o-suite, blue: MACC fcnrt TM5/MACC CIFS TM5/control, orange: MACC fcnrt MOZ) for different latitude bands. See text for details. The blue line shows MACC_fcnrt_TM5 from November 2011 to November 2012, MACC_CIFS_TM5 results from December 2012 until August 2014 and control results from September 2014 onwards (the model run without data assimilation is termed control since Sep 2014). The vertical dashed black lines mark the change from SCIAMACHY to GOME-2 based comparisons in April 2012.

As shown in Figure 9.4.1, amplitude and seasonality of satellite stratospheric NO_2 columns are poorly modelled with CB05-based chemistry runs including the more recent versions of the o-suite. The significant differences between observations and CB05 chemistry runs, i.e. a strong underestimation of satellite retrievals by models, can be explained by the missing stratospheric chemistry for these model versions. The only constraint on stratospheric NO_x is implicitly made by fixing the HNO_3/O_3 ratio at the 10 hPa level. This assumption, in combination with the changing model settings for stratospheric O_3 for control compared to MACC_CIFS_TM5, may explain some of the jumps we see in stratospheric NO_2. In any of these runs the stratospheric NO_2 is poorly constrained. It clearly indicates that stratospheric NO_2 in the latest versions of the o-suite is not a useful product and should be disregarded.

Comparison of the o-suite from July 2012 until August 2014 with the other model runs and satellite observations shows that the previous version of the o-suite stratospheric NO_2 columns had a systematic low bias relative to those from MACC_fcnrt_MOZ and satellite observations for all latitude bands. For example, o-suite values are a factor of 2 smaller than satellite values between 60°S to 90°S for October 2013. Best performance was achieved with the MOZART chemistry experiments without data assimilation (MACC_fcnrt_MOZ, running until September 2014), especially northwards of 30°S. Details on the NO_2 evaluation can be found at: http://www.doas-bremen.de/macc/macc_veri_iup_home.html.

10. Validation results for greenhouse gases

This section describes the NRT validation of the pre-operational, high resolution forecast of CO_2 and CH_4 from 1st December 2019 to 1st December 2020 based on observations from 26 surface stations, located in Western Europe; 10 TCCON stations measuring XCO_2 and XCH_4 total columns, and 13 NDACC stations measuring partial and total CH_4 columns. We compare the observations to the high-resolution forecast experiments (*h9sp, Tco1279L137; 9x9 km*), coupled to the analysis experiment (*h72g, Tco399L137, 25x25 km*). Note that these are the Cy46R1 configurations. Cy47R1, which became operational on 1 November, will be discussed in the next report covering Dec 2020 – Feb 2021.

10.1 CH4 and CO2 validation against ICOS observations

The CO_2 and CH_4 simulations from the analysis and high resolution forecast have been compared to 26 ICOS stations. The near–real time data processing of the in-situ measurements is ensured by the Atmospheric Thematic Center (Hazan et al., 2016). All stations follow the ICOS Atmospheric Station specification (Laurent et al., 2017), which is a requirement in the labelling process (Yver Kwok et al., 2020). Among the 26 stations we can distinguish four sites located on top of mountains (PUY, JFJ, CMN, PRS), two background sites (PAL, ZEP), two coastal sites (UTO, MHD) and 17 tall towers. In addition, there is one site in South Hemisphere at La Réunion Island (RUN). For the later we consider only in this report the highest sampling levels which are at least at 100m above the ground.

Figure 10.1.1 shows the time varying biases (CAMS runs minus observations), averaged on a weekly basis, for ICOS stations. The CO_2 biases are characterized by a clear seasonal cycle at most sites with maximum values in Spring/Summer, and minimum in Autumn/Winter. Ispra (IPR), a tall tower located in the Po valley, appears as an outlier probably due to the complex orography in the surroundings. We also observed higher weekly biases at Lutjewad (LUT), Karlsruhe (KIT) and Saclay (SAC) due to the vicinity of emission hot spots or urban areas. Four examples are detailed on Figures 10.1.2 for Monte Cimone (CMN, Italy) and Puy de dôme (PUY, France), and on Figure 10.1.3 for Norunda (NOR, Sweden) and Svarberget (SVB, Sweden). The two mountain sites show quite similar features: a negative bias of almost -1% in December 2019, followed by an overestimation of the CO_2 concentration rising up to 2%, and decreasing back to -1% in late 2020. The main difference can be found in the timing of the maximum bias, which occurs earlier (May) in PUY compared to CMN (July). The two Nordic site (Figure 10.1.3) of Norunda and Svarberget, also show similar patterns. For the two sites the biases remain close to zero till spring. In June the CO_2 drawdown observed at both sites in underestimated by the CAMS experiments, similarly to PUY. Then the highest biases are observed in autumn, when the CAMS runs cannot reproduce the CO_2 enhancements observed at Nordic sites.

The seasonal cycles of the CO_2 biases calculated for all ICOS sites are shown on figure 10.1.6. With the exception of Ispra, the model/observations differences generally range within ±5 ppm, with a maximum value occurring between May and July. Higher negative biases are observed in the peri-urban sits of KIT and SAC. The lowest biases are observed on average at Mace Head, La Réunion Island and the mountain sits (JFJ, PRS).

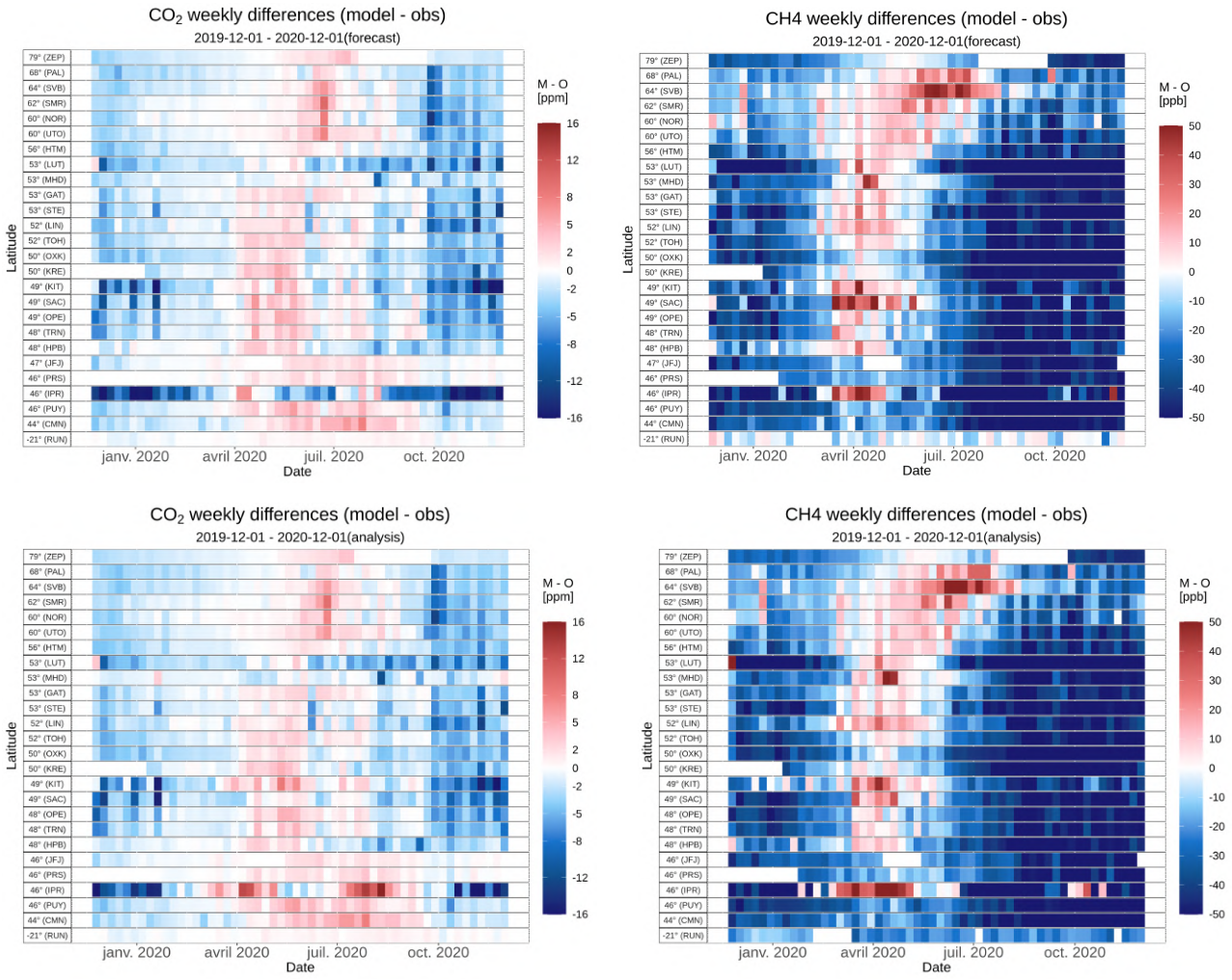

Figure 10.1.1: Mosaic plot of CO_2 (left, in ppm) and CH_4 (right, in ppb) biases of the CAMS high resolution forecast (top panel) and analysis (bottom panel), compared to surface station observations. Each vertical coloured line represents a weekly mean.

For CH_4 the biases show seasonal and latitudinal patterns quite similar to the ones observed for CO_2 (Figure 10.1.1). At the Scandinavian sites the CAMS runs overestimates (up to 50 ppb) the observations from spring to summer. The example of Svarberget station (Figure 10.1.4) clearly shows the overestimation of the baseline and the amplitude of the CH_4 spikes at this season by the CAMS runs, which could indicate that the wetland emissions are overestimated. Then, starting in August, the CAMS experiments underestimate the CH_4 concentrations down to -2%. The more we go at lower latitudes, the more we observe negative biases. In Germany and in the north of France the bias is positive only during a short period in spring. At Ochsenkopf (Figure 10.1.5) the bias just comes to zero in May but remains negative all the year by -2% before spring and -4% afterward. The CAMS runs at Zeppelin site (figure 10.1.5) show a similar comparison to observation. At this site it is worth to note a step increase of the CH_4 concentrations by about 30 ppb in early July. This CH_4 enhancement corresponds to a change in the air masses origins, from the North Sea to Siberia on July 2nd. The CAMS runs represent this change, associated to the CH_4 emissions in Siberia, with the good timing and amplitude. At the southern hemisphere site in La Reunion, we observe a more

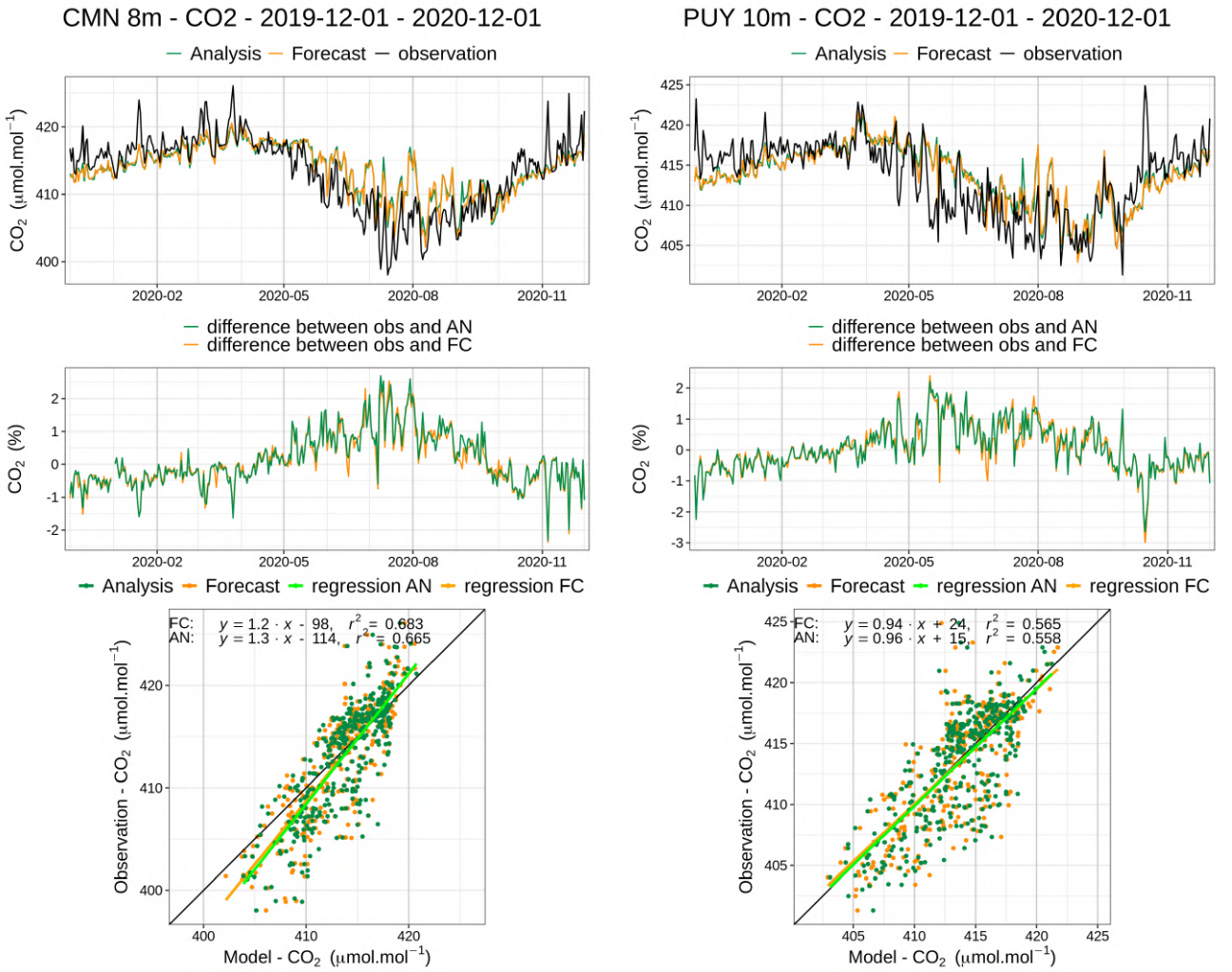

Figure 10.1.2: Comparison of CO_2 daily means observed (black) with the analysis run (green) and the high-resolution forecast (orange) at Monte Cimone (left) and Puy de dôme (right). Middle: differences of the observations minus the simulations. Below: Linear fit between observations and simulations. The dashed vertical line represents the change of experiments in December 2018.

systematic bias over the year. There we can note that the bias of the forecast run is smaller by about 1%, but the correlation is improved in the analysis with a decrease of the amplitude of synoptic events. The seasonal cycle of the CH4 biases (Figure 10.1.6) generally present a maximum value in March and a minimum in September.

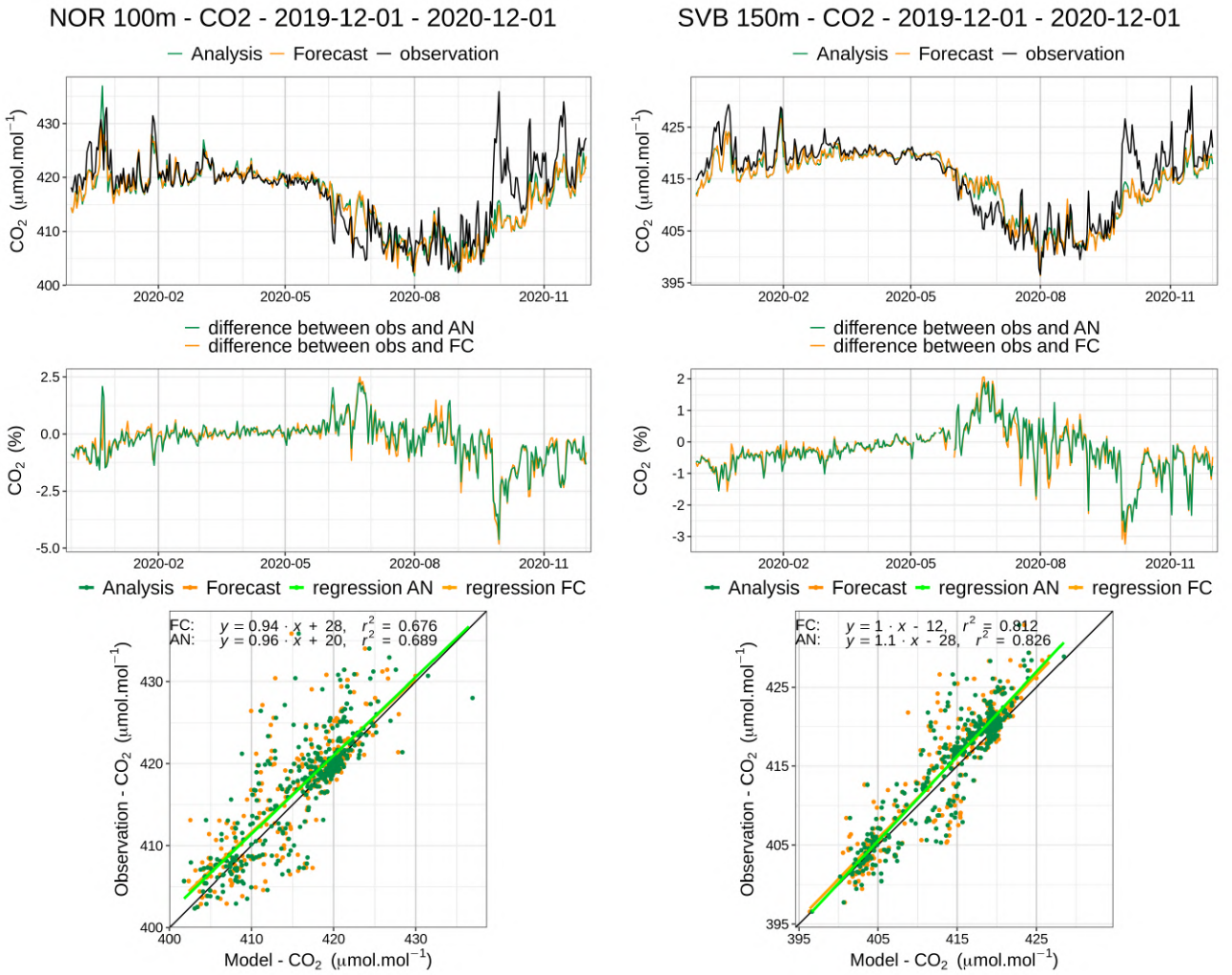

Figure 10.1.3: Same as Figure 10.1.2 for Norunda (NOR) and Svarberget (SVB).

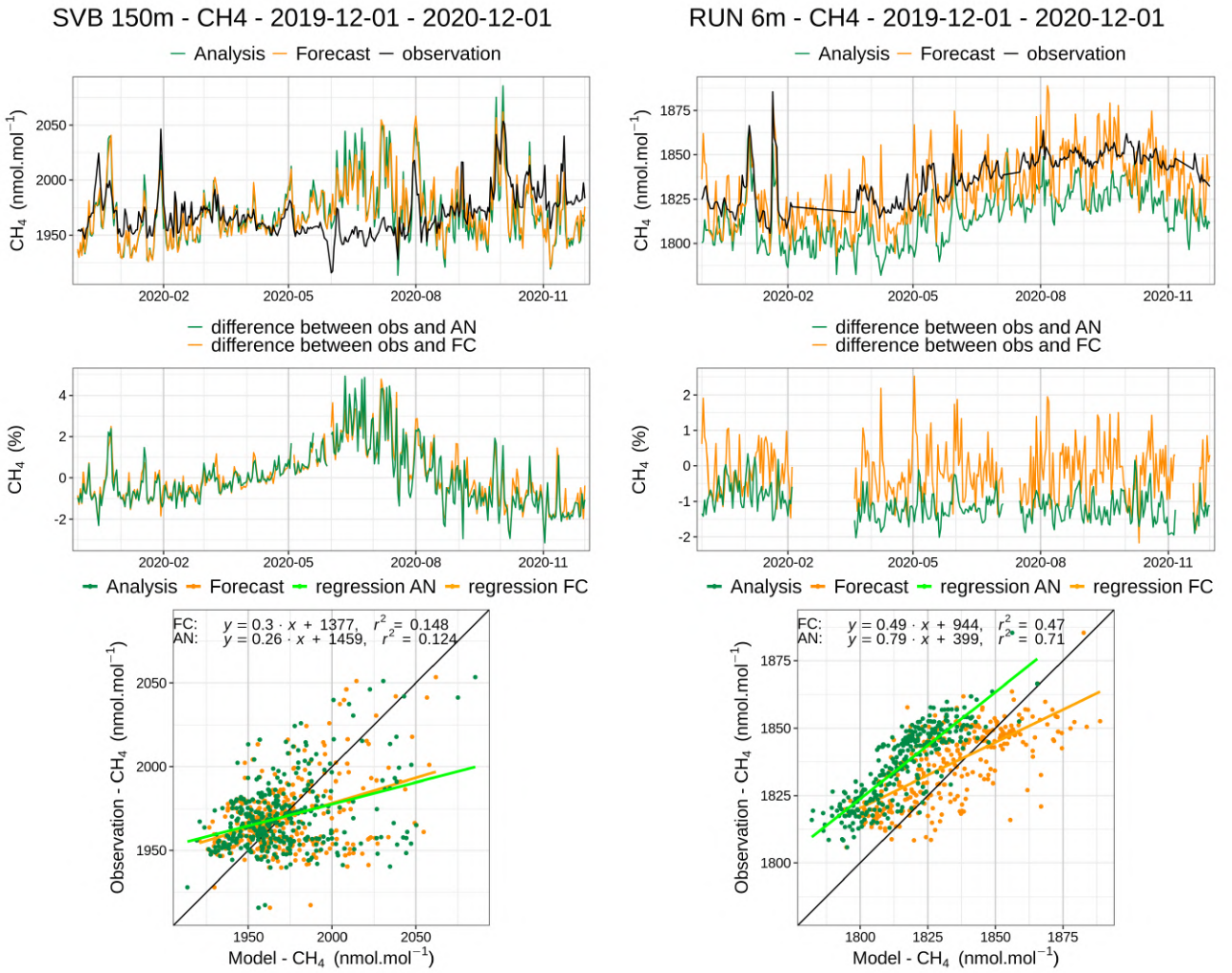

Figure 10.1.4: Comparison of CH_4 daily means observed (black) with the analysis run (green) and the high-resolution forecast (orange) at Svarberget (left) and La Réunion (right). Middle: differences of the observations minus the simulations. Below: Linear fit between observations and simulations. The dashed vertical line represents the change of experiments in December 2018.

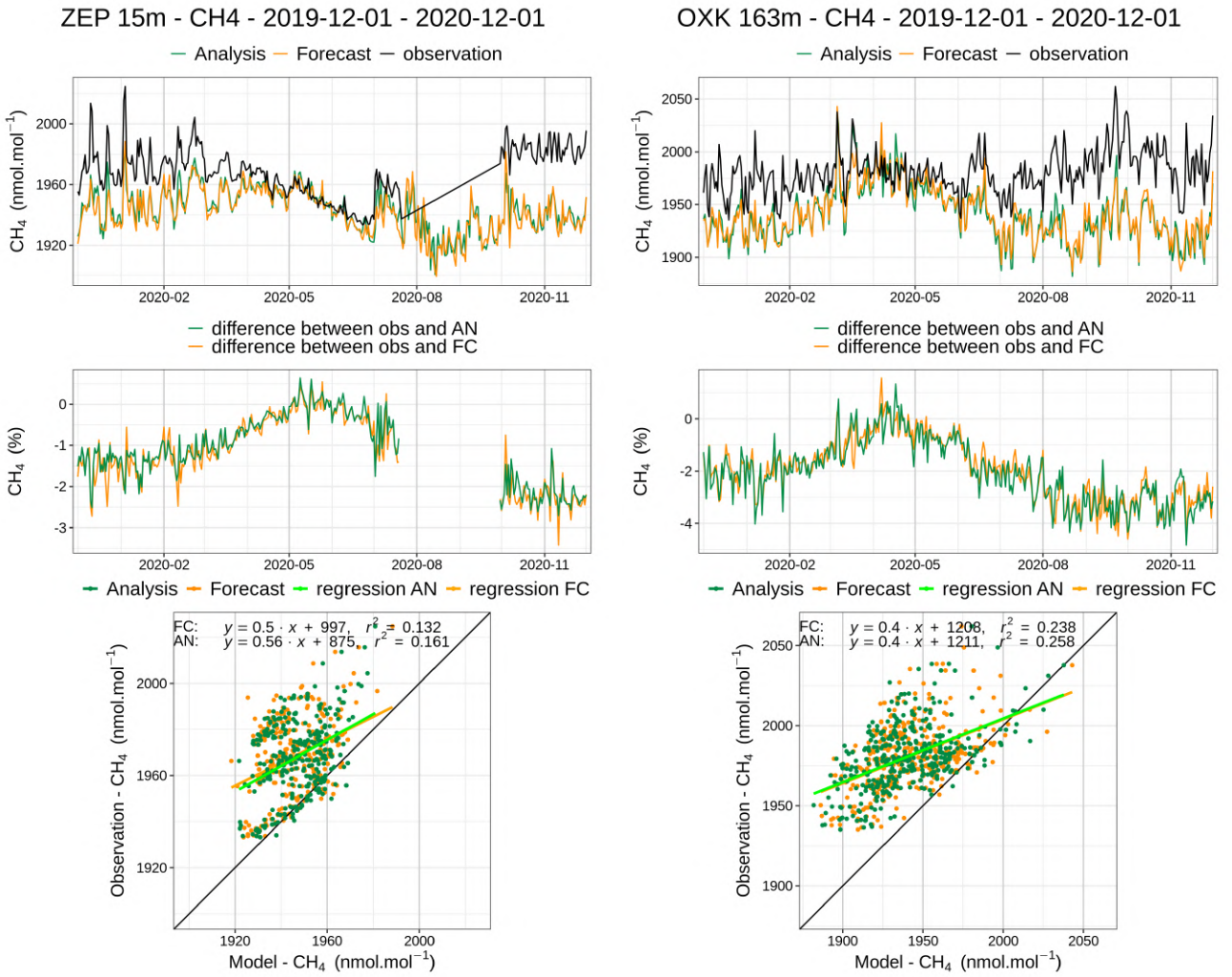

Figure 10.1.5: Same as Figure 10.1.4 for Zeppelin (left) and Ochsenkopf (right).

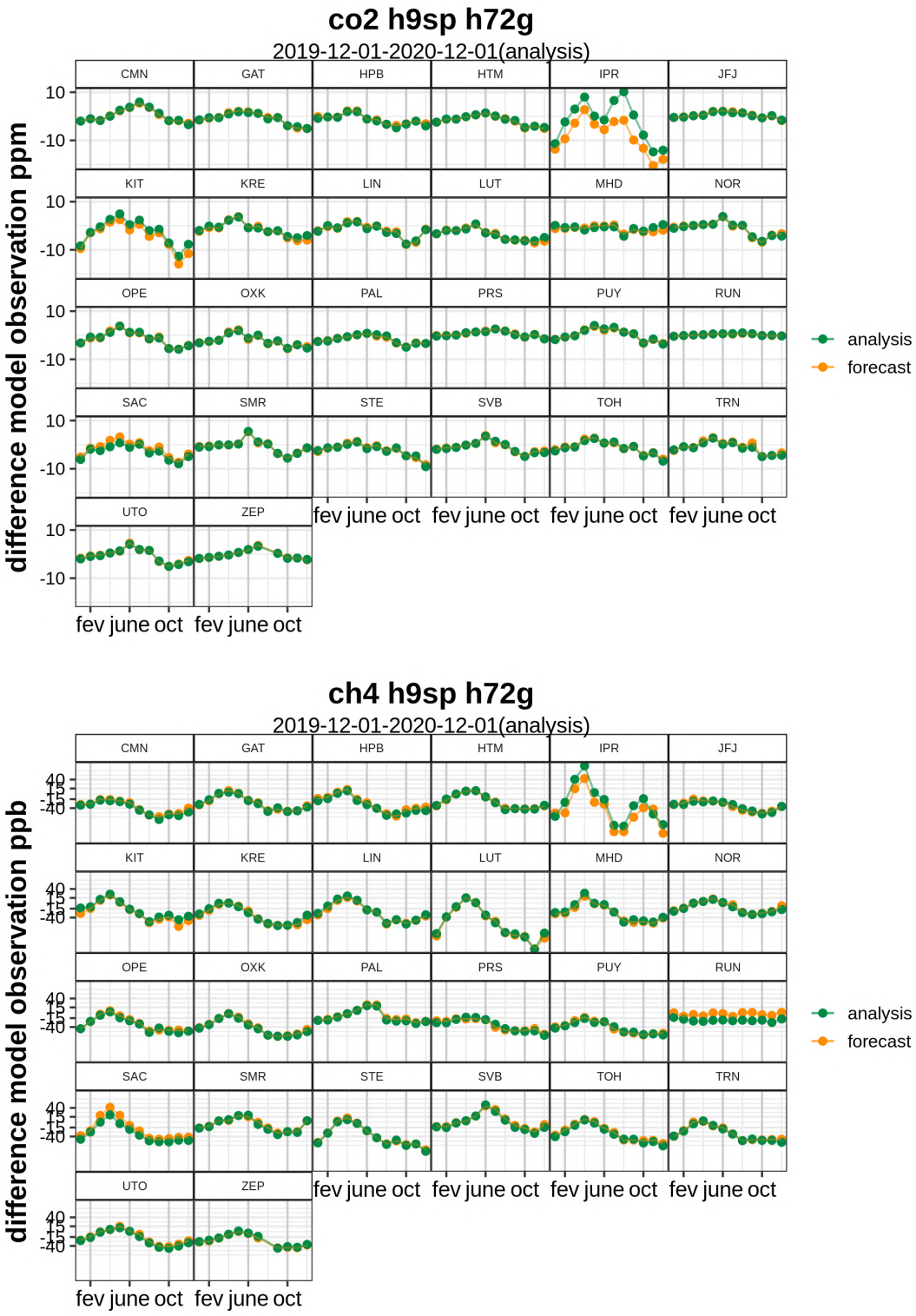

Figure 10.1.6: Mean seasonal cycles of the biases for CO_2 (above, in ppm) and CH_4 (below, in ppb) at ICOS stations. The forecast experiment is shown in orange, and the analysis in green.

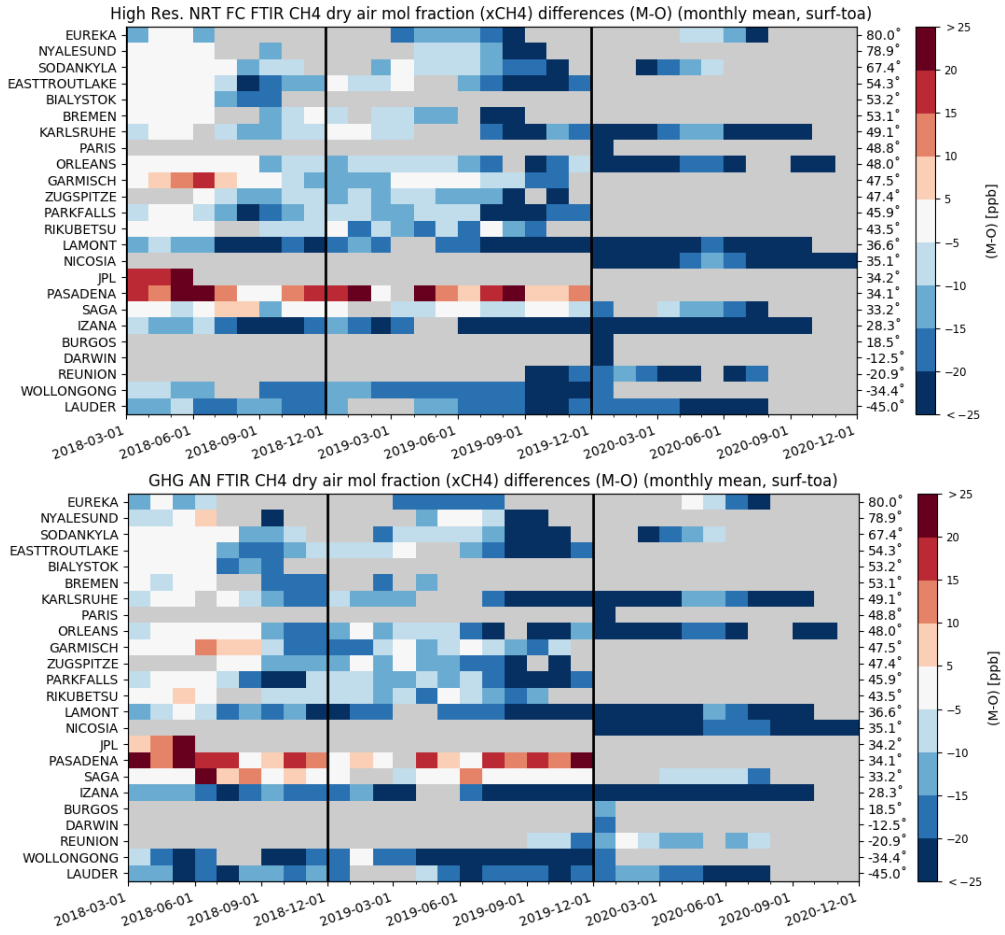

Figure 10.2.1: Monthly differences for the last 2.5 years (upper plot: high res NRT, lower plot: GHG AN). The stations are sorted by latitude (northern to southern hemisphere).

10.2 CH_4 and CO_2 validation against TCCON observations

For the validation column averaged mole fractions of CO_2 and CH_4 (denoted as XCO_2 and XCH_4) from the Total Carbon Column Observing Network (TCCON) are used. Column averaged mole fractions provide different information than the in situ measurements and are therefore complementary to the in situ data. The validation routines used for TCCON data are the same as used for the NDACC network and are documented in Langerock et al. (2015). In this section, we compare column averaged mole fractions of CH_4 and CO_2 of the CAMS models with TCCON retrievals. Data from the following TCCON sites has been used:

Izana (Blumenstock et al., 2017), Reunion (De Mazière et al., 2017), Bialystok (Deutscher et al., 2017), Manaus (Dubey et al., 2017), Four Corners (Dubey et al., 2017), Ascension (Feist et al., 2017), Anmeyondo (Goo et al., 2017), Darwin (Griffith et al., 2017), Wollongong (Griffith et al., 2017), Karlsruhe (Hase et al., 2017), Edwards (Iraci et al., 2017), Indianapolis (Iraci et al., 2017), Saga (Kawakami et al., 2017), Sodankyla (Kivi et al., 2017), Hefei (Liu et al., 2018), Tsukuba (Morino et al., 2017), Burgos (Morino et al., 2018), Rikubetsu (Morino et al., 2017), Bremen (Notholt et al., 2017), Spitsbergen (Notholt et al., 2017), Lauder (Sherlock et al., 2017, Pollard et al., 2019), Eureka (Strong

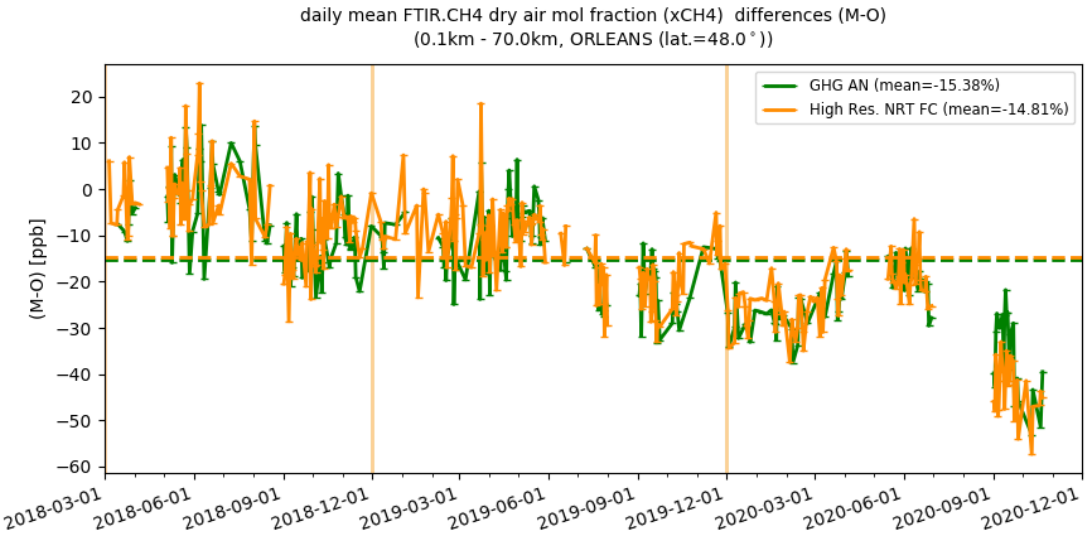

Figure 10.2.2: Comparison of the CH_4 model data with TCCON CH_4 at Orleans.

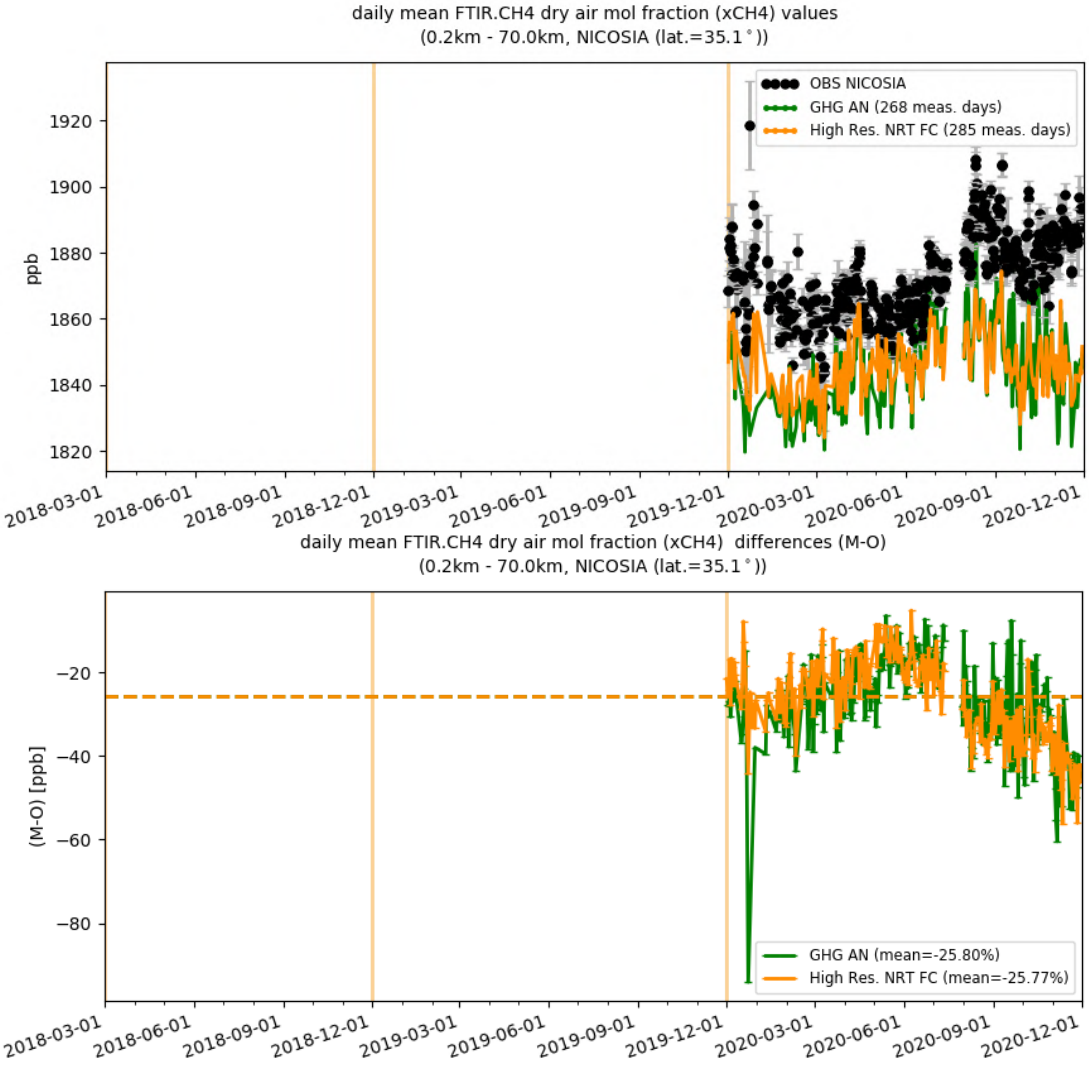

Figure 10.2.3: Comparison of the CH_4 model data with TCCON CH_4 at Nicosia.

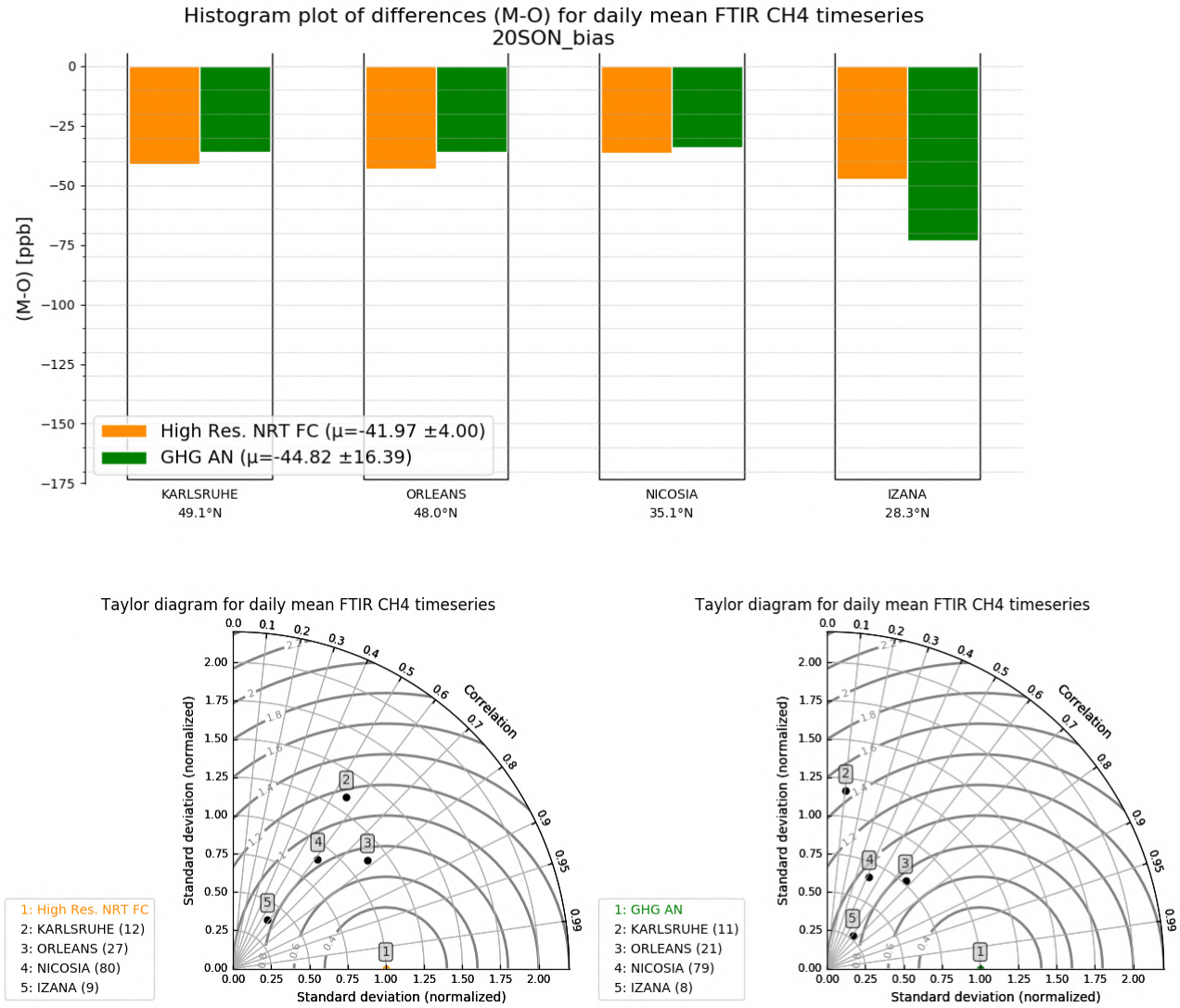

Figure 10.2.4: Histogram plots and Taylor diagrams for the comparison period.

et al., 2018), Garmisch (Sussmann et al., 2017), Zugspitze (Sussmann et al., 2018), Paris (Te et al., 2017), Orleans (Warneke et al., 2017), Park Falls (Wennberg et al., 2017), Caltech (Wennberg et al., 2017), Lamont (Wennberg et al., 2017), Jet Propulsion Laboratory (Wennberg et al., 2017), East Trout Lake (Wunch et al., 2017), Nicosia (Petri et al., 2020)

For the validation of the models in September, October and November TCCON data was available only from the sites Karlsruhe, Orleans, Nicosia and Izana. The data from the stations Orleans and Nicosia used for the comparison period is the rapid delivery data, which has not undergone all TCCON quality checks.

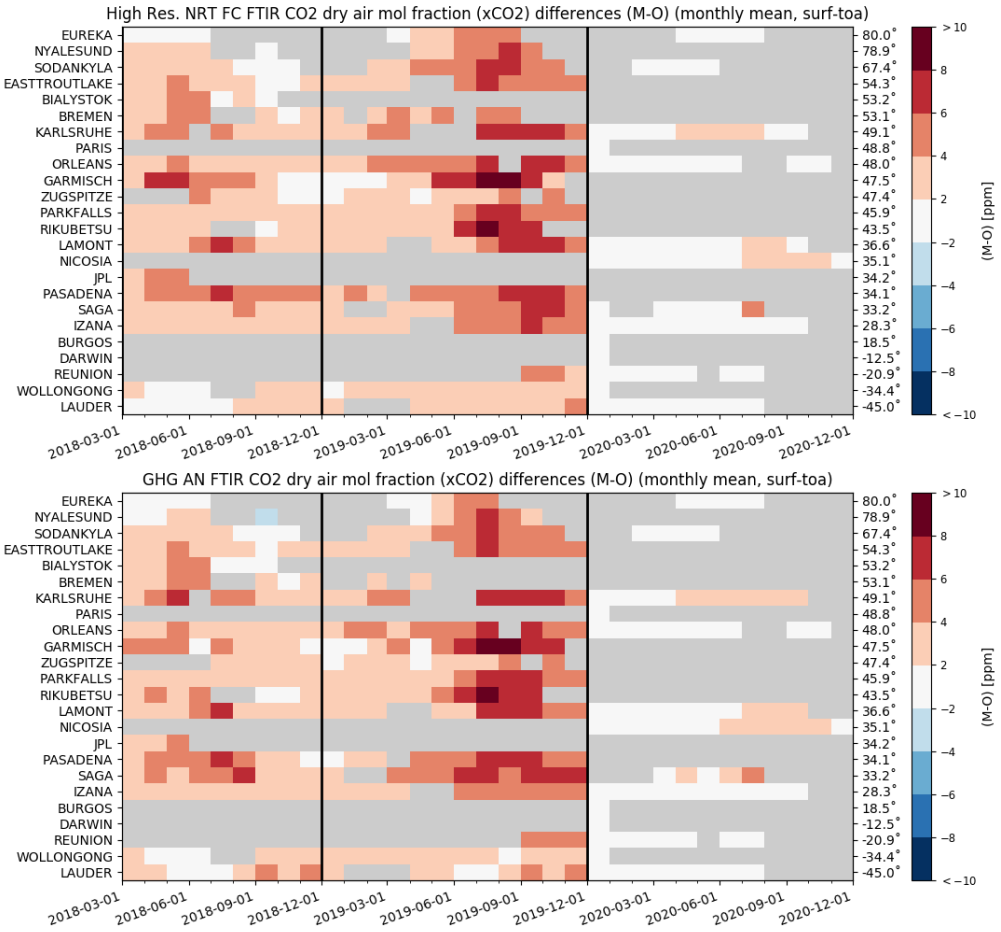

Figure 10.2.5: Monthly differences for the last 4 years (upper plot: high res NRT, lower plot: GHG AN). The stations are sorted by latitude (northern to southern hemisphere).

Methane (CH_4)

Figure 10.2.1 shows the data for the last 2.5 years. The comparison is shown for the sites Orleans (Fig. 10.2.2) and Nicosia (Fig. 10.2.3). The data from these stations show that the model data underestimates the CH_4 for these stations by up to 50 ppb.

Carbon dioxide (CO_2)

Figure 10.2.5 shows the comparisons for the last 2.5 years. For the reporting period the models compare with the measurements within 1%. The comparison is shown for the sites Orleans (Fig. 10.2.6) and Nicosia (Fig. 10.2.7). At Nicosia it obvious that the seasonality is not well captured by the models.

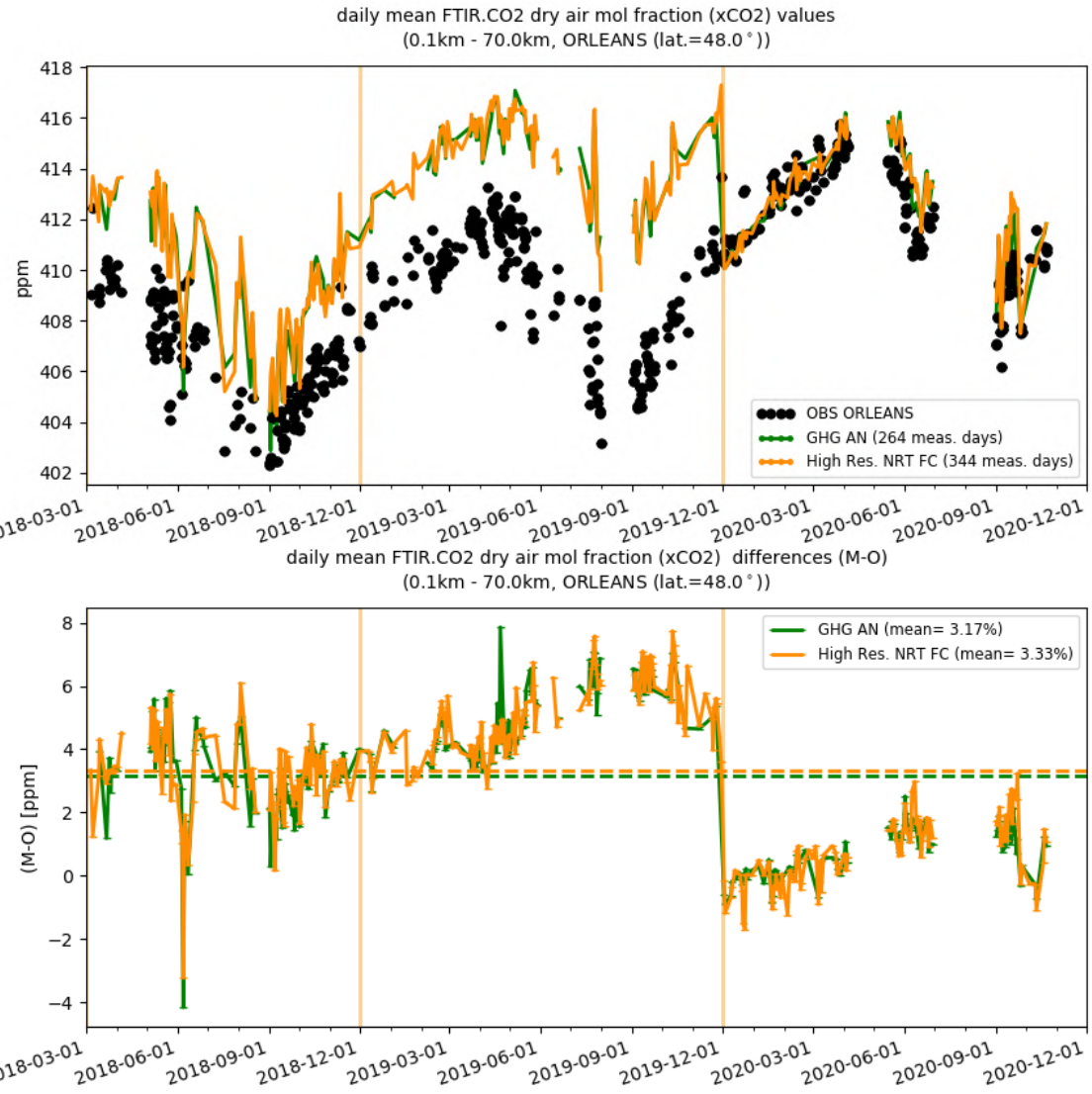

Figure 10.2.6: Comparison of the CO_2 model data with TCCON CO_2 at Orleans.

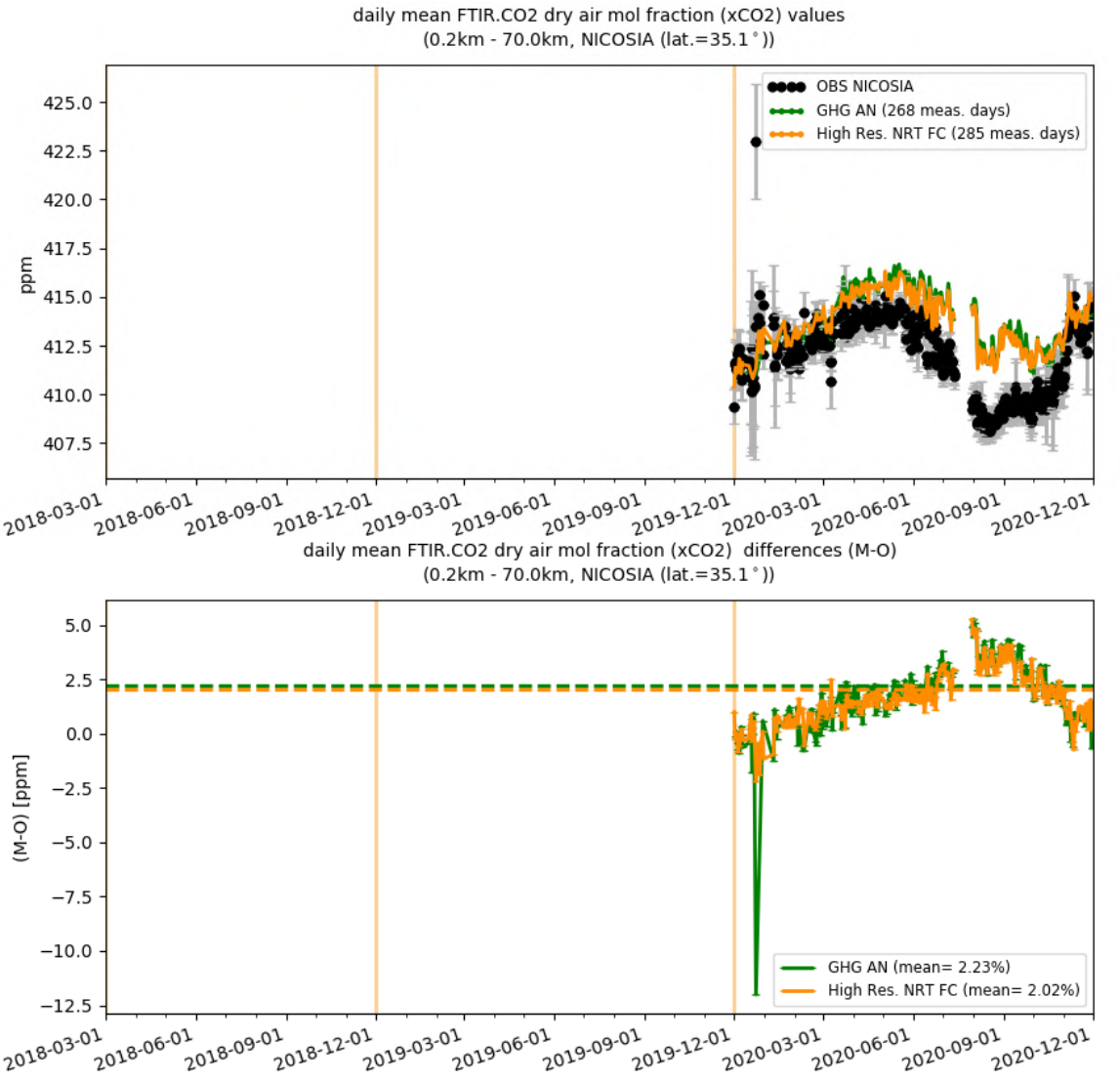

Figure 10.2.7: Comparison of the CO_2 model data with TCCON CO_2 at Nicosia.

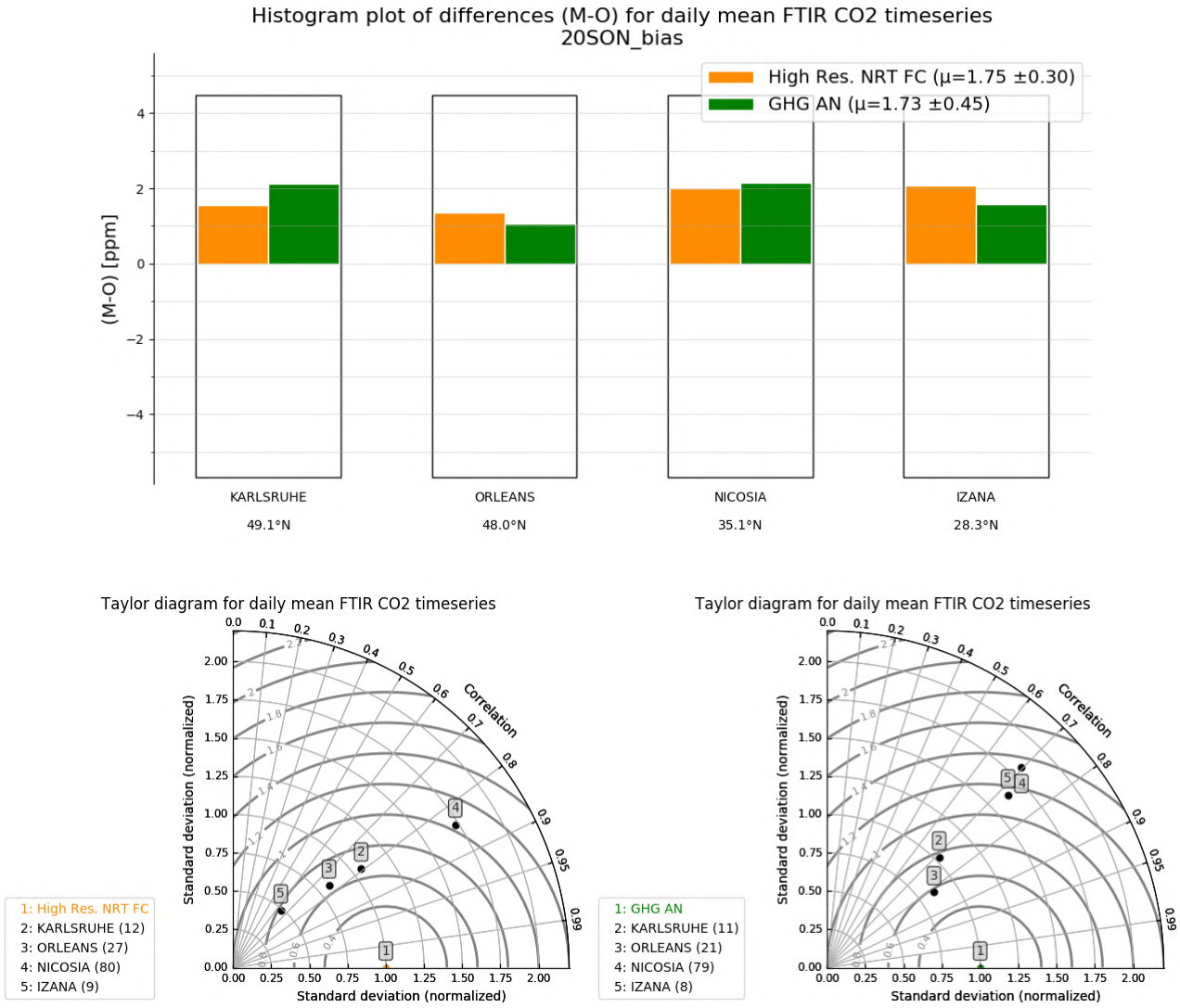

Figure 10.2.8 Histogram plots and Taylor diagrams for the comparison period.

10.3 Validation against FTIR observations from the NDACC network

In this section, we compare the CH_4 profiles of the CAMS GHG products with FTIR measurements at different FTIR stations within the NDACC network. These ground-based, remote-sensing instruments are sensitive to the CH_4 abundance in the troposphere and lower stratosphere, i.e. between the surface and up to 25 km altitude. Tropospheric and stratospheric CH_4 columns are calculated from the FTIR profile data and used to validate corresponding columns obtained from the CAMS data. A description of the instruments and applied methodologies can be found at http://nors.aeronomie.be. The typical uncertainty on the FTIR tropospheric column is 2%, while the uncertainty on the stratospheric column is 7.5%, adding together to a 3% uncertainty on the total column. The systematic uncertainty is large for the NDACC methane product mostly due to higher spectroscopic uncertainties.

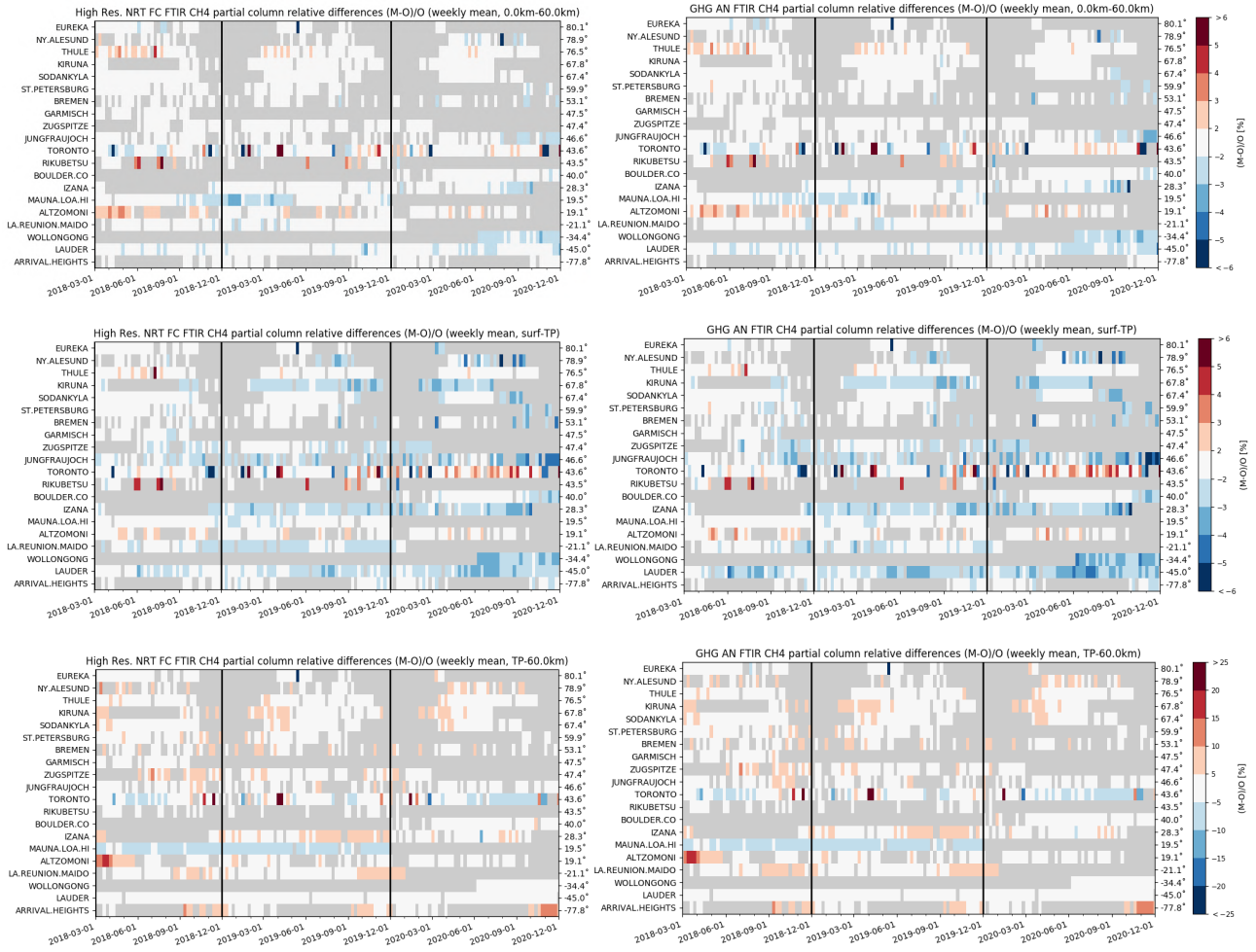

Figure 10.3.1: Weekly mean relative bias for total (top row), tropospheric (middle row) and stratospheric CH_4 columns (bottom row) for the period March 2018 – November 2020 for high resolution forecast (left) and the analysis (right). The overall uncertainty for the CH_4 total column measurements is approximately 4%. The overall uncertainty for the CH_4 total/tropospheric column measurements is approximately 2%, while the stratospheric uncertainty is 7.5% (the colour scale for the mosaic plots follows the uncertainty scale).

Figure 10.3.1 (middle row) shows that the tropospheric columns of CH_4 agree well and only small differences appear between the analysis and the high resolution run. In comparison with the measurement uncertainty, a slight underestimation is observed in the tropospheric columns which is in agreement with the TCCON results. The Paramaribo measurements have reduced sensitivity and the tropospheric/stratospheric split is not valid in this case and the Toronto FTIR time series suffers from too low outliers.

The stratospheric columns (Figure 10.3.1, bottom row) show a slight overestimation compared to the measurement uncertainty.

Figure 10.3.2 shows Taylor diagrams for the SON time period and for a selected number of sites: some stations have limited observations and should be treated with care. Assimilation has a small effect on the correlation coefficients for most sites: the average correlation for 11 stations is 0.76 for the analysis and 0.8 for the high-resolution forecast. Table 10.3.1 contains detailed statistics per site.

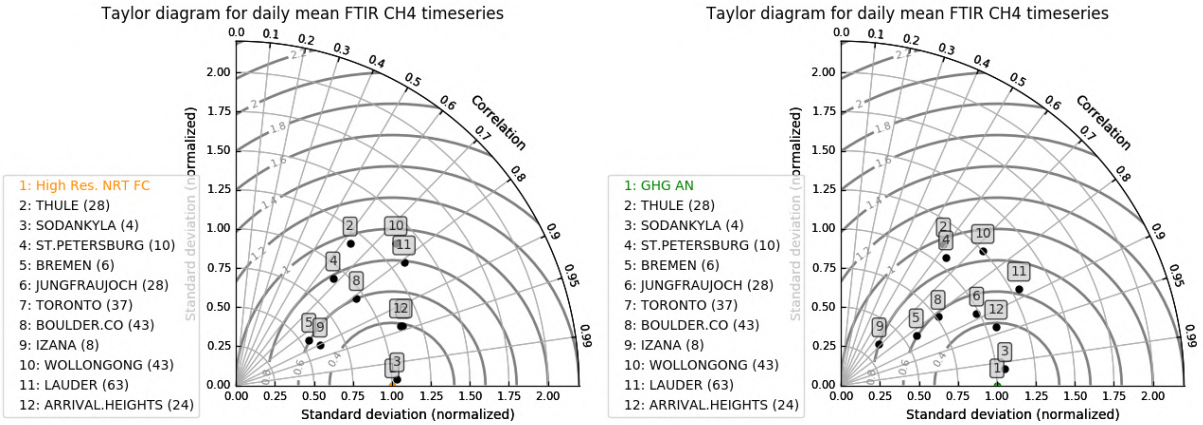

Figure 10.3.2: Taylor diagrams relating the standard deviations for the model /GB time series of total CH_4 column data and their correlation for the period SON 2020 (the stations with a limited number of measurements should be ignored). All time-series are normalized such that the standard deviation of the CAMS column time series is 1.

Table 10.3.1: Detailed statistics for total CH_4 column comparisons against FTIR measurements during SON 2020. Both analysis and highres forecast behave similar.

	Highres Forecast total column					ghg AN total column					
FTIR site	#	rel. std	corr	rel diff (%)	rel diff std(%)	#	rel. std	corr	rel diff (%)	rel diff std(%)	lat
THULE	28	1.2	0.63	-0.12	0.83	28	1.1	0.59	-0.12	0.88	76.5
SODANKYLA	4	1	1	-1.74	0.07	4	1.1	1	-2.12	0.18	67.4
ST.PETERSBURG	10	0.9	0.67	-2.07	0.49	10	1.1	0.64	-2.2	0.48	59.9
BREMEN	6	0.6	0.85	-1.96	0.57	6	0.6	0.83	-1.98	0.54	53.1
JUNGFRAUJOCH	28	1.1	0.94	-2.48	0.48	28	1	0.88	-2.64	0.7	46.6
TORONTO	37	4.5	0.43	0.02	3.74	37	4	0.33	-0.05	3.8	43.6
BOULDER.CO	43	1	0.81	-1.53	0.51	43	0.8	0.82	-1.48	0.68	40
IZANA	8	0.6	0.9	-2.73	0.5	8	0.4	0.68	-3.42	1.26	28.3
WOLLONGONG	43	1.4	0.75	-2.42	1.09	43	1.3	0.73	-2.65	1.13	-34.4
LAUDER	63	1.3	0.81	-1.7	1.05	63	1.3	0.88	-2.07	1.09	-45
ARRIVAL.HEIGHTS	24	1.1	0.94	0.3	0.41	24	1.1	0.94	0.33	0.42	-77.8
		1.3	0.79	-1.49	0.88		1.2	0.76	-1.67	1.01	

10.4 Validation against AIRCORE profiles

The AIRCORE is a new innovative way of sampling the atmospheric air column, initially developed at NOAA/ESRL (Karion et al. 2010). Through a joint research project, LSCE and LMD have worked together to develop an AIRCORE program in France, using the light AirCores developed at LMD (Membrive et al., 2017). The AIRCORE is made of a polystyrene box containing 70m of stainless-steel tubing closed at one end that empties out during the ascending phase and samples the air during the descending phase (Figure 10.4.1). Once at ground level the sampled air is analysed with a CRDS spectrometer to determine the concentrations of CO_2, CH_4 and CO. Knowing the total amount of air contained in the AIRCORE, and the pressure at the maximum elevation and at the ground, concentration-versus-altitude profiles can be derived from those analysis (Membrive et al., 2017).

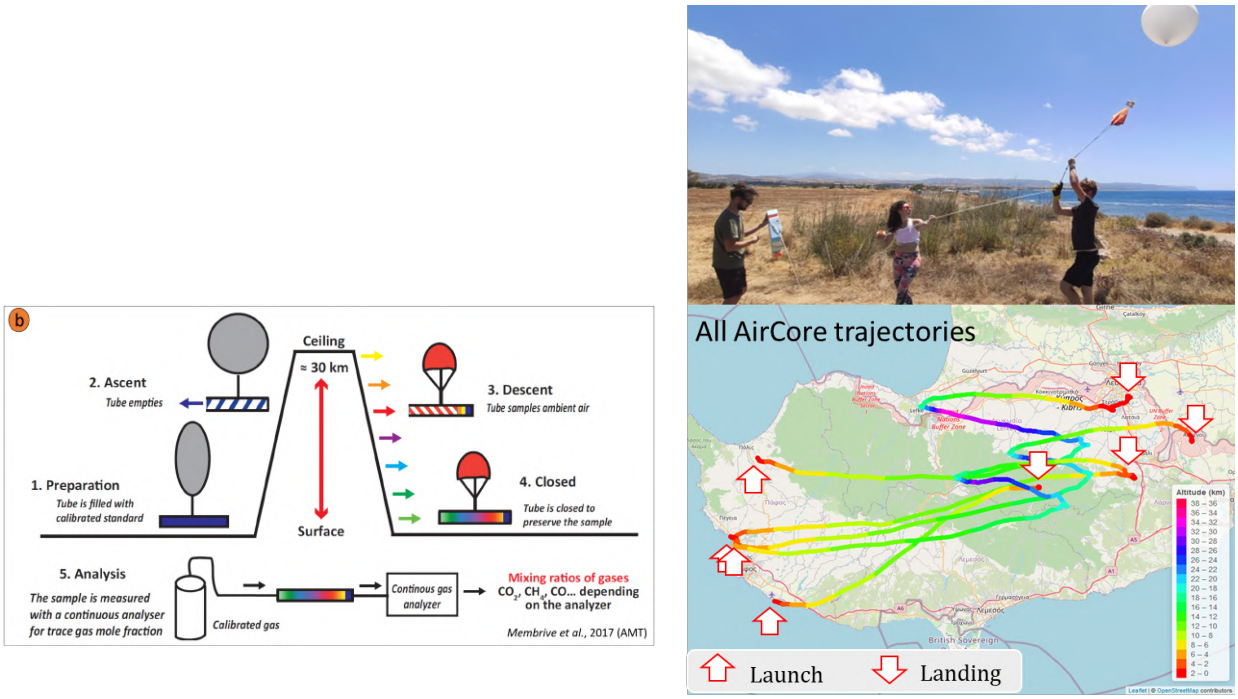

Figure 10.4.1: Left: principle of the AIRCORE. Right: First AIRCORE Campaign in Cyprus (June 2020). The coloured lines show the track of the AIRCORE during its ascent and descent phases.

The first AIRCORE campaign was organized in Cyprus in June 2020, as part of the EMME-CARE (Eastern Mediterranean and Middle East – Climate and Atmosphere Research) project and a collaboration between the Cyprus Institute, LSCE and the French Aircore program. The objective is to initiate in Cyprus a regular program of vertical profiles of greenhouse gases concentrations, combined with surface and total column observations to be integrated in the ICOS and TCCON European networks. Cyprus has a strategic position for greenhouse gases (GHGs) measurements: being situated between the continents of Europe, Africa and Asia; it experiences the overpass of different air masses and the seasonal variation of these air masses.

The first three AIRCORE profiles, up to 24 km, are shown in Figure 10.4.2. A distinct difference is observed between the profile of 19 June and the ones from 29 and 30 June in the upper troposphere lower stratosphere (UTLS) layer. On 29/30 June enhancements were observed in the concentrations between 12 and 17 km. Most of the structures observed during those 3 days are well simulated by the CAMS high resolution forecast. The analysis of the CO_2 dispersion in the UTLS, clearly shows a plume of pollutant coming from Asia. It corresponds to long range transport of pollutants lifted up in the upper troposphere by intense convection over India and transported by the easterly tropical jet stream over North Africa and the eastern Mediterranean. This enhancement due to long-range pollution transport is observed also from the TCCON measurements for CH_4 (+10 to 15 ppb) and CO (+10 to 20 ppb) total columns, a signal correctly represented by the CAMS experiments. For CO_2 the observations indicate a small decrease, whereas the CAMS experiments indicate constant values before and after this event.

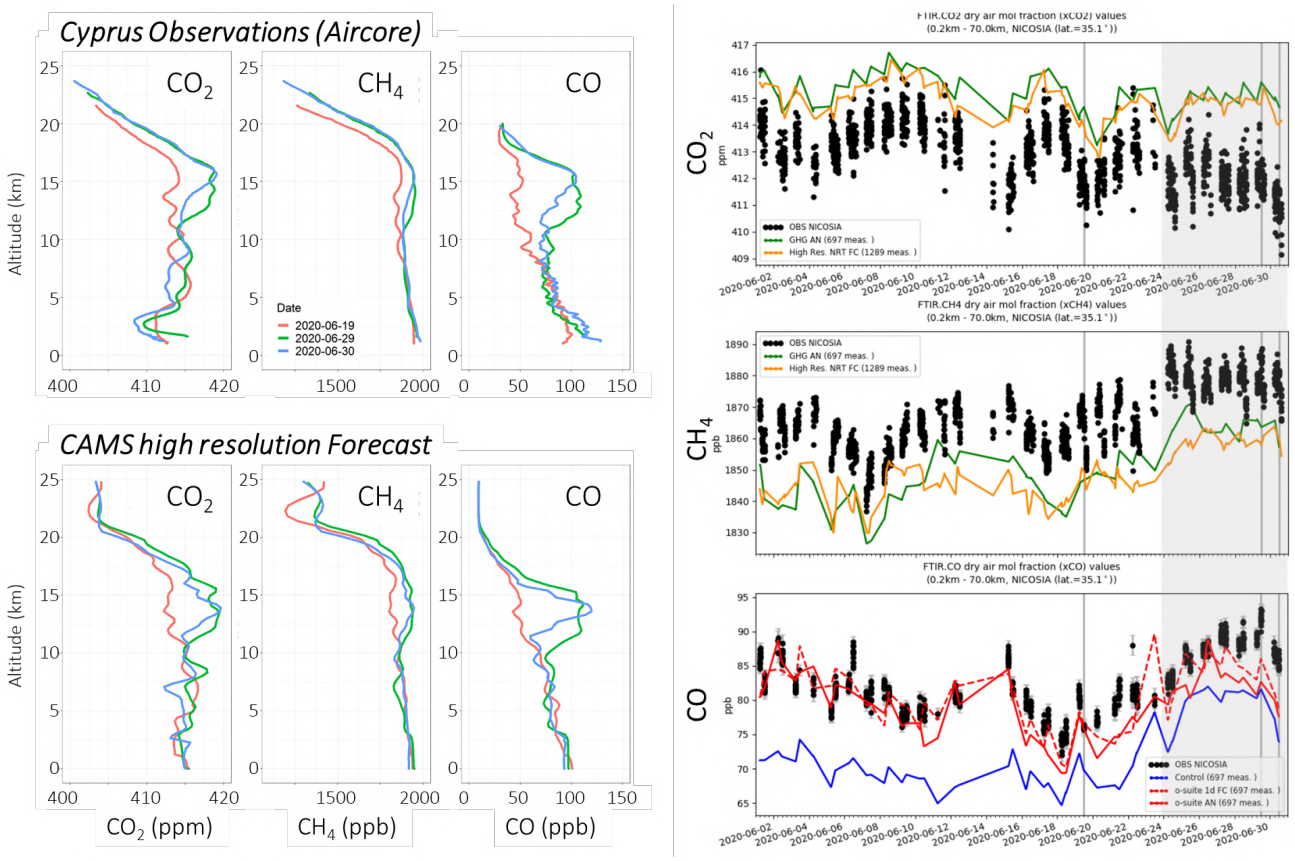

Figure 10.4.2: Left: vertical profiles of CO_2, CH_4 and CO concentrations from AIRCOREs (top panel) and from the high-resolution forecast (bottom panel) on 19 (red), 29 (green) and 30 (blue) June 2020. Right: comparison of the CO_2, CH_4 and CO model data with TCCON at Nicosia in June 2020. Green: CAMS GHG analysis; orange: CAMS high-resolution forecast; red: o-suite analysis (solid) and 1-day forecast (dashed); blue: control run; black: TCCON observations.

According to the AIRCORE profiles the positive offset in the UTLS is compensated by lower concentrations in the low troposphere. At this elevation, back trajectories indicate that the air mass sampled over Cyprus were previously circulating over Central Europe for several days. The carbon uptake by the biosphere in June explains this CO_2 decrease, and the smaller impact in the CAMS profiles is consistent with the underestimations of the CO_2 decrease observed at ICOS stations at this season (Figure 10.1.1).

A second example of a comparison with AIRCORE profiles is based on the measurements made at the Trainou tall tower in France in September 2020. On the vertical profile measured on 15 September we observe elevated CO layers at the surface and in the high troposphere (Figure 10.4.4), well captured by the CAMS experiment. The lowest peak appears to be related to a fire 60km south of Trainou. The CO layers observed in the high troposphere, between 8 and 12 km, correspond to long-range transport of pollutants *e*mitted by the fires on the American west coast. It is interesting to note that, according to CAMS, the CO plume over Trainou was much more intense on September 11 to 13, just in between the two AIRCORE launches (Figure 10.4.5). The 15 September profile shows, both in the observation and the CAMS simulation, a CO_2 and CH_4 enhancement in the stratosphere at about 18 km, which may be interpreted as an intrusion of tropospheric air.

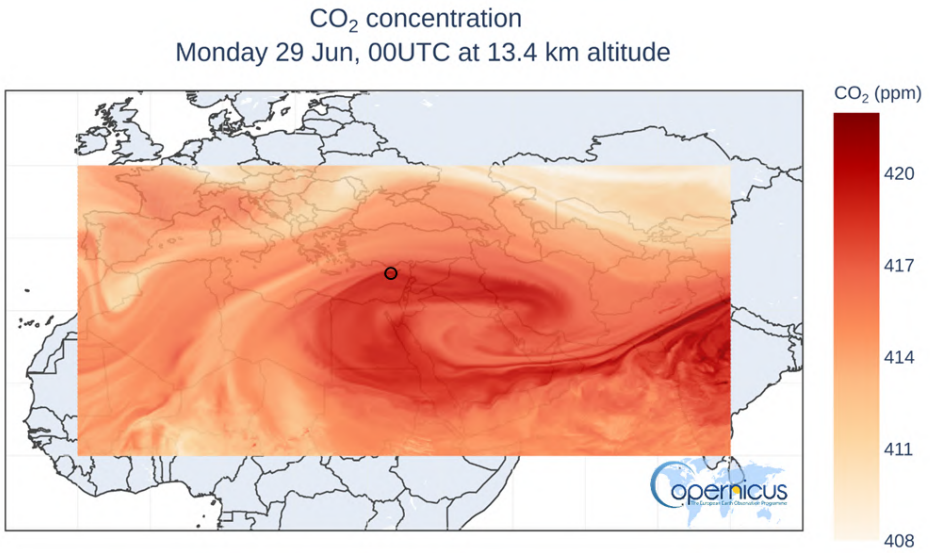

Figure 10.4.3: CO_2 concentrations from the high-resolution forecast experiment at 13.4 km on June 29. The black circle corresponds to the location of the Aircore profiles in Cyprus.

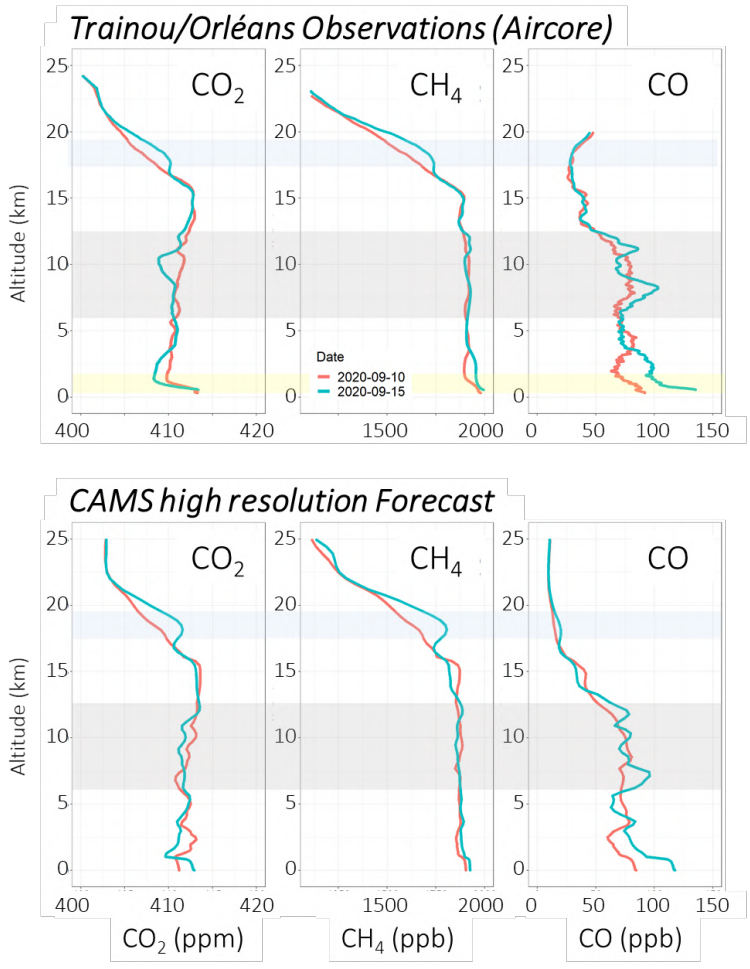

Figure 10.4.4: Vertical profiles of CO_2, CH_4 and CO concentrations from AIRCOREs (top panel) and from the high-resolution forecast (bottom panel) on 10 (red) and 15 (green) September 2020.

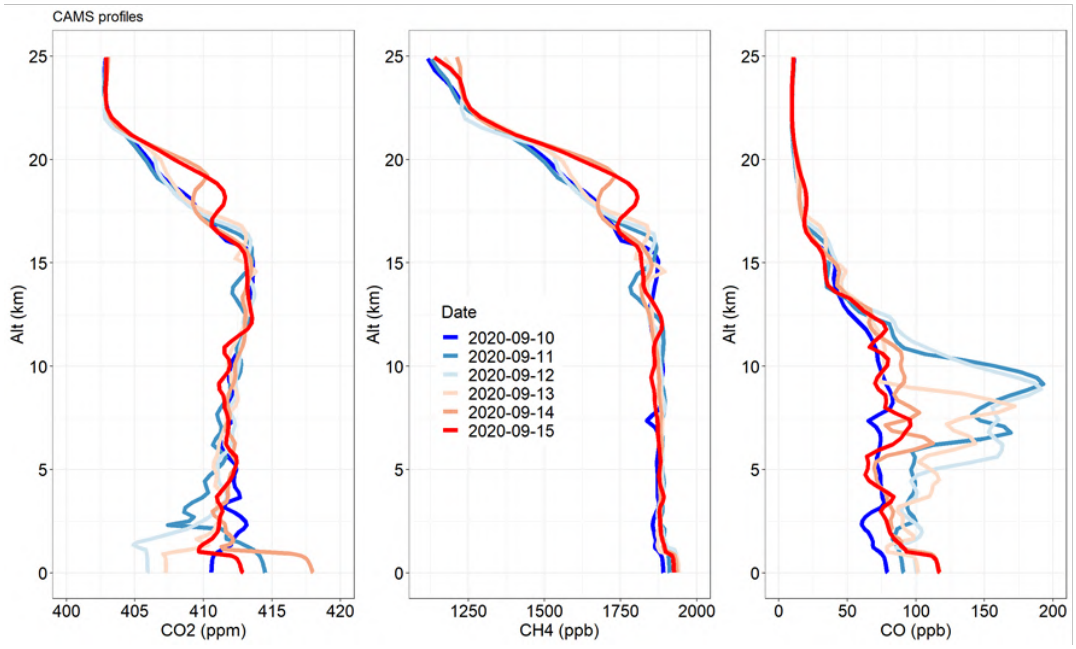

Figure 10.4.5: Vertical profiles of CO_2, CH_4 and CO concentrations from the high-resolution forecast from 10 to 15 September 2020.

11. Event studies

11.1 Dust event in November 2020 in Europe

In early-November 2020, MODIS satellite detected an intense dust outbreak that reached the Iberian Peninsula (see Figure 11.1.1) and moved towards northern Europe the next days. The dust plume origin is located in Algeria and moved to the Iberian Peninsula on 6th November, and continued moving towards northern latitudes reaching France, United Kingdom and Germany on 7-8 November.

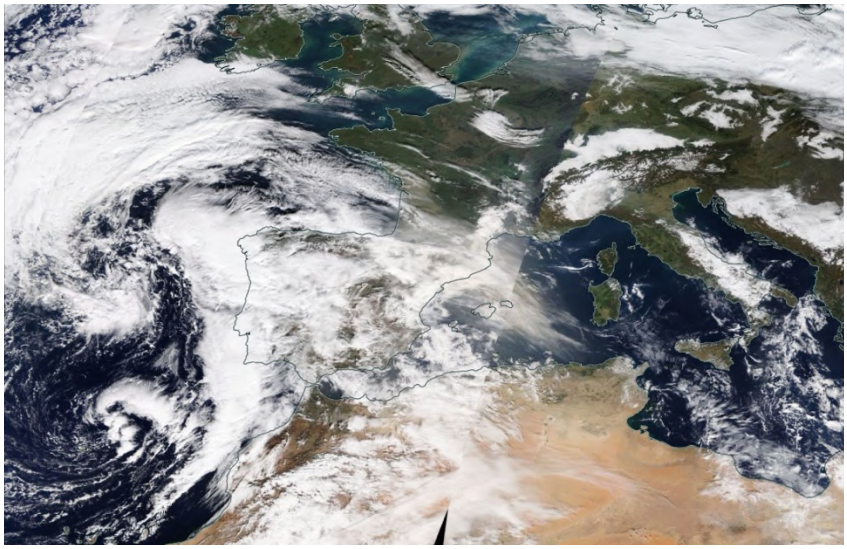

Figure 11.1.1: Daily visible composite of NASA MODIS Terra on 6th November over Iberian Peninsula and the Mediterranean. These images are a zoom of the images included in the comparison with CAMS o-suite in Figure 11.1.2.

The CAMS o-suite (see Figure 11.1.2) shows AOD values above 0.3 across the Western Mediterranean and the Iberian Peninsula during the event from 6 to 9 November. The comparison with MODIS shows that the o-suite reproduces the spatial and temporal distribution of the observed AOD plume with the origin of the plume over Algeria and following an arc that was crossing Spain, France, United Kingdom, and Germany. The comparison with AERONET shows that the CAMS model predicted a maximum peak of DOD over Barcelona (Spain, see Figure 8.4.2) on 6th November. PM10 concentration above 100 µg/m^3 are predicted in the Western Mediterranean and the Iberian Peninsula on 6th November (see Figure 11.1.2). These PM10 values are a little bit overestimated as shown in the comparison with an EEA Spanish site (see ES1569A in Figure 8.4.5b).

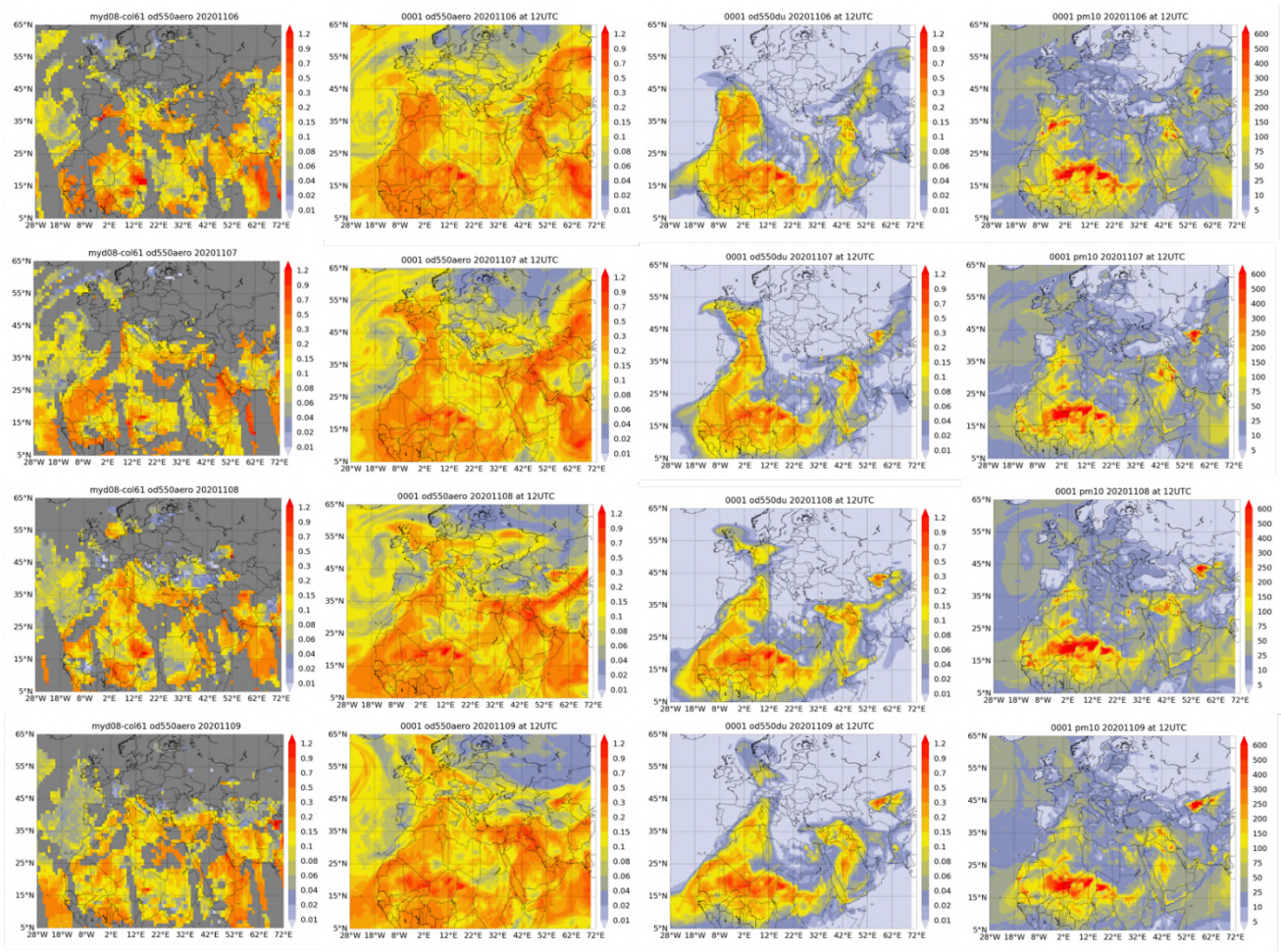

Figure 11.1.2: Observed AOD from MODIS/Aqua Level 3 and modelled o-suite AOD, DOD and PM10 (in µg/m^3) at 12UTC from o-suite for 6-9 November 2020.

12. References

Albert, M. F. M. A., Anguelova, M. D., Manders, A. M. M., Schaap, M., and de Leeuw, G.: Parameterization of oceanic whitecap fraction based on satellite observations, Atmos. Chem. Phys., 16, 13725–13751, https://doi.org/10.5194/acp-16-13725-2016, 2016.

Agusti-Panareda, A., Monitoring upgrades of analysis/forecast system, MACC-III Deliverable D44.04, June 2015.

Bai, K., Li, K., Guo, J., Yang, Y., & Chang, N.-B., Filling the gaps of in situ hourly PM2.5 concentration data with the aid of empirical orthogonal function analysis constrained by diurnal cycles, Atmospheric Measurement Techniques, 13(3), 1213–1226. https://doi.org/ 10.5194/amt-13-1213-2020, 2020.

Basart, S, A. Benedictow, Y. Bennouna, A.-M. Blechschmidt, S. Chabrillat, Y. Christophe, E. Cuevas, H. J. Eskes, K. M. Hansen, O. Jorba, J. Kapsomenakis, B. Langerock, T. Pay, A. Richter, N. Sudarchikova, M. Schulz, A. Wagner, C. Zerefos, Upgrade verification note for the CAMS near-real time global atmospheric composition service: Evaluation of the e-suite for the CAMS upgrade of July 2019, Copernicus Atmosphere Monitoring Service (CAMS) report, CAMS84_2018SC1_D3.2.1-201907_esuite_v1.pdf, July 2019.

Beirle, S., Hörmann, C., Jöckel, P., Liu, S., Penning de Vries, M., Pozzer, A., Sihler, H., Valks, P., and Wagner, T.: The STRatospheric Estimation Algorithm from Mainz (STREAM): estimating stratospheric NO_2 from nadir-viewing satellites by weighted convolution, Atmos. Meas. Tech., 9, 2753–2779, https://doi.org/10.5194/amt-9-2753-2016, 2016.

Bergamaschi, P., Frankenberg, C., Meirink, J. F., Krol, M., Villani, M. G., Houweling, S., Dentener, F., Dlugokencky, E. J., Miller, J. B., Gatti, L. V., Engel, A., and Levin, I.: Inverse modeling of global and regional CH4 emissions using SCIAMACHY satellite retrievals, J. Geophys. Res., 114, D22301, doi:10.1029/2009JD012287, 2009.

Benedetti, A., J.-J. Morcrette, O. Boucher, A. Dethof, R. J. Engelen, M. Fisher, H. Flentjes, N. Huneeus, L. Jones, J. W. Kaiser, S. Kinne, A. Mangold, M. Razinger, A. J. Simmons, M. Suttie, and the GEMS-AER team: Aerosol analysis and forecast in the ECMWF Integrated Forecast System. Part II : Data assimilation, J. Geophys. Res., 114, D13205, doi:10.1029/2008JD011115, 2009.

Birmili, W., Schepanski, K., Ansmann, A., Spindler, G., Tegen, I., Wehner, B., Nowak, A., Reimer, E., Mattis, I., Müller, K., Brüggemann, E., Gnauk, T., Herrmann, H., Wiedensohler, A., Althausen, D., Schladitz, A., Tuch, T., and Löschau, G.: A case of extreme particulate matter concentrations over Central Europe caused by dust emitted over the southern Ukraine, Atmos. Chem. Phys., 8, 997–1016, https://doi.org/10.5194/acp-8-997-2008, 2008.

Boussetta, S., Balsamo, G., Beljaars, A., Agusti-Panareda, A., Calvet, J.-C., Jacobs, C., van den Hurk, B., Viterbo, P., Lafont, S., Dutra, E., Jarlan, L., Balzarolo, M., Papale, D., and van der Werf, G.: Natural carbon dioxide exchanges in the ECMWF Integrated Forecasting System: implementation and offline validation, J. Geophys. Res.-Atmos., 118, 1–24, doi: 10.1002/jgrd.50488, 2013.

Braathen, WMO Arctic Ozone Bulletin No 1/2016, DOI:10.13140/RG.2.1.4929.6403, 2016.

Cammas, J.P., Brioude J., Chaboureau J.-P., Duron J., Mari C., Mascart P., Nédélec P., Smit H., Pätz H.-W., Volz-Thomas A., Stohl A., and Fromm M., Injection in the lower stratosphere of biomass fire emissions followed by long-range transport: a MOZAIC case study. Atmos. Chem. Phys., 9, 5829-5846, 2009

Cariolle, D. and Teyssèdre, H.: A revised linear ozone photochemistry parameterization for use in transport and general circulation models: multi-annual simulations, Atmos. Chem. Phys., 7, 2183-2196, doi:10.5194/acp-7-2183-2007, 2007.

Carn, S. A., V. E. Fioletov, C. A. McLinden, C. Li & N. A. Krotkov, A decade of global volcanic SO2 emissions measured from space, Scientific Reports volume 7, Article number: 44095 (2017).

Dee, D. P. and S. Uppala, Variational bias correction of satellite radiance data in the ERA-Interim reanalysis. Quart. J. Roy. Meteor. Soc.,135, 1830-1841, 2009.

Deeter, M. N., Emmons, L. K., Edwards, D. P., Gille, J. C., and Drummond, J. R.: Vertical resolution and information content of CO profiles retrieved by MOPITT, Geophys. Res. Lett., 31, L15112, doi:10.1029/2004GL020235, 2004.

Deeter, M. N., et al. (2010), The MOPITT version 4 CO product: Algorithm enhancements, validation, and long-term stability, J. Geophys. Res., 115, D07306, doi:10.1029/2009JD013005.

Dentener, F., et al., 2006: Emissions of primary aerosol and precursor gases in the years 2000 and 1750 prescribed data-sets for AeroCom, Atmos. Chem. Phys., 6, 4321 – 4344, http://www.atmos-chem-phys.net/6/4321/2006/acp-6-4321-2006.pdf.

Deshler, T., J.L. Mercer, H.G.J. Smit, R. Stubi, G. Levrat, B.J. Johnson, S.J. Oltmans, R. Kivi, A.M. Thompson, J. Witte, J. Davies, F.J. Schmidlin, G. Brothers, T. Sasaki (2008) Atmospheric comparison of electrochemical cell ozonesondes from different maufacturers, and with different cathode solution strengths: The Balloon Experiment on Standards for Ozonsondes. J. Geophys. Res.113, D04307, doi:10.1029/2007JD008975

Dupuy, E., et al.: Validation of ozone measurements from the Atmospheric Chemistry Experiment (ACE), Atmos. Chem. Phys., 9, 287-343, doi:10.5194/acp-9-287-2009, 2009.

Elbern, H., Schwinger, J., Botchorishvili, R.: Chemical state estimation for the middle atmosphere by four-dimensional variational data assimilation: System configuration. Journal of Geophysical Research (Atmospheres) 115, 6302, 2010.

Emmons, L. K., D. P. Edwards, M. N. Deeter, J. C. Gille, T. Campos, P. Nédélec, P. Novelli, and G. Sachse, Measurements of Pollution In The Troposphere (MOPITT) validation through 2006 Atmos. Chem. Phys., 9, 1795-1803, 2009

Errera, Q., Daerden, F., Chabrillat, S., Lambert, J. C., Lahoz, W. A., Viscardy, S., Bonjean, S., and Fonteyn, D., 4D-Var Assimilation of MIPAS chemical observations: ozone and nitrogen dioxide analyses, Atmos. Chem. Phys., 8, 6169-6187, 2008.

Errera, Q. and Ménard, R.: Technical Note: Spectral representation of spatial correlations in variational assimilation with grid point models and application to the belgian assimilation system for chemical observations (BASCOE), Atmos. Chem. Phys. Discuss., 12, 16763-16809, doi:10.5194/acpd-12-16763-2012, 2012.

Eskes, H. J., S. Basart, A. Benedictow, Y. Bennouna, A.-M. Blechschmidt, S. Chabrillat, Y. Christophe, K. M. Hansen, J. Kapsomenakis, B. Langerock, M. Pitkänen, M. Ramonet, A. Richter, N. Sudarchikova, M. Schulz, A. Wagner, T. Warneke (UBC), C. Zerefos, Upgrade verification note for the CAMS near-real time global atmospheric composition service: Evaluation of the e-suite for the CAMS 47R1 upgrade of October 2020, Copernicus Atmosphere Monitoring Service (CAMS) report, CAMS84_2018SC2_D3.2.1- 202009_esuite.pdf, 2 October 2020, doi:10.24380/fzdx-j890.

Eskes, H.J., S. Basart, A. Benedictow, Y. Bennouna, A.-M. Blechschmidt, S. Chabrillat, Y. Christophe, E. Cuevas, H. Flentje, K. M. Hansen, J. Kapsomenakis, B. Langerock, M. Ramonet, A. Richter, M. Schulz, N. Sudarchikova, A. Wagner, T. Warneke, C. Zerefos, Observation characterisation and validation methods document,

Copernicus Atmosphere Monitoring Service (CAMS) report, CAMS84_2018SC2_D6.1.1-2020_observations_v5.pdf, January 2021. Available from: http://atmosphere.copernicus.eu/user-support/validation/verification-global-services

Eskes, H. J., S. Basart, A. Benedictow, Y. Bennouna, A.-M. Blechschmidt, S. Chabrillat, Y. Christophe, H. Clark, E. Cuevas, K. M. Hansen, U. Im, J. Kapsomenakis, B. Langerock, K. Petersen, M. Schulz, A. Wagner, C. Zerefos, Upgrade verification note for the CAMS near-real time global atmospheric composition service, Copernicus Atmosphere Monitoring Service (CAMS) report, CAMS84_2015SC3_D84.3.1.5_201802_esuite_v1.pdf, February 2018 (2018b)

Eskes et al., Upgrade verification note for the CAMS near-real time global atmospheric composition service, Addendum July 2018, CAMS84_2015SC3_D84.3.1.5_201802_esuite_v1.pdf (2018c).

Flemming, J., Huijnen, V., Arteta, J., Bechtold, P., Beljaars, A., Blechschmidt, A.-M., Diamantakis, M., Engelen, R. J., Gaudel, A., Inness, A., Jones, L., Josse, B., Katragkou, E., Marecal, V., Peuch, V.-H., Richter, A., Schultz, M. G., Stein, O., and Tsikerdekis, A.: Tropospheric chemistry in the Integrated Forecasting System of ECMWF, Geosci. Model Dev., 8, 975-1003, doi:10.5194/gmd-8-975-2015, 2015.

Flemming, J., Benedetti, A., Inness, A., Engelen, R. J., Jones, L., Huijnen, V., Remy, S., Parrington, M., Suttie, M., Bozzo, A., Peuch, V.-H., Akritidis, D., and Katragkou, E.: The CAMS interim Reanalysis of Carbon Monoxide, Ozone and Aerosol for 2003–2015, Atmos. Chem. Phys., 17, 1945-1983, doi:10.5194/acp-17-1945-2017, 2017.

Franco, B., et al., Retrievals of formaldehyde from ground-based FTIR and MAX-DOAS observations at the Jungfraujoch station and comparisons with GEOS-Chem and IMAGES model simulations, Atmos. Meas. Tech., 8, 1733-1756, 2015

Gielen, C., Van Roozendael, M., Hendrick, F., Pinardi, G., Vlemmix, T., De Bock, V., De Backer, H., Fayt, C., Hermans, C., Gillotay, D., and Wang, P.: A simple and versatile cloud-screening method for MAX-DOAS retrievals, Atmos. Meas. Tech., 7, 3509-3527, doi:10.5194/amt-7-3509-2014, 2014.

Granier, C. et al.: Evolution of anthropogenic and biomass burning emissions of air pollutants at global and regional scales during the 1980–2010 period. Climatic Change (109), 2011

Holben, B. N., Eck, T. F., Slutsker, I., Tanré, D., Buis, J. P., Setzer, A., Vermote, E., Reagan, J. A., Kaufman, Y. J., Nakajima, T., Lavenu, F., Jankowiak, I., and Smirnov A.: AERONET – a federated instrument network and data archive for aerosol characterization, Remote Sens. Environ., 66, 1–16, 5529, 5533, 5537, 5544, 1998.

Hommel, R., Eichmann, K.-U., Aschmann, J., Bramstedt, K., Weber, M., von Savigny, C., Richter, A., Rozanov, A., Wittrock, F., Khosrawi, F., Bauer, R., and Burrows, J. P.: Chemical ozone loss and ozone mini-hole event during the Arctic winter 2010/2011 as observed by SCIAMACHY and GOME-2, Atmos. Chem. Phys., 14, 3247-3276, doi:10.5194/acp-14-3247-2014, 2014.

Huijnen, V., et al.: The global chemistry transport model TM5: description and evaluation of the tropospheric chemistry version 3.0, Geosci. Model Dev., 3, 445-473, doi:10.5194/gmd-3-445-2010, 2010.

Inness, A., Blechschmidt, A.-M., Bouarar, I., Chabrillat, S., Crepulja, M., Engelen, R. J., Eskes, H., Flemming, J., Gaudel, A., Hendrick, F., Huijnen, V., Jones, L., Kapsomenakis, J., Katragkou, E., Keppens, A., Langerock, B., de Mazière, M., Melas, D., Parrington, M., Peuch, V. H., Razinger, M., Richter, A., Schultz, M. G., Suttie, M., Thouret, V., Vrekoussis, M., Wagner, A., and Zerefos, C.: Data assimilation of satellite-retrieved ozone, carbon monoxide and nitrogen dioxide with ECMWF's Composition-IFS, Atmos. Chem. Phys., 15, 5275-5303, doi:10.5194/acp-15-5275-2015, 2015.

Janssens-Maenhout, G., Dentener, F., Aardenne, J. V., Monni, S., Pagliari, V., Orlandini, L., Klimont, Z., Kurokawa, J., Akimoto, H., Ohara, T., Wankmueller, R., Battye, B., Grano, D., Zuber, A., and Keating, T.: EDGAR-HTAP: a Harmonized Gridded Air Pollution Emission Dataset Based on National Inventories, JRC68434,

EUR report No EUR 25 299–2012, ISBN 978-92-79- 23122-0, ISSN 1831-9424, European Commission Publications Office, Ispra (Italy), 2012.

Jaross, G., Bhartia, P.K., Chen, G., Kowitt, M., Haken, M., Chen, Z., Xu, Ph., Warner, J., Kelly, T. : OMPS Limb Profiler instrument performance assessment, J. Geophys. Res. Atmos 119, 2169-8996, 2014.

Joly, M. and Peuch, V. H., Objective classification of air quality monitoring sites over Europe, Atmospheric Environment, 47, 111-123, 2012.

Kaiser, J. W., Heil, A., Andreae, M. O., Benedetti, A., Chubarova, N., Jones, L., Morcrette, J.-J., Razinger, M., Schultz, M. G., Suttie, M., and van der Werf, G. R.: Biomass burning emissions estimated with a global fire assimilation system based on observed fire radiative power, Biogeosciences, 9, 527-554, doi:10.5194/bg-9-527-2012, 2012.

Karion, A., C. Sweeney, P. Tans and T. Newberger (2010). AirCore: An Innovative Atmospheric Sampling System. Journal of Atmospheric and Oceanic Technology 27(11): 1839-1853.

Kramarova, N. A., Nash, E. R., Newman, P. A., Bhartia, P. K., McPeters, R. D., Rault, D. F., Seftor, C. J., Xu, P. Q., and Labow, G. J.: Measuring the Antarctic ozone hole with the new Ozone Mapping and Profiler Suite (OMPS), Atmos. Chem. Phys., 14, 2353-2361, doi:10.5194/acp-14-2353-2014, 2014.

Lahoz, W. A., Errera, Q., Viscardy, S., and Manney G. L., The 2009 stratospheric major warming described from synergistic use of BASCOE water vapour analyses and MLS observations, Atmos. Chem. Phys. 11, 4689-4703, 2011

Lambert, A, et al., Aura Microwave Limb Sounder Version 3.4 Level-2 near real-time data user guide, http://disc.sci.gsfc.nasa.gov/Aura/data-holdings/MLS/documents/NRT-user-guide-v34.pdf

Langerock, B., De Mazière, M., Hendrick, F., Vigouroux, C., Desmet, F., Dils, B., and Niemeijer, S.: Description of algorithms for co-locating and comparing gridded model data with remote-sensing observations, Geosci. Model Dev., 8, 911-921, doi:10.5194/gmd-8-911-2015, 2015.

Lefever, K., van der A, R., Baier, F., Christophe, Y., Errera, Q., Eskes, H., Flemming, J., Inness, A., Jones, L., Lambert, J.-C., Langerock, B., Schultz, M. G., Stein, O., Wagner, A., and Chabrillat, S.: Copernicus stratospheric ozone service, 2009–2012: validation, system intercomparison and roles of input data sets, Atmos. Chem. Phys., 15, 2269-2293, doi:10.5194/acp-15-2269-2015, 2015.

Liu, Z., et al., Exploring the missing source of glyoxal (CHOCHO) over China, Geophys. Res. Lett., 39, L10812, doi: 10.1029/2012GL051645, 2012

Massart, S., Flemming, J., Cariolle, D., Jones, L., High resolution CO tracer forecasts, MACC-III Deliverable D22.04, May 2015, available from http://www.gmes-atmosphere.eu/documents/macciii/deliverables/grg

Membrive, O., C. Crevoisier, C. Sweeney, F. Danis, A. Hertzog, A. Engel, H. Bönisch and L. Picon (2017). AirCore-HR: a high-resolution column sampling to enhance the vertical description of CH4 and CO2. Atmos. Meas. Tech. 10(6): 2163-2181

Morcrette, J.-J., O. Boucher, L. Jones, D. Salmond, P. Bechtold, A. Beljaars, A. Benedetti, A. Bonet, J. W. Kaiser, M. Razinger, M. Schulz, S. Serrar, A. J. Simmons, M. Sofiev, M. Suttie, A. M. Tompkins, and A. Untch: Aerosol analysis and forecast in the ECMWF Integrated Forecast System. Part I: Forward modelling, J. Geophys. Res., 114, D06206, doi:10.1029/2008JD011235, 2009.

Ramonet, M., A. Wagner, M. Schulz, Q. Errera, H. J. Eskes, S. Basart, A. Benedictow, Y. Bennouna, A.-M. Blechschmidt, S. Chabrillat, Christophe, Y., E. Cuevas, A. El-Yazidi, H. Flentje, P. Fritzsche, K.M. Hansen, U. Im, J. Kapsomenakis, B. Langerock, A. Richter, N. Sudarchikova, V. Thouret, T. Warneke, C. Zerefos, Validation report of the CAMS near-real-time global atmospheric composition service: Period June - August 2020,

Copernicus Atmosphere Monitoring Service (CAMS) report, CAMS84_2018SC2_D1.1.1_JJA2020.pdf, January 2021, doi:10.24381/8pxn-q362.

Rémy, S., Kipling, Z., Flemming, J., Boucher, O., Nabat, P., Michou, M., Bozzo, A., Ades, M., Huijnen, V., Benedetti, A., Engelen, R., Peuch, V.-H., and Morcrette, J.-J.: Description and evaluation of the tropospheric aerosol scheme in the European Centre for Medium-Range Weather Forecasts (ECMWF) Integrated Forecasting System (IFS-AER, cycle 45R1), Geosci. Model Dev., 12, 4627–4659, https://doi.org/10.5194/gmd-12-4627-2019, 2019.

Richter, A., Burrows, J. P., Nüß, H., Granier, C, Niemeier, U.: Increase in tropospheric nitrogen dioxide over China observed from space, Nature, 437, 129-132, doi: 10.1038/nature04092, 2005

*Richter, A., Begoin, M., Hilboll, A., and Burrows, J. P.: An improved NO2 retrieval for the GOME-2 satellite instrument, Atmos. Meas. Tech. , **4**, 1147-1159, doi:10.5194/amt-4-1147-2011, 2011*

Sindelarova, K., Granier, C., Bouarar, I., Guenther, A., Tilmes, S., Stavrakou, T., Müller, J.-F., Kuhn, U., Stefani, P., and Knorr, W.: Global data set of biogenic VOC emissions calculated by the MEGAN model over the last 30 years, Atmos. Chem. Phys., 14, 9317-9341, doi:10.5194/acp-14-9317-2014, 2014.

Smit, H.G.J., W. Straeter, B.J. Johnson, S.J. Oltmans, J. Davies, D.W. Tarasick, B. Hoegger, R. Stubi, F.J. Schmidlin, T. Northam, A.M. Thompson, J.C. Witte, I. Boyd: Assessment of the performance of ECC-ozonesondes under quasi-flight conditions in the environmental simulation chamber: Insights from the Juelich Ozone Sonde Intercomparison Experiment (JOSIE), J. Geophys. Res. 112, D19306, doi:10.1029/2006JD007308, 2007.

Solomon, S., Haskins, J., Ivy, D. J. and Min, F.: Fundamental differences between Arctic and Antarctic ozone depletion, PNAS 2014 111 (17) 6220-6225, doi:10.1073/pnas.1319307111, 2014.

Stauffer, R. M., Thompson, A. M., Kollonige, D. E., Witte, J. C., Tarasick, D. W., and Davies, J., Voemel, H., Morris, G. A., VanMalderen, R., Johnson, B. J. J., Querel, R.R., Selkirk, H.B., Stübi, R., Smit, H.G.J: A Post-2013 Drop-off in Total Ozone at Half of Global Ozonesonde Stations: ECC Instrument Artifacts? Earth and Space Science Open Archive JF M310.1002/essoar.10501543.1, 2020.

Stavrakou,T., First space-based derivation of the global atmospheric methanol fluxes, Atm. Chem. Phys., 11, 4873-4898, 2013.

Strahan, S.E., A.R. Douglass, and P.A. Newman, The contributions of chemistry and transport to low arctic ozone in March 2011 derived from Aura MLS observations, J. Geophys. Res. Atmos., 118, 1563–1576, doi:10.1002/jgrd.50181, 2013.

Taha, G.; Jaross, G. R.; Bhartia, P. K.: Validation of OMPS LP Ozone Profiles Version 2.0 with MLS, Ozone Sondes and Lidar Measurements, American Geophysical Union, Fall Meeting 2014, abstract #A33J-3322, 2014.

Taylor, K.E.: Summarizing multiple aspects of model performance in a single diagram. J.Geophys. Res., 106, 7183-7192, 2001.

Thompson, A. M., Witte, J. C., Sterling, C.,Jordan, A., Johnson, B. J., Oltmans, S. J.,Thiongo, K. (2017). First reprocessing of Southern Hemisphere Additional Ozonesondes (SHADOZ) ozone profiles (1998\u20132016): 2. Comparisons with satellites and ground-based instruments. Journal of Geophysical Research: Atmospheres, 122, 13,000\u201313,025. https://doi.org/10.1002/2017JD027406, 2017.

van der A, R. J. , M. A. F. Allaart, and H. J. Eskes, Multi sensor reanalysis of total ozone, Atmos. Chem. Phys., 10, 11277–11294, doi:10.5194/acp-10-11277-2010, www.atmos- chem-phys.net/10/11277/2010/, 2010

van der A, R., M. Allaart, H. Eskes, K. Lefever, Validation report of the MACC 30-year multi-sensor reanalysis of ozone columns Period 1979-2008, MACC-II report, Jan 2013, MACCII_VAL_DEL_D_83.3_OzoneMSRv1_20130130.docx/pdf.

van der A, R. J., Allaart, M. A. F., and Eskes, H. J.: Extended and refined multi sensor reanalysis of total ozone for the period 1970–2012, Atmos. Meas. Tech., 8, 3021-3035, doi:10.5194/amt-8-3021-2015, 2015.

van Geffen, J., Boersma, K. F., Eskes, H., Sneep, M., ter Linden, M., Zara, M., and Veefkind, J. P.: S5P TROPOMI NO2 slant column retrieval: method, stability, uncertainties and comparisons with OMI, Atmos. Meas. Tech., 13, 1315–1335, https://doi.org/10.5194/amt-13-1315-2020, 2020.

*Vrekoussis, M., Wittrock, F., Richter, A., and Burrows, J. P.: GOME-2 observations of oxygenated VOCs: what can we learn from the ratio glyoxal to formaldehyde on a global scale?, Atmos. Chem. Phys., **10**, 10145-10160, doi:10.5194/acp-10-10145-2010, 2010*

Wennberg, P. O., Mui, W., Wunch, D., Kort, E. A., Blake, D. R., Atlas, E. L., Santoni, G. W., Wofsy, S. C., Diskin, G. S., Jeong, S., and Fischer, M. L.: On the sources of methane to the Los Angeles atmosphere, Environ. Sci. Technol., 46, 9282–9289, https://doi.org/10.1021/es301138y, 2012

Wittrock, F., A. Richter, H. Oetjen, J. P. Burrows, M. Kanakidou, S. Myriokefalitakis, R. Volkamer, S. Beirle, U. Platt, and T. Wagner, Simultaneous global observations of glyoxal and formaldehyde from space, Geophys. Res. Lett., 33, L16804, doi:10.1029/2006GL026310, 2006

Witte, J. C., Thompson, A. M., Smit, H. G. J., Vömel, H., Posny, F., & Stübi, R. : First reprocessing of Southern Hemisphere ADditional OZonesondes profile records: 3. Uncertainty in ozone profile and total column. Journal of Geophysical Research: Atmospheres, 123, 3243\u20133268. https://doi.org/10.1002/2017JD027791, 2018.

WMO (2010), Guidelines for the Measurement of Atmospheric Carbon Monoxide, GAW Report No. 192, World Meteorological Organization, Geneva, Switzerland, 2010.

WMO (2013), Guidelines for the Continuous Measurements of Ozone in the Troposphere, GAW Report No. 209, World Meteorological Organization, Geneva, Switzerland, 2013.

Wunch, D., Wennberg, P. O., Toon, G. C., Keppel-Aleks, G., and Yavin, Y. G.: Emissions of greenhouse gases from a North American megacity, Geophys. Res. Lett., 36, 1–5, https://doi.org/10.1029/2009GL039825, 2009.

Annex 1: Acknowledgements

Listed below are the authors contributing to the sections in this report. The authors contributing to the model description are also provided, as well as acknowledgements to the validation datasets.

Tropospheric reactive gases reactive gases

Annette Wagner, MPG (editor, O3 sondes, GAW data)
Yasmine Bennouna, Valerie Thouret, CNRS-LA (IAGOS)
Harald Flentje, DWD (O3 sondes, GAW data)
Anne Blechschmidt and Andreas Richter, IUB Bremen (GOME-2 NO2, HCHO)
John Kapsomenakis, Christos Zerefos, AA (ESRL)
Natalia Sudarchikova, satellite IR observations (MPG)
Kaj Hansen, Ulas Im, AU (Arctic theme)
Bavo Langerock, BIRA (NDACC)

Tropospheric aerosol

Michael Schulz, MetNo (editor, Aerocom, Aeronet)
Anna Benedictow, Jan Griesfeller, MetNo (Aerocom, Aeronet)
Sara Basart, MTeresa Pay, Oriol Jorba, BSC-CNS (Aeronet, MODIS, AirBase, SDS-WAS NAMEE RC)
Emilio Cuevas, AEMET (Aeronet, MODIS, AirBase, SDS-WAS NAMEE RC)
Harald Flentje, DWD (Backscatter profiles)

Stratospheric reactive gases

Yves Christophe, BIRA (editor, model-satellite intercomparisons)
Simon Chabrillat, BIRA (model intercomparisons)
Annette Wagner, MPI-M (O_3 sondes)
Bavo Langerock, BIRA (NDACC FTIR, MWR, UVVIS DOAS, LIDAR)
Anne Blechschmidt and Andreas Richter, IUB-UB Bremen (SCIAMACHY/GOME-2 NO_2)

Greenhouse gases

Michel Ramonet, IPSL (ICOS)
Abdelhadi El-Yazidi and Leonard Rivier, LSCE (ICOS)
Thorsten Warneke, UBC (TCCON)
Bavo Langerock, BIRA (TCCON)

Reactive gases and aerosol modeling

Johannes Flemming (ECMWF), Antje Inness (ECMWF), Angela Benedetti (ECMWF), Sebastien Massart (ECMWF), Anna Agusti-Panareda (ECMWF), Johannes Kaiser (KCL/MPIC/ECMWF), Samuel Remy (LMD), Olivier Boucher (LMD), Vincent Huijnen (KNMI), Richard Engelen (ECMWF)

Acknowledgements for the validation datasets used

We wish to acknowledge the provision of NRT GAW observational data by: Institute of Atmospheric Sciences and Climate (ISAC) of the Italian National Research Council (CNR), South African Weather Service, National Centre for Atmospheric Science (NCAS, Cape Verde), National Air Pollution Monitoring Network (NABEL) (Federal Office for the Environment FOEN and Swiss Federal Laboratories for Materials Testing and Research EMPA), Atmospheric Environment Division Global Environment and Marine Department Japan Meteorological Agency, Chinese Academy of Meteorological Sciences (CAMS), Alfred Wegener Institut, Umweltbundesamt (Austria), National Meteorological Service (Argentina), Umweltbundesamt (UBA, Germany)

We are grateful to the numerous operators of the Aeronet network and to the central data processing facility at NASA Goddard Space Flight Center for providing the NRT sun photometer data, especially Ilya Slutker and Brent Holben for sending the data.

The authors thank to all researchers, data providers and collaborators of the World Meteorological Organization's Sand and Dust Storm Warning Advisory and Assessment System (WMO SDS-WAS) for Northern Africa, Middle East and Europe (NAMEE) Regional Node. Also special thank to Canary Government as well as AERONET, MODIS, U.K. Met Office MSG, MSG Eumetsat and EOSDIS World Viewer principal investigators and scientists for establishing and maintaining data used in the activities of the WMO SDS-WAS NAMEE Regional Center (http://sds-was.aemet.es/).

We wish to acknowledge the provision of ozone sonde data by the World Ozone and Ultraviolet Radiation Data Centre established at EC in Toronto (http://woudc.org), by the Data Host Facility of the Network for the Detection of Atmospheric Composition Change established at NOAA (http://ndacc.org), by the Norwegian Institute for Air Research and by the National Aeronautics and Space Administration (NASA).

We wish to thank the NDACC investigators for the provision of observations at Ny Alesund, Bern, Jungfraujoch, Izaña, Xianghe, Harestua, Reunion Maido, Uccle, Hohenpeissen, Mauna Loa, Lauder and Haute Provence.

The authors acknowledge the NOAA Earth System Research Laboratory (ESRL) Global Monitoring Division (GMD) for the provision of ground-based ozone concentrations.

The MOPITT CO data were obtained from the NASA Langley Research Center ASDC. We acknowledge the LATMOS IASI group for providing IASI CO data.

SCIAMACHY lv1 radiances were provided to IUP-UB by ESA through DLR/DFD.

GOME-2 lv1 radiances were provided to IUP-UB by EUMETSAT.

S5P lv1 radiances and NO_2 operational were provided by EU Copernicus.

The authors acknowledge Environment and Climate Change Canada for the provision of Alert ozone data and Sara Crepinsek – NOAA for the provision of Tiksi ozone data. Surface ozone data from the Zeppelin Mountain, Svalbard are from www.luftkvalitet.info. Surface ozone data from the Villum Research Station, Station Nord (VRS) were financially supported by "The Danish Environmental Protection Agency" with means from the MIKA/DANCEA funds for Environmental Support to the

Arctic Region. The Villum Foundation is acknowledged for the large grant making it possible to build VRS in North Greenland.

We acknowledge the National Aeronautics and Space Administration (NASA), USA for providing the OMPS limb sounder data (http://npp.gsfc.nasa.gov/omps.html), the SAGE III-ISS ozone data https://eosweb.larc.nasa.gov/project/sageiii-iss/sageiii-iss_table and the Aura-MLS offline data (http://mls.jpl.nasa.gov/index-eos-mls.php).

We thank the Canadian Space Agency and ACE science team for providing level 2 data retrieved from ACE-FTS on the Canadian satellite SCISAT-1.

The European Environment Information and Observation Network (Eionet) Air Quality portal provides details relevant for the reporting of air quality information from EU Member States and other EEA member and co-operating countries. This information is submitted according to Directives 2004/107/EC and 2008/50/EC of the European Parliament and of the Council.

We are grateful to the IAGOS operators from the various institutes which are members of IAGOS-AISBL (http://www.iagos.org). The authors also acknowledge the strong support of the European Commission, Airbus, and the airlines (Lufthansa, Air France, Austrian, Air Namibia, Cathay Pacific, Iberia, China Airlines and Hawaiian Airlines so far) which have carried the MOZAIC or IAGOS equipment and undertaken maintenance since 1994. In the last 10 years of operation, MOZAIC has been funded by INSU-CNRS (France), Météo-France, Université Paul Sabatier (Toulouse, France) and Research Center Jülich (FZJ, Jülich, Germany). IAGOS has been additionally funded by the EU projects IAGOS-DS and IAGOS-ERI. The MOZAIC–IAGOS database (http://www.iagos-data.fr) is supported by AERIS (CNES and INSU-CNRS). Data are also available via AERIS web site www.aeris-data.fr.

We acknowledge the contribution of the ICOS Atmospheric Thematic Center (Lynn Hazan, Amara Abbaris, and Leonard Rivier) for the near real time data processing of surface CO_2 and CH_4 concentrations. The ICOS monitoring sites are maintained by the national networks: ICOS-Belgium (Martine De Mazière , Mahesh Kumar Sha , Nicolas Kumps), ICOS-Czech Rep. (Michal Marek, Katerina Komínková, Gabriela Vítková), ICOS-Finland (Olli Peltola, Janne Levula, Tuomas Laurila, Juha Hatakka, Ari Leskinen, Ivan Mammarella, Petri Keronen), ICOS-France (Michel Ramonet, Marc Delmotte, Sebastien Conil, Laurent Langrene , Morgan Lopez, Victor Kazan, Aurélie Colomb, Jean Marc Pichon, Olivier Laurent, Camille Yver-Kwok, Zineb Mandrick, Jean-Marc Metzger), ICOS Germany (Matthias Lindauer, Dagmar Kubistin, Christian Plass-Duelmer, Dietmar Weyrauch, Jennifer Müller-Williams), ICOS-Italy (Paolo Cristofanelli, Michela Maione, Francesco Apadula, Pamela Trisolino), ICOS-Netherlands (Huilin Chen, Bert Scheeren), ICOS-Norway (Cathrine Lund Myhre, Ove Hermansen, Chris Lunder), ICOS-Sweden (Jutta Holst, Michal Heliasz, Meelis Molder, Mikaell Ottosson Lofvenius, Irene Lehner, Per Marklund, Paul Smith), ICOS-Switzerland (Martin Steinbacher, Markus Leuenberger), European Commission, Joint Research Centre, Directorate for Energy, Transport and Climate (Peter Bergamaschi, Giovanni Manca).

In collaboration with LSCE and the French Aircore program, the Cyprus Institute has coordinated the first AIRCORE campaign in Cyprus within the framework of the EMME-CARE (Eastern Mediterranean and Middle East – Climate and Atmosphere Research). Thanks to C. Rousogenous, P.Y. Quéhé, Th. Laemmel, C. Keleshis, P.Antoniou, and J.Sciare. The AIRCORE campaign at Trainou was coordinated by Th. Laemmel and J.Moyé from LSCE, with funding from CEA, OVSQ and CNES.

References (ICOS):

Hazan, L., Tarniewicz, J., Ramonet, M., Laurent, O., and Abbaris, A.: Automatic processing of atmospheric CO2 and CH4 mole fractions at the ICOS Atmosphere Thematic Centre, Atmos. Meas. Tech., 9, 4719–4736, https://doi.org/10.5194/amt-9-4719-2016, 2016.

Laurent, O., ICOS Atmosphere Monitoring Station Assembly, and ICOS Atmosphere Thematic Centre (ATC): ICOS Atmospheric Station Specifications v1.3, ICOS ERIC, doi:10.18160/SDW6-BX90, 2017.

Yver-Kwok, C., C. Philippon, P. Bergamaschi, T. Biermann, F. Calzolari, H. Chen, S. Conil, P. Cristofanelli, M. Delmotte, J. Hatakka, M. Heliasz, O. Hermansen, K. Komínková, D. Kubistin, N. Kumps, O. Laurent, T. Laurila, I. Lehner, J. Levula, M. Lindauer, M. Lopez, I. Mammarella, G. Manca, P. Marklund, J. M. Metzger, M. Mölder, S. M. Platt, M. Ramonet, L. Rivier, B. Scheeren, M. K. Sha, P. Smith, M. Steinbacher, G. Vítková and S. Wyss (2021). Evaluation and optimization of ICOS atmosphere station data as part of the labeling process. Atmos. Meas. Tech. 14(1): 89-116.

The TCCON site at Orleans is operated by the University of Bremen and the RAMCES team at LSCE (Gif-sur-Yvette, France). The TCCON site at Bialystok is operated by the University of Bremen. Funding for the two sites was provided by the EU-project ICOS-INWIRE and the University of Bremen. The TCCON site at Réunion is operated by BIRA-IASB, in cooperation with UReunion and is funded by BELSPO in the framework of the Belgian ICOS program.

References (TCCON):

Blumenstock, T., F. Hase, M. Schneider, O. E. García, and E. Sepúlveda. 2017. "TCCON data from Izana (ES), Release GGG2014.R1." CaltechDATA. doi:10.14291/tccon.ggg2014.izana01.r1.

De Mazière, M., M. K. Sha, F. Desmet, C. Hermans, F. Scolas, N. Kumps, J.-M. Metzger, V. Duflot, and J.-P. Cammas. 2017. "TCCON data from Réunion Island (RE), Release GGG2014.R1." CaltechDATA. doi:10.14291/tccon.ggg2014.reunion01.r1.

Deutscher, N. M., J. Notholt, J. Messerschmidt, C. Weinzierl, T. Warneke, C. Petri, and P. Grupe. 2017. "TCCON data from Bialystok (PL), Release GGG2014.R1." CaltechDATA. doi:10.14291/tccon.ggg2014.bialystok01.r1/1183984.

Dubey, M. K., B. G. Henderson, D. Green, Z. T. Butterfield, G. Keppel-Aleks, N. T. Allen, J.-F. Blavier, C. M. Roehl, D. Wunch, and R. Lindenmaier. 2017. "TCCON data from Manaus (BR), Release GGG2014.R0." CaltechDATA. doi:10.14291/tccon.ggg2014.manaus01.r0/1149274.

Dubey, M. K., R. Lindenmaier, B. G. Henderson, D. Green, N. T. Allen, C. M. Roehl, J.-F. Blavier, et al. 2017. "TCCON data from Four Corners (US), Release GGG2014.R0." CaltechDATA. doi:10.14291/tccon.ggg2014.fourcorners01.r0/1149272.

Feist, D. G., S. G. Arnold, N. John, and M. C. Geibel. 2017. "TCCON data from Ascension Island (SH), Release GGG2014.R0." CaltechDATA. doi:10.14291/tccon.ggg2014.ascension01.r0/1149285.

Goo, T.-Y., Y.-S. Oh, and V. A. Velazco. 2017. "TCCON data from Anmeyondo (KR), Release GGG2014.R0." CaltechDATA. doi:10.14291/tccon.ggg2014.anmeyondo01.r0/1149284.

Griffith, D. W. T., N. M. Deutscher, V. A. Velazco, P. O. Wennberg, Y. Yavin, G. Keppel-Aleks, R. A. Washenfelder, et al. 2017. "TCCON data from Darwin (AU), Release GGG2014.R0." CaltechDATA. doi:10.14291/tccon.ggg2014.darwin01.r0/1149290.

Griffith, D. W. T., V. A. Velazco, N. M. Deutscher, C. Paton-Walsh, N. B. Jones, S. R. Wilson, R. C. Macatangay, G. C. Kettlewell, R. R. Buchholz, and M. O. Riggenbach. 2017. "TCCON data from Wollongong (AU), Release GGG2014.R0." CaltechDATA. doi:10.14291/tccon.ggg2014.wollongong01.r0/1149291.

Hase, F., T. Blumenstock, S. Dohe, J. Groß, and M.ä. Kiel. 2017. "TCCON data from Karlsruhe (DE), Release GGG2014.R1." CaltechDATA. doi:10.14291/tccon.ggg2014.karlsruhe01.r1/1182416.

Iraci, L. T., J. R. Podolske, P. W. Hillyard, C. Roehl, P. O. Wennberg, J.-F. Blavier, J. Landeros, et al. 2017. "TCCON data from Edwards (US), Release GGG2014.R1." CaltechDATA. doi:10.14291/tccon.ggg2014.edwards01.r1/1255068.

—. 2017. "TCCON data from Indianapolis (US), Release GGG2014.R1." CaltechDATA. doi:10.14291/tccon.ggg2014.indianapolis01.r1/1330094.

Kawakami, S., H. Ohyama, K. Arai, H. Okumura, C. Taura, T. Fukamachi, and M. Sakashita. 2017. "TCCON data from Saga (JP), Release GGG2014.R0." CaltechDATA. doi:10.14291/tccon.ggg2014.saga01.r0/1149283.

Kivi, R., P. Heikkinen, and E. Kyrö. 2017. "TCCON data from Sodankylä (FI), Release GGG2014.R0." CaltechDATA. doi:10.14291/tccon.ggg2014.sodankyla01.r0/1149280.

Liu, Cheng, Wei Wang, and Youwen Sun. 2018. "TCCON data from Hefei (PRC), Release GGG2014.R0." CaltechDATA. doi:10.14291/tccon.ggg2014.hefei01.r0.

Morino, I., N. Yokozeki, T. Matsuzaki, and M. Horikawa. 2017. "TCCON data from Rikubetsu (JP), Release GGG2014.R2." CaltechDATA. doi:10.14291/tccon.ggg2014.rikubetsu01.r2.

Morino, I., T. Matsuzaki, and M. Horikawa. 2017. "TCCON data from Tsukuba (JP), 125HR, Release GGG2014.R2." CaltechDATA. doi:10.14291/tccon.ggg2014.tsukuba02.r2.

Morino, Isamu, Voltaire A. Velazco, Akihiro Hori, Osamu Uchino, and David W. T. Griffith. 2018. "TCCON data from Burgos, Ilocos Norte (PH), Release GGG2014.R0." CaltechDATA. doi:10.14291/tccon.ggg2014.burgos01.r0.

Notholt, J., C. Petri, T. Warneke, N. M. Deutscher, M. Palm, M. Buschmann, C. Weinzierl, R. C. Macatangay, and P. Grupe. 2017. "TCCON data from Bremen (DE), Release GGG2014.R0." CaltechDATA. doi:10.14291/tccon.ggg2014.bremen01.r0/1149275.

Notholt, J., T. Warneke, C. Petri, N. M. Deutscher, C. Weinzierl, M. Palm, and M. Buschmann. 2017. "TCCON data from Ny Ålesund, Spitsbergen (NO), Release GGG2014.R0." CaltechDATA. doi:10.14291/tccon.ggg2014.nyalesund01.r0/1149278.

Pollard, David Frank, John Robinson, and Hisako Shiona. 2019. "TCCON data from Lauder (NZ), Release GGG2014.R0." CaltechDATA. doi:10.14291/tccon.ggg2014.lauder03.r0.

Sherlock, V., B. Connor, J. Robinson, H. Shiona, D. Smale, and D. F. Pollard. 2017. "TCCON data from Lauder (NZ), 120HR, Release GGG2014.R0." CaltechDATA. doi:10.14291/tccon.ggg2014.lauder01.r0/1149293.

—. 2017. "TCCON data from Lauder (NZ), 125HR, Release GGG2014.R0." CaltechDATA. doi:10.14291/tccon.ggg2014.lauder02.r0/1149298.

Strong, K., S. Roche, J. E. Franklin, J. Mendonca, E. Lutsch, D. Weaver, P. F. Fogal, J. R. Drummond, R. Batchelor, and R. Lindenmaier. 2018. "TCCON data from Eureka (CA), Release GGG2014.R3." CaltechDATA. doi:10.14291/tccon.ggg2014.eureka01.r3.

Sussmann, R., and M. Rettinger. 2017. "TCCON data from Garmisch (DE), Release GGG2014.R2." CaltechDATA. doi:10.14291/tccon.ggg2014.garmisch01.r2.

—. 2018. "TCCON data from Zugspitze (DE), Release GGG2014.R1." CaltechDATA. doi:10.14291/tccon.ggg2014.zugspitze01.r1.

Té, Y., P. Jeseck, and C. Janssen. 2017. "TCCON data from Paris (FR), Release GGG2014.R0." CaltechDATA. doi:10.14291/tccon.ggg2014.paris01.r0/1149279.

Warneke, T., J. Messerschmidt, J. Notholt, C. Weinzierl, N. M. Deutscher, C. Petri, and P. Grupe. 2017. "TCCON data from Orléans (FR), Release GGG2014.R0." CaltechDATA. doi:10.14291/tccon.ggg2014.orleans01.r0/1149276.

Wennberg, P. O., C. M. Roehl, D. Wunch, G. C. Toon, J.-F. Blavier, R. Washenfelder, G. Keppel-Aleks, N. T. Allen, and J. Ayers. 2017. "TCCON data from Park Falls (US), Release GGG2014.R1." CaltechDATA. doi:10.14291/tccon.ggg2014.parkfalls01.r1.

Wennberg, P. O., C. M. Roehl, J.-F. Blavier, D. Wunch, and N. T. Allen. 2017. "TCCON data from Jet Propulsion Laboratory (US), 2011, Release GGG2014.R1." CaltechDATA. doi:10.14291/tccon.ggg2014.jpl02.r1/1330096.

Wennberg, P. O., D. Wunch, C. M. Roehl, J.-F. Blavier, G. C. Toon, and N. T. Allen. 2017. "TCCON data from Caltech (US), Release GGG2014.R1." CaltechDATA. doi:10.14291/tccon.ggg2014.pasadena01.r1/1182415.

—. 2017. "TCCON data from Lamont (US), Release GGG2014.R1." CaltechDATA. doi:10.14291/tccon.ggg2014.lamont01.r1/1255070.

Wennberg, P. O., D. Wunch, Y. Yavin, G. C. Toon, J.-F. Blavier, N. T. Allen, and G. Keppel-Aleks. 2017. "TCCON data from Jet Propulsion Laboratory (US), 2007, Release GGG2014.R0." CaltechDATA. doi:10.14291/tccon.ggg2014.jpl01.r0/1149163.

Wunch, D., J. Mendonca, O. Colebatch, N. T. Allen, J.-F. Blavier, S. Roche, J. Hedelius, et al. 2017. "TCCON data from East Trout Lake, SK (CA), Release GGG2014.R1." CaltechDATA. doi:10.14291/tccon.ggg2014.easttroutlake01.r1.

Wunch, D., Toon, G. C., Sherlock, V., Deutscher, N. M., Liu, C., Feist, D. G., & Wennberg, P. O. (2015). The Total Carbon Column Observing Network's GGG2014 Data Version. Tech. rep., California Institute of Technology, Pasadena. doi:10.14291/tccon.ggg2014.documentation.R0/1221662

Copernicus Atmosphere Monitoring Service

ECMWF - Shinfield Park, Reading RG2 9AX, UK

Contact: info@copernicus-atmosphere.eu

atmosphere.copernicus.eu copernicus.eu ecmwf.int